

Oceano Dunes State Vehicular Recreation Area Dust Control Program
DRAFT 2023 Annual Report and Work Plan

August 1, 2023

ATTACHMENTS

- Attachment 01: 2011 to 2021 Dust Control Measures
- Attachment 02: 2022/2023 ODSVRA Dust Control Program Vegetation Restoration Projects
(State Parks ARWP Work Product)
- Attachment 03: Oceano Dunes: Status 2023 (DRI Presentation)
- Attachment 04: Increments of Progress Toward Air Quality Objectives, ODSVRA Dust Control
2022 Update (DRI Document)
- Attachment 05: Computation Fluid Dynamics Modeling of the ODSVRA 48-Acre Foredune
Restoration Project (DRI Document)
- Attachment 06: SAG Recommendations for Establishing Emissivity Grids to be Used in the
Modeling of Pre-Disturbance Conditions and Future Excess Emissions
Reductions (SAG Memorandum)
- Attachment 07: In-Park Increments of Progress, TPM₁₀:TPWD, April to September 2022 (DRI
Document)
- Attachment 08: Summary of Vegetation Monitoring of Restoration Sites at ODSVRA (2022)
(State Parks ARWP Work Product)
- Attachment 09: Preliminary Analysis of Time-Lapse Photo Monitoring Stations at the ODSVRA
Foredune Restoration Site (UCSB Document)
- Attachment 10: 2023 PMRP Evaluation Metrics
- Attachment 11: Compilation of Studies Reviewed and Comments Provided by the Scientific
Advisory Group from 08/01/22 to 07/31/23
 - 11-01: Increments of Progress Towards Air Quality Objectives – ODSVRA Dust
Controls 2022*
 - 11-02: Quantifying the Source Attribution of PM₁₀ Measured Downwind of the
ODSVRA*
 - 11-03: PI-SWERL September 2022 Results and Implications for
Emissivity/Dispersion Modeling*
 - 11-04: SAG Framework for Assessing Excess Emissions of PM₁₀ from the
ODSVRA*
- Attachment 12: ODSVRA Public Relations Campaign (State Parks ARWP Work Product)
- Attachment 13: 2022/2023 ODSVRA Dust Control Program Vegetation Restoration Projects
(State Parks ARWP Work Product)

THIS PAGE WAS INTENTIONALLY LEFT BLANK.

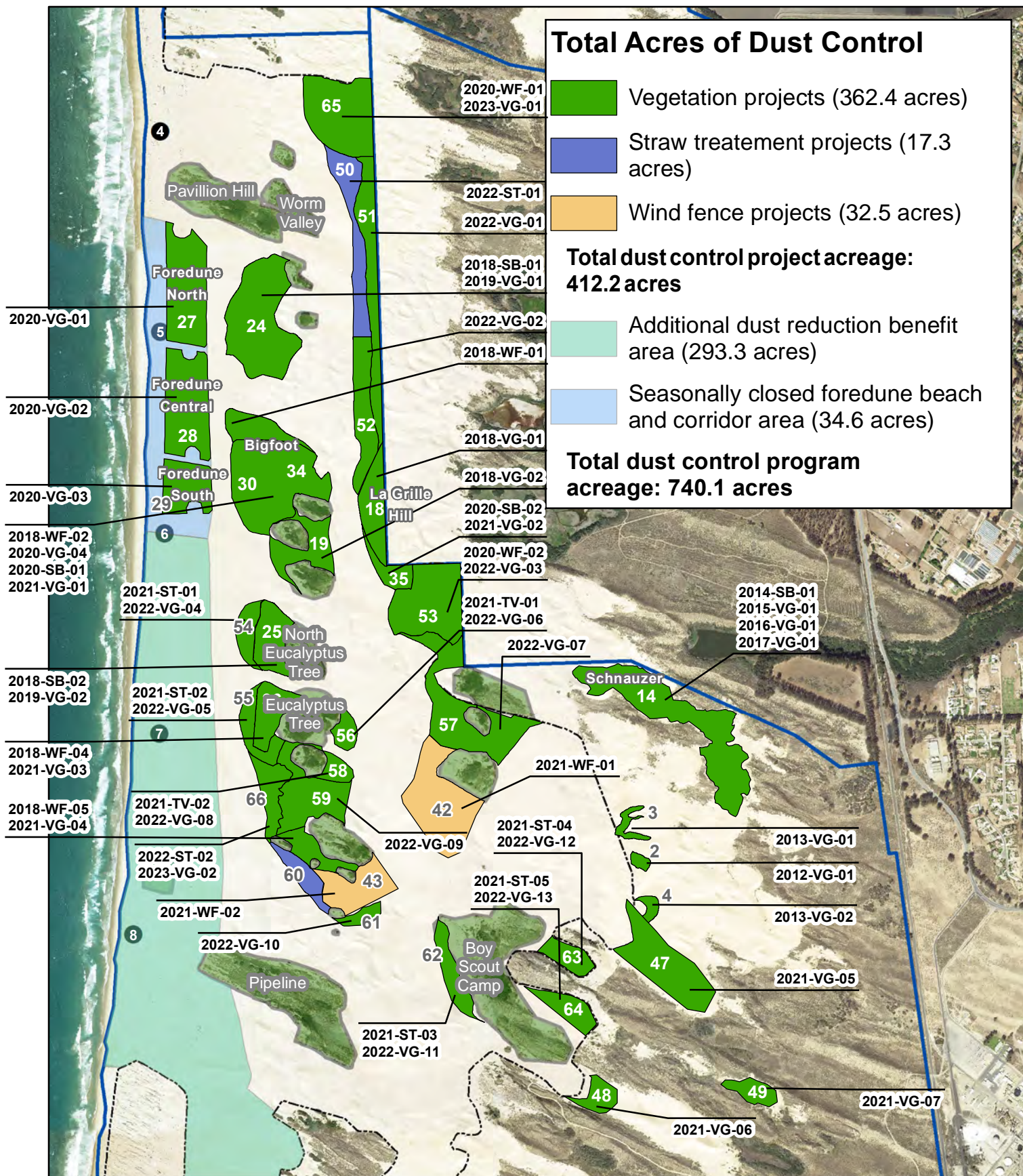
Oceano Dunes State Vehicular Recreation Area Dust Control Program

DRAFT 2023 Annual Report and Work Plan

ATTACHMENT 01

2011 to 2021 Dust Control Measures

THIS PAGE WAS INTENTIONALLY LEFT BLANK.



Source: CDPR, MIG Imagery: 2014 NAIP

6/27/2023



0 500 1,000 2,000 Feet



A01-01: Cumulative Dust Control as of 7/31/23

2023 ARWP

- Marker post
- Existing fenced vegetated islands
- Park boundary
- Open riding and camping area boundary fence

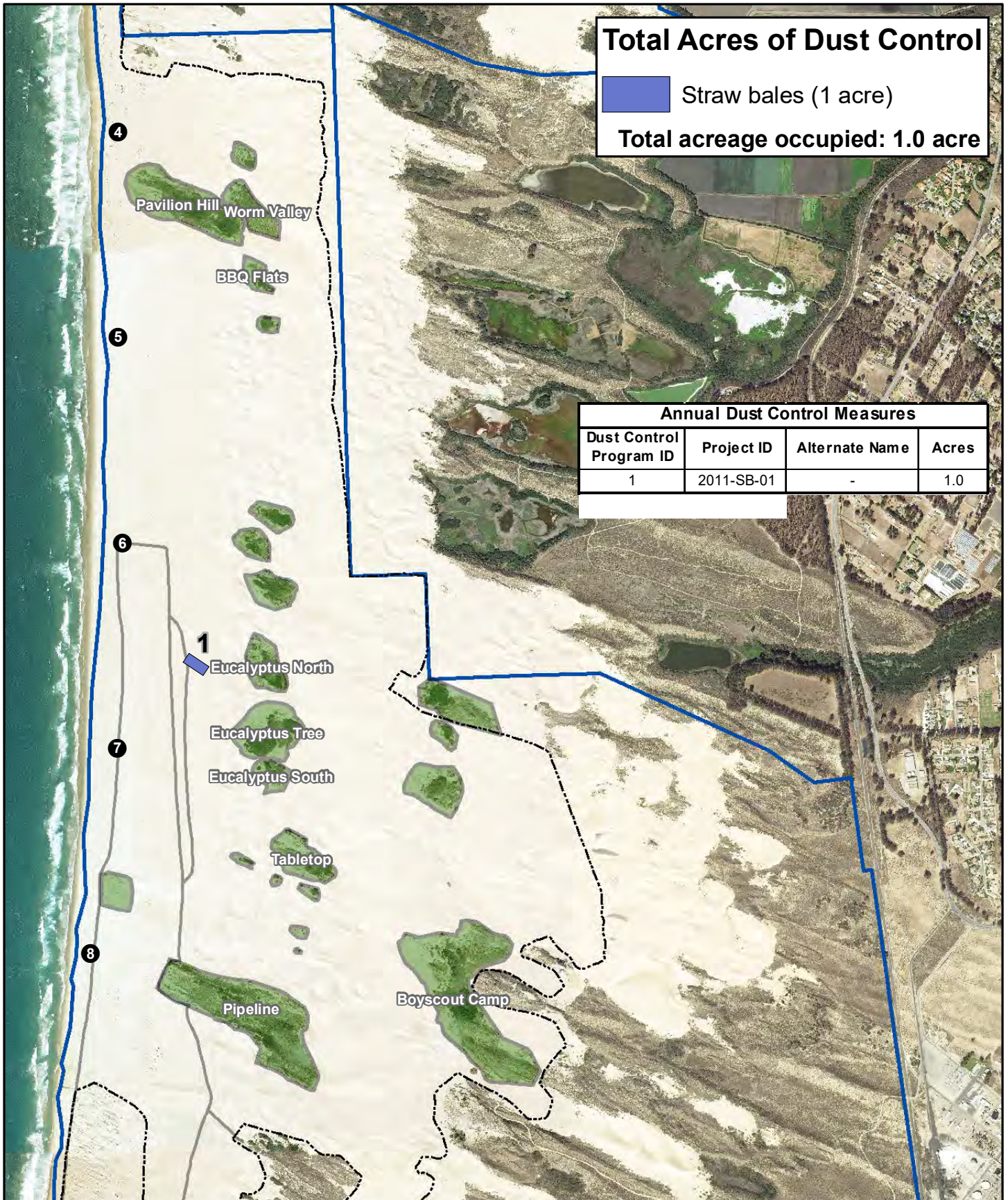
Total Acres of Dust Control

Straw bales (1 acre)

Total acreage occupied: 1.0 acre

Annual Dust Control Measures

Dust Control Program ID	Project ID	Alternate Name	Acres
1	2011-SB-01	-	1.0



Source: CDPR, MIG Imagery: 2014 NAIP

9/13/2021



0 500 1,000 2,000 Feet



● Marker post

— Nesting enclosure from 2020



Existing fenced vegetated islands

----- Open riding and camping area boundary fence



Park boundary

A01-02: 2011 Dust Control Treatment Areas

2023 ARWP

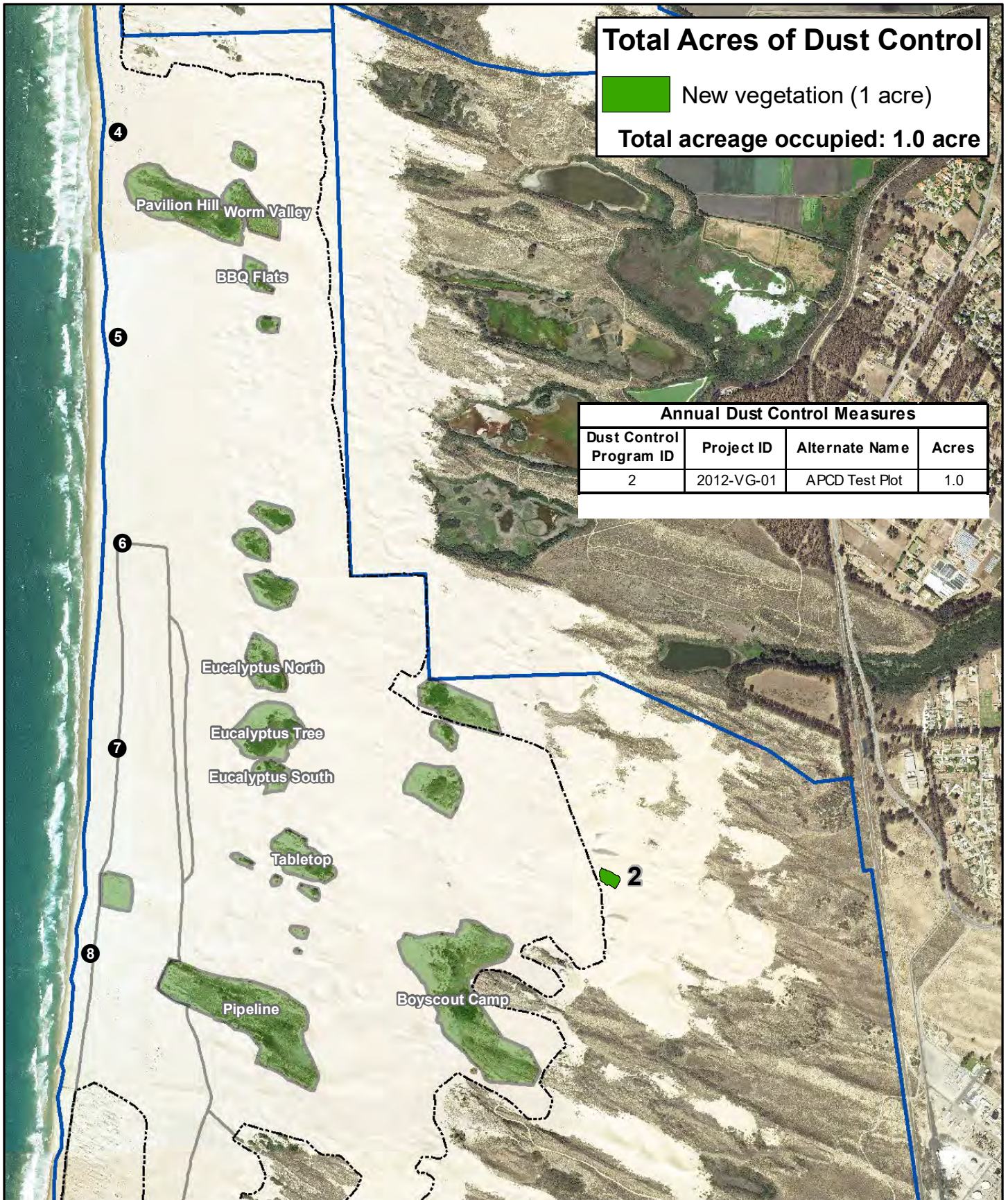
Total Acres of Dust Control

 New vegetation (1 acre)

Total acreage occupied: 1.0 acre

Annual Dust Control Measures

Dust Control Program ID	Project ID	Alternate Name	Acres
2	2012-VG-01	APCD Test Plot	1.0



Source: CDPR, MIG Imagery: 2014 NAIP

9/13/2021



0 500 1,000 2,000 Feet



● Marker post

— Nesting enclosure from 2020



Existing fenced vegetated islands

----- Open riding and camping area boundary fence



Park boundary

A01-03: 2012 Dust Control Treatment Areas

2023 ARWP

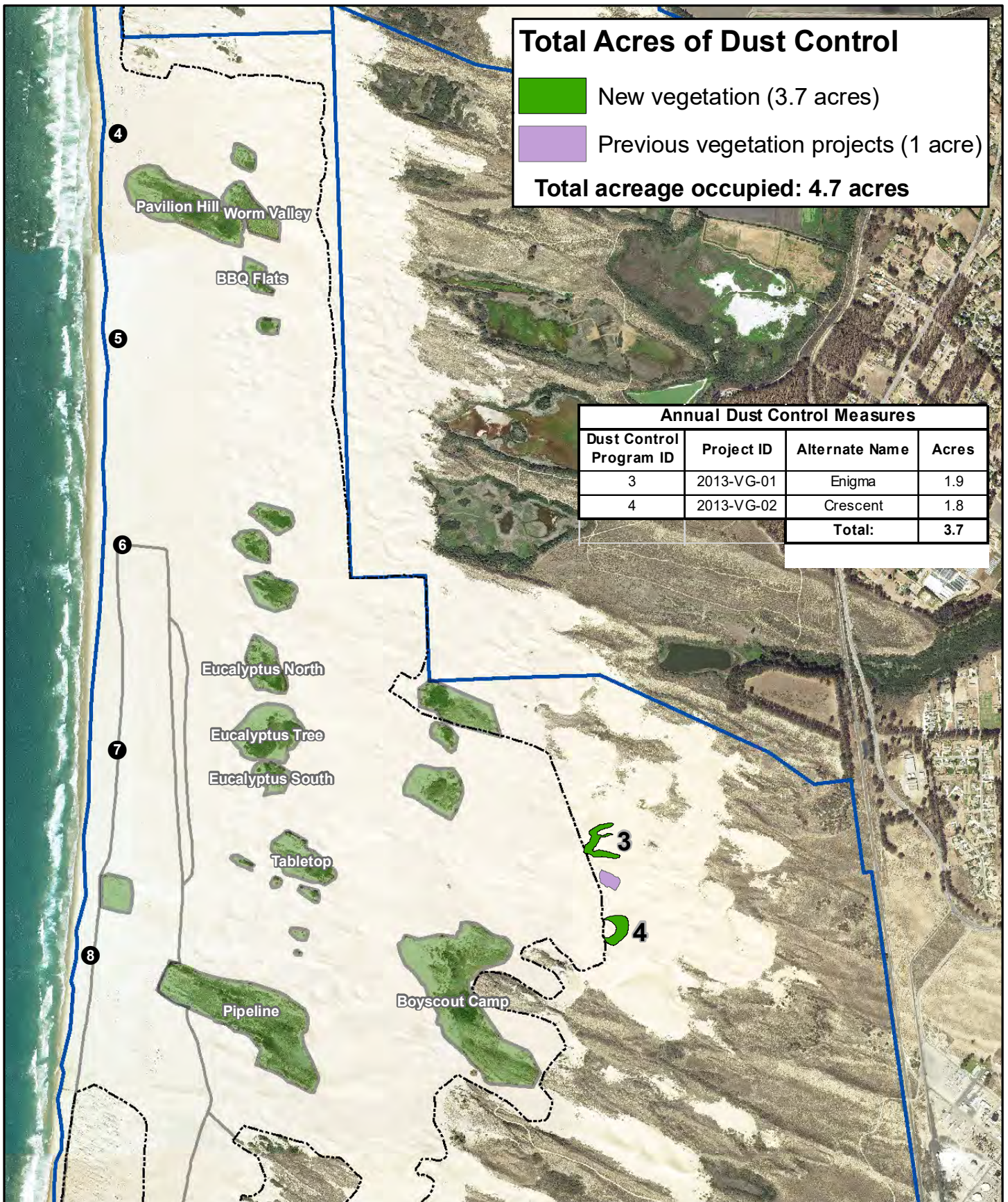
Total Acres of Dust Control

- New vegetation (3.7 acres)
- Previous vegetation projects (1 acre)

Total acreage occupied: 4.7 acres

Annual Dust Control Measures

Dust Control Program ID	Project ID	Alternate Name	Acres
3	2013-VG-01	Enigma	1.9
4	2013-VG-02	Crescent	1.8
Total:			3.7



Source: CDPR, MIG Imagery: 2014 NAIP

0 500 1,000 2,000 Feet



● Marker post

— Nesting enclosure from 2020



Existing fenced vegetated islands

----- Open riding and camping area boundary fence

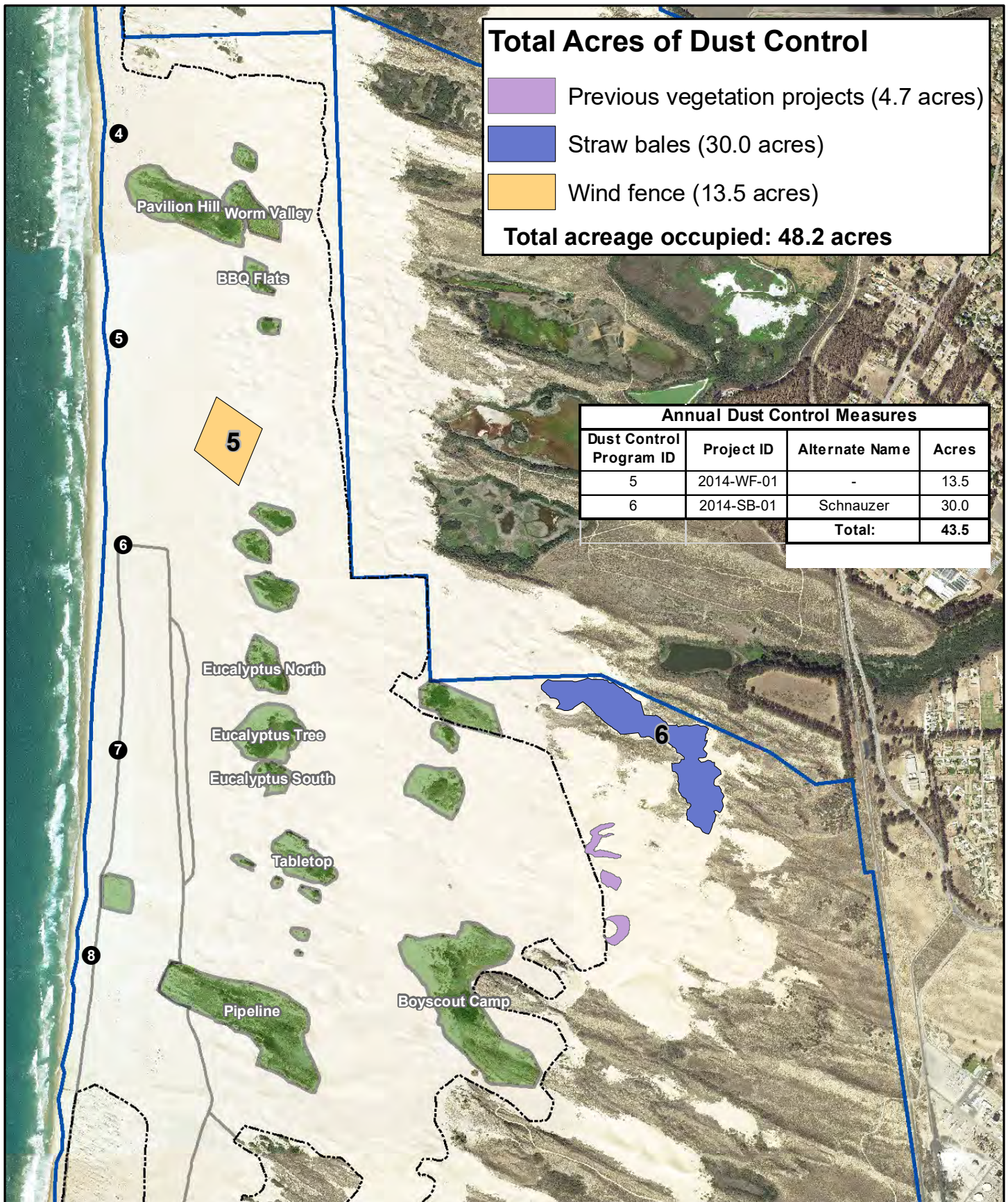


Park boundary

A01-04: 2013 Dust Control Treatment Areas

2023 ARWP

9/13/2021



Source: CDPR, MIG Imagery: 2014 NAIP

0 500 1,000 2,000 Feet



● Marker post

— Nesting enclosure from 2020



Existing fenced vegetated islands

----- Open riding and camping area boundary fence

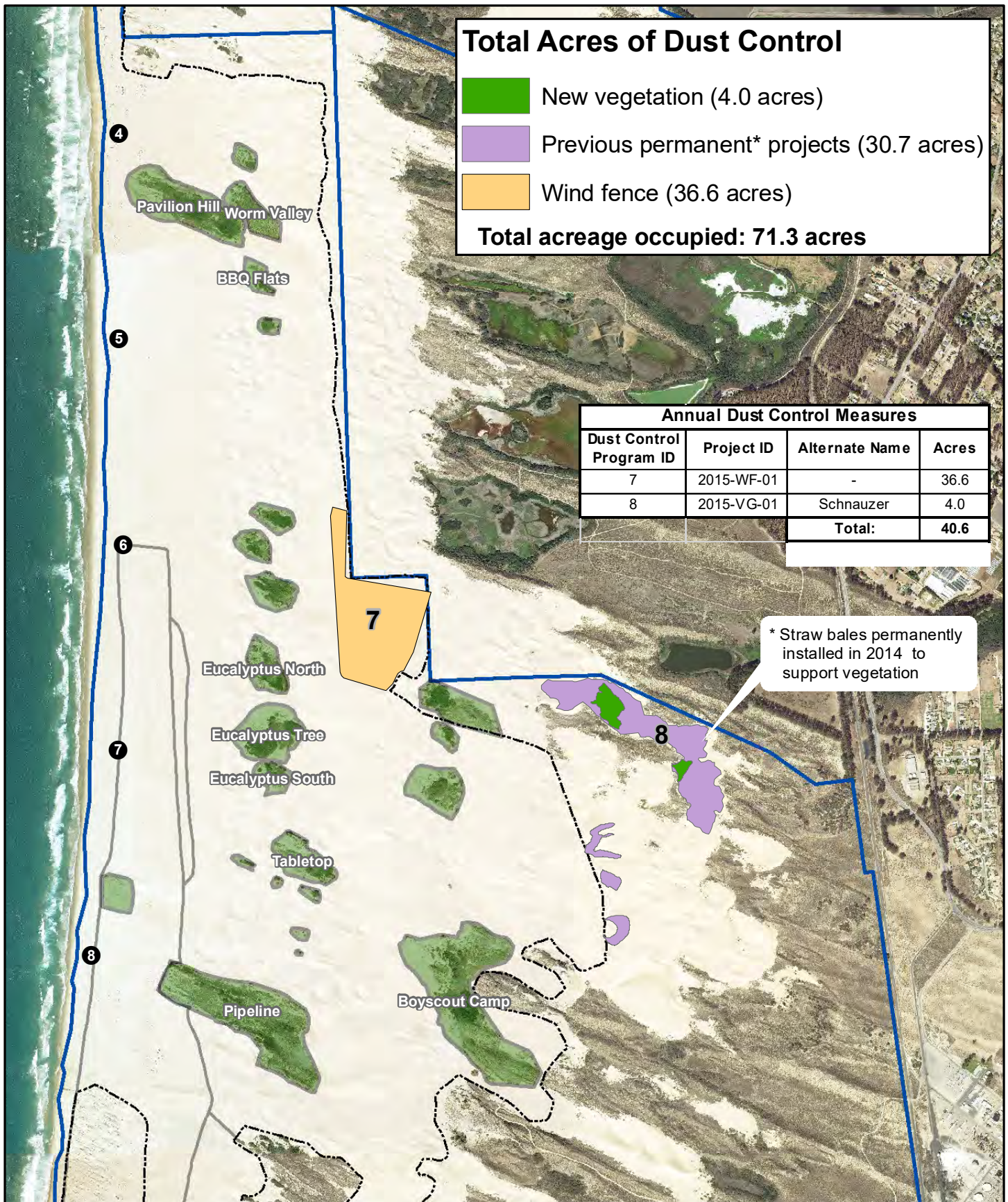


Park boundary

A01-05: 2014 Dust Control Treatment Areas

2023 ARWP

9/13/2021



Source: CDPR, MIG Imagery: 2014 NAIP

0 500 1,000 2,000 Feet



● Marker post

— Nesting enclosure from 2020



Existing fenced vegetated islands

----- Open riding and camping area boundary fence

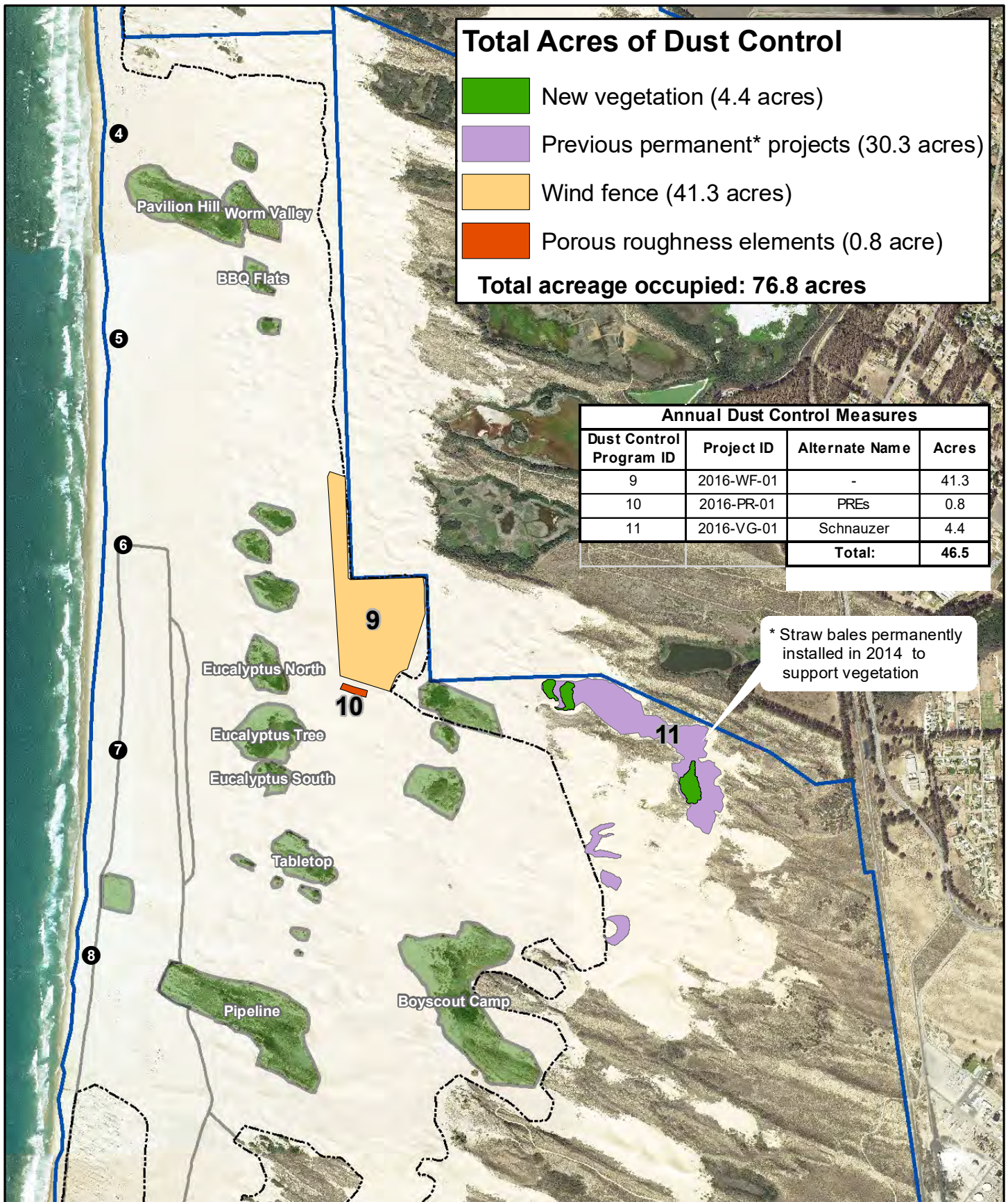


Park boundary

A01-06: 2015 Dust Control Treatment Areas

2023 ARWP

9/13/2021



Source: CDPR, MIG Imagery: 2014 NAIP

0 500 1,000 2,000 Feet



● Marker post

— Nesting enclosure from 2020



Existing fenced vegetated islands

----- Open riding and camping area boundary fence

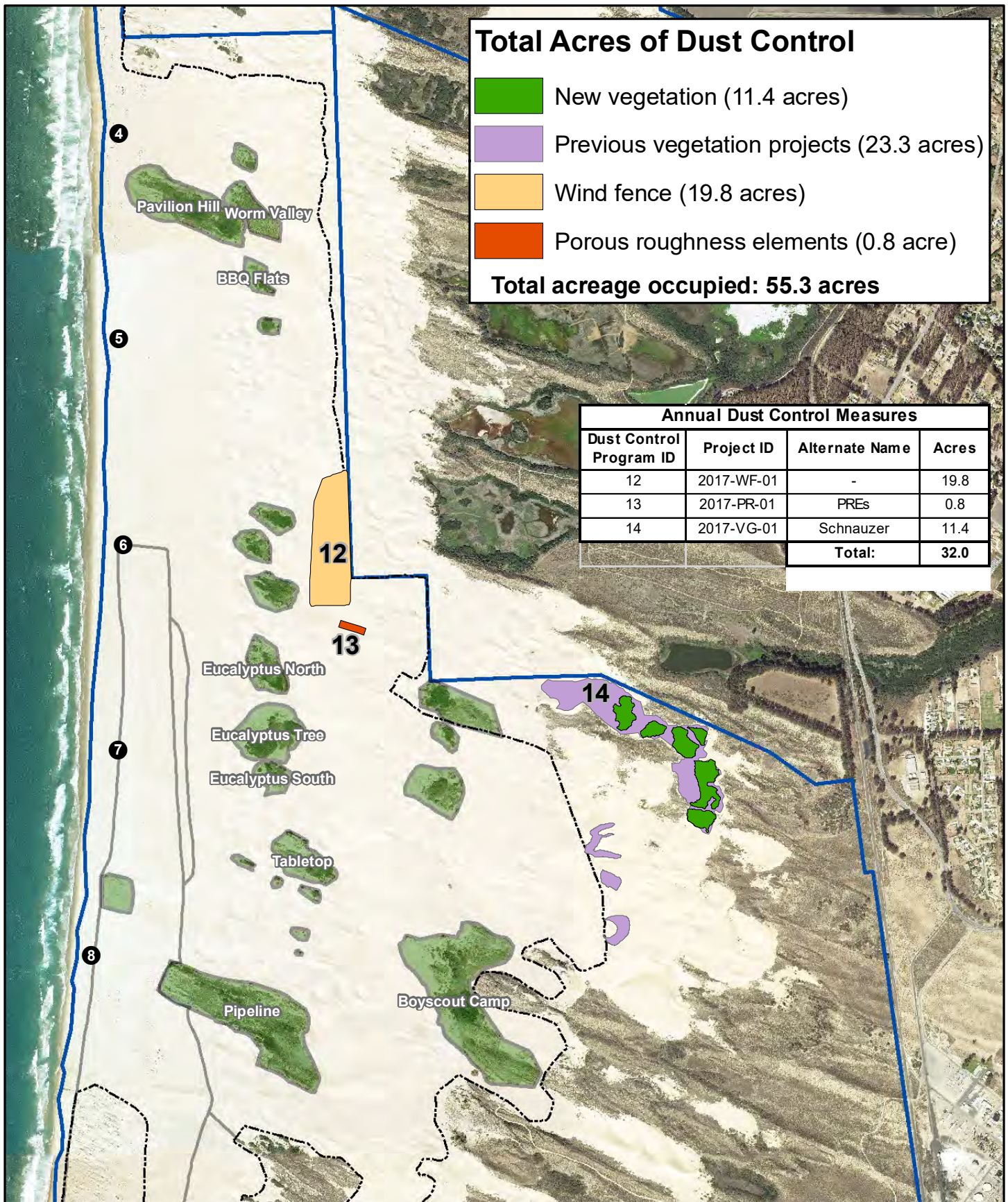


Park boundary

A01-07: 2016 Dust Control Treatment Areas

2023 ARWP

9/13/2021



Source: CDPR, MIG Imagery: 2014 NAIP

0 500 1,000 2,000 Feet



● Marker post

— Nesting enclosure from 2020



Existing fenced vegetated islands

----- Open riding and camping area boundary fence

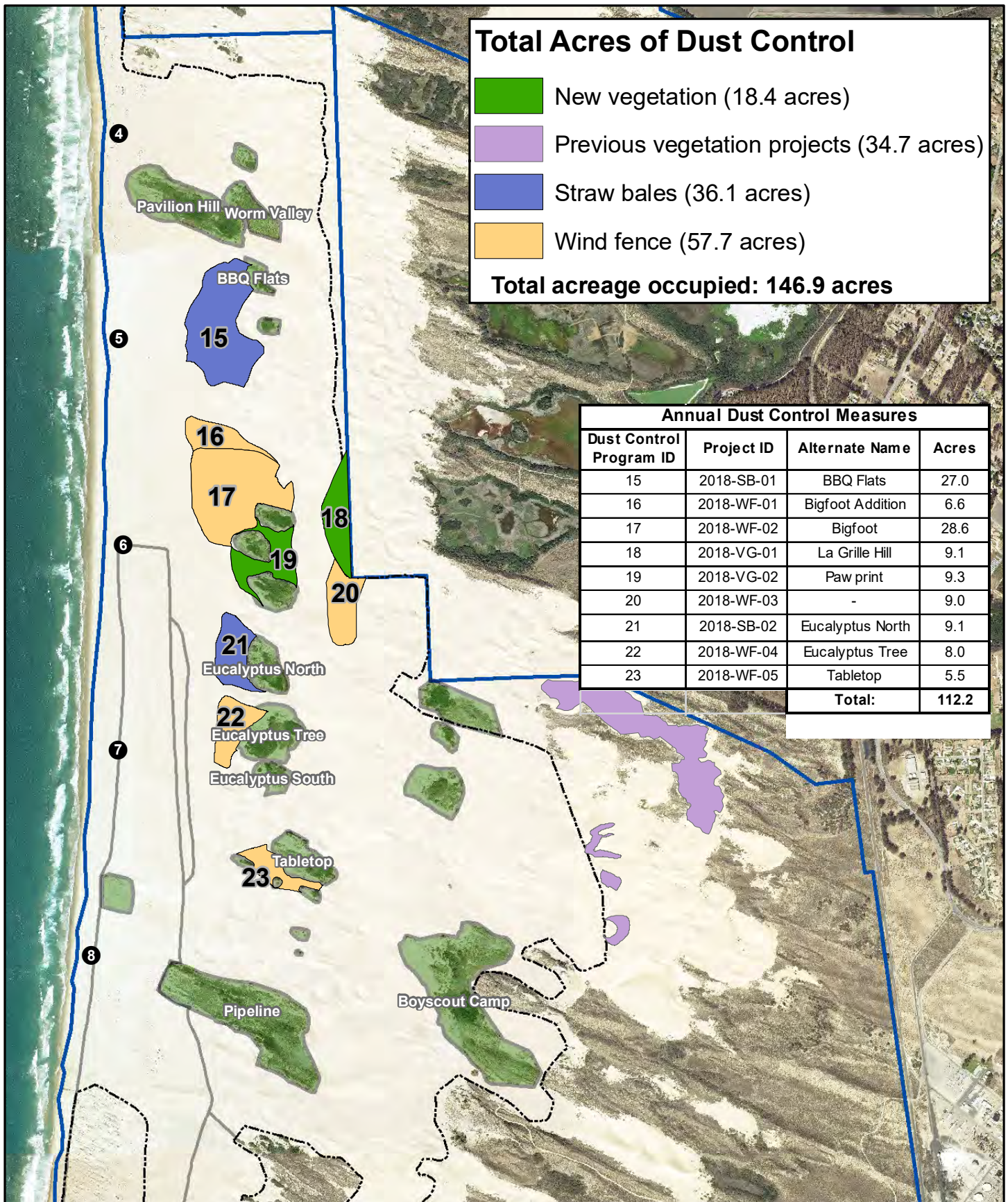


Park boundary

A01-08: 2017 Dust Control Treatment Areas

2023 ARWP

9/13/2021



Source: CDPR, MIG Imagery: 2014 NAIP

0 500 1,000 2,000 Feet



● Marker post

— Nesting enclosure from 2020



Existing fenced vegetated islands



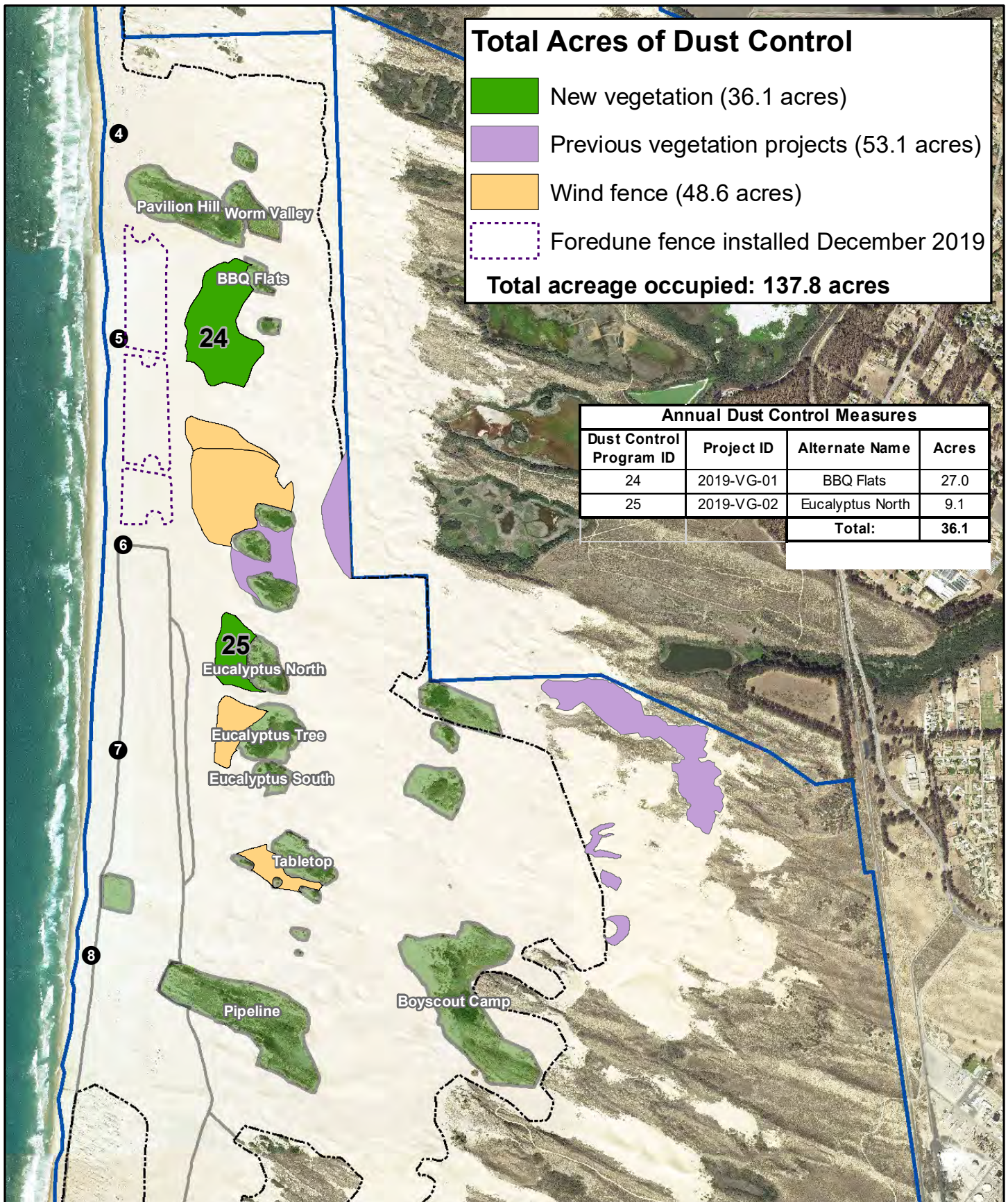
Park boundary

----- Open riding and camping area boundary fence

A01-09: 2018 Dust Control Treatment Areas

2023 ARWP

9/13/2021



Source: CDPR, MIG Imagery: 2014 NAIP

0 500 1,000 2,000 Feet



● Marker post

— Nesting enclosure from 2020



Existing fenced vegetated islands



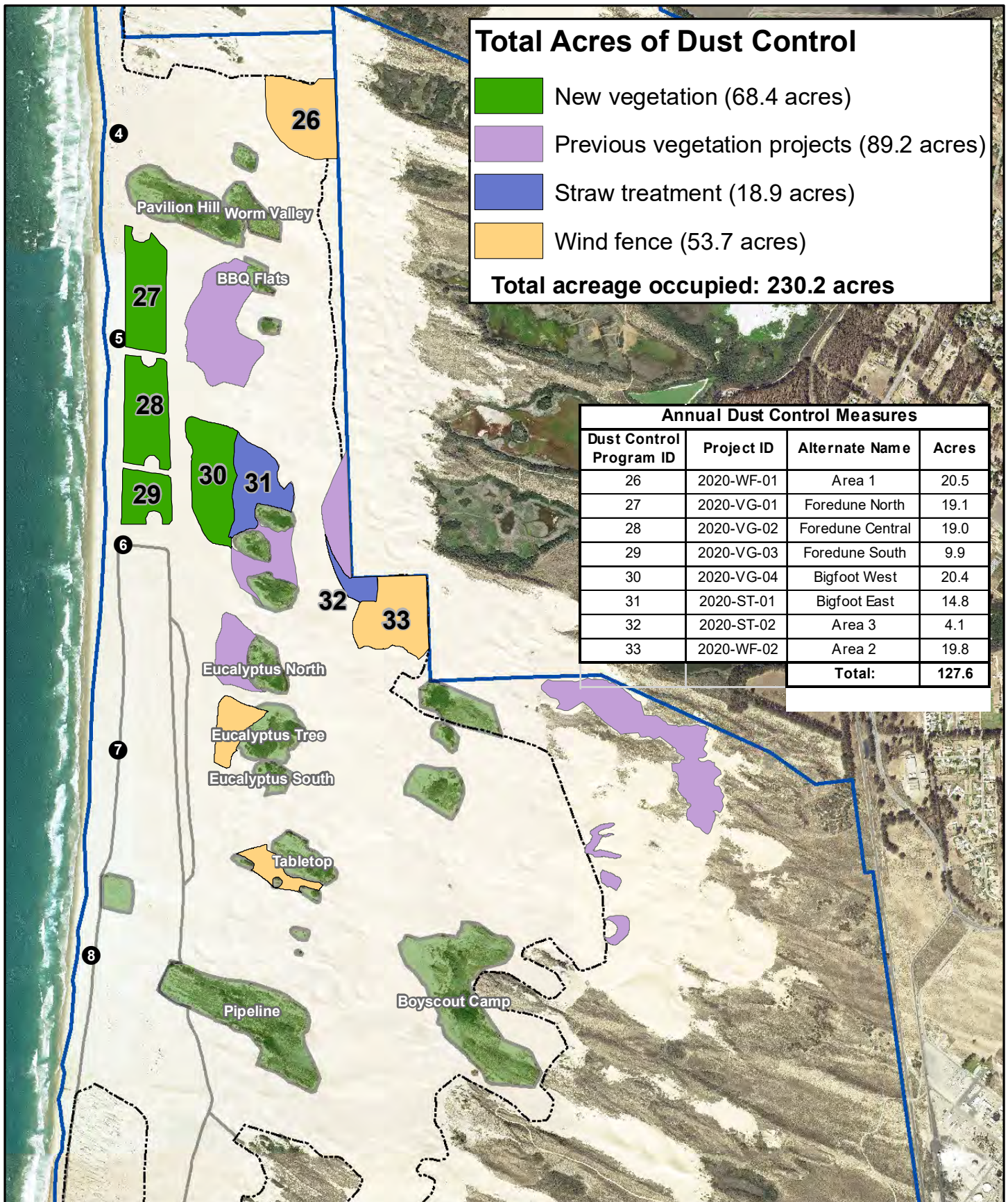
Park boundary

----- Open riding and camping area boundary fence

A01-10: 2019 Dust Control Treatment Areas

2023 ARWP

9/14/2021



Source: CDPR, MIG Imagery: 2014 NAIP

0 500 1,000 2,000 Feet



● Marker post

— Nesting enclosure from 2020



Existing fenced vegetated islands



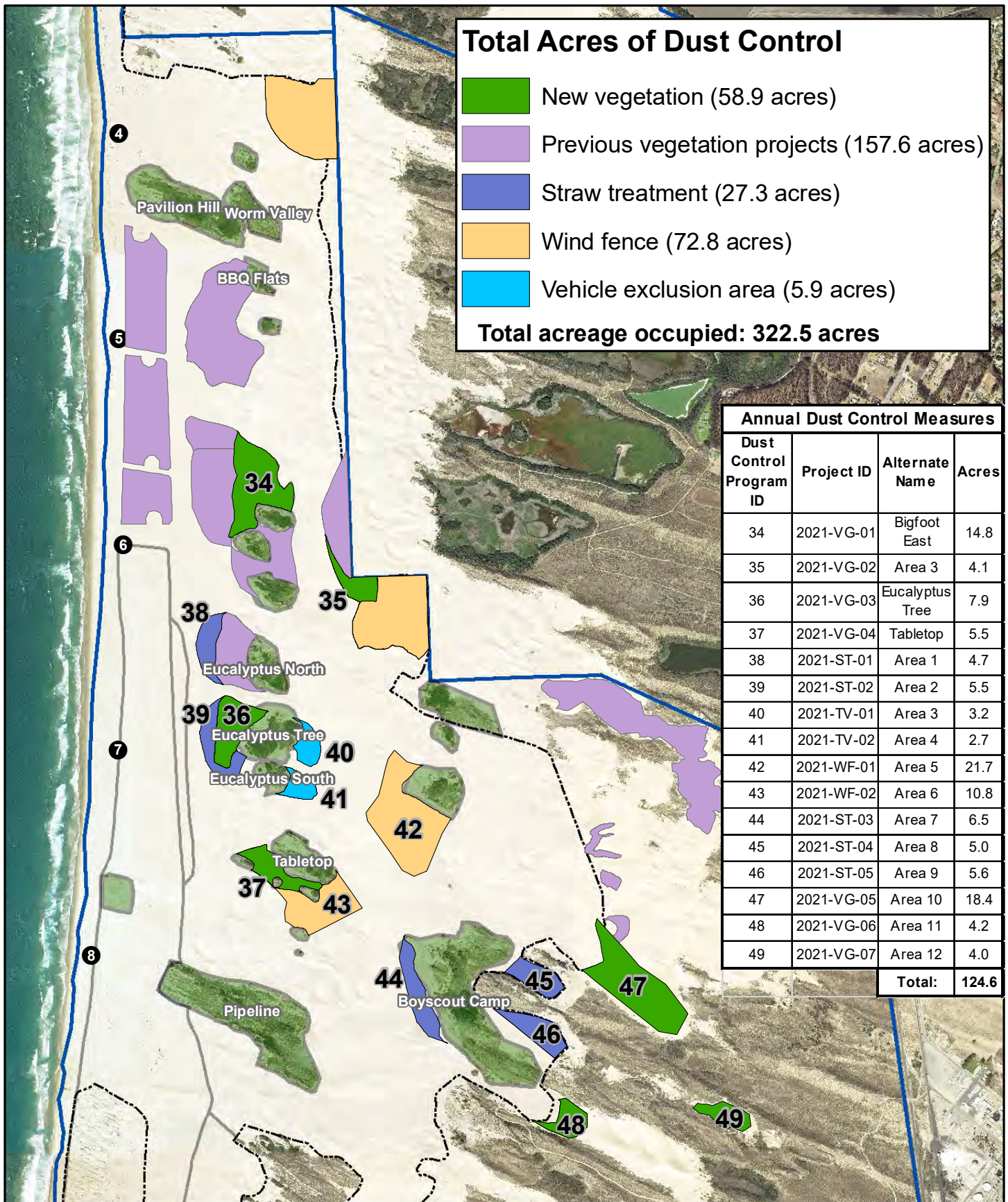
Park boundary

----- Open riding and camping area boundary fence

A01-11: 2020 Dust Control Treatment Areas

2023 ARWP

9/14/2021



Source: CDPR, MIG Imagery: 2014 NAIP

0 500 1,000 2,000 Feet



● Marker post

— Nesting enclosure from 2020



Existing fenced vegetated islands



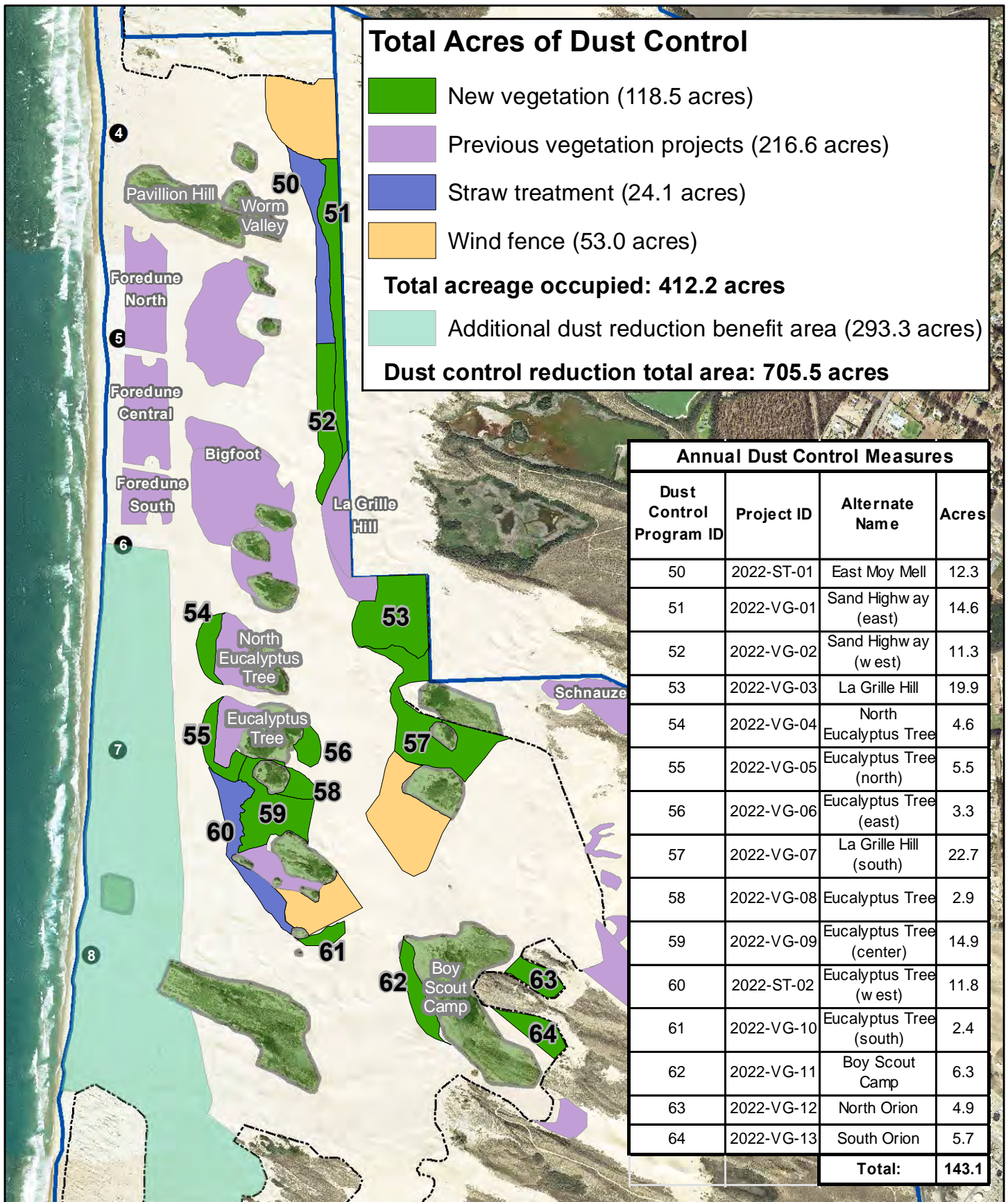
Park boundary

----- Open riding and camping area boundary fence

A01-12: 2021 Dust Control Treatment Areas

2023 ARWP

9/13/2021



Source: CDPR, MIG Imagery: 2014 NAIP

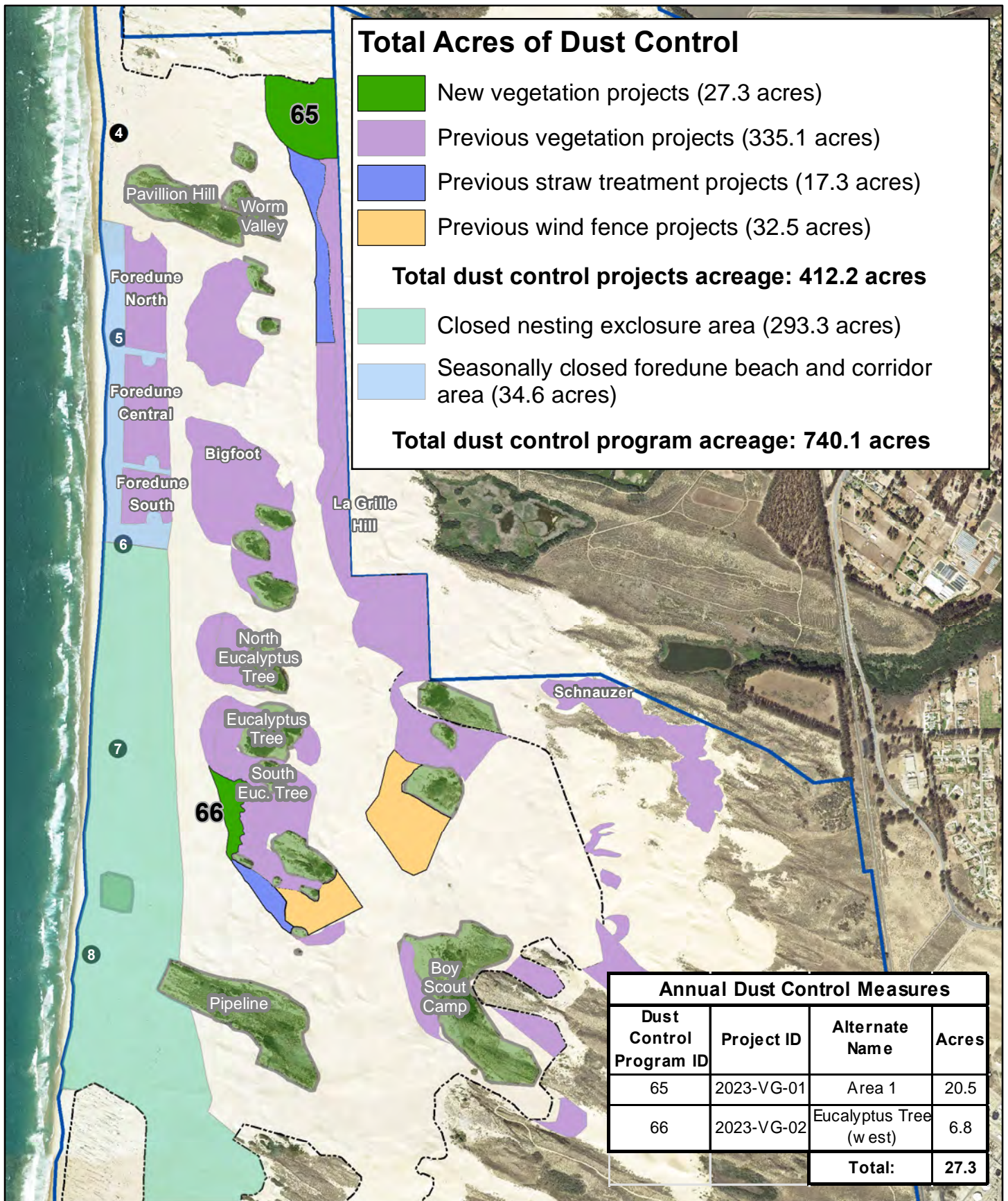
0 500 1,000 2,000 Feet



A01-13: 2022 Dust Control Treatment Areas

2023 ARWP

- Marker post
- Existing fenced vegetated islands
- Park boundary
- Open riding and camping area boundary fence



Source: CDPR, MIG Imagery: 2014 NAIP

0 500 1,000 2,000 Feet



Figure A01-14: 2023 Dust Control Measures

2023 ARWP

- Marker post
- Existing fenced vegetated islands
- Park boundary
- Open riding and camping area boundary fence

Oceano Dunes State Vehicular Recreation Area Dust Control Program

DRAFT 2023 Annual Report and Work Plan

ATTACHMENT 02

**2022/2023 ODSVRA Dust Control Program Vegetation Restoration Projects
(State Parks ARWP Work Product)**

THIS PAGE WAS INTENTIONALLY LEFT BLANK.

2022/2023 ODSVRA Dust Control Program - Restoration Projects								
<i>Scientific Name</i>	Plant Counts	Season Totals	Area 1 2023-VG-01 (New Planting)	Eucalytus Tree West 2023 VG-02 (New Planting)	Eucalyptus Tree Center 2022- VG-09 (Supplemental Planting)	Eucalyptus North 2022-VG-04 (Supplemental Planting)	Eucalyptus Tree 2022-VG-05 (Supplemental Planting)	Lagrange Hill 2022- VG-03 (Supplemental Planting)
Common Name	Native Seed (lbs)							
Acreage		47.5	20.5	6.8	14.9	2.8	1.4	1.1
Straw - (large bales)		433	251	25	97	36	12	12
Fertilizer (lbs) - 15-15-15		2350	1000	350	750	125	75	50
Triticale Seed (lbs) - sterile		2350	1000	350	750	125	75	50
Jute Netting (acres)		1.43	0.81	-	0.62	-	-	-
<i>Total plants</i>		121,724	51,184	19,457	38,091	6,918	3,600	2,474
Total Native Seed (lbs)		516.5	203.0	99.0	152.7	29.7	18.2	14.0
<i>Abronia latifolia</i>		341	98	147	-	60	36	-
Yellow sand verbena		1.1	0.2	0.7	-	0.1	0.1	0.1
<i>Abronia maritima</i>		414	147	147	-	60	36	24
Sticky sand verbena		29.9	6.9	14.0	-	5.0	3.0	1.0
<i>Abronia umbellata</i>		26	-	9	17	-	-	-
Beach sand verbena		1.3	0.7	-	0.6	-	-	-
<i>Acmispon glaber</i>		4,574	1,855	735	1,372	367	147	98
Deerweed		12.5	7.1	0.5	4.5	-	0.2	0.2
<i>Acmispon heermannii</i>		-	-	-	-	-	-	-
Heermann's lotus		1.1	-	-	1.1	-	-	-
<i>Achillea millefolium</i>		8,771	3,822	1,470	2,695	367	221	196
Common yarrow		34.0	13.0	3.5	10.5	1.3	0.8	5.0
<i>Ambrosia chamissonis</i>		1,274	343	441	-	245	147	98
Beach bur		50.9	9.9	28.0	-	7.5	4.5	1.0
<i>Amsinckia spectabilis</i>		-	-	-	-	-	-	-
Seaside fiddleneck		2.7	1.7	-	1.0	-	-	-
<i>Astragalus nuttallii</i>		864	130	-	734	-	-	-
Nuttall's milkvetch		1.8	-	1.8	-	-	-	-
<i>Castilleja affinis</i>		1,120	420	182	336	60	73	49
Indian paintbrush		0.5	0.3	-	0.2	-	-	-
<i>Camissoniopsis cheiranthifolia</i>		3,486	717	368	1,666	367	221	147

<i>Scientific Name</i>	Plant Counts			Eucalytus Tree West 2023	Eucalyptus Tree Center 2022	Eucalyptus North 2022-VG-04	Eucalyptus Tree 2022-VG-05	Lagrange Hill 2022- VG-03
Common Name	Native Seed (lbs)	Season Totals	Area 1 2023-VG-01 (New Planting)	VG-02 (New Planting)	VG-09 (Supplemental Planting)	2022-VG-04 (Supplemental Planting)	2022-VG-05 (Supplemental Planting)	(Supplemental Planting)
Beach evening-primrose		0.9	0.4	0.1	0.3	0.1	0.03	0.02
<i>Carex praegracilis</i>		917	522	49	346	-	-	-
Field sedge		-	-	-	-	-	-	-
<i>Cirsium occidentale</i>		-	-	-	-	-	-	-
Cobweb thistle		2.1	1.2	-	0.9	-	-	-
<i>Corethrogyne filaginifolia</i>		7,434	3,857	1,102	2,303	123	-	49
Common sandaster		33.4	15.0	5.3	11.3	0.9	0.6	0.4
<i>Croton californicus</i>		-	-	-	-	-	-	-
California croton		0.3	-	-	0.3	-	-	-
<i>Cryptantha clevelandii</i>		-	-	-	-	-	-	-
Common cryptantha		0.5	0.4	0.0	0.1	-	-	-
<i>Dudleya lanceolata</i>		1,834	865	220	577	123	-	49
Southern California dudleya		0.2	0.1	-	0.1	-	-	-
<i>Erigeron blochmaniae</i>		7,756	3,740	1,102	2,302	367	147	98
Blochman's leafy daisy		19.1	8.0	2.8	6.0	1.0	0.8	0.5
<i>Eriastrum densifolium</i>		3,058	1,391	368	931	123	147	98
Giant eriastrum		1.9	1.0	-	0.9	-	-	-
<i>Ericameria ericoides</i>		478	292	61	125	-	-	-
Mock heather		79.0	37.0	7.0	30.0	2.5	1.5	1.0
<i>Eriogonum parvifolium</i>		7,512	3,175	1,470	2,499	123	147	98
Coastal buckwheat		1.9	20.0	7.0	22.5	2.5	1.5	1.0
<i>Eriophyllum staechadifolium</i>		7,936	3,674	1,102	2,303	367	294	196
Seaside golden yarrow		51.9	23.4	7.0	16.5	2.5	1.5	1.0
<i>Erysimum suffrutescens</i>		6,961	3,457	1,102	2,304	-	-	98
Suffrutescent wallflower		0.0	-	-	-	-	-	-
<i>Eschscholzia californica</i>		-	-	-	-	-	-	-
California poppy		0.2	0.1	-	0.1	-	-	-
<i>Frangula californica</i>		109	52	14	43	-	-	-
California coffeeberry		-	-	-	-	-	-	-

<i>Scientific Name</i>	Plant Counts			Eucalytus Tree West 2023	Eucalyptus Tree Center 2022	Eucalyptus North 2022-VG-04	Eucalyptus Tree 2022-VG-05	Lagrange Hill 2022- VG-03
Common Name	Native Seed (lbs)	Season Totals	Area 1 2023-VG-01 (New Planting)	VG-02 (New Planting)	VG-09 (Supplemental Planting)	(Supplemental Planting)	(Supplemental Planting)	(Supplemental Planting)
<i>Horkelia cuneata</i>		2,503	1,009	367	931	-	147	49
Wedge leaved horkelia	4.8		2.6	-	2.3	-	-	-
<i>Juncus lescurii/breweri</i>		1,673	902	109	662	-	-	-
Dune rush	-		-	-	-	-	-	-
<i>Lupinus chamissonis</i>		32,242	13,328	5,292	9,702	2,450	882	588
Dune bush lupine	16.9		7.6	2.1	6.0	0.6	0.4	0.3
<i>Malacothrix incana</i>		748	158	294	100	123	73	-
Dunedelion	0.6		0.3	-	-	0.1	0.1	0.1
<i>Morella californica</i>		198	78	-	120	-	-	-
Wax myrtle	3.8		-	-	3.8	-	-	-
<i>Monardella undulata ssp crispa</i>		4,891	849	1,102	2,058	490	294	98
Crisp monardella	15.5		5.8	3.5	3.8	1.3	0.8	0.5
<i>Phacelia distans</i>		-	-	-	-	-	-	-
Common phacelia	0.8		0.5	-	0.3	-	-	-
<i>Phacelia ramosissima</i>		7,112	2,801	1,102	2,057	613	294	245
Branching phacelia	60.5		25.0	10.5	18.8	3.1	1.9	1.3
<i>Populus trichocarpa</i>		68	23	-	45	-	-	-
Black cottonwood	-		-	-	-	-	-	-
<i>Salix lasiolepis</i>		452	158	-	294	-	-	-
Arroyo willow	-		-	-	-	-	-	-
<i>Senecio blochmaniae</i>		6,972	3,321	1,102	1,569	490	294	196
Dune ragwort	34.3		15.0	5.3	11.3	1.3	0.8	0.8
Total plants		121,724	51,184	19,457	38,091	6,918	3,600	2,474
Total Seed		516.5	203.0	99.0	152.7	29.7	18.2	14.0

THIS PAGE WAS INTENTIONALLY LEFT BLANK.

Oceano Dunes State Vehicular Recreation Area Dust Control Program

DRAFT 2023 Annual Report and Work Plan

ATTACHMENT 03

Oceano Dunes: Status 2023

(DRI Presentation)

THIS PAGE WAS INTENTIONALLY LEFT BLANK.

ODSVRA Dust Control Program – 2023 ARWP Status Report

Dr. Jack Gillies, Dr. John Mejia



As of July 31, 2023

- Begin with the 2019 Emissivity Grid
- Convert the Plover Exclosure, 4-dune restoration area, and seasonal beach and corridors grid cells to be represented by the 2022 PI-SWERL mean emissivity relations
- Convert polygon 11 (20.5 acres) from wind fence to straw/vegetated cover
- Overlay the current vegetation layer (same as last year)
- Use the 10 baseline days meteorology (same as last year)
- Remove the emissions from the other managed areas as in previous years

As of July 31, 2023

- Emissions from 2019 grid with changes to PEx, 4-dune, and seasonal
154.1 metric tons/day
- Apply vegetation filter
139.2 metric tons/day
- Apply other reductions from managed areas including polygon 11

Total emissions: 100.9 metric tons/day

Current 1939 estimate 108 metric tons/day

As of July 31, 2023 (addition accounting details)

							SAG assumptions	
Domain						Original 2019 data	AWRP 2022	AWRP 2023
Foredune						6.61	3.37	1.28
PloverExclosure contribution						18.50	9.25	7.42
Beach and Corridors						4.16	2.10	2.20
Computational Fluid Dynamics (Foredure and Oso flaco wake effect)						26.42	1.86	1.86

As of July 31, 2024

- Begin with the 2019 Emissivity Grid
- Convert the Plover Exclosure, 4-dune restoration area, and seasonal beach and corridors grid cells to be represented by the 2022 PI-SWERL mean emissivity relations
- Convert polygons 56 (10.8 acres) and 57 (21.7 acres) from wind fence to straw/vegetated cover
- Overlay the current vegetation layer (same as last year)
- Use the 10 baseline days meteorology (same as last year)
- Remove the emissions from the managed areas as in previous years

As of July 31, 2024

- Emissions from 2019 grid with changes to Pex, 4-dune, and seasonal
154.1 metric tons/day
- Apply vegetation filter
139.2 metric tons/day
- Apply other reductions from managed areas including polygon 56 and 57

Total Emissions: 99.9 metric tons/day

Current 1939 estimate 108 metric tons/day

Revised DRI Model: 2022 Dust Control Program Concentration Reductions Estimates at CDF

CDF		
		% Change from 2013 Baseline, Pre-OHV Baseline 1939 & 1966 Vegetation
10 Highest Emission Days	PM ₁₀ [µg m ⁻³]	
Observations	128.2	
Modeled Baseline 2013	124.7	
Modeled Pre-disturbance Baseline & 1939 vegetation removal	88.0	
Modeled Pre-disturbance Baseline & 1966 vegetation removal	87.0	
2021 Controls in Place (322.5 acres) Current	72.2	-42.1 (2013), -17.9 (1939), -17.0 (1966)
2022 Controls in Place (412.5 acres) Current	66.4	-46.7 (2013), -24.5 (1939), -23.7 (1966)
2022 Controls in Place (412.5 acres) + revised model (SAG Revisions)	61.9	-50.3 (2013), -29.6 (1939), -28.8 (1966)
ARWP 2023	2019 grid (11) = 60.903 2019 grid (11, 56, 57) = 60.719	

Revised DRI Model: 2022 Dust Control Program

Concentration Reductions Estimates at Mesa 2

Mesa 2		
		% Change from 2013 Baseline, Pre-OHV Baseline 1939 & 1966 Vegetation
10 Highest Emission Days	PM ₁₀ [µg m ⁻³]	
Observations	95.4	
Modeled Baseline 2013	97.5	
Modeled Pre-disturbance Baseline & 1939 vegetation removal	71.2	
Modeled Pre-disturbance Baseline & 1966 vegetation removal	75.7	
2021 Controls in Place (322.5 acres) Current	73.8	-24.3 (2013), +3.7 (1939), -2.6 (1966)
2022 Controls in Place (412.5 acres) Current	66.9	-31.3 (2013), -6.0 (1939), -11.6 (1966)
2022 Controls in Place (412.5 acres) + revised model (SAG Revisions)	63.6	-34.7 (2013), -10.6 (1939), -15.9 (1966)
ARWP 2023	2019 grid (11) = 62.504 2019 grid (11, 56, 57) = 62.162	

Oceano Dunes State Vehicular Recreation Area Dust Control Program

DRAFT 2023 Annual Report and Work Plan

ATTACHMENT 04

**Increments of Progress Toward Air Quality Objectives, ODSVRA Dust Control 2022 Update
(DRI Document)**

THIS PAGE WAS INTENTIONALLY LEFT BLANK.

Placeholder. This DRI document is currently under review by the SAG.

THIS PAGE WAS INTENTIONALLY LEFT BLANK.

Oceano Dunes State Vehicular Recreation Area Dust Control Program

DRAFT 2023 Annual Report and Work Plan

ATTACHMENT 05

**Computation Fluid Dynamics Modeling of the ODSVRA 48-Acre Foredune Restoration Project
(DRI Document)**

THIS PAGE WAS INTENTIONALLY LEFT BLANK.

Computation Fluid Dynamics Modeling of the ODSVRA 48-Acre Foredune Restoration Project

The 40 acre coastal foredune restoration project was implemented in 2020. Six distinct treatment areas were created to evaluate if foredune development could be accelerated and how the developmental stages could modulate sand transport and dust emissions leading to reduced contributions of emitted PM₁₀. As part of the evaluation of the individual treatments to modulate the surface shear stress distribution and the associated dust emissions, DRI performed CFD simulations of airflow over defined sections of these treatments (Figure 1) using high-spatial resolution topographic data received from UCSB and high-temporal resolution velocity measurements to create the incoming boundary wind conditions. Measurements of wind speed profiles upwind and downwind of the treatment areas were also used to compare measurements with model predicted wind speeds for verifying the veracity of model outputs following Furtak-Cole et al. (2022).

Each of the six treatment areas evolved distinct topography and vegetation patterns from the time of their establishment in 2019 through to the time represented by the model simulations, i.e., February 2022. Simulations of airflow over the six foredune restoration treatments approximately 24 months after their establishment were performed, driven by a boundary condition constructed from measured wind speed data at the site. Each simulation closely matched wind speeds measured on the leeward side of the restoration areas, which provides confidence that the model effectively reproduced the wind flow conditions across the modeling domain (Table 1). The degree of matching between measured and modeled was defined as the Wind Speed Ratio (WSR), which was calculated as modeled wind speed at 3.5 m AGL/measured wind speed at 3.5 m AGL. The modeled wind speed and measured wind speeds at 3.5 m AGL were associated with the towers on the eastern side of each foredune restoration area. The surface identified as T0 was created to represent a smooth, sloping beach, for comparing shear stress production and emission potential with the developing restoration areas and their individual topographies and vegetation covers.

Table 1. Wind speed ratios (WSR) for the measured and simulated velocity at 3.26 m above the ground at the location of the towers on the eastern edges of the treatment areas. Field data do not exist for T0 (hypothetical flat sloping surface) or T6 (no access permitted due to Snowy Plover restrictions).

	Treatment Identifier						
	T0	T1	T2	T3	T4	T5	T6
Measured WSR	N/A	1.004	0.989	0.905	1.015	1.036	N/A
Simulated WSR	0.972	0.97	0.983	0.967	1.019	1.017	1.029
% Difference		3.4	0.6	-6.2	-0.4	1.9	

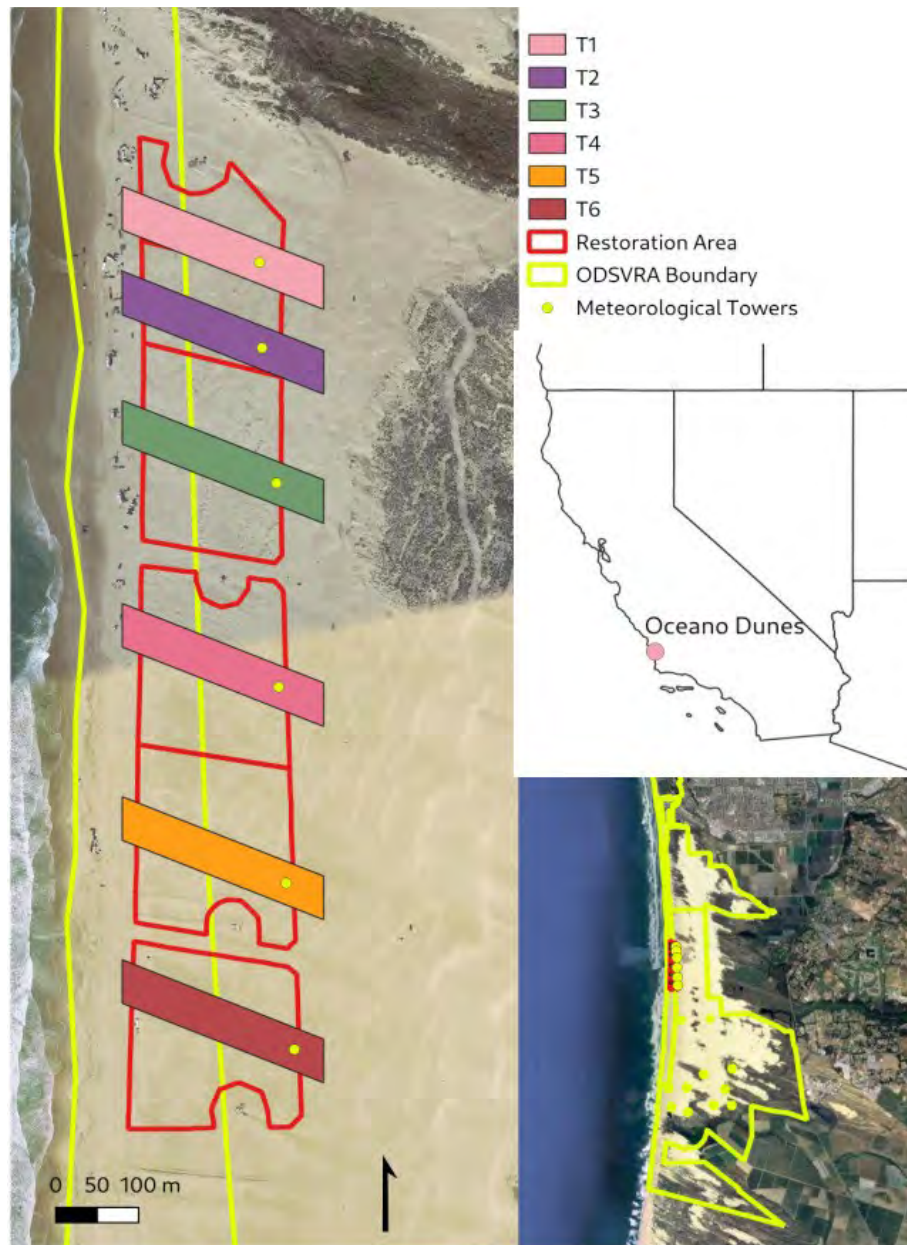


Figure 1. Left: a map showing the restoration area, meteorological tower locations (yellow circles), and simulation domains. Lower right: a map of the ODSVRA boundary and surrounding land surface. Upper right: the position of the study area in the south-west United States.

For the period represented by the topographic and vegetation cover data, i.e., February 2022, there were no recent measurements of surface emissivity made with the PI-SWERL for the restoration areas. To make comparison of the effect of the surface topography and vegetation cover on emissions of PM₁₀ from the foredune restoration treatments, the mean PM₁₀ emissivity relation of the ODSVRA riding area (See Figure 9 of Gillies et al., 2022) was assigned to all the areas ($F \text{ mg m}^{-2} \text{ s}^{-1} = 23.65 u_*^{5.59}$). The threshold shear stress for sand movement ($\tau_s \text{ N m}^{-2}$) within the test areas was assigned based on an

assumed mean grain size of 350 μm and the application of the Bagnold threshold equation (Bagnold, 1941). This results in a threshold shear stress of 0.09 N m^{-2} (note $\tau_s = \rho_a u_*^2$, where ρ_a is air density). The threshold shear stress and the relation for emissivity were used in the simulations to estimate where saltation would occur across the area of each treatment and the strength of the dust emissions for above threshold transport conditions for the developed boundary condition. Using uniform emissivity relation and threshold shear stress isolated the effect of shear stress on the topography and vegetation cover to generate dust emissions, and should not be considered representative of actual emissivity conditions.

The simulated shear stress for the set boundary condition on each of the treatment areas is shown in Figure 2. For each of the surfaces presented in Figure 2, surface integrals were performed to compute the vegetation area, total surface area, total shear stress, and area-normalized total shear stress. These quantities are presented in Table 2.

Due to the differing distances across each treatment from shoreline to inland, these integrals are only performed over a distance of 100 m upwind from the locations of the meteorological towers. A vegetation mask of the foredune restoration area was merged with the simulation output allowing for surface integrals over bare ground and vegetated areas to be computed separately. The important quantity affecting emissions is the integral for the bare ground (BG). Area normalization calculations (N m^{-2}) are computed using the total surface area accounting for the complexity of the topography (SAN) in each treatment.

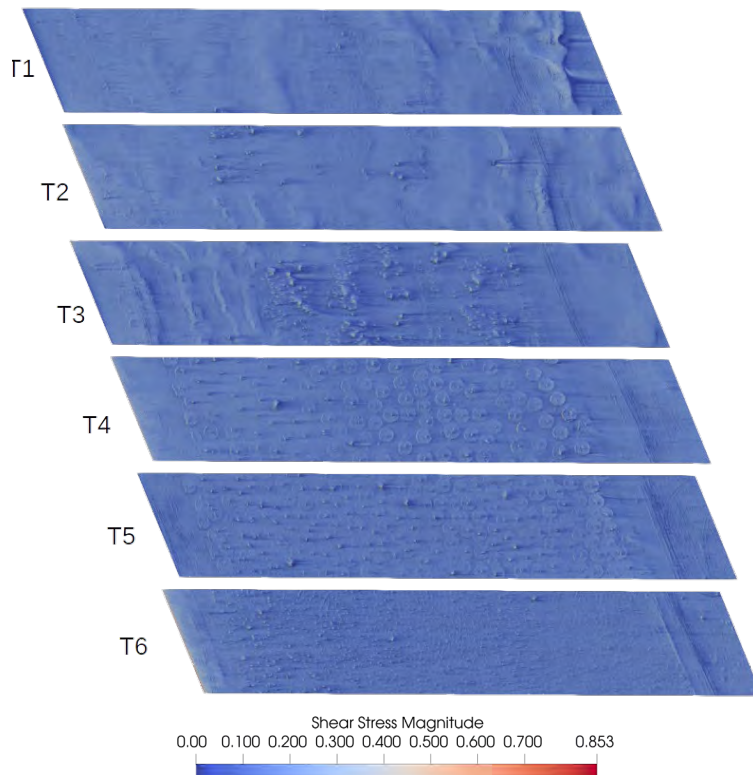


Figure 2. Shear stresses on the six treated surfaces (T1-T6). Flow is from left to right.

As shown in Table 2, T3 has the greatest surface and vegetated areas. T3 also has the lowest total shear stress, 31.9% lower than for a smooth sloping surface, i.e., T0. T6 ranks as the second most effective treatment for reducing shear stress (24.9% lower than T0), which is consistent with its second highest cover of vegetation. T4 and T5, have greater surface areas than T6, but lower vegetation covers, however, the overall reduction in shear stress compared to T0 for T4 and T5 is quite similar to T6 (24.6% and 23.6, respectively). Treatments 1 and 2 also show a reduction in total shear stress compared to T0, by 15.0% and 17.8%, respectively, which is due solely to the topographic adjustment of the surfaces due to the creation of transverse bedforms by the wind and sediment transport processes.

Table 2. The vegetation and total surface areas and shear stress generated on the seven surfaces for the modeled boundary condition.

	T0	T1	T2	T3	T4	T5	T6
Vegetation Area (m ²)	0	5	20.7	234.7	77.8	117.3	177.4
Total Surface Area (m ²)	5001.4	5009.7	5009.3	5048.7	5033.1	5030.1	5026.4
Total Shear (N)	926.8	789.1	762.4	636.5	703.3	712.4	699.3
Total Shear on Bare Ground (N)	926.8	788.6	759.9	608.8	694.7	699.4	676.1
Surface Area Normalized Shear (N m ⁻²)	0.185	0.156	0.152	0.126	0.14	0.142	0.139

Emissions from each surface for the wind condition investigated can be calculated by integrating the emissivity relation over the shear surface data (Furtak-Cole et al., 2022) presented in Figure 2. The most realistic case is to only integrate over BG areas and where the calculated shear stress is above the assigned threshold value. Emissions values for this case are presented in Table 3. Additionally, the PM10 that would be emitted by vegetated areas if the vegetation was removed (E vegetation deficit), and the total surface area below the Bagnold threshold are reported in Table 3. The E vegetation deficit correlates with the total area of vegetation cover. The area below the threshold for transport is effectively a function of the amount of shelter in the lee of the roughness elements such as individual nebkha, plants, and transverse bedforms in the case of T1 and T2. This is illustrated in Figure 3 that shows the vegetation and the below threshold areas for T3 and T4. T3 has the greatest amount of below-threshold shelter area, though significant values are observed for the straw node treatments T4 and T5. Formation of topographic highs are linked to vegetation growth in T3, resulting in vegetation heavily influencing the location and size of shelter zones.

Table 3. Predicted emissions from the 5000 m² planar area upwind of the tower locations in the seven simulations. E values are calculated using only surface area at the intersection of shear values above threshold and bare ground surfaces. E vegetation deficit denotes the amount of predicted emissions from vegetated surface area, which is not included in bare ground (BG) calculations.

	T0	T1	T2	T3	T4	T5	T6
E Bare Ground (mg s ⁻¹)	603.5	408.0	369.3	244.2	323.5	325.7	296.7
E Bare Ground (mg m ⁻² s ⁻¹)	0.121	0.082	0.074	0.048	0.064	0.065	0.059
E Vegetation Deficit (mg s ⁻¹)	0.00	0.15	1.14	15.00	4.59	6.53	9.25
Area Below Bagnold Threshold (m ²)	0	57.7	90.5	719.5	282.2	255.8	195.4

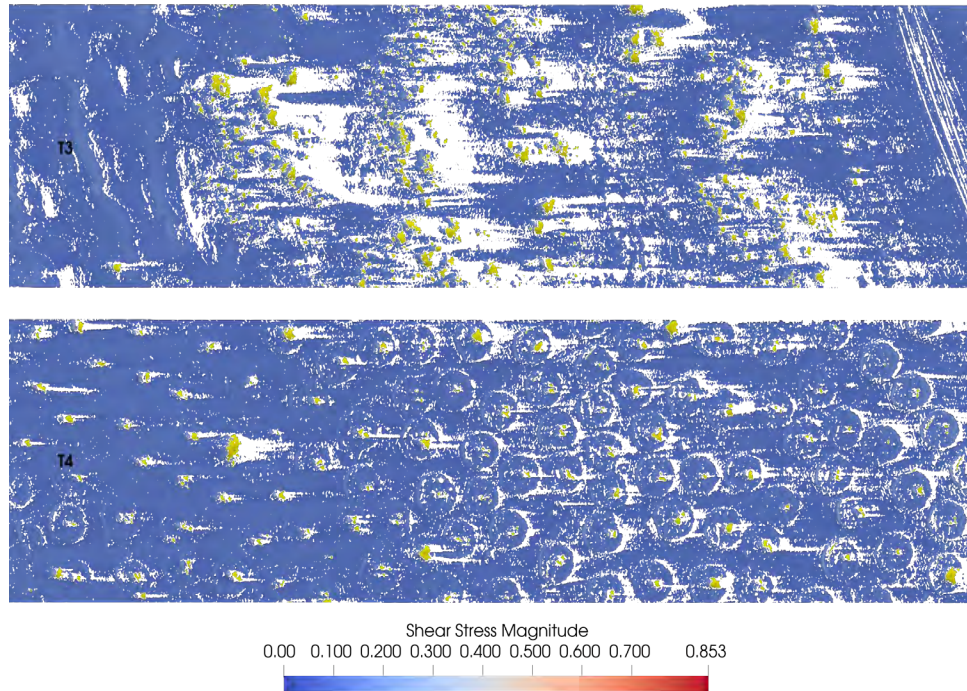


Figure 3. Maps of the vegetation (yellow) and areas below threshold (white) for T3 (upper) and T4 (lower) for the modeled boundary wind condition.

The CFD simulations of flow over the six foredune restoration area treatments provide a means to characterize how topography and vegetation cover modulate sand transport and dust emissions. As the foredune restoration areas evolve, simulations using digital surface maps created by UCSB two times per year, and the established boundary wind condition can be used to update the metrics in Table 2. These metrics serve as indicators how potential sand transport and dust emissions change as a function of changes in the topography and vegetation development, and inform, in part, the system performance (Walker et al., 2022). Updated simulations (i.e., using the most up-to-date digital surface maps) could be used to inform adaptive management decisions.

CFD simulations may also provide information on how foredune emissions modulate PM10 emissions within the DRI emission/dispersion model. This is a more complex undertaking as the emissions scale as a function of shear stress, which also affects the amount of surface area that is above or below threshold. The effect of the different foredune restoration areas on emissions presented here simulate only one boundary wind condition, whereas under real-world or modeled conditions the incoming wind changes continually. Evaluations could be undertaken to investigate how data from CFD simulations of flow over the foredune restoration areas or a defined foredune configurations (e.g., north Oso Flaco) could be used to modify the emission/dispersion model to better account for the aerodynamic effect of roughness and vegetation on PM10 emissions.

References

- Furtak-Cole, E., J.A. Gillies, I.J. Walker, Z. Hilgendorf, G. Nikolich (2022). Simulation of air flow and shear stress distribution on the Oceano Dunes, implications for saltation and dust emissions. *Environmental Fluid Mechanics*, 22, 1399-1420, doi: 10.1007/s10652-022-09902-0.
- Gillies, J.A., E. Furtak-Cole, G. Nikolich, V. Etyemezian (2022). The role of off highway vehicle activity in augmenting dust emissions at the Oceano Dunes State Vehicular Recreation Area, Oceano CA. *Atmospheric Environment: X*, 13, 100146, doi: 10.1016/j.aeaoa.2021.100146.
- Walker, I.J., Z. Hilgendorf, C. Turner, J.A. Gillies, E. Furtak-Cole, G. Nikolich (2022). Assessing performance of a 'nature-based' foredune restoration project, Oceano Dunes, California, USA. *Earth Surface Processes and Landforms*, 48 (1), 143-162, doi: 10.1002/esp.5478.

Oceano Dunes State Vehicular Recreation Area Dust Control Program

DRAFT 2023 Annual Report and Work Plan

ATTACHMENT 06

**SAG Recommendations for Establishing Emissivity Grids to be Used in the Modeling of Pre-Disturbance Conditions and Future Excess Emissions Reductions
(SAG Memorandum)**

THIS PAGE WAS INTENTIONALLY LEFT BLANK.

June 21, 2023

Memo: SAG Recommendations for Establishing Emissivity Grids to be used in Modeling of Pre-Disturbance Conditions and Future Excess Emissions Reductions

From: Scientific Advisory Group (SAG)

To: Jon O'Brien, California Department of Parks and Recreation
Karl Tupper, San Luis Obispo Air Pollution Control District

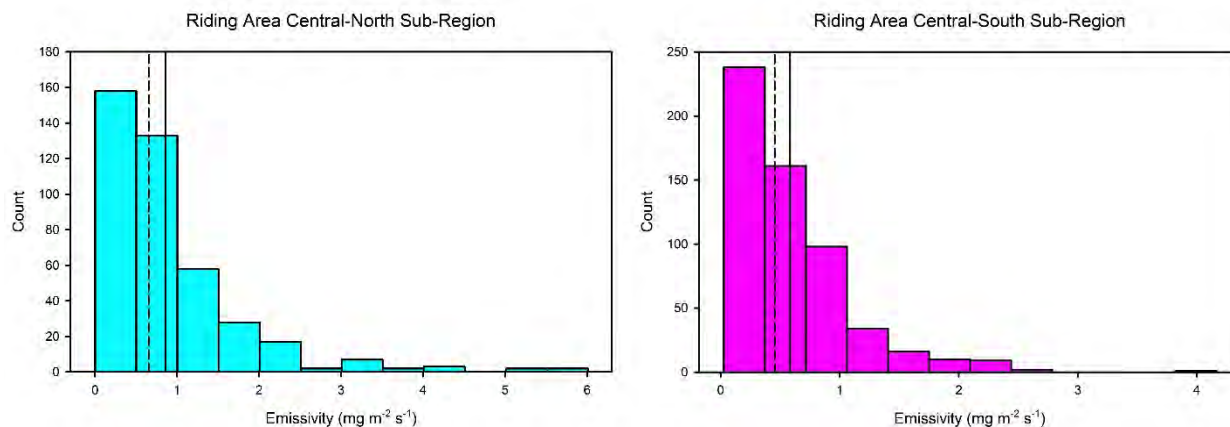
Cc: Sarah Miggins, California Department of Parks and Recreation
Gary Willey, San Luis Obispo Air Pollution Control District

The recently revised Stipulated Order of Abatement (SOA), filed on October 18, 2022, requires that Annual Report and Work Plans (ARWP) submitted by the California Department of Parks and Recreation (CDPR) “**shall be designed to eliminate emissions in excess of naturally occurring emissions from the ODSVRA [Oceano Dunes State Vehicular Recreation Areas] that contribute to downwind violations of the state and federal PM₁₀ air quality standards**” (Section 3.b.), and that to meet this objective, CDPR “**shall initially reduce mass-based PM₁₀ emissions within the ODSVRA to a level consistent with the pre-disturbance scenario identified by the SAG [Scientific Advisory Group]**” (Section 3.c.). Taken together, these directives place a great deal of emphasis on dust emissions from the ODSVRA both past and present. ‘Past’ refers to expected baseline emissions from a pre-disturbance¹ state (i.e., prior to significant human impact, specifically from vehicular traffic) and ‘present’ refers to emissions from the contemporary landscape, including a combination of riding and non-riding areas.

Of course, past conditions are unknowable with absolute certainty. But sophisticated modeling with rational, scientifically-defensible assumptions, informed by historical reconstructions from aerial photographs of land cover change, can provide reasonable estimates of probable conditions on a natural or a potentially restored landscape absent of OHV traffic. Modeling of present conditions have the further advantage of complementary measurements that can be used to calibrate and validate the model results, thereby providing confidence in interpretation of contemporary processes of dust emission, transport, and dispersion from the ODSVRA.

A key component of representing and quantifying past and present air quality conditions is properly parameterizing the emissivity (dust-releasing nature) of sand surfaces within the ODSVRA dune landscape. To this end, the Desert Research Institute (DRI) has undertaken an

¹ It is recognized that human activities, including vehicular traffic, horse riding, hiking, and camping, have been a part of the Oceano Dunes landscape for many decades, prior to establishment of ODSVRA in the 1970s. There is very limited photographic evidence of landscape configuration prior to the early 1900s when human recreational activities began to influence the natural landscape. The earliest historical aerial photography from the 1930s reflects some level of disturbance, and as such, the term 'pre-disturbance' state is somewhat of a misnomer. Nevertheless, for consistency with the language used in the SOA regarding modeling of a pre-disturbance scenario, we will continue to use the term 'pre-disturbance' (as well as 'naturally occurring' emissions). As explained in the UCSB Vegetation Cover Analysis Report (February 2022), the 1939 imagery dataset is considered to be the best available indication of landscape configuration (i.e., vegetation cover, dune presence) prior to extensive Off-Highway Vehicle (OHV) activity within the Oceano Dunes.



extensive series of field campaigns since 2013 to measure surface emissivity using an instrument referred to as a “PI-SWERL (Portable In-Situ Wind EROsion Laboratory). DRI has reported on the results of these field campaigns, and most recently submitted another report entitled “**PI-SWERL September 2022 Results and Implications for Emission/Dispersion Modeling**” that describes the September 2022 PI-SWERL campaign. The 2022 field campaign quantified PM₁₀ emissivity in three zones of management that had not been previously measured: (1) new foredune restoration area (FRA); (2) the permanently exclosed Western Snowy Plover nesting area (PE), and (3) other seasonal exclosure (SE) areas. In the CDPR **2022 Annual Report and Work Plan** (ARWP), all of these areas were identified as requiring further study to refine PM₁₀ emissions estimates via the DRI Emission/Dispersion Model (Mejia et al., 2019), with the goal of reporting updated modeling of PM₁₀ emissions for the 2023 ARWP (in progress). DRI made several recommendations regarding how to utilize the PI-SWERL data in future modeling scenarios, and Table 1 provides a summary.

Table 1: DRI proposed approaches to modeling PM₁₀ emissivity for specific dust control management areas not previously measured.

Dust control management area	Previous modeling approach (for 2022 ARWP)	Proposed new modeling approach (for 2023 ARWP)
Foredune restoration area	Use mean (average) 2019 PI-SWERL non-riding PM ₁₀ emissivity curve	Use mean (average) 2022 PI-SWERL measurements in foredune restoration area to create PM ₁₀ emissivity curve
Permanent plover exclosure	Use 50% of mean (average) 2019 PI-SWERL plover exclosure PM ₁₀ emissivity curve	Use mean (average) 2022 PI-SWERL measurements in plover exclosure to create PM ₁₀ emissivity curve
Seasonal beach exclosures	Use mean (average) 2019 PI-SWERL non-riding PM ₁₀ emissivity curve	Use mean (average) 2022 PI-SWERL measurements in the seasonal beach exclosure area to create PM ₁₀ emissivity curve

Seasonal transportation corridor exclosures	Use mean (average) 2019 PI-SWERL non-riding PM ₁₀ emissivity curve	Use mean (average) 2022 PI-SWERL measurements in seasonal corridors to create PM ₁₀ emissivity curve
---	--	--

The DRI 2022 PI-SWERL report was reviewed but not yet endorsed by the SAG (**SAG Review of Desert Research Institute (DRI) report, “PI-SWERL September 2022 Results and Implications for Emission/Dispersion Modeling”**, February 10, 2023). SAG members made several recommendations for clarification and improvement of the report. One area of concern was with regard to the specifics of the emissivity grids that DRI proposed to use in updated modeling runs. The SAG review indicates the following points of clarification (reproduced verbatim with italics added):

- (1) ***Underlying emissivity grid.** The use of an amalgamated 2013-2019 PI-SWERL emissivity grid for the pre-disturbance scenario, versus use of the 2019 PI-SWERL emissivity grid for mitigation scenarios, is potentially an “apples-to-oranges” comparison that needs to be further justified. The issue is that the 2013 PI-SWERL grid, used as the “baseline year” under the previous terms of the SOA, appears to display anomalously high PM₁₀ emissivity as compared to any other year or long-term trend. By including 2013 emissivity data for the baseline and pre-disturbance scenario, CDPR may therefore be claiming credit for a greater percentage emissions reduction than is actually merited. (See comment “C” in SAG review of 2022 ARWP.)*

On October 21, 2022, the San Luis Obispo County Air Pollution Control District (SLOAPCD) conditionally approved the 2nd Draft 2022 Annual Report and Work Plan (SLOAPCD, 2022). However, the SLOAPCD shared many of the SAG’s concerns about modeling assumptions, which may be crediting CDPR dust mitigation measures with achieving a greater level of PM₁₀ emissions reductions than may actually be merited. Therefore, as the condition for its approval of the 2022 ARWP, SLOAPCD mandated that these model issues be addressed in the 2023 ARWP. SLOAPCD’s conditional approval letter stated, “Emission calculations in the 2023 ARWP shall be based on assumptions recommended by the SAG and preapproved, in writing, by the APCO.”

The purpose of this memorandum is to present a comprehensive analysis of the existing PI-SWERL data of actual dust emissivity within ODSVRA, and to make recommendations regarding an emissivity grid that could be incorporated into future modeling efforts leading to implementation of the excess emissions framework proposed by SAG (**SAG Memo – Framework for Assessing “Excess Emissions” of PM₁₀ from the Oceano Dunes**, January 30, 2023), thereby satisfying the requirement of the conditional approval letter. Model updates are also important for the purpose of quantifying changing emission conditions due to mitigation strategies undertaken within the yearly ARWPs.

The analysis of the PI-SWERL data is broken into several distinct sections appended to this memo below, which concludes with recommendations for the proposed emissivity grid.

Respectfully,

The Scientific Advisory Group²

Bernard Bauer (Chair), Carla Scheidlinger (Vice-Chair), Mike Bush, Jack Gillies, Jenny Hand, Leah Mathews, Ian Walker

² As a co-author of the DRI 2022 PI-SWERL report, SAG member John A. Gillies did not contribute to the review of the report, but was part of the discussions leading to the recommendations in this memorandum. Although Raleigh Martin (former SAG Chair) recently left SAG, he provided a substantive review of this memorandum, having had a lengthy engagement with the particulars of the emissivity grids that constitutes invaluable knowledge. His efforts are warmly acknowledged.

OVERVIEW OF PI-SWERL MEASUREMENTS

DRI began collecting PI-SWERL data in August, 2013, and have conducted measurement campaigns for most years up to September, 2022. The PI-SWERL instrument and its field application have been described extensively in numerous publications (e.g., Mejia et al., 2019 and references therein). The PI-SWERL data are generally categorized as either Riding Area (RA) or Non-Riding Area (NRA). **A total of 1516 distinct measurement locations have been sampled (Table 2), with sampling in the RA prioritized over the NRA at a split of 984 to 532. An additional 69 PI-SWERL measurements were taken in areas that are 'seasonally exclosed',** which means that riding is allowed during part of the year (October 1 through February 28) followed by a period of exclosure (March 1 through September 30) when riding is not allowed. These 69 measurements will be treated separately toward the end of this document.

Table 2: Summary of PI-SWERL Measurements at ODSVRA

YEAR_Month(s)	Riding Area	Non-Riding Area
2013_08	186	143
2014_09	45	35
2015_06	100	2
2015_9/10	165	6
2016_03	58	34
2019_05	337	124
2019_10	42	28
2022_05	51	27
2022_09		133
TOTAL	984	532

The footprint of the zones designated for riding and non-riding has evolved over time due to management interventions directed at dust mitigation. The majority of the land base has not changed designation, but significant acreage originally open for riding has transitioned to non-riding status, typically with fenced exclosures and surface treatments (i.e., straw, surface texturing, scattered seeds, and planted vegetation) or sand fencing. Thus, there are areas considered as 'transitional' because they have not had sufficient opportunity to revert to naturalized conditions and may be displaying residual effects from OHV riding. As an example, the Foredune Restoration Area (FRA) was exclosed in December, 2019 and, prior to that date, this zone was accessible to OHV traffic and camping activities. A total of 71 measurements were taken in this zone while it was designated as RA, and 110 measurements were taken in September, 2022, 31 months (~2.5 years) following implementation of restoration treatments in February, 2020. The data from the FRA are included in the summary values presented in Table 2, but the FRA will be treated separately for purposes of modeling. The same situation applies to the Western Snowy Plover Exclosure (PE), which was seasonally accessible to OHV use during the non-nesting/rearing season (October through February, inclusive) but is now permanently closed. As mentioned above, there is a relatively small area (34.6 acres) that is currently

managed for both OHV access and seasonal exclosure during different times of the year, and since it is neither fully riding nor non-riding, as are other parts of the ODSVRA, it will be assessed separately (and is not included in Table 2).

Due to logistical challenges associated with changes in surface cover, dune movement, evolving restoration treatments and habitat protection, the PI-SWERL measurements are not equally distributed over time or in space. Rather, the sampling design from year-to-year addressed strategic operational needs (e.g., parameterizing the zones most likely to influence air quality or identifying areas for management interventions) rather than statistical requirements (e.g., quantifying uncertainty). Therefore, the sampling approach was neither (stratified) random nor regularly spaced. Moreover, access to certain locations is restricted during certain times of the year because of regulations regarding protected species (e.g., Snowy Plover, California Least Tern). Nevertheless, the large number of measurements within the ODSVRA in both riding and non-riding areas ensures that statistical testing can be conducted with some degree of confidence in the results. **When interpreting the results, however, it is important to appreciate that there may be some sampling bias with respect to either time or space depending on how the data are clustered when assessing group differences or similarities.** The following two sections deal with the temporal and spatial elements of the PI-SWERL measurements independently.

TEMPORAL DIMENSIONS OF PI-SWERL SAMPLING

It is to be expected that there will be seasonal influences on dust emissions from the ODSVRA because of weather-related (i.e., moisture, temperature, windiness) differences between spring (wet) and fall (dry) conditions. In addition, the intensity of OHV traffic and camping use varies during the year. In an attempt to tease out some of these influences, the PI-SWERL measurement results from the Riding Area (RA) were disaggregated according to month/year of sampling and represented using box-and-whisker plots (Figure 1).

A Theil trend analysis (Wilcox, 2005) resulted in no statistically significant trends ($p < 0.01$) in emissivity over time for any of the percentiles shown in the panels in Figure 1 (see Appendix 1 for analysis results). The relatively large dust emissions during the 2013 campaign were noted previously (e.g., 2022 ARWP, Section 2.3.5.1; https://storage.googleapis.com/slocleanair-org/images/cms/upload/files/2ndDraft2022ARWP_2022914.pdf) and were likely due to an extended drought in California (2011-2017); 2013 was a particularly dry year (<https://weather.com/news/news/much-california-2013-was-driest-year-record-20140101>). Moreover, the 2013 campaign was conducted in August, which is characteristically dry, as well as coinciding with intense OHV use of the park. Nevertheless, inclusion of the 2013 data in the regression did not change the final result that there was no significant temporal trend.

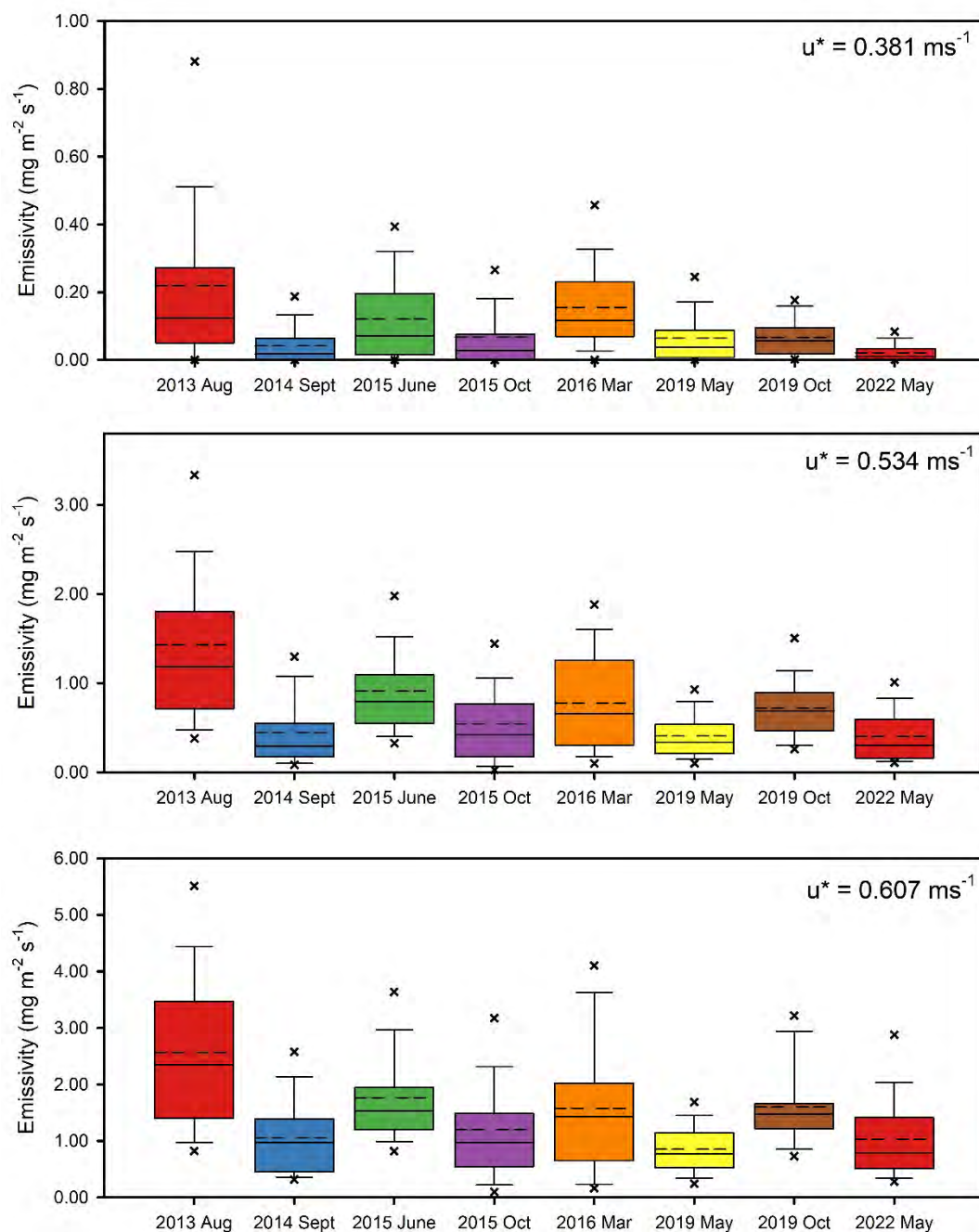


Figure 1: Box-and-whisker plots of PI-SWERL measurements made in the Riding Area (RA) from each field campaign from 2013 through 2022. The colored boxes define the range of the 25th and 75th percentiles; the whiskers correspond to the 10th and 90th percentiles; and the outer symbols (x) indicate the 5th and 95th percentiles. The median value is given by the horizontal solid line within the box, whereas the arithmetic mean (average value) is shown by the horizontal dashed line. The three panels correspond to the three RPM speeds used in the PI-SWERL device to characterize dust emissions at any single measurement location.

Figure 2 shows summary results from an Analysis of Variance (ANOVA) on Ranks using Dunn's test, which is a nonparametric test that does not require equal sample sizes or assuming that all samples were drawn from normally distributed populations with equal variances. Invoking Dunn's test was necessary because none of the measurement campaigns yielded emissivity distributions that were normally distributed. The significance level for all ANOVA on Ranks tests in this report was $p < 0.01$. The results show that the August 2013 data ($n = 186$) are significantly different from most other years (indicated by red boxes), with the exception of June 2015 ($n = 100$) and October 2019 ($n = 42$), which are not statistically different. Overall, it appears as if the lower emissivity periods (September 2014, October 2015, May 2019, and May 2022) are statistically similar to each other but different from the higher emissivity periods (June 2015, March 2016, and October 2019). Of interest for the purposes of this temporal analysis is the fact that there were two measurement campaigns in 2015 (June and October) and in 2019 (May and October), with the June 2015 campaign having greater overall emissivity than in October 2015, whereas the opposite is true for the May 2019 and October 2019 campaigns. As noted earlier, it is important to keep in mind that field campaigns in different years/seasons had different areal coverage, varying sample sizes, and did not regularly re-occupy the same locations, which makes a temporal analysis challenging. Developing a sampling framework that would allow a robust statistical analysis of ODSVRA emissivity data is a challenge due to its size, temporal changes in emissivity on multiple scales, the logistical difficulties of measurement campaigns, and the expense of those campaigns.

Riding Area	Aug 2013	Sep 2014	Jun 2015	Oct 2015	Mar 2016	May 2019	Oct 2019	May 2022
Aug 2013	-							
Sept 2014	Y	-						
Jun 2015	N	Y	-					
Oct 2015	Y	N	Y	-				
Mar 2016	Y	N	N	N	-			
May 2019	Y	N	Y	Y	Y	-		
Oct 2019	N	Y	N	Y	N	Y	-	
May 2022	Y	N	Y	N	N	N	Y	-

Figure 2: Summary results from ANOVA on Ranks test to determine whether there are significant differences ($P < 0.01$) between measurement results from different campaigns for the Riding Area. Boxes in red with 'Y' indicate that there are significant differences between the two sets of data (column vs row) whereas boxes in green with 'N' indicate that the data sets are not statistically different. This analysis considers only the high RPM ($u^* = 0.61 \text{ m s}^{-1}$) PI-SWERL data, but the other two sets of data (low and mid RPM) produced similar results.

Figure 3 shows box-and-whisker plots of the PI-SWERL measurement results from the Non-Riding Area (NRA) disaggregated according to year/month of sampling. As with the RA data, Theil regression demonstrated that there is no statistically significant temporal trend (Appendix 1). Relatively low emissivity values occurred in the two 'transitional' areas—i.e., the Foredune Restoration Area (FRA) and the permanent Plover Exclosure (PE). The March 2016 data (n = 34) had the largest mean and median values, whereas the October 2019 data (n = 28) had the smallest mean and median (aside from the 2015 measurements with an n = 8 when the June and October data were clustered). The May 2022 data (n = 27) show an increase in emissivity relative to the October 2019 low.

Figure 4 shows the results of the ANOVA on Ranks tests for the Non-Riding Area campaigns. The 2015 data set was excluded from this analysis because it comprised only 8 measurements in the Non-Riding Area. Many of the data sets from individual years are statistically different from each other. Of interest is that the August 2013 data set is different from most others with the exception of the two sampling campaigns immediately following (2014 and 2016). The October 2019 campaign appears to be a 'swing' year, being statistically different from earlier campaigns but not different from later campaigns. Also, of note is that the May 2022 data set cannot be considered statistically different from most other years with the exception of August 2013 (much higher emissivity). Moreover, the May 2022 data for the NRA are also statistically different from both the Foredune Restoration Area and Plover Exclosure, both of which were measured later in the same year and have very low emissivity.

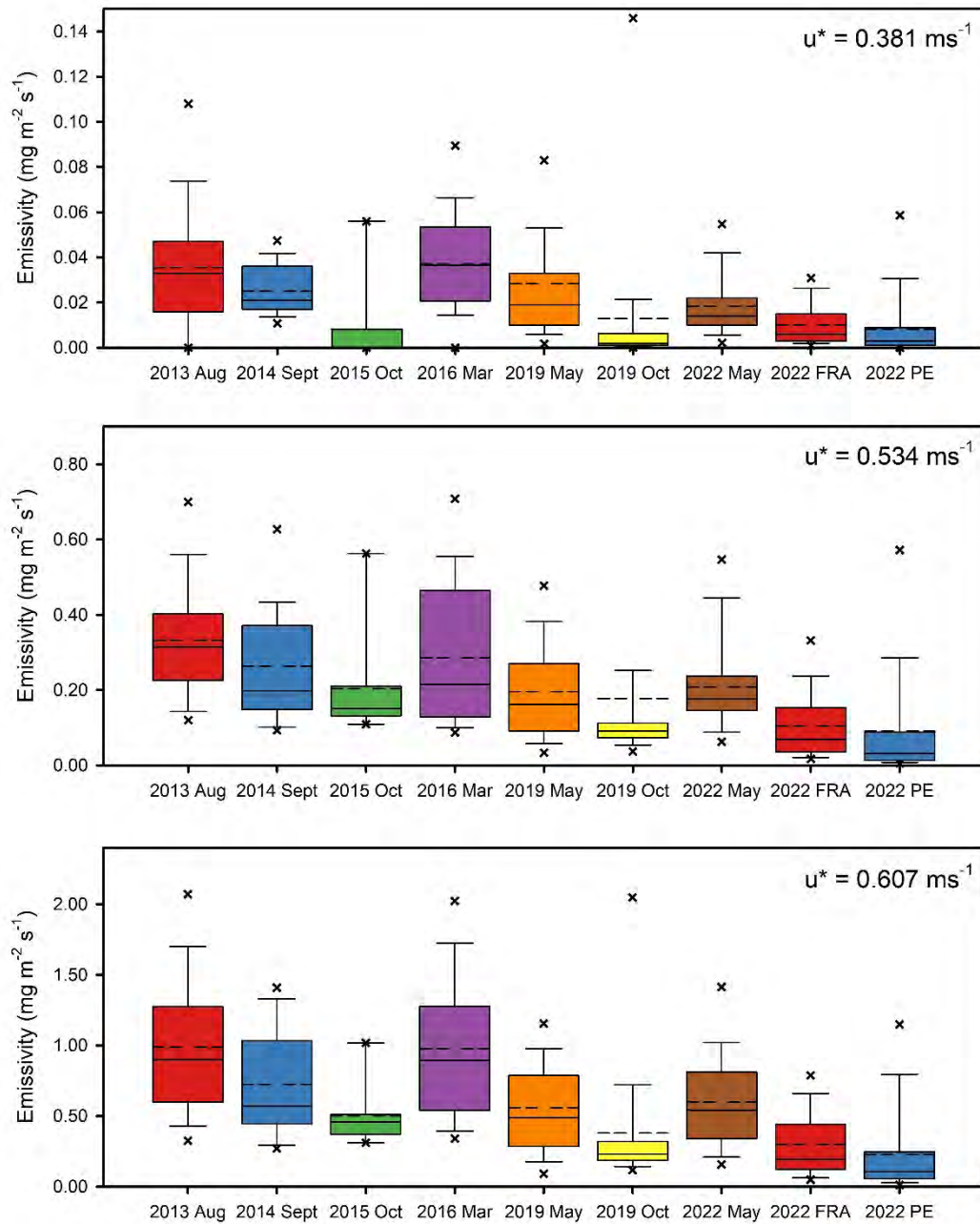


Figure 3: Box-and-whisker plots of PI-SWERL measurements made in the Non-Riding Area (NRA) from each field campaign from 2013 through 2022. The colored boxes define the range of the 25th and 75th percentiles; the whiskers correspond to the 10th and 90th percentiles; and the outer symbols (x) indicate the 5th and 95th percentiles. The median value is given by the horizontal solid line within the box, whereas the arithmetic mean (average value) is shown by the horizontal dashed line. The three panels correspond to the three RPM speeds used in the PI-SWERL device to characterize dust emissions at any single measurement location. “FRA” refers to Foredune Restoration Area; “PE” refers to Plover Exclosure.

Non-Riding Area	Aug 2013	Sep 2014	Mar 2016	May 2019	Oct 2019	May 2022	Sep 2022 FRA	Sep 2022 PE
Aug 2013	-							
Sept 2014	N	-						
Mar 2016	N	N	-					
May 2019	Y	N	Y	-				
Oct 2019	Y	y	Y	N	-			
May 2022	Y	N	N	N	N	-		
Sep 2022 FRA	Y	Y	Y	Y	N	Y	-	
Sep 2022 PE	Y	y	Y	y	N	y	N	-

Figure 4: Summary results from ANOVA on Ranks test to determine whether there are significant differences between measurement results from different campaigns for the Non-Riding Area. Boxes in red with 'Y' indicate that there are significant differences between the two sets of data (column vs row) whereas boxes in green with 'N' indicate that the data sets are not statistically different. FRA means foredune restoration area; PE means permanent plover exclosure. This plot considers only the high RPM ($u^* = 0.61 \text{ m s}^{-1}$) PI-SWERL data, but the other two sets of data (low and mid RPM) produced similar results.

This initial statistical assessment suggests that, despite notable temporal variability in the RA and NRA data, there is no statistically significant temporal trend in emissivity. Part of this outcome relates to the fact that moisture and temperature conditions are highly variable in coastal areas, yet the PI-SWERL sampling strategy does not, and logistically is unable to, control for this variability. Surface moisture conditions can change hourly, daily, weekly, monthly, seasonally, and inter-annually, and it would require a significantly more intensive effort to account for surface moisture conditions in relation to precipitation, relative humidity, and temperature changes. Moreover, there may be a co-dependency on the spatial distribution of measurements from year-to-year, which will be considered next.

SPATIAL DIMENSIONS OF PI-SWERL SAMPLING

The PI-SWERL data were imported into an open-source geographic information system (QGIS) to render a spatial view of the sampling locations. Figure 5 shows the measurement locations relative to the park boundaries. Most areas have been sampled extensively although there are certain areas where the density of points is much greater than in others. The FRA, for example, has a relatively large density of measurements, the majority of which (110 of 181 points) were

collected in September 2022 after 33 months (~2.75 years) of exclosure to OHV access. The PE, in contrast, has relatively few points given the large size of the area, and all these measurements were made in September 2022. There are no measurements in this area during the period when it was seasonally open for OHV riding. The sampling strategy in the PE appears to have followed a longitudinal north-south transect along the middle of the preserve, with points in the north being slightly closer to the shore than points in the south where the exclosure is wider. Many of the other data points in the rest of the park follow west-east transects that run parallel with the prevailing (effective) wind direction out of the WNW.

The points in Figure 5 are color-coded to reflect the date of the measurement campaign (browns indicating older measurements taken in 2013-2015, neutral colors indicating mid-decade, and blue colors indicating recent measurements). Many points are not visible in this graphic either because the sampling was performed in tight spatial clusters or because multiple measurements in different years fall in approximately the same location (i.e., the symbols are stacked with only the most recent appearing on the map).

Figure 6 shows the same data but disaggregated according to year of the field campaign (measurements made between 2014 and 2016 are represented on one map because of the relatively small number). Despite the multitude of measurements covering most of the area of the ODSVRA, it is evident that the sampling was performed unevenly, both temporally and spatially, as mentioned earlier. The two largest field campaigns were in 2013 (RA n=186; NRA n=143) and 2019 (RA n=379; NRA=152) with measurements spanning most of the park. The Dune Preserve to the north (also an NRA) was sampled intensely in 2013 covering most of the area and was revisited in 2019 to duplicate two of the transects. A similar sampling approach was taken to the south in the Oso Flaco NRA zone with intense sampling in 2013 and re-sampling of a west-east transect in 2019.

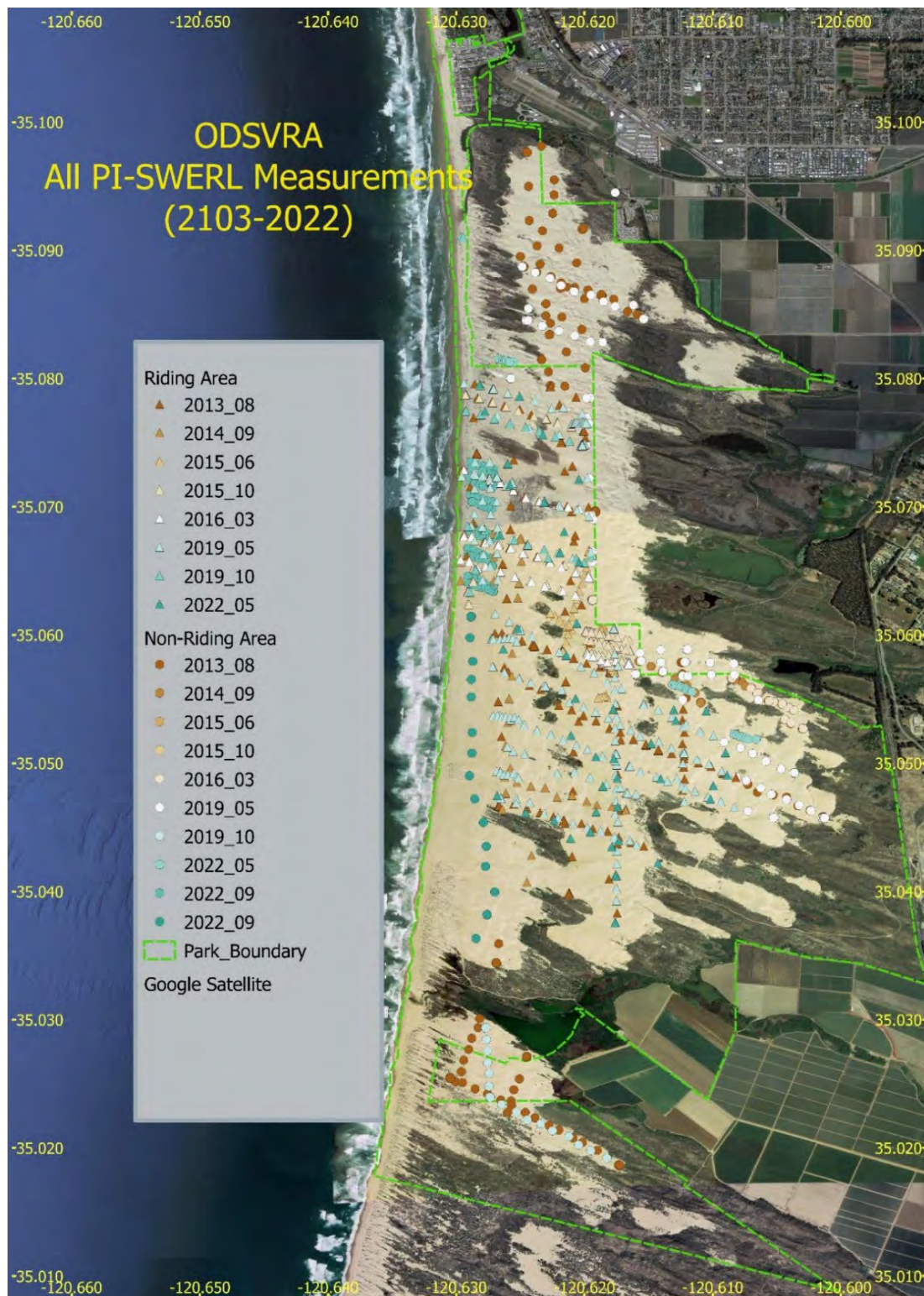


Figure 5: Location of all PI-SWERL measurements from 2013 to 2022. Triangles designate samples taken within the Riding Area (OHV accessible) and circles designate Non-Riding Area samples. Samples in the Seasonal Exclusion area from 2022 are not shown.

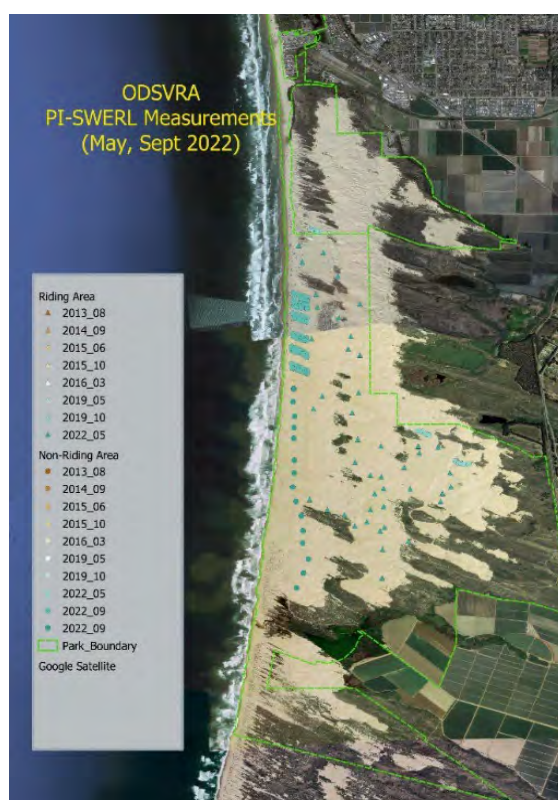
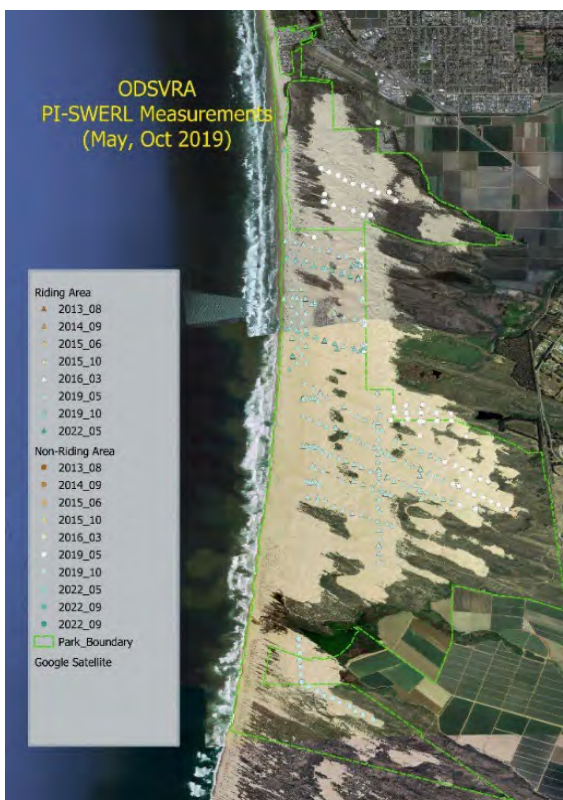
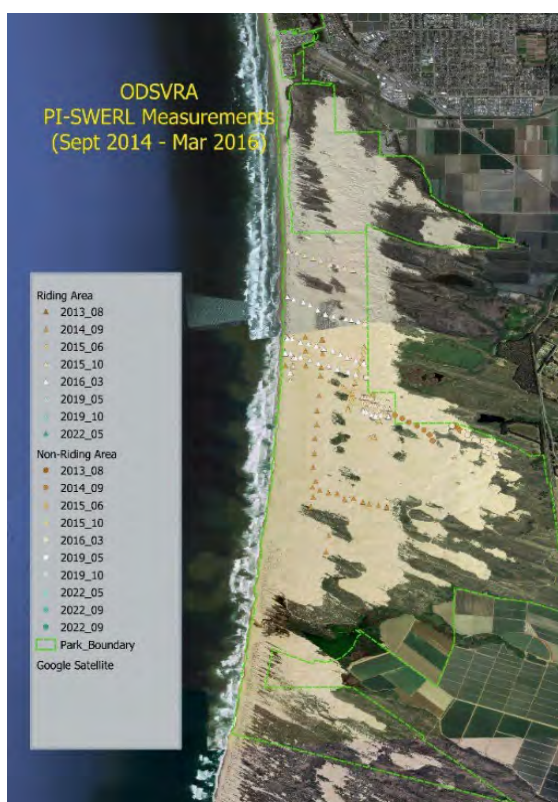
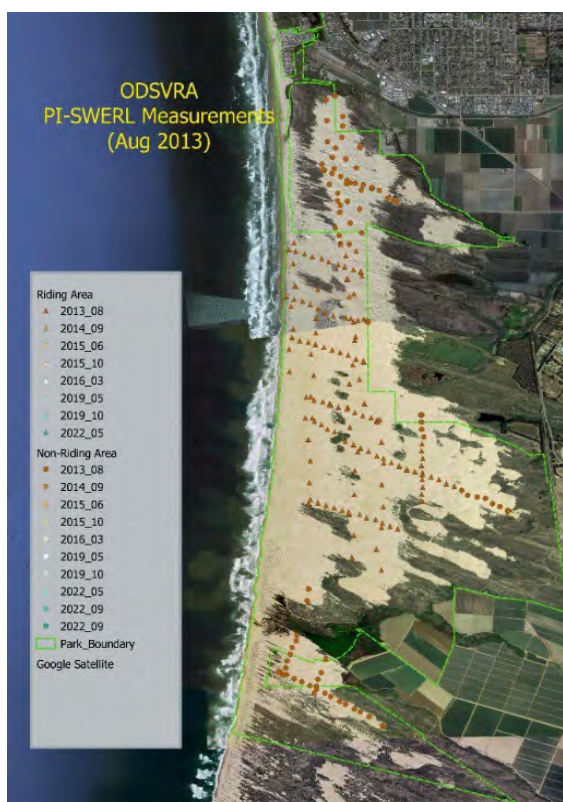


Figure 6: Location of PI-SWERL measurements during different field campaigns from 2013 to 2022. Triangles designate Riding Area and circles designate Non-Riding Area.

The measurements from 2014-2016 were focused on the central region, largely targeting the Riding Area upwind of the CDF and Mesa2 air quality monitoring stations. Measurements in 2022 also focused on the central region with prioritization of the FRA, PE, the SE areas, and the RA. There were no PI-SWERL measurements collected in 2017, 2018, 2020, and 2021.

As noted in the previous section, there were no discernable long-term trends in the PI-SWERL data. A more thorough statistical investigation is hampered by the fact that the sampling design did not call for replication of measurement locations across multiple years (except for a few instances where certain transects were re-occupied in different years, e.g., 2013 and 2019). Therefore, there is an added spatial dimension to consider to the data distributions. It has been suggested, for example, that due to mean grain size increases from north to south (see Scientific Advisory Group Report, February 2023, *Oceano Dunes: State of the Science*) there may be a corresponding decrease in dust emissions from north to south. This possibility was recognized in earlier modeling efforts by DRI, and this will be considered for both the RA and NRA data below.

When examining the spatial distribution of the Non-Riding Area measurements, it becomes clear from Figures 5 and 6 that there are three distinct zones: (1) the Dune Preserve to the north (demarcated by N 35.0794° latitude as the southern boundary, which is slightly south of the park boundary); (2) a Southern Zone falling to the south of the Plover Exclosure and the riding area (referred to as Oso Flaco); and (3) a Central Zone that covers all the remaining area in between these lines of latitude. The PI-SWERL measurements were clustered into these three zones for statistical analysis, with the exception that the data from the Foredune Restoration Area and the Plover Exclosure were kept aside and treated independently.

Figure 7 shows box-and-whisker plots for the North, Central, and South zones as well as the FRA and PE zones, retaining the year of collection as an additional variable. Visually, the emissivity values to the south are generally smaller than the north, despite considerable scatter. The data from 2013, for example, stand out as having comparatively large emissivity relative to other years, especially in the North and South zones. In the Central zone, this difference is not quite as apparent because the data from 2016 (brown bar) have a very wide distribution despite a relatively small sample size (n=34). Approximately one third of these measurements were taken directly east of the fence that marks the riding area, whereas the remainder were taken just south of Black Lake (west of Callender) and far from the riding area. Once again, the measurements from 2015 (yellow bar) can be discounted because of small sample size (n=8).

For the purposes of testing whether there is indeed a north-south trend in emissivity, the data from each of the three zones were clustered (i.e., combining data from all years). The resulting box-and-whisker plots are shown in Figure 8. From this rendering, it becomes much clearer that **there is indeed a reduction in emissivity from north to south. In addition, the FRA and PE also show very low emissivity in comparison to the Central and North zones.** The ANOVA on Ranks results (for the high RPM case) are shown in Figure 9, from which it is evident that the groupings are all statistically different with one exception--the FRA measurements cannot be considered to be statistically different from the PE measurements, but they are both different from the South, Central, and North zones.

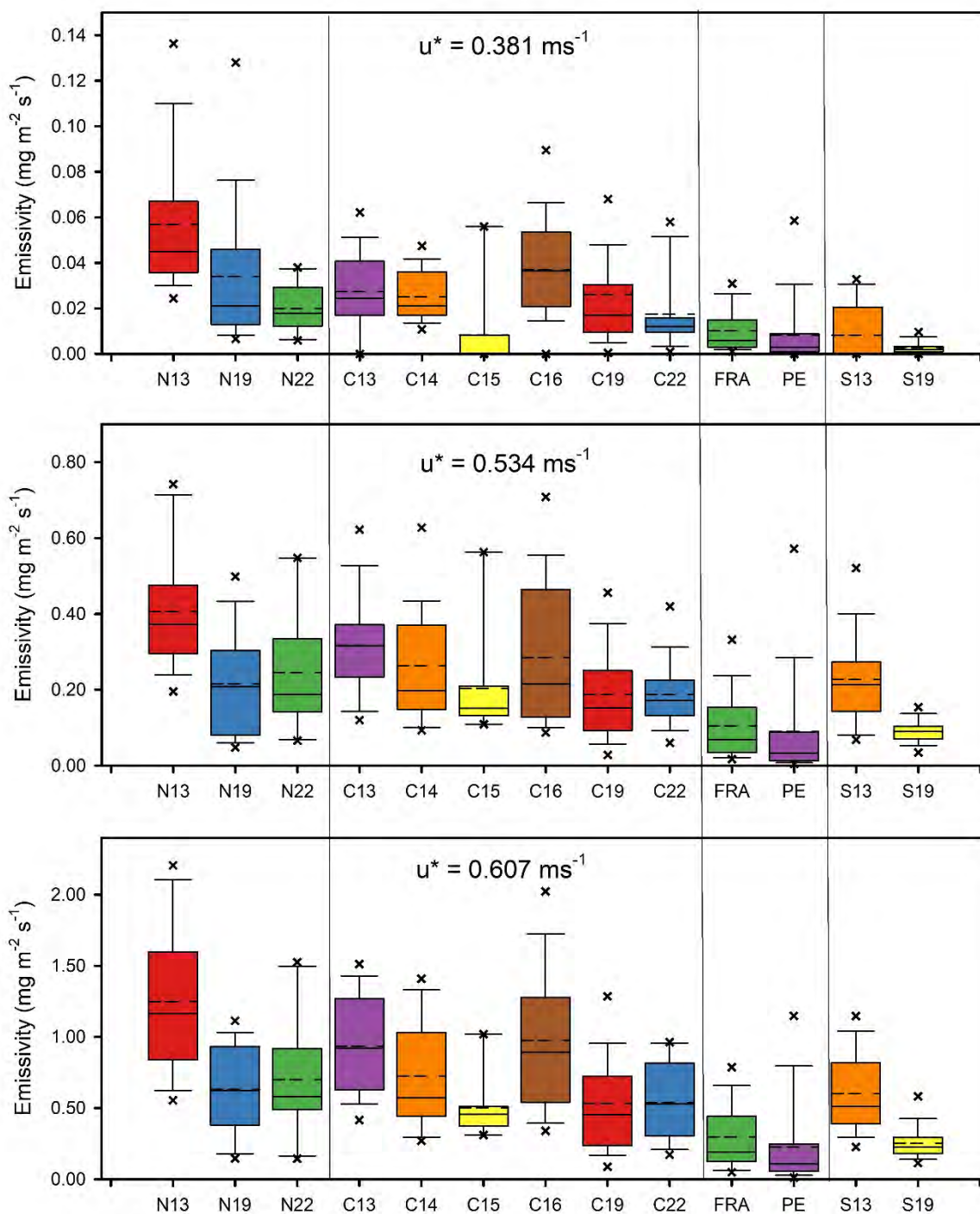


Figure 7: Box-and-whisker plots of PI-SWERL measurements made in the Non-Riding Area (NRA) from each field campaign from 2013 through 2022 disaggregated into North, Central, and South zones (delineated by vertical thin lines). Foredune Restoration Area (FRA) and Plover Exclosure (PE) are treated separately. See Figure 1 for explanation of symbols. The three panels correspond to the three RPM speeds used in the PI-SWERL device to characterize dust emissions at any single measurement location.

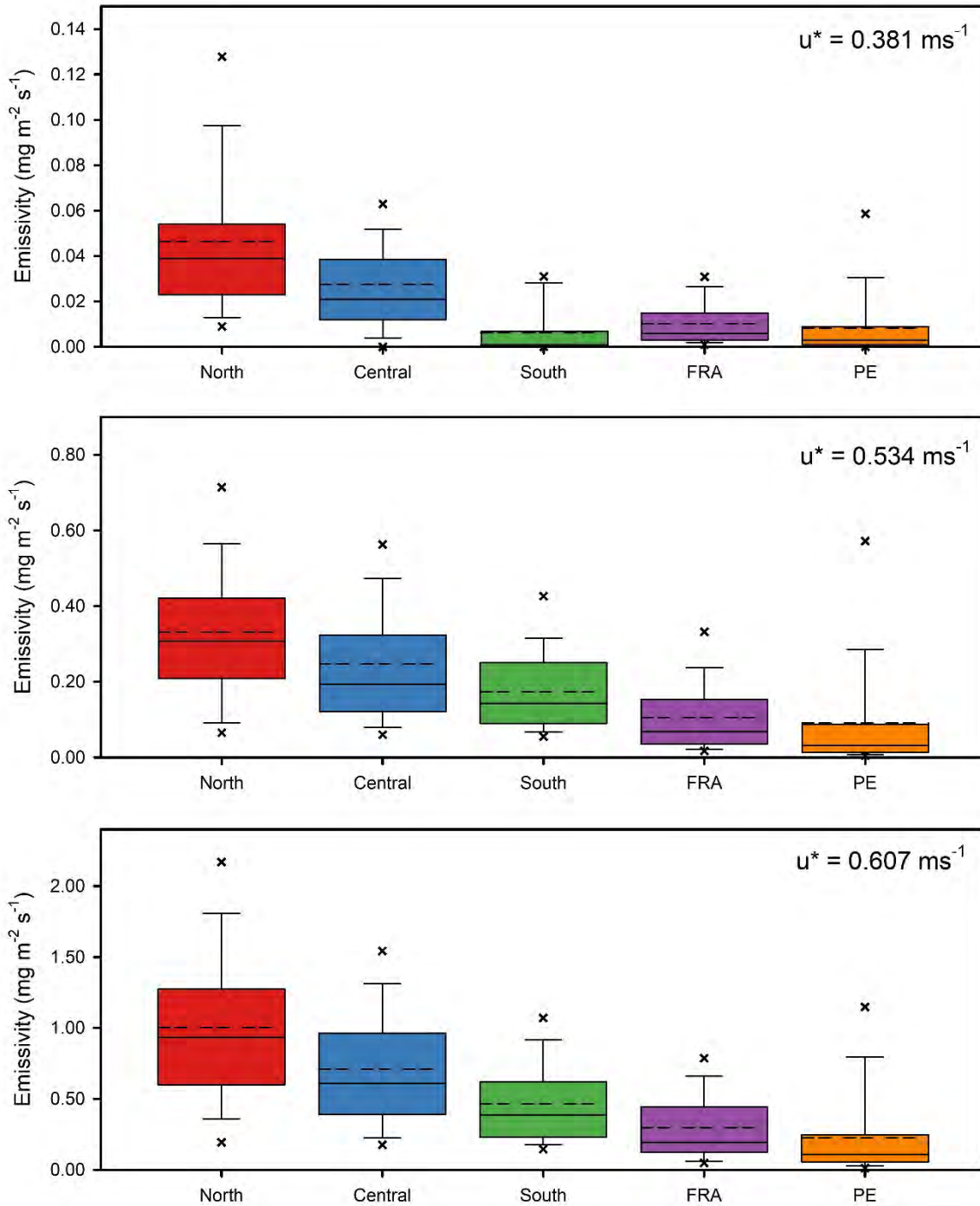


Figure 8: Box-and-whisker plots of PI-SWERL measurements made in the Non-Riding Area (NRA) aggregated into North, Central, and South zones. Foredune Restoration Area (FRA) and Plover Exclosure (PE) are treated separately. See Figure 1 for explanation of symbols. The three panels correspond to the three RPM speeds used in the PI-SWERL device to characterize dust emissions at any single measurement location.

Non-Riding Area	North	Central	South	FRA	PE
North	-				
Central	Y	-			
South	Y	Y	-		
FRA	Y	Y	Y	-	
PE	Y	y	y	N	-

Figure 9: Summary results from ANOVA on Ranks test to determine whether there are significant differences between measurement results for the Non-Riding Area clustered into zones in the north-south direction. Refer to Figure 7 for zones. Boxes in red with 'Y' indicate that there are significant differences between the two sets of data (column vs row) whereas boxes in green with 'N' indicate that the data sets are not statistically different. This plot considers only the high RPM ($u^* = 0.61 \text{ m s}^{-1}$) PI-SWERL data, but the other two sets of data (low and mid RPM) produced similar results.

Although an analysis of potential west-east trends was undertaken for the NRA data, the differences were not as apparent as for the north-south trends. Moreover, there is considerable subjectivity with regard to placement of separation boundaries for data aggregation, so this line of inquiry was not pursued further.

The Riding Area data shown in Figure 5 were all located within the central zone that was defined for the NRA data, and there are no obvious break points to create zones for the RA as was the case for the NRA. **The RA data were plotted according to latitude (Figure 10) to determine whether there was visual evidence to justify a separation. There is an evident decrease in emissivity toward the south, which is gradual but progressive.** The resulting R^2 values for the regression suggest that latitude is a weak explanatory variable given how much scatter there is at any single line of latitude. The scatter is skewed to much larger emissivity values in the north where the OHV use is more intense and spatially constrained than in the south. Visually, there appears to be a break at about $N 35.062^\circ$, which aligns roughly with the northern boundary of the PE and follows a parallel trajectory inland. The sub-region to the north of this line has characteristically larger emissivity values and large scatter than the sub-region to the south of this line.

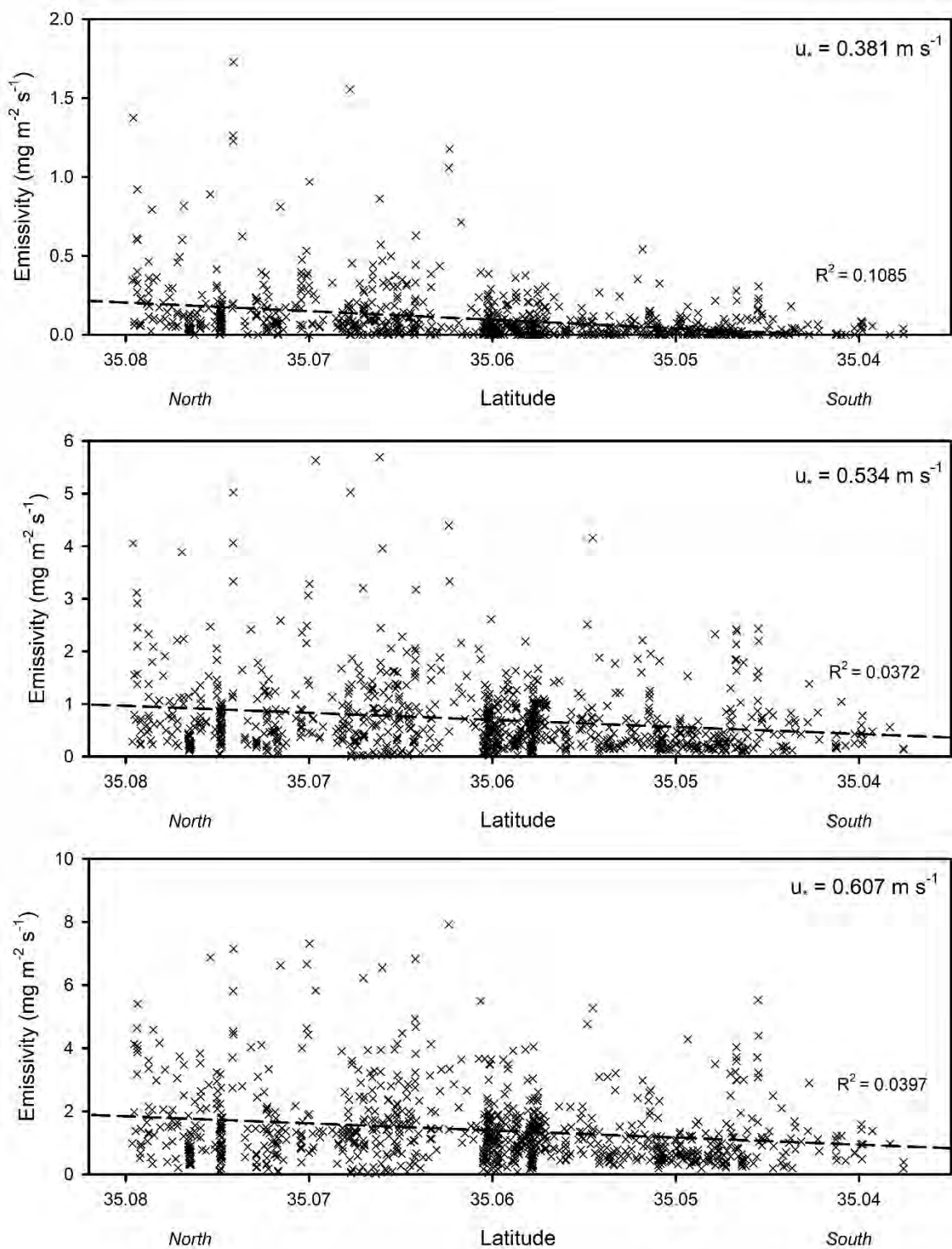


Figure 10: North-South trend in emissivity for Riding Area PI-SWERL data from 2013-2022. Dashed line is the best-fit linear regression line with R^2 values shown in each panel.

Following on the visual cues from Figure 10, the PI-SWERL RA data were pooled into two sub-regions (Central-North and Central-South) for additional analysis. Figure 11 provides the box-and-whisker plots that graphically portray the data distributions in each zone. Although the Central-South sub-region has generally smaller emissivity values, there is considerable overlap in the distributions. The Mann-Whitney Rank Sum Test was performed on the three sets of PI-SWERL data corresponding to the Lo-, Mid-, and Hi-RPM measurements to determine whether the data from the Central-North sub-region were statistically different from the Central-South sub-region. The results are provided in Table 3, and the very small p value indicates that the null hypothesis (no difference in samples) is to be rejected. Thus, there is a significant difference between the paired sub-regions. As with the NRA data, the analysis of west-east trends proved less revealing.

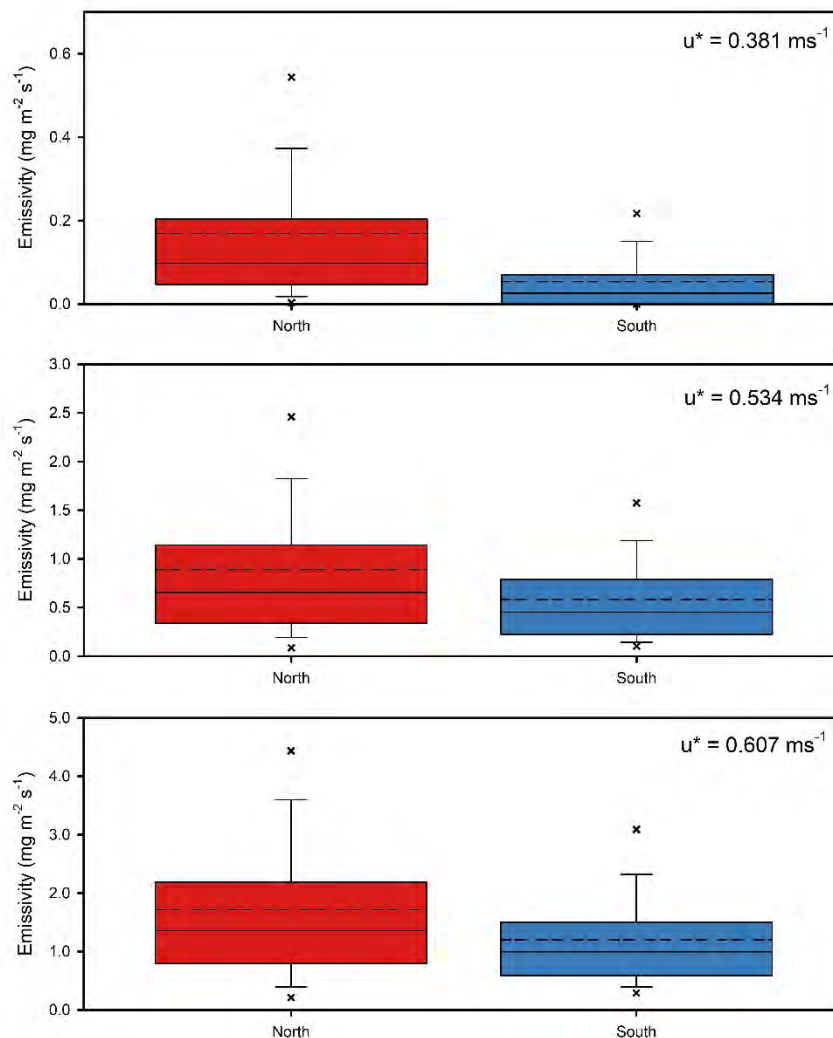


Figure 11: Box-and-whisker plots of PI-SWERL measurements made in the Riding Area (NA) aggregated into Central-North and Central-South sub-regions See Figure 1 for explanation of symbols. The three panels correspond to the three RPM speeds used in the PI-SWERL device to characterize dust emissions at any single measurement location.

Table 3: Results from Mann-Whitney Rank Sum Tests on PI-SWERL data from the Central-North (CN) and Central-South (CS) sub-regions of the Riding Area (2013-2022).

u^* (m s⁻¹)	Median Emissivity (mg m⁻² s⁻¹)		U statistic	T value	p
	CN (n = 415)	CS (n = 569)			
0.381	0.098	0.026	56,062	264,422	< 0.001
0.534	0.655	0.454	89,606	229,900	< 0.001
0.607	1.360	0.996	88,582	224,646	< 0.001

RECOMMENDATIONS LEADING TOWARD MODEL EMISSIVITY GRIDS

Spatial Sub-Division (Zones and Sub-Regions)

The above analysis of the PI-SWERL data collected between 2013 and 2022 suggests that the **Riding Area** can be subdivided in two sub-regions (Central-North and Central-South) while the **Non-Riding Area** can be subdivided into three zones (North, Central, and South). Figure 12 shows these five primary areas as well as two additional areas designated as non-riding: (i) Foredune Restoration Area; (ii) Plover Exclosure, and the areas managed for Seasonal Exclosure (SE). The vegetated zones should be treated separately by overlaying a cover mask on the GIS model. Each of the zones and sub-regions are then allocated different emissivity characteristics for purposes of future dust emissions modeling.



Figure 12: Proposed zonation for disaggregating the PI-SWERL measurements (2013-2022) into three zones for the Non-Riding Area (NRA North, NRA Central, NRA South, separated by purple and blue dashed lines) and two sub-regions for the Riding Area (RA Central-North, RA Central-South separated by orange dashed line). Also shown are the boundaries of the Foredune Restoration Area (FRA), the Plover Exclosure (PE), and the Seasonal Exclosure (SE) areas. The current extent of the Riding Area is mapped in a light tan color. See also Figure 17.

The following recommendations are made with regard to the zonation of the ODVSRA, based on the PI-SWERL analysis presented above:

For the Riding Area, the Central-North and Central-South sub-regions should be delineated by a separation line that parallels the northern fenced boundary of the Plover Exclosure from the beach inland, and then following N 35.062° latitude past the eastern park boundary (Figure 13) to the end of the modeling domain. The northern and southern boundaries of the Riding Area are the same as the boundaries for the Non-Riding Areas, as described below.

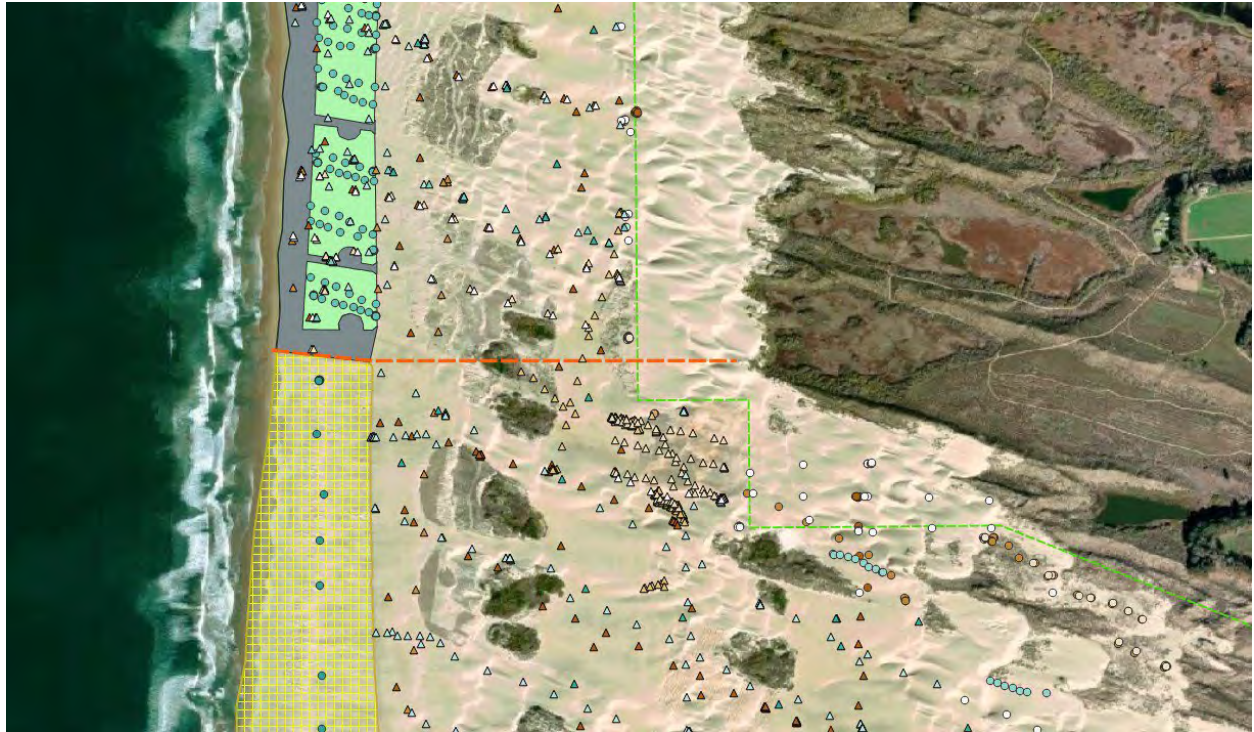


Figure 13: Proposed boundary line (orange dashed line) between the Central-North and Central-South sub-regions of the Riding Area. Refer to Figure 12 for location, and see Figure 5 for definition of symbols.

For the Non-Riding Area, three zones were identified (North, Central, South) from the statistical analysis. Figure 12 shows an overview of the recommended boundaries for these zones. A close-up of the boundary between the North and Central zones is shown in Figure 14, and it also serves as the northern boundary for the Riding Area. The boundary is delineated by a fence line that trends west-east in zig-zag fashion, which then follows along the northern boundary of a sand-fencing area, and then trends eastward along N 35.0794° latitude to the eastern boundary of the ODVRA. On the western side, the boundary follows the park fence line heading north to the mouth of Arroyo Grande Creek.

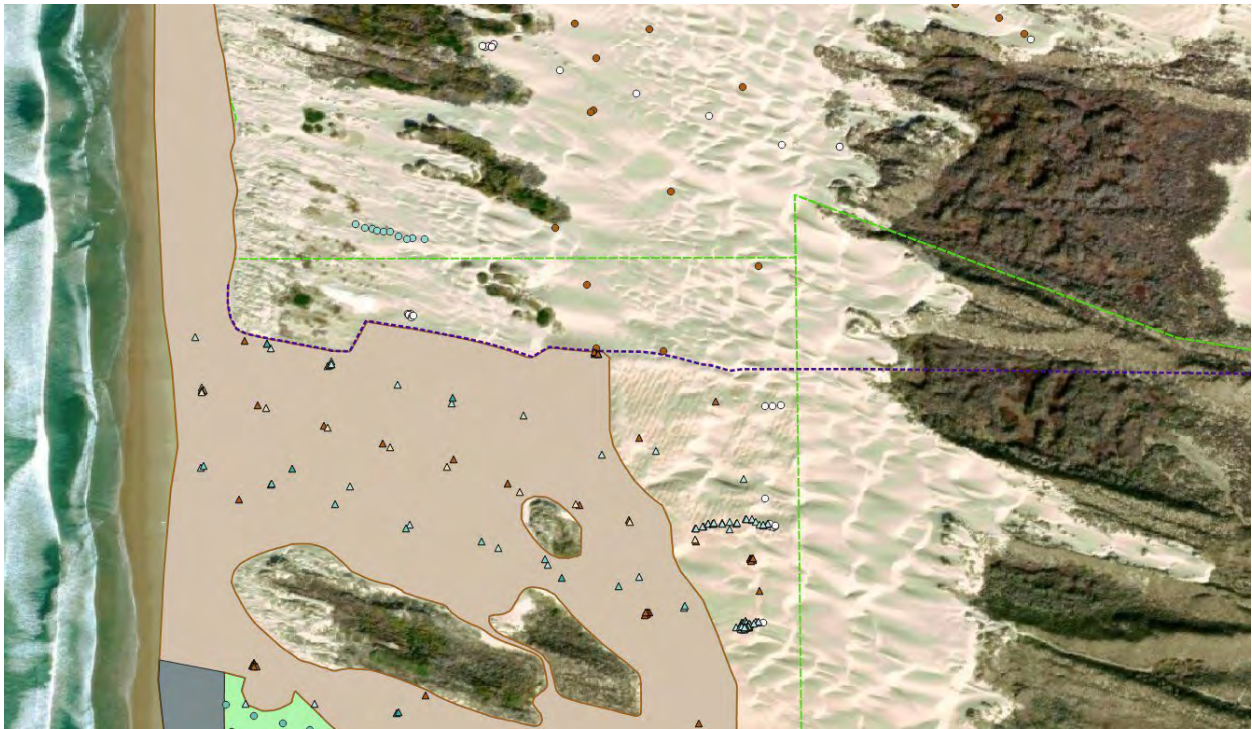


Figure 14: Proposed boundary line (purple dashed line) between the North and Central zones for the Non-Riding Area, which also delineates the northern boundary of the Riding Area. Refer to Figure 12 for location, and see Figure 5 for definition of symbols.

A close-up of the boundary between the NRA Central and NRA South is shown in Figure 15. This boundary begins on the beach and follows the fence line along the southern margin of the Plover Exclosure. It then transitions to the fence line delineating the southern margin of the Riding Area (RA Central-South), and from the most southerly point of the Riding Area takes a straight line to the nearest corner of the ODSVRA boundary and continues east along the park boundary through a thickly vegetated area.

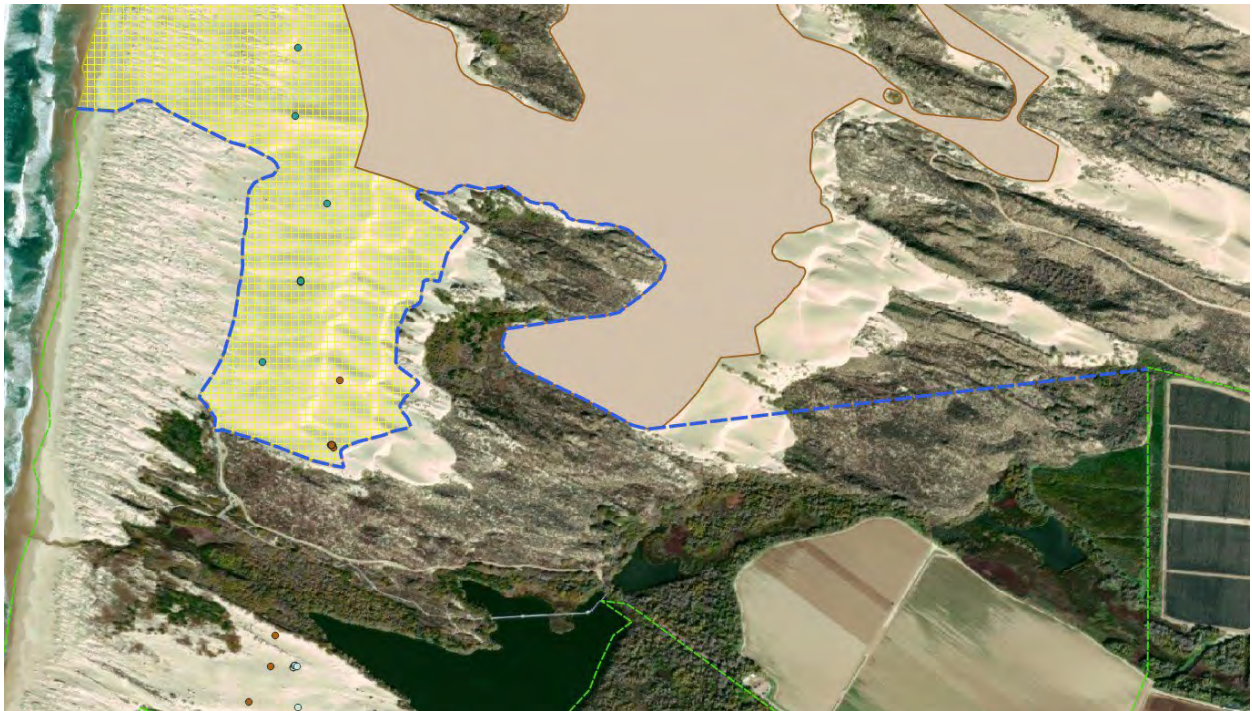


Figure 15: Proposed boundary line (dashed blue line) between NRA Central and NRA South zones, which also delineates the southern boundary of the Riding Area. Refer to Figure 12 for location, and see Figure 5 for definition of symbols.

A close-up of the FRA, the northern portion of the PE, and the Seasonal Exclosure (SE) area is presented in Figure 16. Also shown are some of the vegetation islands. All these zones are defined by GIS shapefiles managed by CDPR (T. Carmona, personal communication), and each of them is assigned a separate emissivity relation (as described below).

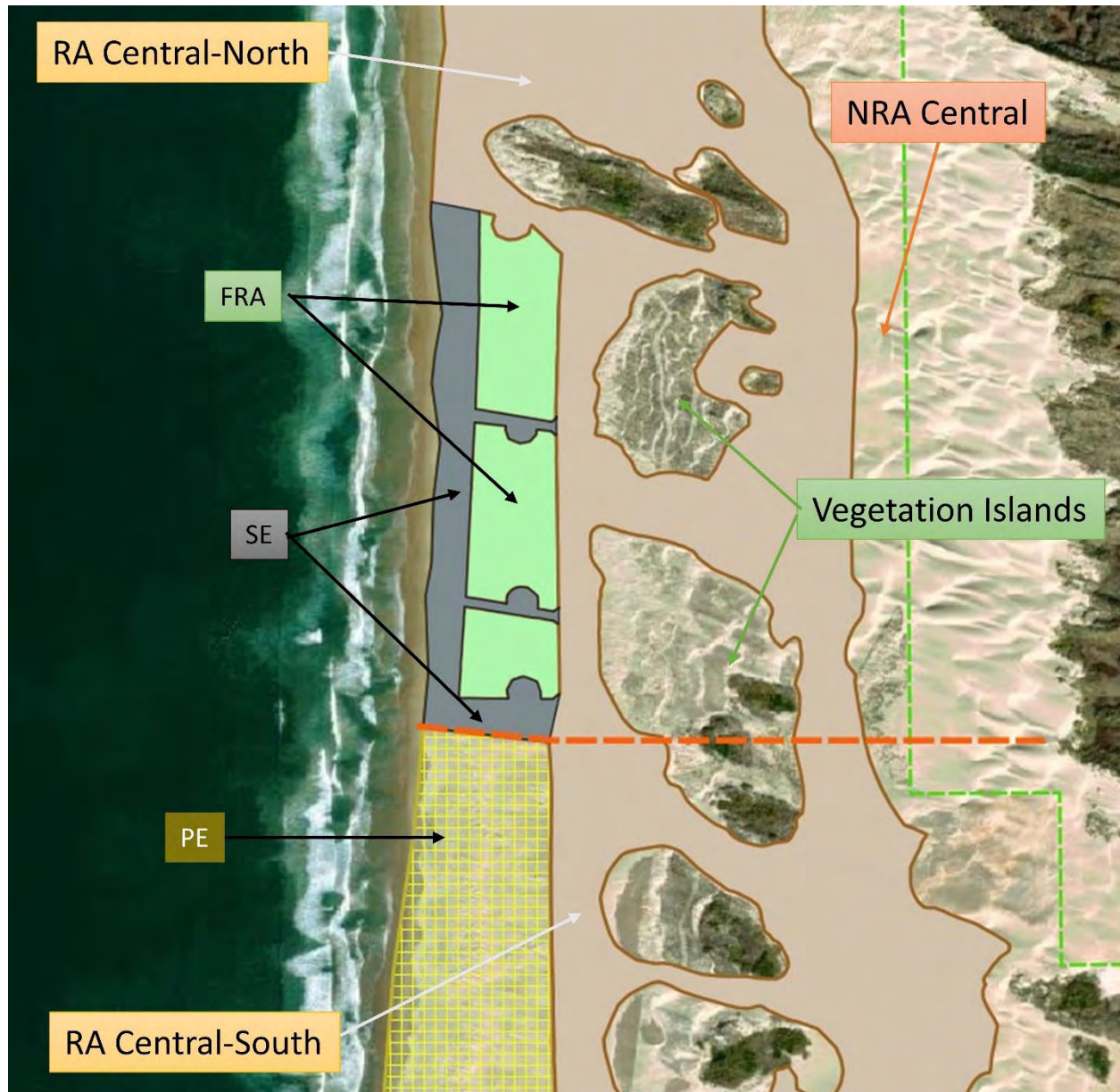


Figure 16: Outlines of the Foredune Restoration Area (FRA), Plover Exclosure (PE), and the Seasonal Exclosure (SE) areas. The Riding Area is shown in tan color. Refer to Figure 12 for location.

The excess emissions framework proposed by SAG (SAG Memo – Framework for Assessing “Excess Emissions” of PM₁₀ from the Oceano Dunes, January 30, 2023) identifies the need to develop emissions grids for various modeling scenarios. This requires development of emissivity relations for each of the zones and sub-regions identified above, based on PI-SWERL measurement that are clustered or pooled accordingly.

For Current (2023) Conditions, it is recommended that the ODSVRA area be subdivided into nine zones (Figure 17), as follows:

1. Non-Riding Area North Zone
2. Non-Riding Area Central Zone
3. Non-Riding Area South Zone
4. Riding Area Central-North Sub-Region
5. Riding Area Central-South Sub-Region
6. Foredune Restoration Area (FRA)
7. Plover Exclosure (PE)
8. Seasonal Exclosures (SE)
9. Vegetated Areas (VEG)

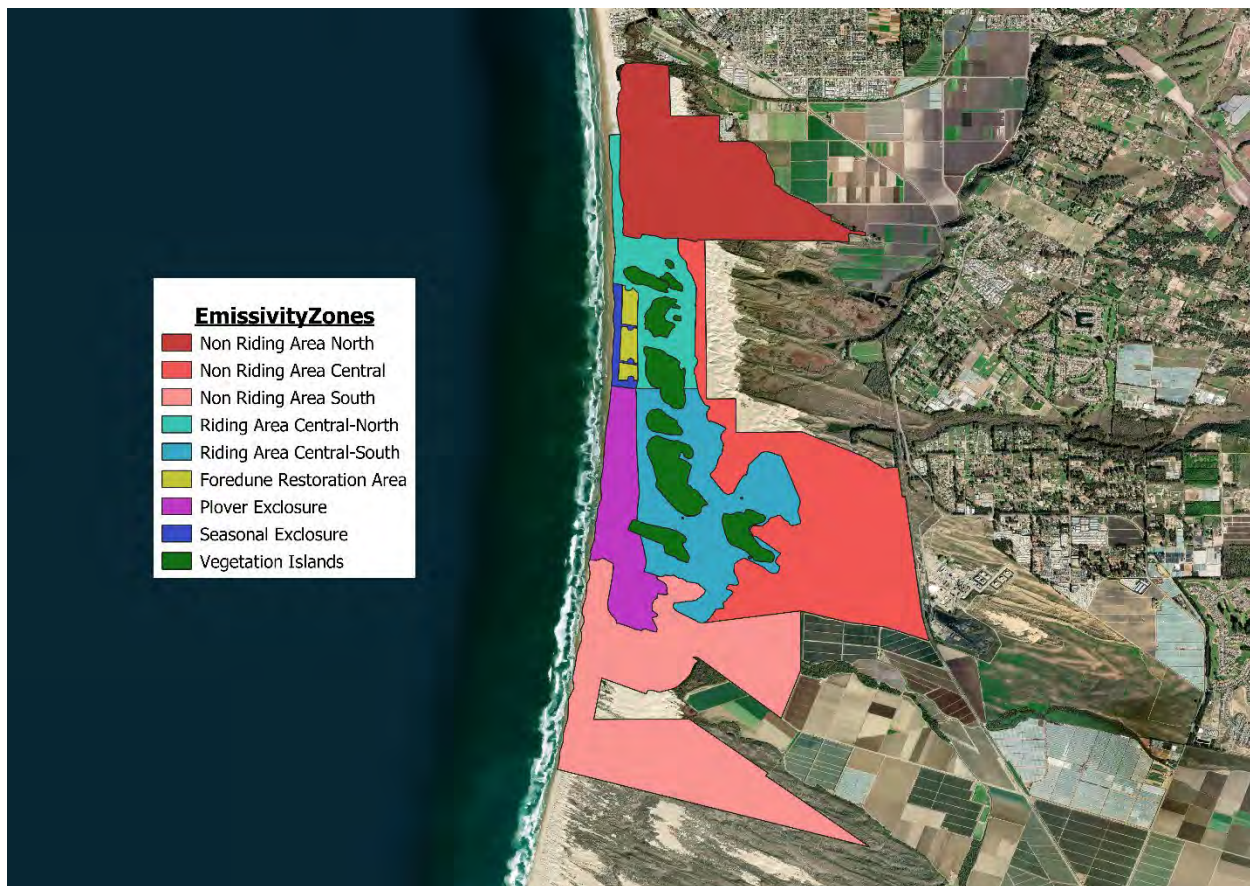


Figure 17: Emissivity zone polygons proposed for modeling the Current (2023) Conditions scenarios.

For the Pre-Disturbance (1939) scenario, it is recommended that the ODSVRA area be subdivided into three large NRA zones (North, Central, and South), as delineated by the boundaries shown in Figure 14 (between North and Central) and Figure 15 (between Central and South). Each of the three zones (Figure 18) will have a different emissions relation. The North zone is essentially the same as the Dune Preserve, which has not had OHV access for a long time. Similarly, the South zone encompasses the Oso Flaco area for which there has been no recent riding allowed. The Central zone, which currently has a mix of zones and riding access, will be classified in its entirety as "non-riding" for the pre-disturbance scenario, and only non-riding data from NRA Central will be used to characterize the emissivity relation. The 1939 vegetation cover mask developed by UCSB should be applied to this modeling scenario, yielding four distinct modeling zones (North, Central, South, Vegetation) all of which have non-riding characteristics.

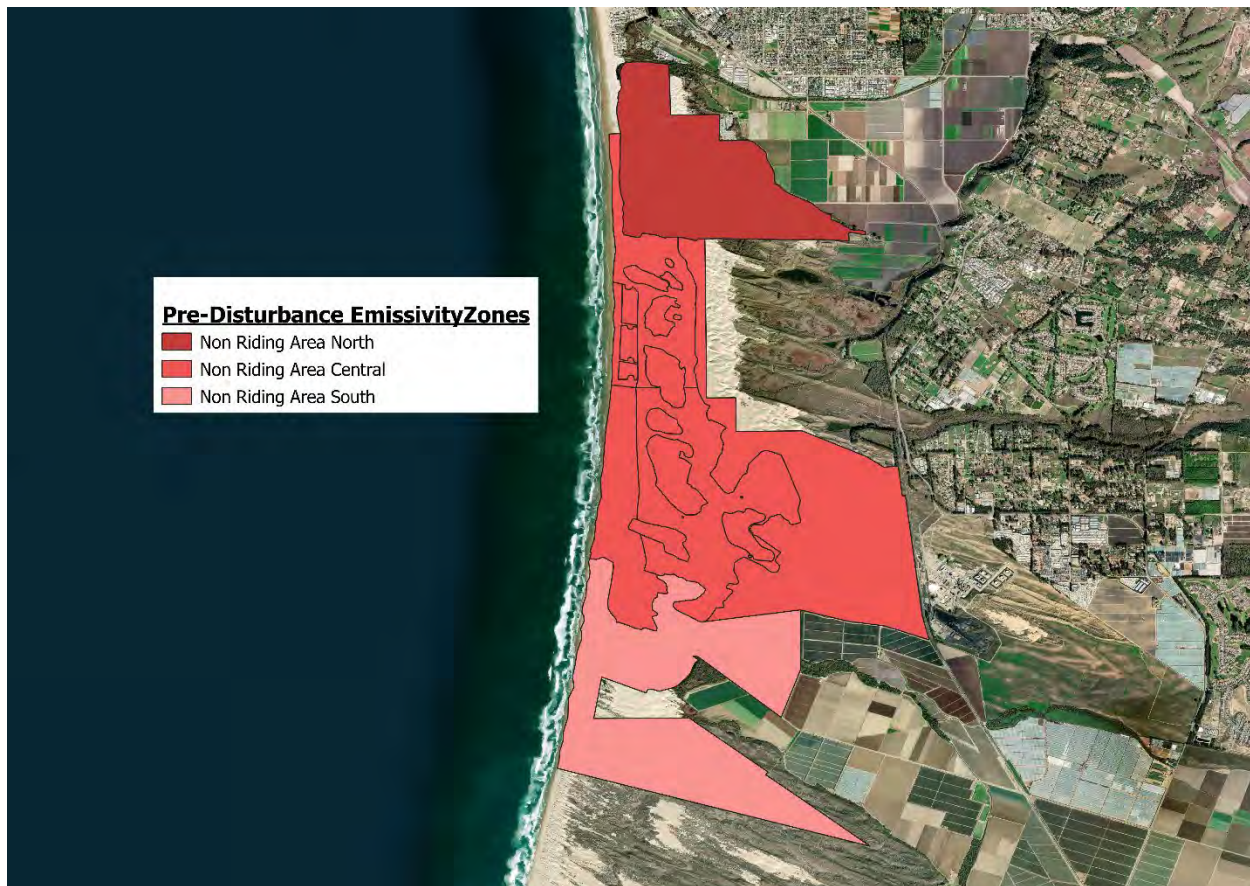


Figure 18: Emissivity zone polygons proposed for modeling the Pre-Disturbance (1939) scenarios. Vegetation cover mask to be superimposed.

Emissivity Curves

For each of the proposed zones and sub-regions identified above, emissivity relations will need to be assigned for purposes of modeling. These relations take the form of a power function:

$$F = a u_*^b$$

where F is the emissive flux ($\text{mg m}^{-2} \text{s}^{-1}$), u_* is shear velocity (m s^{-1}), a and b are coefficients from regression analysis of the PI-SWERL results for the three rotational speeds (Etyemezian et al., 2007). Such emissivity relations are deemed to be representative of the entire zone or sub-region, regardless of intra-area variations in surface characteristics (e.g., texture, mineralogy, slope, aspect, moisture content, degree of disturbance). Accounting for all such micro-scale controls is logistically impractical. Fortunately, there are a very large number of PI-SWERL measurements across the entire park area, making a statistical approach viable.

In past modeling efforts, emissivity grids were developed for both the 2013 and then the 2019 PI-SWERL measurement campaigns using a spatial interpolation algorithm superimposed on a 20 m by 20 m grid for the entire modeling domain. Each grid cell was given a different emissivity relation based on the spatially interpolated emissivity surface derived from the PI-SWERL measurements at unevenly distributed point locations. The proposal for moving forward is to define emissivity relations for each of the zones and sub-regions rather than for the 20 m by 20 m grid used earlier. Since each of the zones and sub-regions includes multiple measurements, a statistical approach implies using some measure of central dispersion (e.g., mean, mode, median) to quantify a representative emissivity value for each of the RPM speeds (shear velocities) of the PI-SWERL measurements.

Figure 19 shows two characteristic data distributions based on all the measurements (2013-2022) in the Central-North and Central-South Sub-Regions of the Riding Area. It is clear that the distributions are heavily skewed, with a large number of measurements falling at the low end of the emissivity range and a handful of measurements at the extreme high end of the emissivity range. Tests for normality consistently yield negative results, and as a consequence, standardized parameters used to describe Gaussian distributions (e.g., mean, standard deviation) are not strictly applicable.

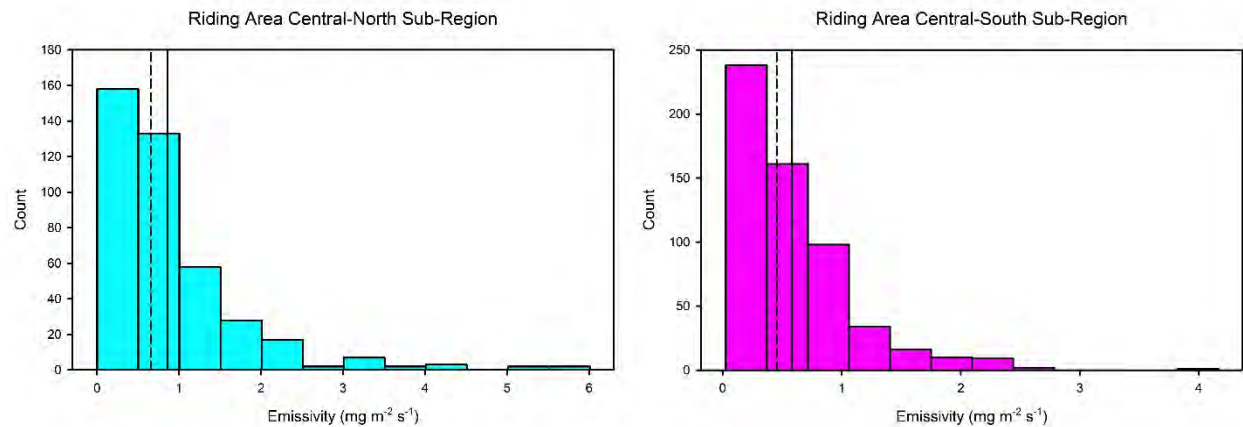


Figure 19: Histograms of PI-SWERL emissivities (Hi-RPM setting) for Central-North Sub-Region (left) and Central-South Sub-Region (right) of the Riding Area for all measurements from 2013 to 2022. Solid vertical line is the arithmetic mean; dashed vertical line is the median.

Although non-parametric statistics typically have reduced explanatory power, **it is recommended that future emissivity relations be based on the median** rather than the mean. The median is defined as the 'middle' value of the distribution, which is arguably more representative of the typical emissivity because it is not influenced by a few extreme values as is the mean. Figure 19 indicates that for the PI-SWERL data, the median is marginally smaller than the mean, although in some cases the mean can be considerably larger when skewed by a few measurements with extremely large emissivity values. This difference between using the median rather than the mean will yield updated values for modeled PM_{10} , and when applied to both the pre-disturbance and present conditions, it will facilitate a direct comparison of emissions for purposes of assessing the effectiveness of dust control measures.

The following recommendations are made in regard to assigning emissivity curves to the various zones and sub-regions:

Current (2023) Conditions Scenarios

<i>Zone or Sub-Region</i>	<i>Emissivity curves based on data from...</i>
NRA North	All 2013-2022 PI-SWERL measurements located in NRA North Zone
NRA Central	All 2013-2022 PI-SWERL measurements located in NRA Central Zone (not including FRA, PE, SE)
NRA South	All 2013-2022 PI-SWERL measurements located in NRA South Zone
RA Central-North	All 2013-2022 PI-SWERL measurements located in RA Central-North Sub-Region
RA Central-South	All 2013-2022 PI-SWERL measurements located in RA Central-South Sub-Region
FRA	Only 2022 PI-SWERL measurements located in the FRA
PE	Only 2022 PI-SWERL measurements located in the PE
SE	Weighted average of riding and non-riding measurements in SE areas (see below for details)

Pre-Disturbance (1939) Scenario

<i>Zone or Sub-Region</i>	<i>Emissivity curves based on data from...</i>
North (same as NRA North)	All 2013-2022 PI-SWERL measurements located in NRA North Zone
Central (same as NRA Central but also including footprint of RA areas between the north and south boundaries)	All 2013-2022 PI-SWERL measurements located in NRA Central Zone (not including FRA, PE, SE)
South (same as NRA South)	All 2013-2022 PI-SWERL measurements located in NRA South Zone

Note that for both the Current Conditions and Pre-Disturbance Scenarios, **the recommendation is to take advantage of the complete set of PI-SWERL measurements collected between 2013 and 2022**. Despite 2013 being an exceptionally dry year with demonstrably larger emissivity values (refer to discussion of Figures 1, 3 and 7), such dry years are part of the normal climatology of the region, and prolonged droughts are projected to become more frequent in the future. There is no defensible reason to exclude these data from consideration, and they help to

define the natural variability in the system, which should be accounted for when considering model uncertainty. Similarly, there are no defensible reasons for excluding any of the other PI-SWERL measurements (e.g., inordinately small or large emissivity) because they have been thoroughly quality controlled for errors associated with instrumental failure and transcription/coding inaccuracies by DRI personnel.

Table 4 provides the results for the emissivity relations developed for the Non-Riding and Riding Areas as well as the Foredune Restoration Area and Plover Exclosure area, based on the recommendations presented above. Graphic renditions of the data and power relations are shown in Figure 20. The same axis scaling is used for quick visual comparison, and it is apparent that the RA Central-North sub-region has the largest median emissivity. Interestingly, the RA Central-South sub-region has median emissivity that are not too dissimilar from the NRA North zone and NRA South zone, despite OHV restrictions in the latter two zones. The PE and FRA have the smallest median emissivity.

Table 4: Data used in developing emissivity relations. Power function coefficients (a, b) are shown at the bottom.

	Non-Riding Areas			Riding Areas		FRA	PE
	North	Central	South	Central-North	Central-South		
n =	111	221	67	403	574	110	23
u* (m s⁻¹)							
0.381	0.039	0.021	0.001	0.094	0.024	0.006	0.003
0.534	0.307	0.193	0.142	0.640	0.432	0.068	0.032
0.607	0.932	0.610	0.388	1.349	0.964	0.192	0.107
F = a (u*)^b							
a	66.376	51.649	20.786	24.340	24.395	10.710	11.416
b	8.547	8.893	7.972	5.795	6.466	8.060	9.355
r ²	.999	.999	.999	1.000	0.999	1.000	1.000

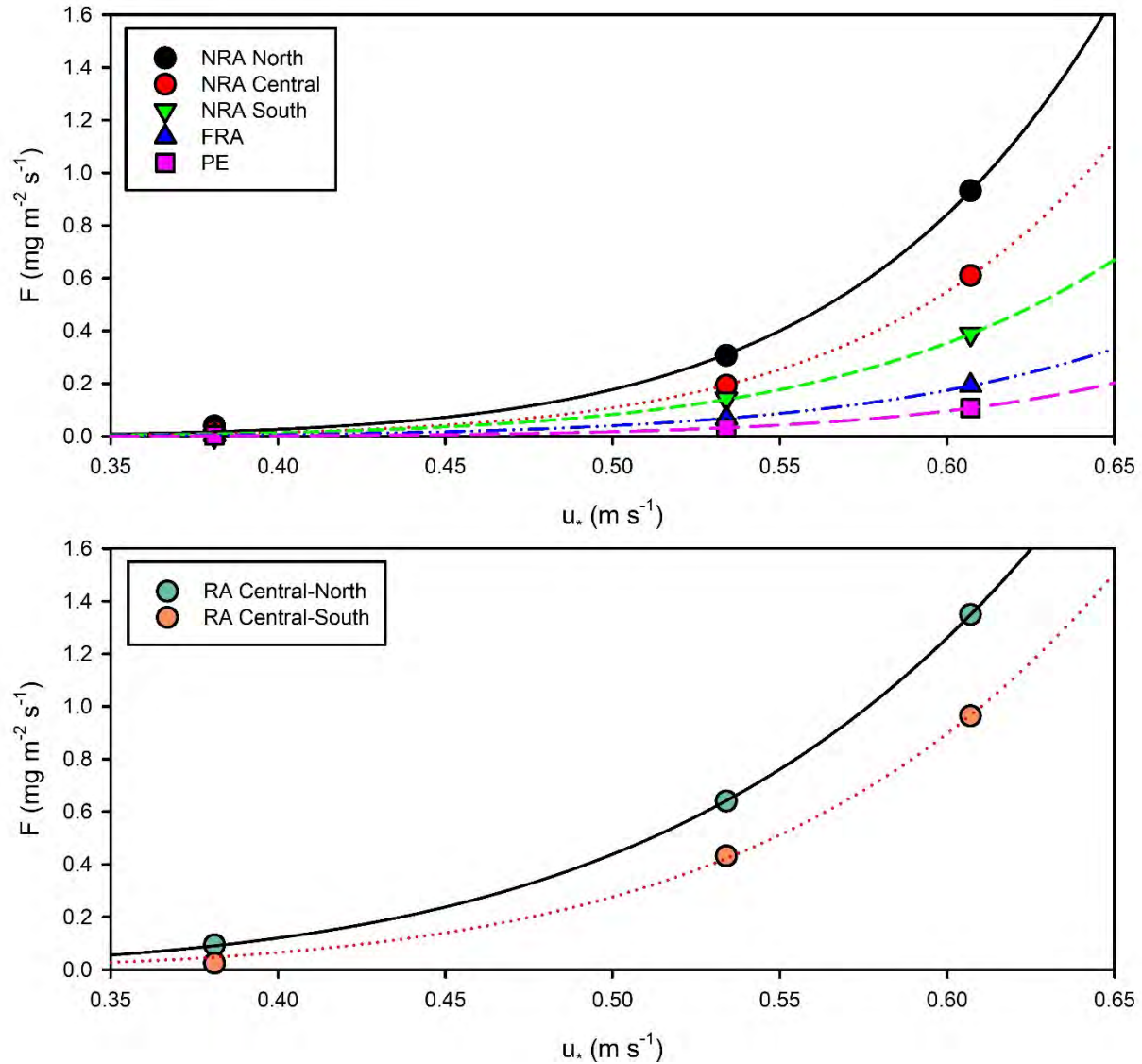


Figure 20: Emissivity relations for various zones in future modeling scenarios. Refer to Table 4 for details.

As mentioned previously, the Seasonal Exclusion areas require separate treatment because they are neither exclusively 'riding' nor 'non-riding.' There are two sub-zones within the SE area: (1) the narrow beach strip that lies to the west of the FRA; and (2) two access corridors that divide parts of the FRA and another access corridor between the PE and FRA (see Figure 16). The beach strip is closed to OHV use between March 1 and September 30, but accessible for OHV recreational use between October 1 and February 28. The corridors are managed similarly with the exception of the eastern entry areas that provide year-around rider access to toilet facilities.

A total of 69 PI-SWERL measurements were taken along the beach and corridor areas on September 30, 2022, which is at the end of exclusion period. Thus, these measurements are thought to be characteristic of the sand surface at the conclusion of the non-riding season after a

7-month period of continual adjustment. Some of these measurements were made in the year-around entry areas to the toilets and therefore are considered to be characteristic of the riding period. Several other measurements were made in corridors where it was noted that there had been recent disturbance of the surface by bulldozers as part of regular park maintenance. Therefore, of the 69 PI-SWRL measurements made in the SE area, 24 are classified as 'riding' whereas 45 are considered to be representative of 'non-riding' conditions. The 'riding' measurements were supplemented with another 34 measurements that were taken in the footprint of the SE area between 2013 and 2019 when OHV riding was allowed all year (i.e., before seasonal closure). These 34 measurements were extracted from the data set used to characterize RA Central-North using a GIS map to locate the relevant points. Table 5 presents the data and power function exponents, whereas Figure 21 shows the curves in graphical form.

Because there is a 'riding' period and a 'non-riding' period, each with different emissivity relations, it is necessary, for the purposes of modeling, to combine these to create a single curve. The simplest approach is to average the median values from both periods for each of the shear velocity increments, and then to develop a third relation based on the average of the medians. The results from this approach are also shown in Table 5 and Figure 21. Alternative approaches to yield a weighted average were explored using relaxation and ramp-up factors in an attempt to quantify the adjustments taking place on the landscape as the surface transitions from a highly emissive surface at the end of the riding period (February 28) to a less emissive surface at the end of the non-riding period (September 30), and back when OHV access is again allowed. However, very little is known about how rapidly these transitions occur and how they are influenced by meteorological conditions. In the end, the results were not that different from the simple averaging approach, lying somewhere in the middle between the two relations defining the riding and non-riding periods, so the simplest averaging approach was adopted.

Table 5: Data used in developing emissivity relations for the Seasonal Exclosure area. Power function coefficients (a, b) are shown at the bottom.

	Riding Affected Period (2013-2022)	Non-Riding Period (Sep 2022)	Average
n =	58	45	2
u* (ms⁻¹)			
0.381	0.049	0.006	0.028
0.534	0.295	0.065	0.180
0.607	0.678	0.200	0.439
E = a(u*)^b			
a	15.875	15.450	13.042
b	6.322	8.709	6.798
r ²	.999	1.000	.999

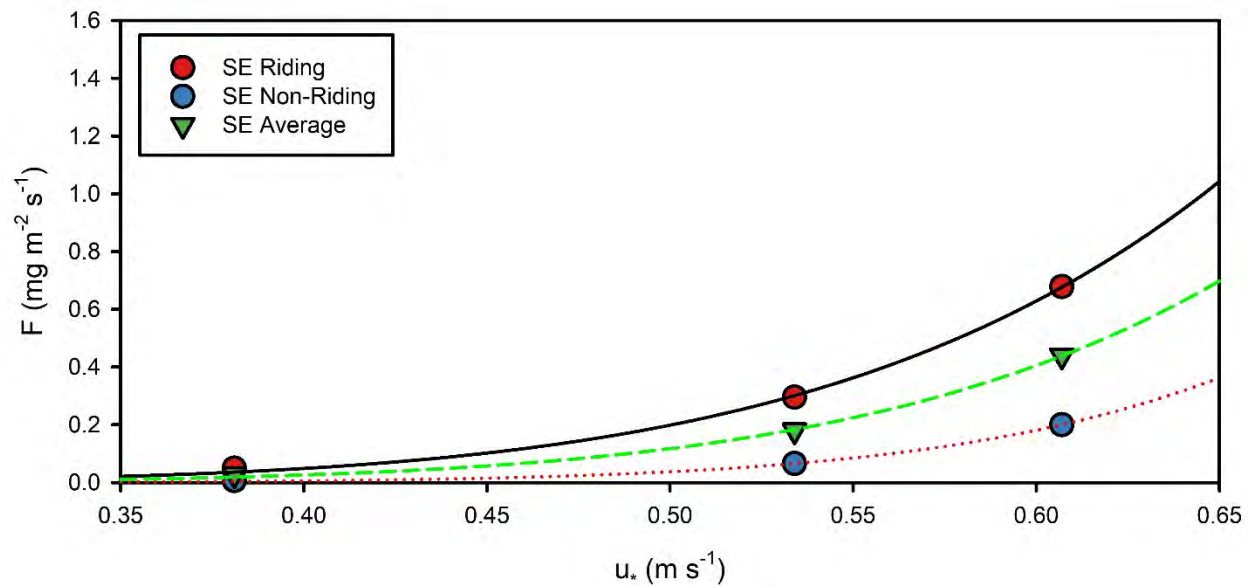


Figure 21: Emissivity relations for the Seasonal Exclusion area. Refer to Table 5 for details.

The pre-disturbance landscape would not have had zones equivalent to the FRA, PE, or SE, and there would have been limited influence from OHV riding. Therefore, **for the purposes of defining emissivity relations that characterize the Pre-Disturbance (1939) surface, it is recommended that all PI-SWRL measurements (2013-2022) from the NRA North zone be pooled to define a single power relation that applies to that zone only, and similarly so for the NRA Central zone and NRA South zone.** The rationale for not including any of the measurements from the FRA, PE, and SE areas is that these are all 'managed' landscapes in one way or another. For example, the FRA has six different treatments (species, planting densities, surface pre-treatments) and it is not known with any certainty how these varying surfaces, which are in continual stages of evolution, relate to a pre-disturbance condition. There is evidence from the air-photo reconstruction of the 1939 surface that foredunes were a component of the landscape, but given limited resolution and exposure in this early imagery, it is difficult to identify the exact extent of these areas, and there is no information on plant densities or heights from that time, which are critical factors in quantifying the sand-trapping and dust-retention characteristics of these former vegetated surfaces. More monitoring is needed over the next decade to better understand how the FRA will evolve and how the emissions characteristics will change. This does not undermine the use of the 2022 PI-SWRL measurements for the purposes of modeling the current (2023) landscape.

Similarly, the PE surface is a somewhat recently adjusted surface that is also managed for bird habitat, including the introduction of large woody debris that has, combined with emergent vegetation, lead to the development of appreciable incipient nebkha dune cover. One can imagine similar surfaces having evolved in the pre-disturbance environment after a major storm event that caused coastal inundation and erosion, for example. But it would likely still take a decade or longer for a disturbed sand surface to return to a completely natural state. This would involve multiple meteorological events across a range of speeds, directions, temperatures, and moisture conditions that serve to reorganize the sand surface in terms of texture, vegetation

cover, and dune development, but not yet reaching the stage of foredune development with mature plant communities. Thus, there is uncertainty as to how the measurements taken in the PE in 2022 might apply to a pre-disturbance landscape. The SE surface clearly has no counterpart in a pre-disturbance landscape given that it is seasonally subject to OHV disturbance, so these measurements will also not be used to characterize the pre-disturbance landscape.

Finally, all vegetated areas are treated identically in the current DRI model, with zero dust emissions, and it is recommended that this practice be followed in the near future for both the pre-disturbance and current conditions scenarios. This assumption is somewhat simplistic because there are areas in the ODSVRA that are densely vegetated (for which the assumption is clearly valid) and other areas that are sparsely vegetated or recently planted (for which there is likely to be some dust emission from open sand surfaces, especially under extreme wind events). However, in most of the managed areas where recent planting has taken place (with the exception of the FRA), it has been standard practice to spread straw on the surface, which prevents dust emissions for several years until the plants spread. In addition, there is relatively little understanding of how different plant species and assemblages prevent saltation and dust emissions even though it is generally appreciated that there is a dependency on plant height and stem density. Thus, given current uncertainty surrounding this issue, invoking a more complex dust emission scheme that is a function of plant characteristics across the treated surfaces is not yet viable nor recommended. The most expedient approach is to ensure that the shapefiles defining the vegetated areas truly reflect the geometry of the areas that are 'heavily' vegetated (with dense, mature vegetation covers or straw treatments with recently planted areas). These may not always follow enclosure fence lines, and the shapefiles will need to be continually updated, ideally using the UAS-derived surface cover maps.

CONCLUDING REMARKS

In respect of PM₁₀ emissions within the ODSVRA, Section 3.c. of the revised Stipulated Order of Abatement (SOA), filed on October 18, 2022, states that,

"Emissions shall be calculated using...a representative emissivity grid derived from PI-SWERL measurements as recommended by the SAG, ..."

In response to the second draft 2022 ARWP, the APCD's Conditional Approval letter (October 21, 2022) states that,

"Emission calculations in the 2023 ARWP shall be based on assumptions recommended by the SAG and preapproved, in writing, by the APCO."

The purpose of this memo is to satisfy both these requirements by presenting a detailed analysis of the PI-SWERL data collected to date and offer several recommendations that follow therefrom.

Appendix 1. Linear Theil Regression Analysis

Linear Theil regression (Theil, 1950; Wilcox, 2005) was performed on the PI-SWERL data to evaluate changes in emissivity over time. Theil regression is a non-parametric method that fits a line to data by computing the median of the slopes of all the possible combinations of pairs of data points. An advantage of the Theil regression is its insensitivity to outliers. The regression was performed on PI-SWERL data from 2013 through 2022, aggregated by percentile for both riding and non-riding areas (see Figures 1 and 3, respectively). Kendall tau statistics were used to determine statistical significance; a statistically significant trend was assumed at the 99% significance level ($p < 0.01$), meaning there is a 99% chance that the slope was not due to random chance.

Results for the three PI-SWERL speeds are shown in Tables A1 and A2 for the riding and non-riding areas, respectively. None of the trends were statistically significant ($p < 0.01$).

Table A1. Regression results for temporal trend analysis for PI-SWERL data for the **riding areas**. The percentile corresponds to the data distribution, the slope ($\text{mg m}^{-2} \text{s}^{-1} \text{day}^{-1}$) corresponds to data from 2013 through 2022, and p is the statistical significance. Three speeds (u^* is shear velocity) were used in the PI-SWERL instrument.

	$u^* = 0.381 \text{ ms}^{-1}$		$u^* = 0.534 \text{ ms}^{-1}$		$u^* = 0.607 \text{ ms}^{-1}$	
Percentile	slope	p	slope	p	slope	p
5	3.8E-07	0.02	-1.3E-05	1.00	-3.0E-05	0.62
10	4.1E-07	0.09	-4.3E-05	0.46	-3.5E-05	0.46
25	-4.5E-06	0.71	-5.5E-05	0.22	-4.3E-05	0.46
50	-1.7E-05	0.32	-1.1E-04	0.32	-2.2E-04	0.14
75	-5.5E-05	0.32	-1.9E-04	0.22	-2.2E-04	0.32
90	-1.0E-04	0.05	-2.8E-04	0.08	-5.2E-04	0.14
95	-1.3E-04	0.05	-3.7E-04	0.22	-3.2E-04	0.46

Table A2. Regression results for temporal trend analysis for PI-SWERL data for the **non-riding areas**. The percentile corresponds to the data distribution, the slope ($\text{mg m}^{-2} \text{s}^{-1} \text{day}^{-1}$) corresponds to data from 2013 through 2019, and p is the statistical significance. Three speeds (u^* is shear velocity) were used in the PI-SWERL instrument.

	$u^* = 0.381 \text{ ms}^{-1}$		$u^* = 0.534 \text{ ms}^{-1}$		$u^* = 0.607 \text{ ms}^{-1}$	
Percentile	slope	p	slope	p	slope	p
5	0	0.71	-2.5E-05	0.05	-5.7E-05	0.29
10	4.4E-07	0.64	-2.6E-05	0.02	-8.4E-05	0.10
25	-2.5E-06	0.54	-3.3E-05	0.05	-9.8E-05	0.05
50	-5.9E-06	0.29	-4.3E-05	0.18	-1.8E-04	0.18
75	-5.9E-06	0.18	-7.0E-05	0.18	-2.0E-04	0.29
90	-1.5E-06	0.88	-6.7E-06	0.65	-9.0E-05	0.45
95	3.2E-06	0.65	-5.2E-05	0.65	7.3E-05	0.65

References

- Etyemezian, V., Nikolich, G., Ahonen, S., Pitchford, M., Sweeney, M., Purcell, R., Gillies, J., Kuhns, H., 2007. The Portable In-Situ Wind EROsion Laboratory (PI-SWERL): a new method to measure PM10 windblown dust properties and potential for emissions. **Atmos. Environ.** 41 (18), 3789–3796. <https://doi.org/10.1016/j.atmosenv.2007.01.018>.)
- Mejia, J.F., Gillies, J.A., Etyemezian, V., Glick, R., 2019, A very-high resolution (20m) measurement-based dust emissions and dispersion modeling approach for the Oceano Dunes, California, **Atmospheric Environment** 218 (2019) 116977. <https://doi.org/10.1016/j.atmosenv.2019.116977>.
- Thiel, H., 1950, A rank-invariant method of linear and polynomial regression analysis, **Proc. Kon. Ned. Akad. V. Wetensch. A.** 53, 386-392, 521-525, 1397-1412.
- Wilcox, R., 2005, "10.2 Theil–Sen Estimator", **Introduction to Robust Estimation and Hypothesis Testing**, Academic Press, pp. 423–427, [ISBN 978-0-12-751542-7](https://doi.org/10.1016/B978-0-12-751542-7))

Oceano Dunes State Vehicular Recreation Area Dust Control Program

DRAFT 2023 Annual Report and Work Plan

ATTACHMENT 07

In-Park Increments of Progress, TPM₁₀:TPWD, April to September 2022

(DRI Document)

THIS PAGE WAS INTENTIONALLY LEFT BLANK.

In-Park Increments of Progress, TPM10:TPWD, April to September 2022

State Parks has installed seasonal and temporary meteorological and PM₁₀ monitoring sites at ODSVRA since the SLOAPCD first began evaluating PM₁₀ emissions on the Nipomo Mesa as part of its Phase 1 and Phase 2 studies. The purpose of these instruments is to help assess individual project effectiveness and update and refine meteorological inputs needed for the SOA's air quality modeling.

State Parks' S1 meteorological tower (located near marker post 6) was installed in June 2010 and continues to operate and support Dust Control Program activities. State Parks' meteorological and PM₁₀ monitoring network varies slightly from year to year depending on specific goals, objectives, and dust control measures identified in the ARWP cycle. From approximately April 1, 2022, to October 31, 2022, State Parks maintained the monitoring network shown in Figure 1, including:

- Six (6) foredune meteorological and PM monitoring sites
- Fifteen (15) other meteorological and PM monitoring sites located throughout and downwind of ODSVRA
- One (1) sonic detection and ranging (SODAR) instrument station (supported by UCSB).

State Parks installed the same monitoring network beginning in April 2022 and maintained this network through approximately October 2022. Typically, the 15 monitoring sites each consist of a suite of instruments affixed to a tripod, platform, or tower located 3.5 to 10 m AGL. Instruments collect wind speed and wind direction (using two-dimensional sonic anemometry), ambient temperature, relative humidity (RH), and barometric pressure. A Sensit instrument is also deployed at/near the ground level to measure saltation activity in active sand transport areas. The SODAR instrument station (originally installed in May 2019, removed March 2023) records three-dimensional velocity vector data from approximately 40 m to 200 m AGL.

The particulate matter at each station is measured using a MetOne 212-2 Particle Profiler that measures particle counts in eight size (geometric mean diameter in micrometers, or μm) bins (0.39 μm , 0.59 μm , 0.84 μm , 1.41 μm , 2.24 μm , 3.53 μm , 7.07 μm , and 10+ μm) per sampled flow volume using an optically based measurement system. These particle count bins are used to derive a PM₁₀ concentration on a minute and hourly basis. The PM₁₀ concentration is derived from environmentally controlled and field calibration relationships between particle count data collected by the Particle Profiler and mass-based PM₁₀ concentration data collected by an EPA Federal Equivalent Method (FEM) Beta Attenuation Mass (BAM) PM₁₀ monitor. This calibration ensures that each MetOne 212-2 Particle Profiler instrument has a specific calibration relationship to provide the best estimate of PM₁₀ during deployment at ODSVRA.

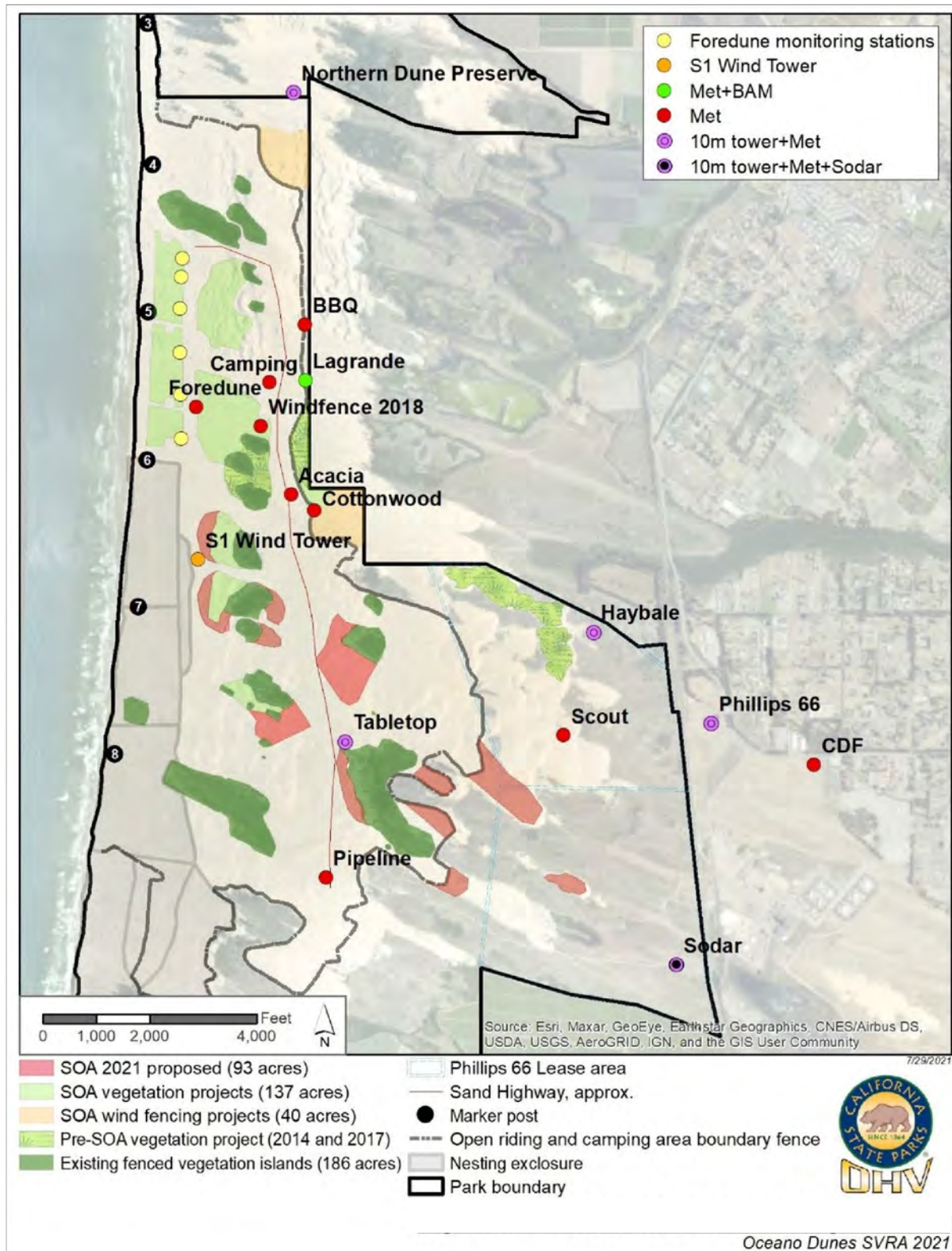


Figure 1. Map showing the locations monitoring stations.

The MetOne 212-2 units deployed in 2022 were calibrated by DRI using the same methodology employed for previous monitoring efforts. The units were first calibrated against a FEM BAM PM₁₀ monitor in an environmental chamber prior to field placement. Some units were then collocated with an in-Park FEM BAM to check if environmentally controlled calibration relationships are, or are not, changing following field deployment. If a significant change is observed, the in-Park derived calibration will be used to convert the PM₁₀ value to BAM-equivalent PM₁₀. All units were brought back to DRI in the fall of 2022 to derive post-field deployment relations to determine if a relation has drifted significantly from the pre-deployment one and to assess the performance specifications (e.g., flow rate).

The key purpose of the monitoring network is to collect PM₁₀ and meteorological data to provide a means to evaluate the relation between wind conditions and PM₁₀ during the primary dust-season (April-September). This annual characterization allows for the assessment of changes in the PM₁₀ levels interior and downwind of the ODSVRA open riding and camping area as it relates to meteorology and dust control projects.

The total wind power density (TWPd) as a function of month for each in-Park station is shown in Fig. 2. This figure shows that there was an abrupt change in the TWPd transitioning from spring (April-June) to summer (July-September) 2022. This was also observed in 2021 (Figure 2). Figure 2 shows as well that TWPd reached much greater values at some stations than was observed at the same stations in 2021.

The meteorological and PM monitoring stations provide data to evaluate the relation between wind and PM₁₀ concentrations across the domain of the ODSVRA and at key points downwind (e.g., Phillips 66, SODAR, and CDF sites) and through time. To quantify WPD at each monitoring location the hourly mean values are summed for the hours identified where the PM₁₀ (MetOne 212-BAM corrected, using chamber-based calibration relationships) concentrations are paired with the station-measured wind speed. To define the relation between monthly TPM₁₀ and TWPd for the in-Park stations in 2021, we calculated mean hourly PM₁₀ and mean hourly wind speed measured at each in-Park monitoring station. To define the relation between monthly TPM₁₀ and TWPd for the stations downwind of the riding areas, we calculated mean hourly PM₁₀ and mean hourly wind speed measured at the respective heights of the anemometers above-ground-level (AGL) for each monitoring station.

To set the threshold of WPD for the summation calculation we first examined the relation between average PM₁₀ and mean wind speed for monitoring stations spanning the north-south dimension of the in-Park network (DP, Cottonwood, and Pipeline) in 2022. Similar to 2021, concentrations of PM₁₀ begin to increase when the 3.5 m AGL wind speed exceeds 5 m s⁻¹, which was typical for most stations. We use 5.5 m s⁻¹ mean hourly wind speed to set the lower limit for WPD (102 W m⁻²) for the summations of total WPD (TWPd, W m⁻²) and total PM₁₀ (TPM₁₀, µg m⁻³) for each month. As the in-Park stations are surrounded by sand that can be mobilized by the wind, no wind direction filter was applied. For the stations out of the Park and downwind of riding areas the data were filtered by the wind direction 236° - 325° to ensure that the PM was originating from the direction of the ODSVRA. It must be noted that for these stations the PM is being actively dispersed by the wind and there are no local contributions of PM by the saltation process.

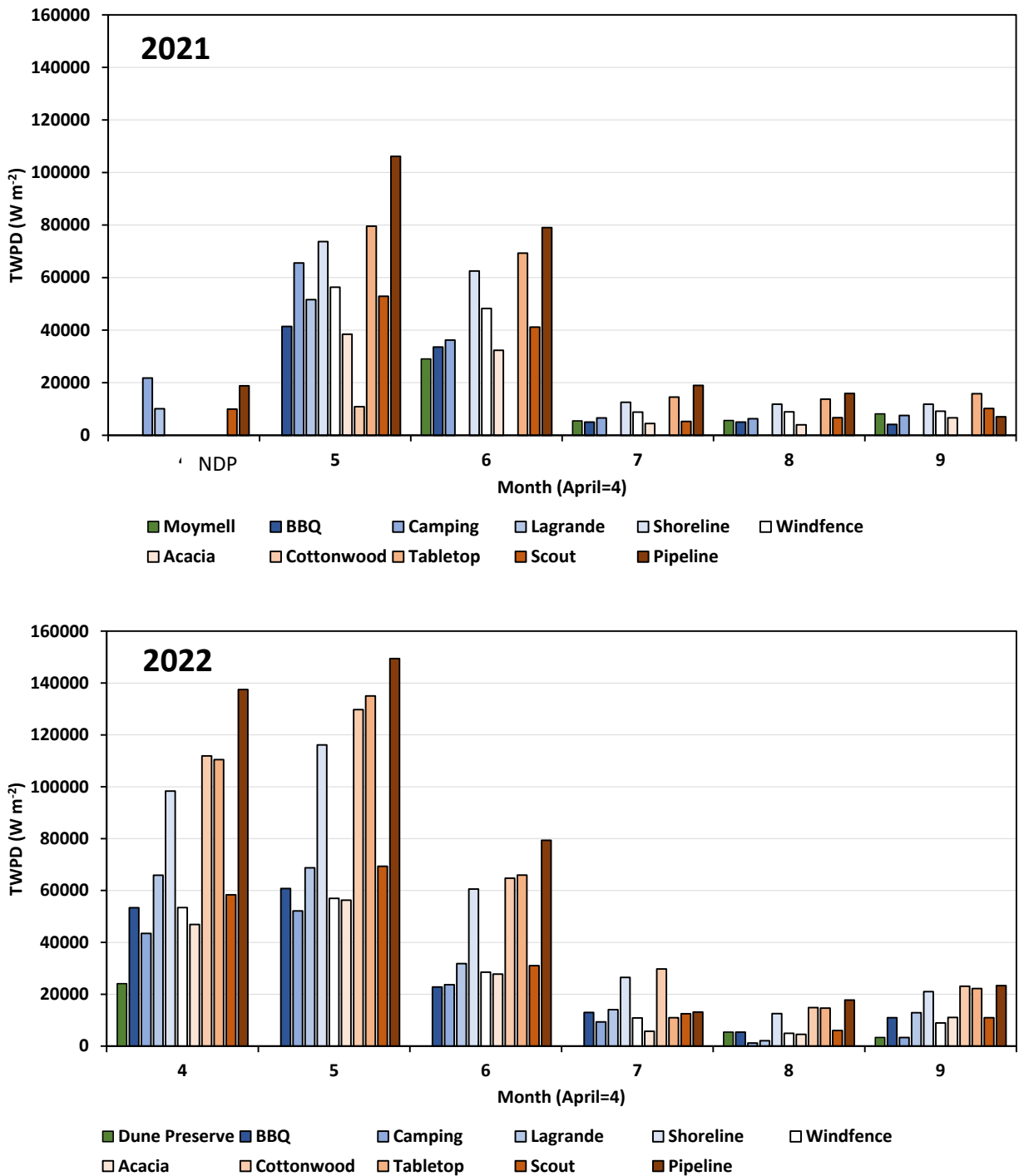


Figure 2. The TWPDP for the in-Park stations for available data from April to September 2021 (top graph) and April to September 2022 (bottom graph).

Examples of relations between TPM₁₀ and TWPD for four in-Park sites that span the north-south dimension of the monitoring network are shown in Figure 3 for 2022. As in previous years monthly TPM₁₀ is strongly correlated with monthly TWPD for all network stations.

The ratio of TPM₁₀:TWPD ($\mu\text{g W}^{-1} \text{m}^{-1}$) serves as a metric to evaluate how the dust emission system is changed by changes to or in the landscape. With no changes to the surface where the emissions originate from, this ratio will reflect the efficiency of the wind and saltation system to produce PM₁₀ for the prevailing environmental conditions during the period of interest and should remain stable if the environmental conditions remain stable. If, however, the surface from which the emissions are originating from is changing, for example, by removal of the PM₁₀ source material or coarsening of the surface sand (i.e., increasing mean grain diameter), the ratio should diminish as dust production by saltation processes becomes less efficient in producing PM₁₀ dust. Conversely, if the ratio increases through time, it indicates that the source area is producing greater amounts of PM₁₀ for similar conditions of WPD, suggesting that the sand is being enriched in PM₁₀ source material. There is a limit to the explanatory power of this ratio, which is that if winds are at, or close to, the designated threshold speed either at the monitoring location or in the source area for a large part of the record, the value becomes unstable due to a potential paucity of data but also because as wind speed diminishes the strength of the coupling between the wind and the saltation-generated PM₁₀ weakens and is subject to influence of PM₁₀ from other sources.

The change in TPM₁₀:TWPD for the in-Park and out-of-Park stations for available data from April to September 2022 is shown Figure 4. Between 2021 and 2022, the mean seasonal TPM₁₀:TWPD ratio for the in-Park stations decreased for at least six of the stations (DP, BBQ, Shoreline, Windfence, Tabletop and Scout) while increasing for at least two, Camping and Lagrande. Data are missing for Cottonwood in 2021 and Pipeline in 2022 due to instrument failures. For the out-of-Park stations Haybale, CDF, and P66 do not appear to have changed between 2021 and 2022 based on the overlap of the standard deviation of the mean values, with only SODAR being lower in 2022 than 2021.

To compare 2022 with 2021 in terms of mean TPM₁₀:TWPD across the riding area of ODSVRA and through time, the mean normalized TPM₁₀:TWPD was calculated by dividing each month's mean value by the mean value for September (Figure 5). The variability of the normalized TPM₁₀:TWPD ratio across the in-Park stations appears to be much greater in 2022 than in 2021. In 2022, however, the differences among the mean normalized TPM₁₀:TWPD ratios for the months April to August are less than what was observed in 2021.

The wind speed and PM₁₀ data for the network stations indicate that the monthly TWPD increased to much higher values in the spring of 2022 than observed in 2021. Similar to the results described in Section 2.2.2.2, the in-Park stations indicate that even though the TWPD values were much greater than in 2021, the production of PM₁₀ in 2022 was lower during the April/May to September period. These data support the observation that the trend of decreasing TPM₁₀:TWPD as a function of increasing acres of dust control (Section 2.2.2.2 Figures 4 and 5) as the majority of stations within the ODSVRA riding area also show a reduction in their TPM₁₀:TWPD ratio from 2021 to 2022.

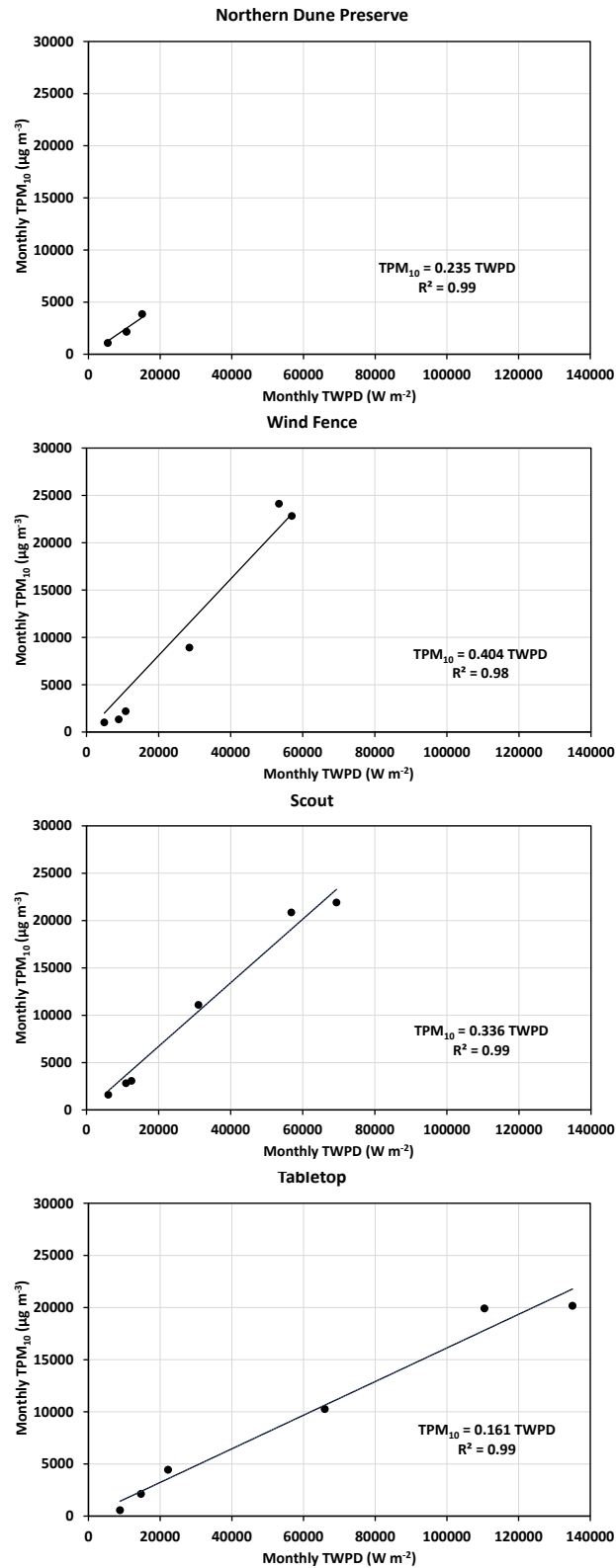


Figure 3. Examples of the relation between monthly TPM₁₀ and monthly TWPD for four in-Park stations covering the north to south span of station locations for the months April to September 2022.

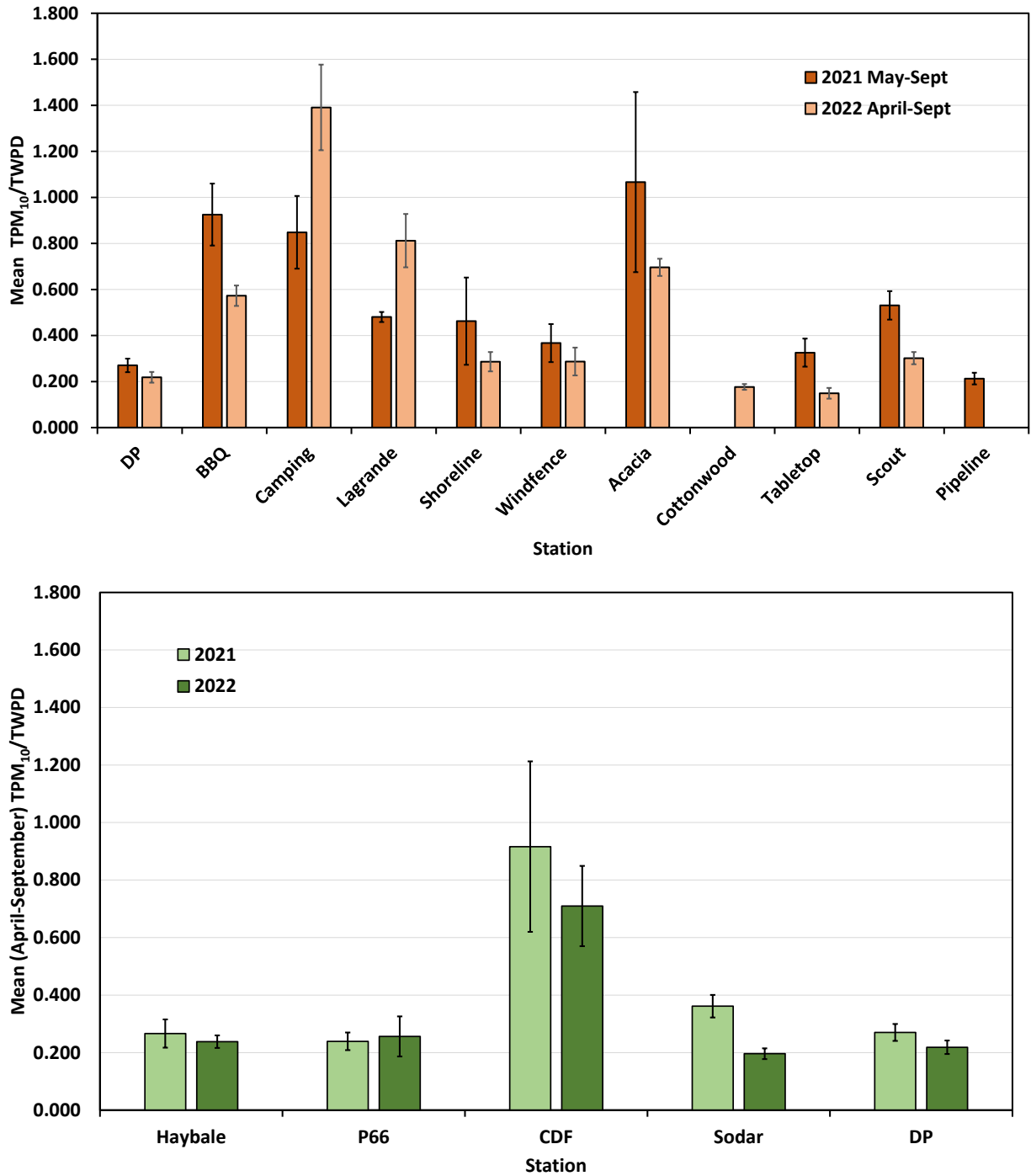


Figure 4. Mean seasonal (April-September) TPM₁₀:TPWD values for 2021 and 2022, for the in-Park (top panel) and out-of-park stations (bottom panel).

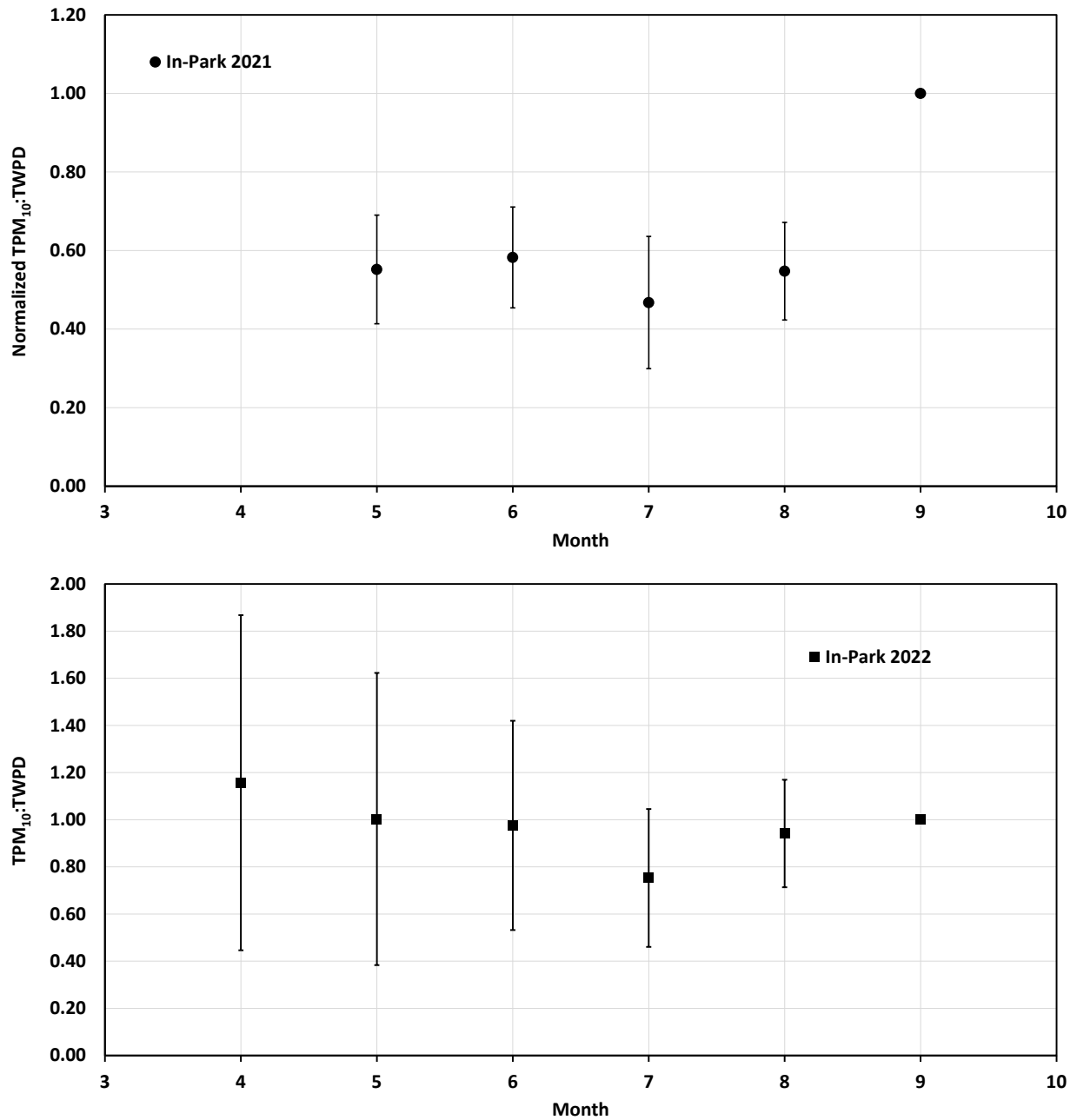


Figure 5. Normalized monthly mean TPM₁₀:TPWD for the in-Park stations in 2021 (top panel) and 2022 (Bottom panel). Error bars represent the standard deviation of the mean normalized ratio value for the 11 in-Park stations.

Oceano Dunes State Vehicular Recreation Area Dust Control Program

DRAFT 2023 Annual Report and Work Plan

ATTACHMENT 08

**Summary of Vegetation Monitoring of Restoration Sites at ODSVRA (2022)
(State Parks ARWP Work Product)**

THIS PAGE WAS INTENTIONALLY LEFT BLANK.

Summary of Vegetation Monitoring of Restoration Sites at ODSVRA

Line Intercept Transect Sampling

Methods

Line Intercept method (Line intercept: % cover = distance a+b+c+d+e+f / total transect length, where a, b, c, etc. are the intercept lengths of vegetation canopy) was used to estimate percent cover of species within each project area.

For this assessment both foredune and back dune project areas were sampled in 2022 and reference sites were sampled in previous years. Reference sites were selected in areas that had been closed to vehicular activity for at least 20 years and had not been subject to restoration plantings in the past. Within back dune habitats, early succession communities (early seral) and climax communities (late seral) can vary considerably in species composition and percent cover. For this reason, both early seral and late seral reference sites were sampled for comparison.

Within each foredune project area and reference site, a total of four transects of 30 meters each were sampled (the same transect lines were also surveyed in 2020, 2021, and 2022). Within each back dune project area and reference site, a total of three transects of 30 meters each were sampled. In 2022, the project areas that were surveyed included the 48-Acre Fore dune, planted February 2020; Bigfoot (western), planted January 2020; Bigfoot (eastern), planted in February; 2021; and Pawprint, planted January 2018.

Starting points for the transect lines were randomly selected within each project area using GIS software. Originally, three transect lines in each project area were randomly selected from the eight cardinal and intermediate directions (i.e. N, NE, E, SE, S, SW, W, and NW). In 2022, within the 48-Acre Fore dune Project Area, a fourth transect line was added in each treatment area running in the direction of the prevailing wind.

A measuring tape was run along the transect and secured with wooden stakes. As the vegetation canopy intersected the line, the species was noted on the datasheet along with the beginning and ending measurements of the canopy under “Start” and “Stop”. When the canopies of two different species overlapped, each species was documented separately as two different canopies. A closed canopy for a given species was assumed until gaps in vegetation exceed the width of 5 centimeters. All dead woody vegetation was included separately and noted as “Dead” unless it was clearly the result of seasonal dieback of a perennial plant that was still viable.

Once each 30-meter transect was surveyed, a reconnaissance level survey was conducted of the project area and any additional species observed were noted.

Results

48-acre Fore dune Project

In 2022, after the third growing season for the project area, none of the treatment areas met the vegetation cover of the reference site at 23.03% vegetation cover and only one of the six treatment areas (Area 6) met the species richness (i.e. the number of different species) of the reference site with at least 10 species represented. An increase in vegetation cover was documented in three of the six

treatment areas with Area 3 and Area 4 both showing a slight decrease in cover. Area 3 (Native Seed & Grain Seed) decreased from 12.3% cover in 2021 to 10.1% cover in 2022 and Area 4 (Low Density Nodes) decreased from 5.7% cover in 2021 to 5.1% cover in 2022. Area 1, the control, showed no change in cover. The treatment area that saw the highest percent cover was Area 6 (Parks Classic) with 13.8% cover (up from 12.7% the previous year) followed closely by Area 3 with 10.1% cover. Both Area 5 and Area 6 showed the highest level of species richness with 9 and 10 species represented respectively in each area. The plant cover was highly variable between transects in all treatment areas due to the clustered pattern of the vegetation. (Refer to Table 1 and Figure 1).

Table 1. Table of results from the 48 Acre Foredune Restoration Project line intercept transect sampling.

Foredune Restoration Project Vegetation Assessment							
*Non-native species P=Present within Area but not on transect line	Area 1 Control	Area 2 Native Seed	Area 3 Native Seed & Grain Seed	Area 4 Low Density Nodes	Area 5 High Density Nodes	Area 6 Parks Classic	Reference North Oso Flaco Foredune
Age of Planting (years)	2.5	2.5	2.5	2.5	2.5	2.5	-
Species Richness	2	3	4	7	9	10	10
Transect 1	0.0%	21.0%	0.0%	5.5%	16.9%	13.9%	6.2%
Transect 2	0.0%	0.0%	24.8%	8.6%	3.8%	8.2%	60.1%
Transect 3	0.0%	0.0%	3.1%	6.5%	0.7%	21.4%	12.1%
Transect 4	0.0%	0.0%	12.6%	0.0%	4.3%	11.7%	13.8%
Mean Percent Cover	0.0%	5.3%	10.1%	5.1%	6.4%	13.8%	23.0%
Species	Mean Percent Cover						
<i>Abronia maritima</i>	-	4.6%	8.7%	1.7%	2.7%	4.3%	15.5%
<i>Ambrosia chamissonis</i>	p	p	2.8%	2.4%	3.1%	5.1%	5.7%
* <i>Cakile maritima</i>	p	0.7%	p	p	p	0.1%	3.2%
* <i>Carpobrotus sp.</i>	-	-	-	-	-	-	1.4%
<i>Malicothrix incana</i>	-	-	-	p	0.2%	0.2%	0.3%
<i>Calestegia soldanella</i>	-	-	-	-	-	-	0.1%
<i>Camissoniopsis cheiranthifolia</i>	-	-	-	p	0.2%	2.8%	0.02%
<i>Abronia latifolia</i>	-	-	p	p	0.4%	p	p
<i>Erigeron blochmaniae</i>	-	-	-	-	-	-	p
<i>Senecio blochmaniae</i>	-	-	-	-	-	-	p
<i>Atriplex leucopylla</i>	-	-	-	0.9%	p	p	-
<i>Eriophyllum staechadifolium</i>	-	-	-	-	p	0.3%	-
<i>Erysimum suffrutescens</i>	-	-	-	-	-	p	-
<i>Fragaria chiloensis</i>	-	-	-	-	-	p	-
<i>Monardella undulata crispa</i>	-	-	-	-	p	-	-
Dead Vegetation	-	-	0.11%	0.32%	-	0.90%	-

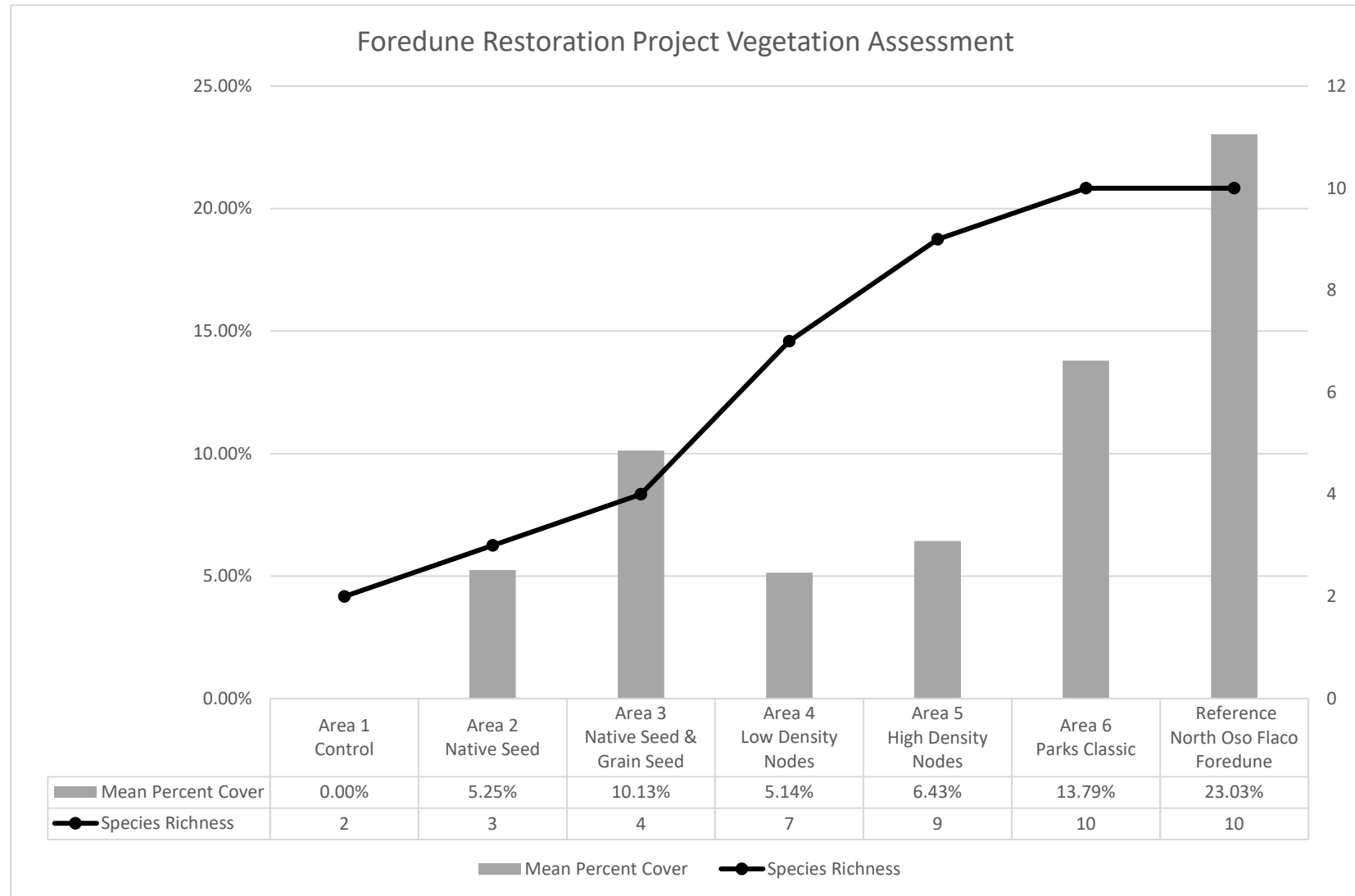


Figure 1. Vegetation composition in 48 Acre Foredune project areas compared to reference site. Four 30-meter transects were sampled in each of the Foredune areas and Reference Site.

Comparison of Line Intercept Transect Sampling Method and Results from Independent Studies

State Parks methods were designed to monitor the establishment of vegetation cover and species richness within specific project areas. Two recent and independent reports also evaluated vegetation cover within the ODSVRA using aerial imagery to analyze total vegetation cover, each using different imagery sources. Both studies were used to cross-reference the State Parks results. These reports include:

UCSB Historical Vegetation Cover Change Analysis (1930-2020) within the Oceano Dunes SVRA" (N. Swet, Z. Hilgendorf, I. Walker, December 28, 2021). Published as Attachment 07-04 in the 2022 ARWP

Hilgendorf, Z., Turner, C, Walker, I.J. UCSB-ASU 2020-2021 ODSVRA Foredune Restoration UAS Survey Report. 37p. Produced for CDPR-ODSVRA and published as Attachment 8 in the 2021 ARWP.

The methods used by Hilgendorf et al., 2021 were continued in subsequent seasons and the results from those surveys are included in Table 2.

The aerial imagery analysis of the North Oso Flaco foredune presented in (Swet et al., 2021) covered the same area as the State Parks transect monitoring reference site in North Oso Flaco and found that vegetation cover ranged from between 24.41% in 2012 and 19.05% in 2020. State Parks vegetation monitoring of the area corroborates these findings with a vegetation cover mean of 23.0% in the fall of 2021. It should be noted that State Parks sampled only four (4) randomly selected 30-meter transects within the area with a high degree of variation between samples (ranging from 6.2% cover to 60.1% cover) and that the aerial imagery analysis looked at the entire area so some variation in the results between the two studies is expected. For the remainder of the study, (Swet et al., 2021) did not analyze project specific areas that are comparable with the State Parks transects so further analysis of their source imagery would need to be conducted to cross-reference their study with State Parks transect monitoring.

In (Hilgendorf et al., 2021) the authors did analyze vegetation cover within specific project areas but limited their analysis to the 48 Acre Foredune Project. A comparison of the two studies can be seen in Table 2 and Figure 2 below. When comparing the results from the State Parks transect monitoring with the results from (Hilgendorf et al., 2021) and their subsequent surveys, it needs to be clarified that the two studies had differing ways of defining vegetation cover and therefore variation in the results is expected. State Parks transect monitoring measured canopy cover, ignoring small gaps between leaves or stems (<5 cm), and included all parts of the vegetation canopy, not only the leaf cover, but also the woody stems, seasonally dormant plants and dead woody vegetation. (Hilgendorf et al., 2021) used 5-band multispectral imagery acquired from uncrewed aerial system (UAS) surveys and Normalized Difference Vegetation Index (NDVI) method to determine vegetation cover. NDVI looks at the differences in reflected near infrared light and red light which in turn is used to determine leaf cover. This is noteworthy because with NDVI method seasonal variations in cover are expected as seasonal changes in the leaf cover occur (i.e., NDVI does not tend to consider live woody stems or dormant vegetation that does not have photosynthesizing leaves). For example, beach primrose is a perennial that actively grows in the early spring but becomes mostly dormant in the fall, leaving woody stems with little leaf cover. With NDVI you would detect high percent cover in February and low percent cover in October but with the transect method plants would be detected in both seasons. This is significant in Treatment 6 because there is a fair amount of beach primrose. This is even more evident with annual species like sea rocket, which in its post season desiccated state would be counted as having cover in the

transect method. This seasonal fluctuation in leaf cover may also account for the reduction in cover in the UAS surveys in some the treatment areas from October to February and then back up in the following October. In the back dunes, seasonal changes using NDVI are very apparent in the willow thickets within the vegetation islands which drop their leaves in the winter. For these reasons, it is expected that the results of the two studies would vary, specifically when data was collected in different seasons.

In general, State Parks results follow a similar pattern as the UAS surveys with vegetation cover generally increasing over time across all treatment areas except the control (Area 1). One exception is that State Parks showed a slight decrease in cover in both Areas 3 and 4 from 2021 to 2022. In addition, the UAS surveys showed a seasonal decrease in cover in Area 6 from February 2021 (4.02%) to October 2021 (3.54%) However, in subsequent seasons cover increased in Area 3 and by February 2023 it had reached 14.83%. Seasonal decreases in cover were also seen from October 2022 to February 2023 in Areas 1, 2, 3 and 4. When comparing results from the most recent surveys of each method, the rankings in cover varied, however, the differences in cover for each Area was less variable. Most notably in the Fall of 2022 State Parks and the UAS surveys showed vegetation cover at similar levels in Area 1 (0% and 0.26%), Area 3 (10.13% and 11.47%), Area 4 (5.14% and 6.03%), and Area 6 (13.79% and 14.82%), However, Area 2 (5.25% and 3.45 %) and Area 5 (6.43 % and 9.57%) showed greater difference when comparing the two methods. This inconsistency is likely a result of the State Parks method having a small sample size and a high degree of variability in cover between transects. This is apparent in the wide range of percent cover in the samples compared to the mean. For example, in 2022 Area 2 had a mean of 5.25% and a sample range of 0% cover to 21.0% cover and Area 5 had a mean of 6.4% with a sample range of 0.7% cover to 16.9% cover. Furthermore, because the UAV method does not include non-photosynthetic woody material and the State Parks transect method does, it is expected that the UAV results would show lower percent cover for data collected within the same season.

Table 2. Vegetation cover comparison between State Parks Transect Monitoring and the UCSB/ASU UAS Surveys.

48 Acre Foredune	Area 1	Area 2	Area 3	Area 4	Area 5	Area 6
Fall 2020 - State Parks Transect Monitoring	0.00%	0.10%	4.02%	0.76%	0.40%	3.57%
Oct 2020 - UCSB/ASU UAS Survey	0.02%	0.41%	2.66%	0.87%	1.65%	2.54%
Feb 2021 - UCSB/ASU UAS Survey	0.02%	0.50%	2.66%	1.08%	2.08%	4.02%
Fall 2021 - State Parks Transect Monitoring	0.00%	1.91%	12.31%	5.69%	2.14%	12.66%
Oct 2021 - UCSB/ASU UAS Survey	0.14%	1.85%	4.87%	1.93%	3.63%	3.54%
Feb 2022 - UCSB/ASU UAS Survey	0.08%	1.74%	4.55%	2.24%	4.64%	11.35%
Fall 2022 - State Parks Transect Monitoring	0.00%	5.25%	10.13%	5.14%	6.43%	13.79%
Oct 2022 - UCSB/ASU UAS Survey	0.26%	3.45%	11.47%	6.03%	9.57%	14.82%
Feb 2023 - UCSB/ASU UAS Survey	0.12%	2.68%	8.93%	5.52%	9.66%	14.83%

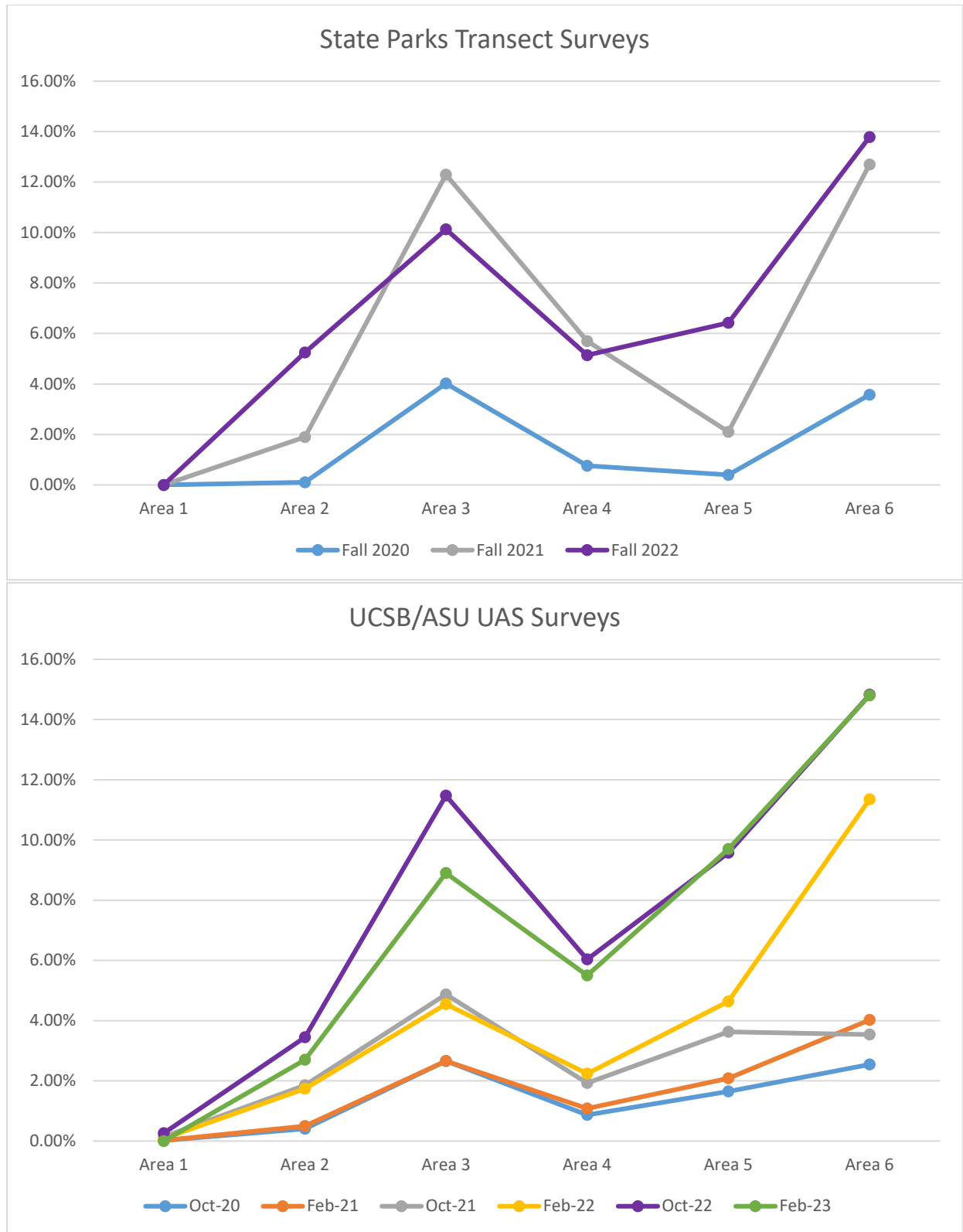


Figure 2. Vegetation cover comparison between State Parks Transect Monitoring and the UCSB/ASU UAS Surveys.

Back Dune Projects

Each of the back dune project areas surveyed showed healthy levels of vegetation cover and showed similar vegetation composition compared to the early seral reference site. Of the 20 native species present within the early seral reference site, the project areas had between 12 and 14 of them and a total richness of between 22 and 26 species. The dominant species within the early seral reference site, *Lupinus chamissonis*, showed similar percent cover in the project areas with 24.6%, 24.0% and 33.9% in each of the project areas and 29.23% in the early seral reference site. All project areas had lower percent cover than both reference sites. However, growth is anticipated to continue and percent cover is anticipated to approach the cover of the reference sites within the upcoming growing seasons. Refer to Table 3 and Figure 3. In addition to transect monitoring, in the fall of 2022, a reconnaissance level survey was conducted of past back dune project areas. Each project area was walked so that full visual coverage of the project area was obtained and all plant species observed were documented. Project areas had a range of 12 to 26 species observed. Refer to Table 4 for results.

Table 3. Table of results from the back dune restoration project line intercept transect sampling.

Back Dune Restoration Project Vegetation Assessment					
*Non-native species P=Present within project area	Bigfoot (western) 2020-VG-04	Bigfoot (eastern) 2021-VG-01	Pawprint 2018-VG-02	Reference - Early Seral	Reference - Late Seral
Age of Planting (years)	2.5	1.5	4.5	-	-
Species Richness	22	26	26	22	15
Transect 1	53.9%	30.1%	20.4%	76.7%	76.3%
Transect 2	18.8%	27.2%	70.5%	63.2%	78.7%
Transect 3	35.6%	32.1%	26.0%	66.4%	76.2%
Mean Percent Cover	36.1%	29.8%	38.9%	68.8%	77.1%
Species					
<i>Abronia maritima</i>	p	-	-	-	-
<i>Abronia umbellata</i>	0.3%	2.1%	p	-	-
<i>Achillea millefolium</i>	0.2%	p	0.2%	4.6%	p
<i>Acmispon glaber</i>	1.0%	0.7%	3.2%	p	3.5%
<i>Acmispon tomentosus</i>	-	p	p	-	-
<i>Ambrosia chamissonis</i>	p	p	p	p	-
<i>Astragalus nuttallii</i>	0.1%	p	p	-	-
<i>Baccharis pilularis</i>	-	-	p	p	0.2%
* <i>Cakile maritima</i>	p	-	-	-	-
<i>Camissoniopsis cheiranthifolia</i>	0.2%	3.1%	p	p	-
<i>Castilleja affinis</i>	-	p	-	p	-
<i>Chenopodium californicum</i>	-	-	-	-	p
<i>Chorizanthe eastwoodiae</i>	-	-	-	p	-
<i>Cirsium occidentale</i>	-	-	-	0.4%	-
* <i>Conicosia pugioniformis</i>	-	-	p	0.9%	0.1%
<i>Corethrogyne filaginifolia</i>	p	p	p	-	6.1%
<i>Croton californica</i>	-	p	-	-	-
<i>Cryptantha clevelandii</i>	-	-	-	p	-

*Non-native species P=Present within project area	Bigfoot (western) 2020-VG-04	Bigfoot (eastern) 2021-VG-01	Pawprint 2018-VG-02	Reference - Early Seral	Reference - Late Seral
<i>*Ehrharta calycina</i>	-	-	-	p	p
<i>Eriastrum densifolium</i>	p	p	p	-	-
<i>Ericameria ericoides</i>	p	0.1%	p	22.6%	57.9%
<i>Erigeron blochmaniae</i>	p	0.3%	p	1.3%	-
<i>Erigeron canadensis</i>	-	-	-	-	-
<i>Eriogonum parvifolium</i>	1.4%	1.1%	1.0%	-	0.03%
<i>Eriophyllum staechadifolium</i>	p	0.2%	0.4%	-	-
<i>Erysimum suffrutescens</i>	0.01%	p	p	p	p
<i>Horkelia cuneata</i>	-	p	p	-	-
<i>Juncus lescurii</i>	-	p	p	-	-
<i>Lupinus chamissonis</i>	24.6%	24.0%	33.9%	29.3%	-
<i>Malicothrix incana</i>	p	-	p	-	-
<i>Monardella undulata crispa</i>	8.6%	p	p	p	-
<i>Mucronea californica</i>	-	p	-	-	-
<i>Oenothera elata</i>	p	-	-	-	-
<i>Phacelia ramosissima</i>	5.9%	1.6%	0.9%	p	-
<i>Pseudognaphalium biolettii</i>	-	-	-	0.1%	p
<i>Pseudognaphalium californicum</i>	-	-	-	p	-
<i>Pseudognaphalium ramosissimum</i>	-	p	p	p	p
<i>Salix lasiolepis</i>	p	p	p	p	-
<i>Senecio blochmaniae</i>	p	p	0.4%	2.5%	p
<i>Silene laciniata</i>	-	-	-	-	p
Dead woody vegetation	0.3%	-	-	12.8%	13.4%

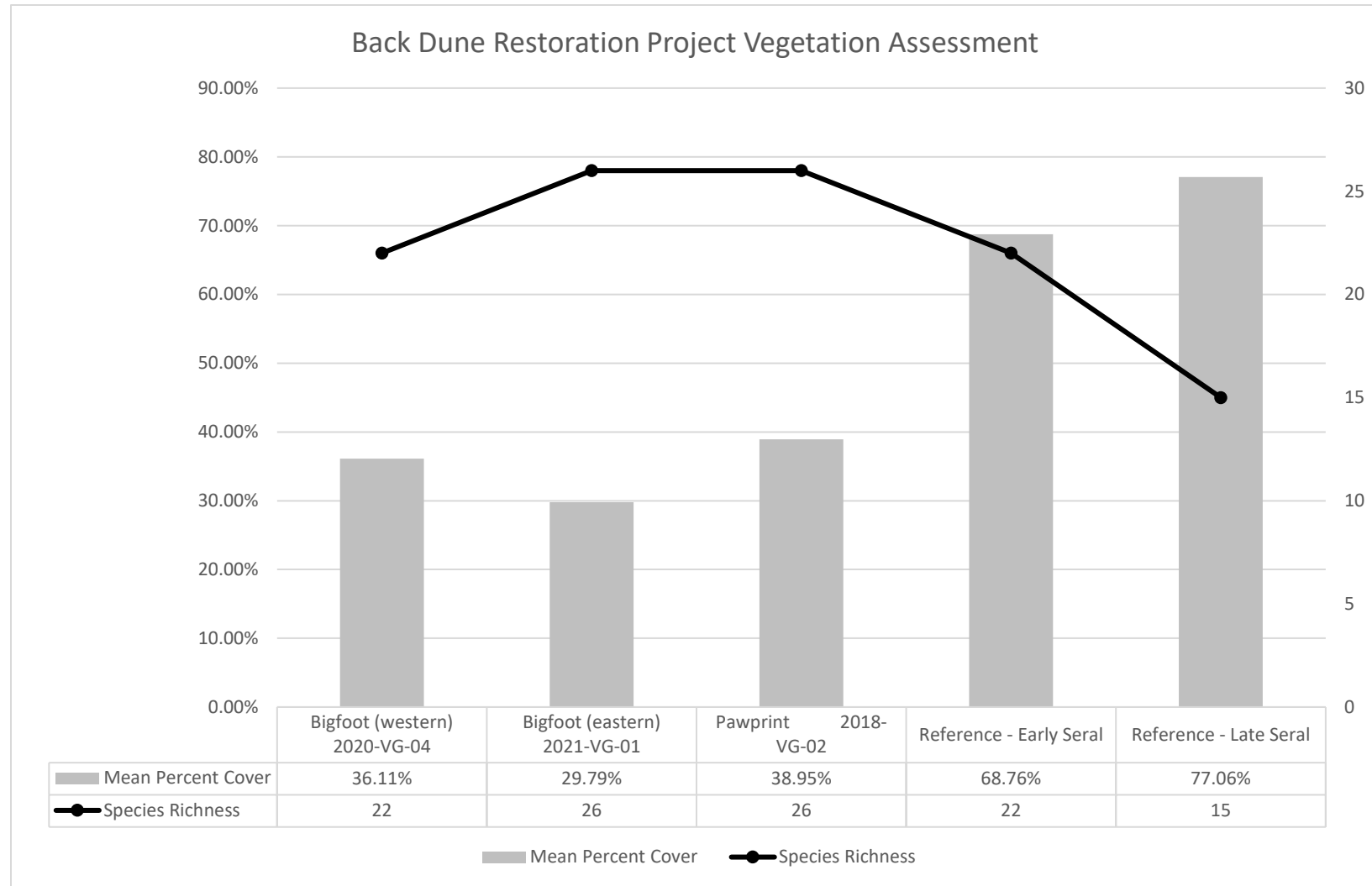


Figure 3. Vegetation composition in back dune project areas compared to reference site. Three 30-meter transects were sampled in each of the back dune areas and reference site.

Table 4. Table of results from the back dune restoration project reconnaissance level species inventory surveys

Restoration Project Follow-up Monitoring - 2022 Species Inventory											
	BBQ Flats 2019- VG- 01	Eucalyptus North 2022-VG- 04	Eucalyptus Tree 2022-VG- 05	Eucalyptus Tree 2021-VG- 03	Bigfoot (Western) 2020-VG- 04	Lagrange Hill 2018-VG- 01	Pawprint 2018-VG- 02	Lagrange Hill 2021- VG-02	Schnauzer 2015-VG-01 2016-VG-01 2017-VG-01	Enigma 2013- VG-01	Crescent 2013- VG-02
Species Richness within Area	22	15	18	21	22	15	26	17	24	12	14
Species (*indicates non-native)	Species Present within Project Area (surveys conducted Sept-Nov 2022)										
<i>Abronia latifolia</i>			X	X							
<i>Abronia maritima</i>	X	X	X		X						
<i>Abronia umbellata</i>	X		X	X	X		X	X	X		
<i>Acmispon glaber</i>	X	X	X	X	X	X	X	X	X		
<i>Acmispon tomentosus</i>							X				
<i>Achillea millefolium</i>	X	X	X	X	X	X	X	X	X	X	X
<i>Ammophila arenaria</i>									X		
<i>Ambrosia chamissonis</i>	X	X	X	X	X	X	X	X		X	X
<i>Artemisia dracunculus</i>									X		
<i>Astragalus nuttallii</i>					X		X				
<i>Baccharis pilularis</i>	X						X		X		
<i>Castilleja affinis</i>	X			X							
<i>Camissoniopsis cheiranthifolia</i>	X	X	X	X	X	X	X	X		X	
* <i>Cakile maritima</i>	X	X	X	X	X						X
<i>Chenopodium californicum</i>									X		
<i>Cirsium occidentale</i>									X		
<i>Corethrogyne filaginifolia</i>	X	X	X	X	X	X	X	X	X	X	
* <i>Conicosia pugioniformis</i>							X		X		X
<i>Croton californica</i>									X		
<i>Dudleya lanceolata</i>							X	X			
<i>Erigeron blochmaniae</i>	X		X	X	X	X	X	X	X		X
* <i>Ehrharta calycina</i>									X		
<i>Eriastrum densifolium</i>					X		X				

	BBQ Flats 2019- VG- 01	Eucalyptus North 2022-VG- 04	Eucalyptus Tree 2022-VG- 05	Eucalyptus Tree 2021-VG- 03	Bigfoot (Western) 2020-VG- 04	Lagrange Hill 2018-VG- 01	Pawprint 2018-VG- 02	Lagrange Hill 2021- VG-02	Schnauzer 2015-VG-01 2016-VG-01 2017-VG-01	Enigma 2013- VG-01	Crescent 2013- VG-02
<i>Ericameria ericoides</i>	X	X	X	X	X	X	X	X	X	X	X
<i>Eriogonum parvifolium</i>	X	X	X	X	X	X	X	X	X	X	X
<i>Eriophyllum staechadifolium</i>	X	X	X	X	X	X	X		X		X
<i>Erysimum suffrutescens</i>	X	X	X	X	X		X	X			
<i>Fragaria chiloensis</i>						X					
<i>Heterotheca grandiflora</i>											X
<i>Horkelia cuneata</i>							X	X			
<i>Juncus lescurii</i>							X	X			
<i>Linanthus californicus</i>									X		
<i>Lupinus chamissonis</i>	X	X	X	X	X	X	X	X	X	X	X
<i>Malicothrix incana</i>	X				X		X				
<i>Monardella undulata crispa</i>	X	X	X	X	X	X	X	X	X	X	X
<i>Mucronea californica</i>				X					X		
<i>Oenothera elata</i>	X				X						
<i>Phacelia ramosissima</i>	X	X	X	X	X	X	X	X	X	X	X
<i>Pseudognaphalium californicum</i>									X		X
<i>Pseudognaphalium ramosissimum</i>							X			X	
<i>Salix lasiolepis</i>	X			X	X	X	X			X	
<i>Sambucus mexicana</i>									X		
<i>Senecio blochmaniae</i>	X	X	X	X	X	X	X	X	X	X	X
<i>Stephanomeria virgata</i>				X							

Photo Point Monitoring

On-the-ground photo point monitoring was conducted at the 48-Acre Foredune project prior to project installation in February 2020 and following project installation in May 2020, October 2020, October 2021 and October 2022. Photo point monitoring is scheduled to continue in October in future years. Photo points are located on all four corners of each treatment area. For each photo point, two photos are taken, each with one of the treatment area boundary lines on the outer edge of the photo with the interior of the treatment area centered in the photo. There is also one photo point overlooking the entire 48-Acre Foredune project from a distance. Refer to figures 4-7. On-the-ground photo point monitoring was also conducted throughout the back dune project areas during the Fall of 2022 and has been conducted annually since 2018. Back dune photo points are positioned to capture changes within the general areas where back dune projects are located. The number of photos for each photo point and the number of photo points varies at each location to sufficiently capture each area. In total, 45 photo points were monitored in the back dunes in 2022. Refer to figures 8-11. In addition to on-the-ground monitoring, drone aerial imagery photo point monitoring was conducted in May 2020, and during the winter in 2020, 2021 and 2022. Within the 48-Acre Foredune, two photo points were taken of each treatment area, one from the east and one from the west for each area. In addition, each winter drone photo points were conducted within the back dune project areas. The number of photos for each photo point and the number of photo points varied at each location to sufficiently capture each area. Refer to figure 12-15. Both on-the-ground and drone photo point monitoring are scheduled to continue annually.



Figure 4. Photo point of 48 Acre Foredune Area 3 facing west prior to treatment. Photo taken on February 4, 2020.



Figure 5. Photo point of 48 Acre Foredune Area 3 facing west 2.5 years after treatment. Photo taken on October 18, 2022.



Figure 6. Photo point of 48 Acre Foredune Area 3 facing north prior to treatment. Photo taken on February 4, 2020.



Figure 7. Photo point of 48 Acre Foredune Area 3 facing north 2.5 years after treatment. Photo taken on October 18, 2022.



Figure 8. Photo point of North Eucalyptus Tree project area facing northeast prior to planting. Photo taken on October 17, 2018.



Figure 9. Photo point of North Eucalyptus Tree project area facing northeast. Photo taken on October 19, 2022.



Figure 10. Drone photo point of 48 Acre Foredune High Density Node Area 5 facing east. Image taken in May 2020.



Figure 11. Drone photo point of 48 Acre Foredune High Density Node Area 5 facing east. Image taken on February 16, 2023.



Figure 12. Drone photo point of Bigfoot restoration project area facing south. Image taken on May 8, 2020.



Figure 13. Drone photo point of Bigfoot restoration project area facing south. Image taken on February 16, 2023.



Figure 14. Drone photo point of La Grille Hill restoration project area facing northwest. Image taken on March 6, 2022.



Figure 15. Drone photo point of La Grille Hill restoration project area facing northwest. Image taken on March 8, 2023.

Oceano Dunes State Vehicular Recreation Area Dust Control Program

DRAFT 2023 Annual Report and Work Plan

ATTACHMENT 09

**Preliminary Analysis of Time-Lapse Photo Monitoring Stations at the ODSVRA Foredune
Restoration Site
(UCSB Document)**

THIS PAGE WAS INTENTIONALLY LEFT BLANK.

Preliminary Analysis of Time-Lapse Photo Monitoring Stations at the ODSVRA Foredune Restoration Site

To observe and examine the development and responses of the foredune restoration treatments to wind and sand transport and events, time-lapse cameras were installed on the masts of the meteorological monitoring stations within each treatment plot. The stations were installed in May 2020 at the landward/eastern edge of the restoration plots (Fig. 3) and the cameras face upwind (roughly WNW) and capture oblique images every 30 minutes from 07:00 - 17:30 local time (PST). Cameras were installed to capture and characterize various formative events (e.g., sediment transport, plant growth, bedform development and migration, erosion events, dust emissions) at a relatively high temporal frequency.

Since deployment of the cameras, over 20,000 images have been captured at each of the restoration sites. Not all images are of acceptable quality, however, so poor images were removed manually from the datasets (Figure 2) because of fog, rain, blurriness, fouling of the lens by salt spray or dust, or overexposure. Some poor images were kept if they indicated some contribution to changing morphology. These pre-processed imagery datasets were then examined in more detail for their potential to characterize formative events and responses. Time lapse videos were also generated from the cleaned imagery to capture representative sediment transport events and their various landscape and treatment responses.

In this report, we provide a sample dataset that shows the mentioned methods. These methods can be applied monthly, seasonally, or annually to the entire dataset depending on project needs. The month of January 2023 was selected because the restoration treatments have had years to develop by this time and differences in sediment transport across the plots could be assessed. Additionally, there were noted sediment transport events in this month and the image quality was high for all treatment plots for comparison.

Preliminary analysis of the pre-processed imagery captured from the cameras by UCSB began in late 2022 and focused on data collected over one month (January 2023) to test and verify methods of photo image analysis and provide insight to next steps, limitations, and benefits of the imagery for the restoration project. Images from this interval for each restoration plot were classified, coded, analyzed, and compiled into time series videos, and related to the wind speed, direction, and thresholded total wind power density (TWPD) collected at the same station. A summary of the preliminary event/response coding is shown in Table 1. An example of imagery obtained from the cameras during a high-magnitude transport event is shown in Figure A detailed explanation of the methods, data, and preliminary results of this analysis are provided in the attached report (Heffentrager et al., 2023, Preliminary Analysis of Time-Lapse Photo Monitoring Stations at the Oceano Dunes Foredune Restoration Site).



Figure 1: Locations of the meteorological stations equipped with time-lapse cameras within each restoration plot. Othomosaic is from February 2022.

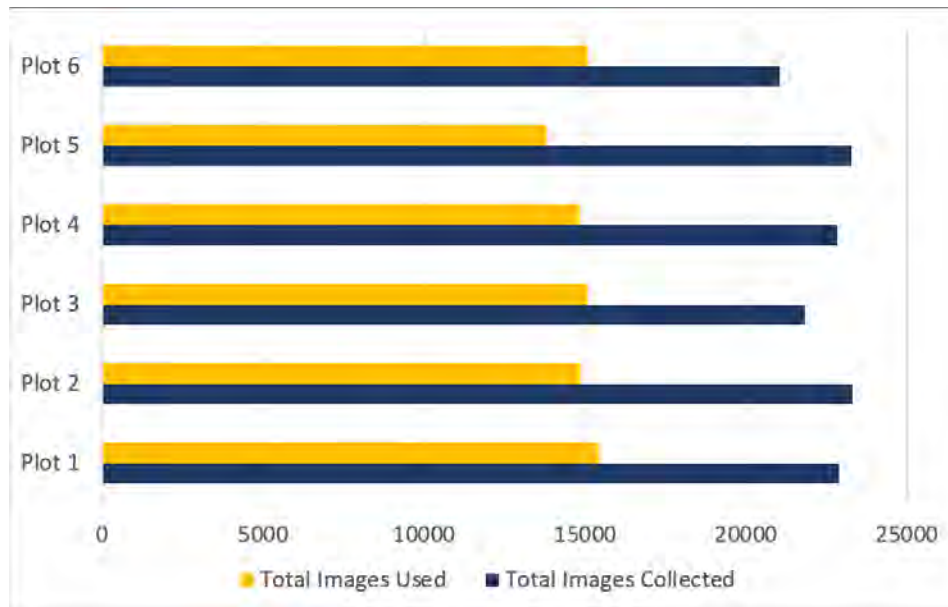


Figure 2: Total images collected (blue) and remaining after poor images were removed from the datasets for each monitoring station (yellow). There are variations in the number of total images collected due to various collection periods resulting from station-specific maintenance and collection differences.

Table 1: Coding key for monitoring camera image classification and analysis. Aeolian transport and associated dune changes are directly related and receive the same code. Meteorological conditions are coded independently of sediment transport and dune morphological responses.

Key	Aeolian Transport	Dune Morphological Changes	Meteorological Conditions
0	Inactive	No change	Dry, Sunny
1	Trace	Dune building, ripple formation/movement, sand accretion	Dry, Cloudy or Overcast
2	Active	Evidence of sediment erosion, sand streamers, surface deflation	Fog
3	Widespread	Widespread saltation cloud	Wet or Rain



Figure 3: Large sediment transport event on 1/9/2023 at 15:32 GMT in Plots 1-6 (labeled).

Oceano Dunes State Vehicular Recreation Area Dust Control Program

DRAFT 2023 Annual Report and Work Plan

ATTACHMENT 10

2023 PMRP Evaluation Metrics

THIS PAGE WAS INTENTIONALLY LEFT BLANK.

PMRP Evaluation Metrics – Annual Record 2022-23

In 2021, the SAG, in consultation with State Parks, updated the PMRP evaluation metrics used to track dust control progress. The updated metrics provide a more streamlined dashboard that make it easier to track progress and to inform adaptative management. “Dust Mitigation Targets” refer to evaluation metrics with specific measurable endpoints. “Dust Mitigation Indicators” refer to values indicating progress but for which specific targets are not defined.

In 2022, the SAG recommended specific changes to the current DRI Model to more accurately account for the effectiveness of dust mitigation treatments (see State Parks’ 2022 ARWP Section 2.2.1.3). The SAG’s recommendations were incorporated into a “revised” DRI model that results in different estimates of PM₁₀ mass emissions and concentration reductions compared to the current DRI model. The revised DRI model does not change the modeled 2013 baseline information against which evaluation metrics and Dust Control Program progress has historically been measured.

This attachment presents previously reported metrics from prior ARWPs for years 2013, 2019, 2020, 2021, and 2022. Metrics for 2023 are as reported in State Parks’ 2023 ARWP, which uses the latest revised DRI model assumptions (see 2023 ARWP Section 2.2.1.1).

As described in State Parks’ 2023 ARWP (Section 2.2), the October 2022 SOA amendments to reduce 2013 baseline emissions by 50% with an excess emissions framework that focuses on reducing the ODSVRA’s contribution to downwind violations of the state and federal ambient air quality standards. The development of this framework will result in updated evaluation metrics.

Evaluation Metric table notes are provided at the end of this document.

EVALUATION METRICS TABLE 1: DUST MITIGATION TARGETS									
Dust mitigation treatments		2013 baseline	2019	2020	2021	2022	2023	2024¹	Current target²
A. Cumulative area under treatment within ODSVRA, as of July 31 of current year, relative to 2013 baseline (acres)	A1. Total	0	137.8	230.2	322.5	740.1	740.1	740.1	N/A
	A2. Back dunes inside riding area	0	103.1	195.5	213.2	288.3	288.3	288.3	
	A3. Back dunes outside riding area	4.7	34.7	34.7	61.3	75.9	75.9	75.9	
	A4. Foredunes	0	0.0	48.0	48.0	48.0	48.0	48.0	
	A5. Nesting enclosure	0	0.0	0.0	0.0	293.3	293.3	293.3	
	A6. Foredune beach and corridor	0	0.0	0.0	0.0	34.6	34.6	34.6	
PM₁₀ mass emissions		2013 baseline	2019	2020	2021	2022	2023³	2024	Current target⁴
B. Riding Area mean PM ₁₀ emissions for 10 baseline days - modeled	B1. Mass emissions (metric tons / day)	182.8	135.0	131.6	123.9	103.8	100.9	99.9	N/A
	B2. Relative to 2013	100%	73.9%	72.0%	67.8%	56.7%	55.2%	54.6%	N/A
PM₁₀ concentrations		2013 baseline	2019	2020	2021	2022	2023	2024⁵	Current target⁶
C. CDF mean PM ₁₀ concentration for 10 baseline days (µg/m ³) - modeled		124.7	N/A	N/A	N/A	61.9	60.9	60.7	N/A
D. Mesa2 mean PM ₁₀ concentration for 10 baseline days (µg/m ³) - modeled		97.5	N/A	N/A	N/A	63.6	62.5	62.2	

EVALUATION METRICS TABLE 2: DUST MITIGATION INDICATORS							
Air quality indicators		2013 baseline	2019	2020	2021	2022	2023
1. Actual number of high wind event days ⁷		59	30	55	51	64	72
2. Actual number of exceedances of California air quality standard ⁸	2a. at CDF	58	16	30	54	54	16
	2b. at Mesa2	43	14	28	38	38	11
3. Actual number of exceedances of Federal air quality standard ⁹	3a. at CDF	1	0	0	0	0	0
	3b. at Mesa2	0	0	0	0	0	0
Foredune restoration		2013 baseline	2019	2020	2021	2022	2023
4. Foredune plant fractional cover, at time of spring survey (%)	4a. Treatment 1	N/A	N/A	N/A	0	0	0
	4b. Treatment 2				0.1	1.9	2.7
	4c. Treatment 3				4.0	12.3	10.1
	4d. Treatment 4				0.8	5.7	5.1
	4e. Treatment 5				0.4	2.1	6.4
	4f. Treatment 6				3.6	12.7	13.8
5. Foredune species richness index relative to Oso Flaco site (10 species) ¹⁰	5a. Treatment 1	N/A	N/A	N/A	0	0	20
	5b. Treatment 2				33	40	30
	5c. Treatment 3				50	50	40
	5d. Treatment 4				100	60	70
	5e. Treatment 5				110	100	90
	5f. Treatment 6				110	80	100
6. Foredune sand volume, current spring survey relative to previous fall survey (m ³ m ⁻² month ⁻¹)	6a. Treatment 1	N/A	N/A	N/A	0.0011	TBD	TBD ¹¹
	6b. Treatment 2				0.0006	TBD	TBD
	6c. Treatment 3				0.0022	TBD	TBD
	6d. Treatment 4				0.0009	TBD	TBD
	6e. Treatment 5				0.0020	TBD	TBD
	6f. Treatment 6				0.0031	TBD	TBD
Back dune stabilization		2013 baseline	2019	2020	2021	2022	2023
7. Cumulative area of back dune stabilization within ODSVRA, as of July 31 of current year (acres)	7a. Planting area	TBD ¹²	89.2	109.6	168.5	287.1	314.4
	7b. Fencing area	0	48.6	53.7	72.8	53.0	32.5
	7c. Straw bales area	0	0	18.9	27.3	24.1	17.3
	7d. Temporary vehicle exclusion areas	0	0	0	5.9	0.0	0.0
	7e. Stabilized vegetation surface area	TBD ¹³	137.8	182.2	274.5	364.2	364.2
8. Native seed harvest for all plants during current ARWP reporting period (kg/year)		N/A	203.2	307.3	193.0	252.6	234.5
9. Plant species cultivation for all plants during current ARWP reporting period (#/year)			106,350	89,433	127,464	125,380	121,724

EVALUATION METRIC TABLE NOTES

¹ 2024 dust mitigation treatment acreage values are based on State Parks 2023 ARWP, Chapter 3, and are subject to change.

² State Parks' June 2019 PMRP included a preliminary compliance analysis, or sensitivity analysis, prepared by DRI, that evaluated the approximate size, scale, and level of effort necessary to comply with the SOA's air quality objectives, namely the 50% reduction in maximum modeled baseline PM₁₀ mass emissions identified in SOA condition 2.c. The preliminary PMRP modeling conducted by DRI indicated that approximately 500 acres of dust control measures could be needed to achieve SOA air quality objectives. State Parks' 2021 ARWP included an updated estimate of the amount of dust control measures that may be required to achieve SOA air quality objectives. The 2021 ARWP's updated sensitivity analysis increased the estimate of the amount of dust control measures necessary to comply with SOA Condition 2.C from 500 acres (as preliminary estimated in the 2019 PMRP) to 602 acres, assuming 100% effectiveness for all dust control measures. This target may be revised in the future based on further modeling of dust mitigation effectiveness and monitoring of actual air quality improvements.

³ 2024 PM₁₀ mass emissions reduction estimates are based on State Parks 2023 ARWP, Table 3-1, and are subject to change.

⁴ The original PM₁₀ mass emissions target is defined according to Stipulated Order of Abatement (SOA) provision 2c, which "...establish[es] an initial target of reducing the maximum 24-hour PM₁₀ baseline emissions by fifty percent (50%), based on air quality modeling based on a modeling scenario for the period May 1 through August 31, 2013." The air quality modeling approach is described in the PMRP. The 10 baseline days for this scenario are defined in the 2020 Annual Report and Work Plan (ARWP), Attachment 6. As described in State Parks' 2023 ARWP (Section 2.2), the October 2022 SOA amendments to reduce 2013 baseline emissions by 50% with an excess emissions framework that focuses on reducing the ODSVRA's contribution to downwind violations of the state and federal ambient air quality standards. The development of this framework may result in new targets and evaluation metrics for PM₁₀ mass emissions.

⁵ 2024 PM₁₀ concentration reduction estimates are based on State Parks 2022 ARWP, Table 3-2 and Table 3-3, and are subject to change.

⁶ Original SOA provision 2b states that "...the [Particulate Matter Reduction] Plan shall be designed to achieve state and federal ambient PM₁₀ air quality standards." However, it does not designate a specific PM₁₀ airborne concentration target for the baseline modeling scenario. Refer to State Parks' 2022 ARWP (Table 2-3) for the current California and National Ambient Air Quality Standards for PM₁₀. As described in State Parks' 2023 ARWP (Section 2.2), the October 2022 SOA amendments to reduce 2013 baseline emissions by 50% with an excess emissions framework that focuses on reducing the ODSVRA's contribution to downwind violations of the state and federal ambient air quality standards. The development of this framework may result in new targets and evaluation metrics for PM₁₀ concentrations.

⁷ Values are determined using the SLO Air Pollution Control District (APCD) definition of “high wind event day” as any day when the 3 p.m. PST hourly wind speed at CDF exceeds 8 mph and the 1 p.m. PST hourly wind direction is between 290 and 360°. The period of consideration is January 1 - June 26, 2023. Data may be preliminary and subject to change.

⁸ The California Ambient Air Quality Standard is a mean value of 50 µg/m³ over a 24-hour period. The period of consideration is January 1 - June 26, 2023. Data may be preliminary and subject to change.

⁹ The National Ambient Air Quality Standard is a mean value of 150 µg/m³ over a 24-hour period. The period of consideration is January 1 - June 26, 2023. Data may be preliminary and subject to change.

¹⁰ The number of native plant species recorded for each treatment area as compared to reference site at Oso Flaco (10 species). Long term goal is to have a stable or increasing richness value versus reference site.

¹¹ 2022 and 2023 Foredune sand volumes will be determined from the latest uncrewed aerial system (UAS) survey conducted by UCSB. The latest survey results are under review by State Parks. Foredune sand volumes will be updated following the State Parks’ review of the UCSB UAS survey data.

¹² The baseline 2013 back dune stabilization “planting area” metric may be estimated from UCSB’s historic vegetation report; however, the SAG has not established the methodology for establishing baseline vegetation conditions. State Parks will coordinate with the SAG to finalize the methodology for determining baseline 2013 back dune stabilization planting areas. Currently, the yearly estimates of planting area for the Dust Control Program (e.g., 89.2 acres in 2019) are based on the amount of back dune vegetation planted under the Dust Control Program (i.e., excludes foredune vegetation and non-vegetation projects such as wind fencing).

¹³ The baseline 2013 back dune “stabilized vegetation surface area” metric may be estimated from vegetation coverage estimates determined from aerial imagery; however, the SAG has not established the methodology for establishing baseline vegetation conditions. State Parks will coordinate with the SAG to finalize the methodology for determining baseline 2013 back dune stabilization planting areas. Currently, the yearly estimates of stabilized vegetation surface area for the Dust Control Program (e.g., 137.8 acres in 2019) reflect the sum of the stabilization approaches in metrics 7a to 7d.

THIS PAGE WAS INTENTIONALLY LEFT BLANK.

Oceano Dunes State Vehicular Recreation Area Dust Control Program

DRAFT 2023 Annual Report and Work Plan

ATTACHMENT 11

**Compilation of Studies Reviewed and Comments Provided by the Scientific Advisory Group
from 08/01/22 to 07/31/23**

**11-01: Increments of Progress Towards Air Quality Objectives – ODSVRA Dust Controls 2022
Update**

11-02: Quantifying the Source Attribution of PM₁₀ Measured Downwind of the ODSVRA

11-03: PI-SWERL September 2022 Results and Implications for Emission/Dispersion Modeling

11-04: SAG Framework for Assessing Excess Emissions of PM₁₀ from the ODSVRA

THIS PAGE WAS INTENTIONALLY LEFT BLANK.

Oceano Dunes State Vehicular Recreation Area Dust Control Program

DRAFT 2023 Annual Report and Work Plan

ATTACHMENT 11-01

DRAFT DRI Report- Increments of Progress Towards Air Quality Objectives (Fall 2022)

SAG Comments on Increments of Progress Towards Air Quality Objectives (October 11, 2022)

FINAL DRI Report - Increments of Progress Towards Air Quality Objectives (February 7, 2023)

THIS PAGE WAS INTENTIONALLY LEFT BLANK.

Placeholder. This DRI document is currently under review by the SAG.

THIS PAGE WAS INTENTIONALLY LEFT BLANK.

Oceano Dunes State Vehicular Recreation Area Dust Control Program

DRAFT 2023 Annual Report and Work Plan

ATTACHMENT 11-02

**SAG Comments on DRI/SLOAPCD Report Quantifying the Source Attribution of PM₁₀
Measured Downwind of the ODSVRA (November 23, 2022)**

**FINAL DRI/SLOAPCD Report Quantifying the Source Attribution of PM₁₀ Measured Downwind
of the ODSVRA (April 15, 2023)**

THIS PAGE WAS INTENTIONALLY LEFT BLANK.

Oceano Dunes State Vehicular Recreation Area Dust Control Program

DRAFT 2023 Annual Report and Work Plan

ATTACHMENT 11-02

**SAG Comments on DRI/SLOAPCD Report Quantifying the Source Attribution of PM₁₀
Measured Downwind of the ODSVRA (November 23, 2022)**

THIS PAGE WAS INTENTIONALLY LEFT BLANK.

November 23, 2022

Memo: SAG Review of “Chemical Speciation and Source Attribution of PM₁₀ Samples Collected in 2021 at the CDF Monitoring Site,” by X. Wang, J.A. Gillies, S. Kohl, and G. Nikolich (Desert Research Institute)

From: Scientific Advisory Group (SAG)

To: Ronnie Glick, California Department of Parks and Recreation (CDPR)

Cc: Sarah Miggins, California Department of Parks and Recreation (CDPR)
Jon O’Brien, California Department of Parks and Recreation (CDPR)

Summary Statement

The Scientific Advisory Group (SAG) welcomes the submission of this new report on chemical speciation analyses of PM₁₀ dust collected at the CDF monitoring site by the San Luis Obispo County Air Pollution Control District (SLOAPCD) and analyzed by Desert Research Institute (DRI) scientists to inform attribution of PM₁₀ sources within and outside the Oceano Dunes State Vehicular Recreation Area (ODSVRA).

Overall, the SAG appreciates the factual, logical, and neutral presentation of these new PM₁₀ speciation analyses, which help to further advance our understanding of the contribution of ODSVRA dust emissions to airborne PM₁₀, relative to other sources, as measured at CDF. Overall, the PM₁₀ sampling techniques appear to be standard and appropriate, though the report would be improved by providing further details regarding specific sampling approaches. In addition, the pairing of both ionic and elemental analyses provides a significant advancement over previous studies by accounting for almost all of the unattributed “other” PM₁₀ mass, which has been an issue with previous studies. However, significant uncertainties remain in the attribution of PM₁₀ dust to the ODSVRA versus other sources, especially regarding “unattributed mass.” Though the present report is appropriately cautious in its interpretation of speciation analyses, the authors are encouraged to provide further context for how the results should be interpreted. Specifically, the component identified as “mineral dust” may not completely capture all sources of PM₁₀ from the ODSVRA, as the elemental analysis assumes a specific source profile for “mineral dust,” and some of other identified sources may in fact originate from within the ODSVRA.

Comments on Sampling Techniques

There is not enough information included in the paper to provide a thorough or authoritative review of the sampling techniques utilized for this research. The paper references use of a Federal Equivalent Method (FEM) sampler, implying but not specifying the sampling techniques, qa/qc, etc. conform to EPA approved regulatory collection of PM₁₀ mass on Teflon filters. What little data is provided adheres to regulatory practices. There is no regulatory standard for sample collection on quartz fiber filters, however standard practices have been developed and utilized in national networks such as IMPROVE and CSN. If the sampling

techniques followed regulatory or standard practices, it may be prudent to say so, or where and why deviations were made.

In that same vein, there is also not enough information provided to thoroughly review the laboratory's gravimetric analysis or filter handling procedures. However, what data is provided appears to conform to regulatory requirements for analysis of PM₁₀ mass on Teflon filters.

There is mention of filter blank samples in the statement: "Any PM₁₀ on the blank filter and its chemical constituents can subsequently be subtracted from the amount that is acquired during active sampling." This is the only reference made to filter blank analysis. What came of this analysis, and how did it affect the results? What adjustment method (if any) was used?

There is some ambiguity regarding this statement: "Paired Teflon-membrane and quartz-fiber filters were used to collect the PM₁₀ using a Partisol (Federal Equivalent Measurement, FEM) sampler. Two Partisol samplers were used in rotation to allow for testing of any sampler-created bias." Partisols are single channel samplers, so both would always have to run simultaneously since there were two separate filter samples (one Teflon, one quartz) for each day. Perhaps we're reading this wrong? Additionally, what was the analysis of the sampler-created bias?

Was the mass measured at the CDF BAM monitor compared to the gravimetric mass filter samples? Of particular curiosity is the 10/7/2021 outlier date.

Comments on Speciation Analysis

This report does a good job of clearly presenting the chemical speciation and source attribution analysis. The analyses are overall clear and well-reasoned. However, the present report is somewhat light on interpretation. Without situating these results within the larger debate regarding the attribution of airborne PM₁₀ at monitoring sites near the ODSVRA, there is a danger that the results could be misinterpreted. Here, the SAG offers some ideas for consideration in the interpretation of these source attribution results.

The present study adds significant clarity to the ongoing debate about chemical speciation by identifying a clear approach to identification of chemical constituents within filter samples. Seven constituents are identified: (1) fresh sea salt (FS), (2) aged sea salt (AS), (3) non-sea salt sulfate (nssSO₄²⁻), (4) mineral dust (MD), (5) elemental carbon (EC), (6) organic matter (OM), and (7) "other." Together, these seven constituents are summed together as "reconstructed mass." Any gap between this reconstructed mass and the total gravimetric mass is considered "unidentified mass."

The inclusion of laboratory ion analyses to determine the contribution of sea salt (both FS and AS) to total reconstructed mass provides a significant advancement over previous speciation studies at the ODSVRA. As shown in Fig. 7 of the present study, FS dominates the combined sea salt contribution on high PM₁₀ days, suggesting an oceanic origin for this component of PM₁₀. As shown in Fig. 8, when such sea salt (both FS and AS) is included within the overall reconstructed mass, linear regression indicates that the remaining unidentified mass is on average about 16% of the total gravimetric mass, providing confidence that most constituents are

accounted for within the analysis. (During PM₁₀ exceedance events, the average unidentified component is slightly higher at 20.4%, as shown in Fig. 27.)

As in past studies, the mineral dust (MD) component is a topic of significant interest. MD is not directly measurable but is instead determined based on an assumed elemental source profile applied to XRF analyses of filter samples, i.e., the modified IMPROVE formula (Eq. 5). Similar assumptions are used to identify nssSO_4^{2-} and OM based on established relations, whereas EC appears to be derived directly from the XRF analysis. “Other” includes the remaining ions and elements not captured within the designated categories. These methods are standard and acceptable; however, the source profile formula for MD (as well as other constituents) assumes a particular elemental composition for mineral dust, which may not reflect the actual chemical character of ODSVRA sands (which are known to be rich in feldspar and quartz). Thus, the component attributed as MD in the present study (identified as “Dust” in most figures), may not represent the full contribution of ODSVRA-derived mineral dust.

The present study provides a detailed analysis of source attribution during 8 PM₁₀ exceedance days in 2021. Such high PM₁₀ events are of the greatest management interest, and thus they are the primary focus of the study. Apart from 5/4/2021, which experienced winds of a more westerly character than the typical northwesterly winds on high PM₁₀ days (see Figs. 12-13), analyses for the remaining high PM₁₀ days (Figs. 14-26) show MD (“Dust”) as constituting an average 48.1% (range: 39.2%-58.2%) of the total sample gravimetric sample mass. (As shown in Fig. 27, inclusion of 5/4/2021 within the analysis yields a lower average MD of 43.1%.) The present study does not speculate on the unusually low MD component on 5/4/2021, but the unusual westerly (rather than northwesterly) wind direction may provide an explanation. For example, the CDF monitoring site may be experiencing PM₁₀ from a less emissive area of the ODSVRA on this particular date.

The present study acknowledges the limitations of ionic and elemental analyses. The study speculates that the “unidentified mass” component of the analysis, constituting an average 20.4% of PM₁₀ on exceedance days (or 19.9% if excluding 5/4/2021), is comprised of particle-bound water on aerosol samples associated with oxide components of quartz and feldspar minerals. Thus, assuming that unidentified mass is an additional component of mineral dust (i.e., total dust = “MD” + “unidentified mass”), yields an estimate that mineral dust is 63.5% of PM₁₀ on exceedance days (mean 68.0% if excluding 5/4/2021).

Regarding the ionic and elemental analyses, it is slightly surprising that K⁺ was attributed largely to seaspray, given what we know about the predominance of feldspars (presumably K-spar, although there are many others) in the sand matrix. Huang et al. (2019) found that feldspars, combined, contributed almost half of the mass of Oceano sands (K-rich feldspar 23% and plagioclase 23%) with another 3% clay (coatings on the grains). The ratio-regression method used to identify K⁺ contributions relative to that in seawater (with Na⁺ concentrations from sea salt as the reference control) generally makes sense, but it is still surprising that K does not contribute more. Also, there are many other types of feldspars and some also contain Na⁺. How can we isolate the sources of elemental K⁺, Na⁺, and even Ca²⁺ if they can be traced to both ocean water and the local sediments? This might call for more detailed mineralogical study of the other minerals in the mix, such as feldspars. Alternatively, it is possible that this distinction is

captured by the paired nature of the ionic versus elemental analyses. Either way, it would help if the present report could further address this question.

Though the present analysis does not pinpoint the mineral dust contribution to PM₁₀ at ODSVRA with total certainty, it does provide significant clarity relative to previous studies. Notably, the “other” component within the reconstructed mass is on average only 1.75% of PM₁₀ on exceedance days (Fig. 27). This finding provides confidence that the reconstructed mass is accurately capturing most constituents. Thus, the study provides high confidence that all PM₁₀ attributed to “MD” (i.e., “Dust”) in Fig. 27 does in fact originate from mineral dust within the ODSVRA. Such analysis therefore places a meaningful lower bound on ODSVRA-derived PM₁₀ on exceedance days, shown as 43.1% in Fig. 27, or 48.1% if excluding 5/4/2021. What remains less clear is how much the other components may also be attributed to an ODSVRA source. Though constituents identified as fresh sea salt (FS) and aged sea salt (AS) would appear to bear at least a partial oceanic origin, it is possible that at least some of these constituents in fact originated from within the ODSVRA, either due to deposit and re-emission of sea salt, or due to issues in distinguishing ionic and elemental components, as described above. The present analysis addresses the possibility that the “unidentified” component is ODSVRA-sourced; however, it is possible that at least some of the other constituents also arise from within the ODSVRA, as opposed to oceanic or other inland sources. Further analyses are needed to better answer these questions.

Other Specific Comments

1. Figure 1 has the first mention of ODSVRA. This should be spelled out, and its relevance to the sampling campaign described.
2. Page 3: misspelled word – “costal” instead of “coastal”.
3. Page 3: “most ions are measured with high quality”. Does this mean with high accuracy? The word “quality” is confusing.
4. Figure 8 caption: what does “top panel” mean?
5. A brief conclusion paragraph would be helpful. Though such a paragraph might compromise the admirably neutral tone of this paper, it may be worth trying to craft something to put the results in context.

Respectfully,
The Scientific Advisory Group

Dr. Raleigh Martin (Chair of SAG); Dr. William Nickling; Dr. Ian Walker; Ms. Carla Scheidlinger; Ms. Leah Mathews; Mr. Mike Bush, Dr. John A. Gillies

References

Huang, Y., Kok, J.F., Martin, R.L., Swet, N., Katra, I., Gill, T.E., Reynolds, R.L., Freire, L.S. (2019). Fine dust emissions from active sands at coastal Oceano Dunes, California. *Atmospheric Chemistry and Physics* 19, 2947–2964. <https://doi.org/10.5194/acp-19-2947-2019>

Oceano Dunes State Vehicular Recreation Area Dust Control Program

DRAFT 2023 Annual Report and Work Plan

ATTACHMENT 11-02

**FINAL DRI/SLOAPCD Report Quantifying the Source Attribution of PM₁₀ Measured Downwind
of the ODSVRA (April 15, 2023)**

THIS PAGE WAS INTENTIONALLY LEFT BLANK.

Article

Quantifying the Source Attribution of PM₁₀ Measured Downwind of the Oceano Dunes State Vehicular Recreation Area

Xiaoliang Wang ¹, John A. Gillies ^{1,*}, Steven Kohl ¹, Eden Furtak-Cole ¹, Karl A. Tupper ² and David A. Cardiel ²

¹ Division of Atmospheric Sciences, Desert Research Institute, Reno, NV 89512, USA; xiaoliang.wang@dri.edu (X.W.); steve.kohl@dri.edu (S.K.); eden.furtak-cole@dri.edu (E.F.-C.)
² San Luis Obispo County Air Pollution Control District, San Luis Obispo, CA 93401, USA; ktupper@co.slo.ca.us (K.A.T.); dacardiel@co.slo.ca.us (D.A.C.)
 * Correspondence: jack.gillies@dri.edu; Tel.: +01-775-674-7035

Abstract: A measurement campaign was undertaken April–October 2021 using PM₁₀ filter samplers to collect 24 h samples downwind of the Oceano Dunes State Vehicular Recreation Area (ODSVRA), an area that allows off-highway driving on its coastal dunes. The PM₁₀ samples were analyzed and these data were used to identify the sources that contributed to the PM₁₀ under varying meteorological conditions. Exposed filters were weighed to calculate mass concentration and analyzed using X-ray fluorescence to quantify elemental composition, ion chromatography to quantify water-soluble ions, and thermal/optical reflectance to quantify organic carbon and elemental carbon in the particulate matter. These speciated data were used to attribute the sources of PM₁₀ for eight days that exceeded the California state 24 h mean PM₁₀ standard and 39 days that were below the standard. The mean attribution of sources for the eight identified exceedance days was mineral dust (43.1%), followed by sea salt (25.0%) and the unidentified category (20.4%). The simultaneous increase in the mineral dust and unidentified categories with increasing levels of PM₁₀ arriving from the direction of the ODSVRA suggests that the unidentified components were unmeasured oxides of minerals and carbonate. This increases the attribution of mineral dust for a mean exceedance day to 63.5%. The source of the mineral dust component of the PM₁₀ is attributable to wind-driven saltation and dust emission processes within the ODSVRA.

Keywords: source attribution; dust emissions; off-highway vehicle activity; dust abatement



Citation: Wang, X.; Gillies, J.A.; Kohl, S.; Furtak-Cole, E.; Tupper, K.A.; Cardiel, D.A. Quantifying the Source Attribution of PM₁₀ Measured Downwind of the Oceano Dunes State Vehicular Recreation Area. *Atmosphere* **2023**, *14*, 718. <https://doi.org/10.3390/atmos14040718>

Academic Editor: Antonio Donateo

Received: 23 March 2023

Revised: 11 April 2023

Accepted: 12 April 2023

Published: 15 April 2023



Copyright: © 2023 by the authors. Licensee MDPI, Basel, Switzerland. This article is an open access article distributed under the terms and conditions of the Creative Commons Attribution (CC BY) license (<https://creativecommons.org/licenses/by/4.0/>).

1. Introduction

The Oceano Dunes, part of the Callender coastal dune system, in San Luis Obispo County, California (Figure 1), is a known source of fugitive dust emissions [1–4]. Under conditions of elevated wind speed for westerly winds, exceedances of the US Federal Standard (150 µg m^{−3}) and the State of California Standard (50 µg m^{−3}) for 24 h time-integrated concentrations of particulate matter ≤ 10 µm aerodynamic diameter (PM₁₀) have been observed downwind of the dunes since air-quality monitoring was initiated in 1989. Exceedance of the State of California Standard continues to be observed to the present day (2022), while the Federal Standard has not been exceeded since 2014, according to the San Luis Obispo County Air Pollution Control District (SLOAPCD) records.

This California State Park allows off-highway vehicle (OHV) recreation on approximately 338 ha of the beach and dune landscapes (as of December 2022) while prohibiting OHV activity outside this area to protect sensitive areas and critical habitat for identified endangered species (e.g., *Charadrius alexandrinus nivosus*, Western Snowy Plover and *Sterna antillarum browni*, California Least Tern). The primary mechanism for emission of dust into the atmosphere from the ODSVRA's sandy areas is wind-generated rather than

OHV recreation actively lofting dust. For winds $> 8 \text{ m s}^{-1}$ with dominant westerly components as measured 10 m above ground level (AGL) within the park, the threshold for sand transport is exceeded, and this is accompanied by dust emissions [1–4]. Gillies et al. [2] reported, however, that OHV activity augments the dust emission potential of the area designated for such activity, producing more PM_{10} than would occur if the sand areas were not impacted by vehicle travel.

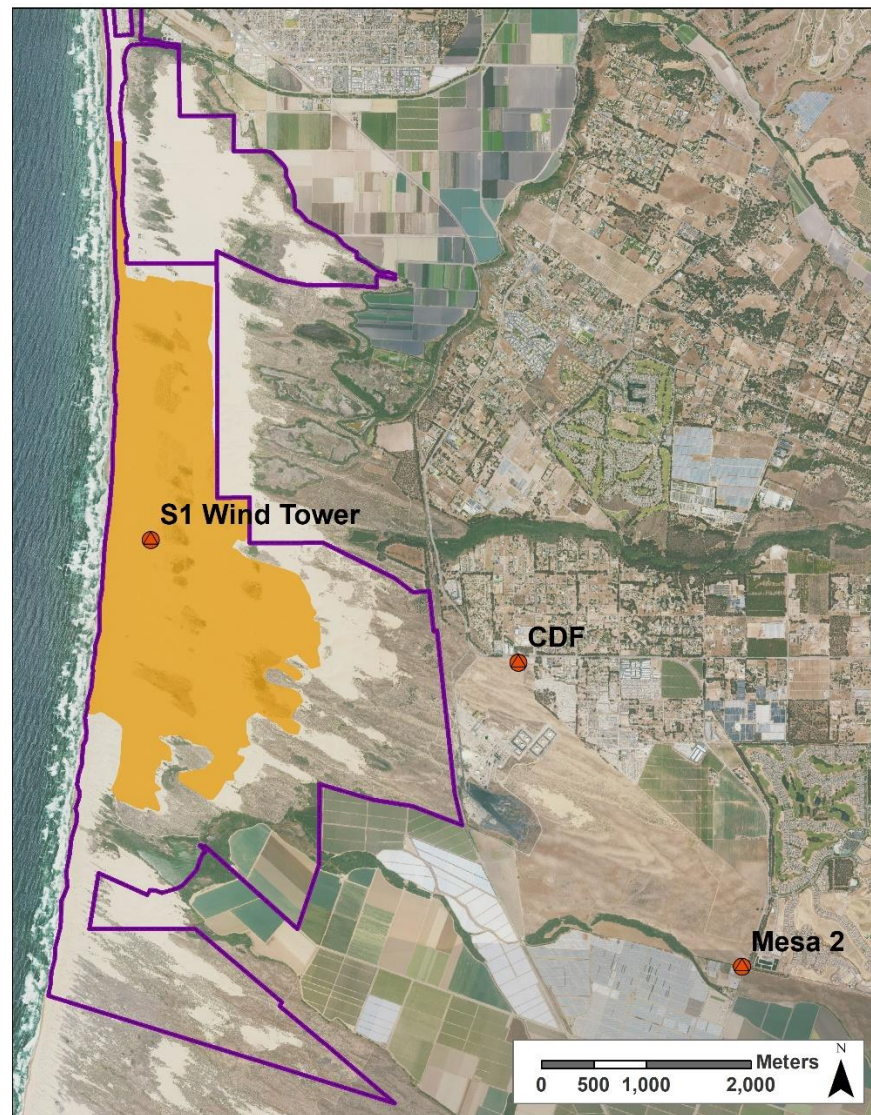


Figure 1. The location of the APCD’s environmental monitoring station, the CDF, with respect to the ODSVRA. The shaded area demarcates the riding area of the ODSVRA. The solid purple line demarcates the boundary of the ODSVRA. A red circle in the shaded area identifies the location of a 10 m tower designated as S1, where in-park meteorological data are collected, and Mesa2 is another of the APCD’s monitoring stations.

A Stipulated Order of Abatement (SOA) approved by the SLOAPCD Hearing Board in April 2018 (Case No. 17-01) required the California Department of Parks and Recreation (Parks) to reduce the PM_{10} attributable to the Oceano Dunes State Vehicular Recreation Area (ODSVRA, i.e., the ODSVRA is the source area) to achieve the state and federal 24 h mean PM_{10} standards. It also identified that to work toward achieving compliance, Parks should develop a management strategy that reduces the emissions of PM_{10} attributable to dust emission processes within the ODSVRA riding area by 50% by the end of 2023. The SOA was amended in November 2019 and again in October 2022. As amended, the SOA

requires that by the end of 2025, PM_{10} emissions from the ODSVRA be reduced to those modeled to approximate the conditions that existed in 1939. This was prior to high levels of OHV activity and assumes a higher degree of vegetation cover than at present [5].

Parks implemented a management strategy in 2014 based on using dust-control measures within the ODSVRA to reduce PM_{10} emissions caused by wind and saltating sand. These measures included increasing the amount of vegetation covering sand dunes and promoting the restoration of a foredune [6,7], which reduced the size of the area from which dust emissions originated as well as modulating the wind energy on and downwind of the control areas [7]. Temporarily installed arrays of sand fences [1] and covering the sand with a layer of straw on designated areas of the dunes have also been emplaced at different times to modify dust emission processes, as they provided immediate suppression of dust emission upon installation. Planted vegetation requires time to reach its full potential to mitigate saltation and dust emission processes as the plants reach maturity and maximize their ability to protect the surface from wind erosion [8].

Although wind-generated dust in the PM_{10} size range within the ODSVRA is the result of dust emissions driven by saltating sand during periods when the wind creates above-threshold conditions, other sources may also be contributing to the observed PM_{10} concentrations measured east of the ODSVRA at the SLOAPCD monitoring site identified as the California Department of Forestry and Fire Station (hereafter CDF) (Figure 1). This station is downwind of the ODSVRA during periods of westerly wind that are often observed to be associated with high hourly PM_{10} , which, if sustained for a sufficient length of time, leads to exceedance of the State of California Standard 24 h mean concentration of PM_{10} .

The attribution of the sources of PM_{10} measured in the study area (Figure 1) has been a focus of measurement efforts of the SLOAPCD. A one-year filter measurement campaign (2004–2005) in the study area showed that during high- PM_{10} events at the CDF and Mesa2 sites, (1) high northwesterly wind was observed from the dune area; (2) mass concentrations of coarse particles ($PM_{10-2.5}$) were higher than those of fine particles ($PM_{2.5}$); and (3) a large fraction of the PM_{10} was windblown crustal materials [9]. This evidence suggested that dust emissions from the upwind ODSVRA were a major PM_{10} source in the study area. This conclusion was supported by a follow-up study in this area [10], which also showed that other sources (e.g., a chemical facility or agricultural fields) were not significant contributors to PM_{10} during high- PM_{10} events. The SLOAPCD also found that the contribution of quartz alone to the total PM_{10} mass approached 12.5% on high- PM_{10} days when winds were predominately from the west [11]; in addition to quartz, ODSVRA dust has been shown to contain significant feldspar and clay components [12]. However, these studies did not analyze the full chemical composition of the PM_{10} , making source attribution less definitive.

A recent study by Lewis et al. [13] argued that the contributions of dust from the ODSVRA to downwind $PM_{2.5}$ and PM_{10} are small and dust abatement measures would not improve downwind air quality. Lewis et al. [13] collected filter samples of 6–8 h duration at different times of the day (post-12:00 pm) in 2019–2021. The filters were analyzed for elements with X-ray fluorescence (XRF) and organic functional groups with Fourier-transform infrared (FTIR) spectroscopy. Lewis et al. [13] reported that the mineral dust fraction was 14% ($\pm 10\%$) of the PM_{10} measured by a Beta Attenuation Monitor (BAM) on high- PM_{10} days, which were defined as days on which BAM-measured PM_{10} at the CDF exceeded $140 \mu g m^{-3}$ for one or more reported hours. We note in their study that the $PM_{2.5}$ and PM_{10} sampling did not comply with the EPA-designated Federal Reference Method (FRM) or Federal Equivalent Method (FEM), and the gravimetric $PM_{2.5}$ and PM_{10} mass concentration had large differences with the FEM BAM concentrations.

Accurate attribution of PM_{10} is needed to inform Parks of the best management practices that will lead to compliance with the SOA. The results presented by Mejia et al. [4] and Gillies et al. [1,2] suggested that the current Parks management strategy to reduce PM_{10} contributions through dust-control measures is a prudent approach to reach compliance with

the SOA, as measurements and modeling have suggested that high PM₁₀ concentrations observed within the ODSVRA contribute substantially to the PM₁₀ measured downwind of the ODSVRA. According to Lewis et al. [13], however, dust-control measures will not be effective, as their results suggested mineral dust is a minor component of PM₁₀ when the hourly mean concentration observed at the CDF is $>140 \mu\text{g m}^{-3}$. Resolving the relative attribution of PM₁₀ to its sources as measured at the CDF has implications for Parks to effectively manage the PM₁₀ contributions from the ODSVRA to regional PM₁₀ levels to meet the SOA.

To aid in resolving the uncertainty of the source attribution of PM₁₀ at the CDF monitoring site, a PM₁₀ measurement campaign was undertaken in 2021. Using Federal Reference Method PM₁₀ filter samplers (Thermo Fisher Scientific, Waltham, MA, USA, Partisol® 2025i Sequential Air Samplers), paired, preweighed 47 mm Teflon-membrane and pretreated 47 mm quartz-fiber filters were used to collect 24 h PM₁₀ samples following the US EPA's one-in-three days sampling schedule from April to October 2021. This period of the year has the greatest probability for exceedances of the state 24 h mean PM₁₀ standard. The exposed filters were weighed to calculate the 24 h mass concentration and analyzed using XRF to quantify the elemental composition (Na to U), ion chromatography to quantify the water-soluble ions, and thermal/optical reflectance to quantify the organic carbon (OC) and the elemental carbon (EC) in the collected particulate matter. Details on the sampling and analytical methods are provided in the Methods Section. Using these speciated data, analyses were undertaken to provide accounting of the source attribution of PM₁₀, with the attribution for days that exceeded the state 24 h mean PM₁₀ standard being of particular interest.

Available data (https://aqs.epa.gov/aqsweb/documents/data_mart_welcome.html (accessed on 3 January 2023)) on the temporal record of hourly PM₁₀ and hourly meteorological data at the CDF (i.e., wind speed and wind direction measured at 10 m AGL, 2019–2022) and within the ODSVRA, at a station designated as the S1 tower (Figure 1) (wind speed and wind direction measured at 10 m AGL), were also examined to determine the likelihood of an exceedance of the state 24 h mean PM₁₀ standard when the direction of particle transport was from the ODSVRA toward the CDF.

2. Materials and Methods

2.1. PM₁₀ Sampling and Analyses

PM₁₀ samples were collected on filters over 24 h periods (midnight to midnight) every three days at the CDF monitoring site between April and October 2021 (Figure 1). Collocated FRM samplers were used to collect PM₁₀ on paired filters for gravimetric-mass and chemical analyses (Figure 2). These analyses were carried out by the Environmental Analysis Facility (EAF) of the Desert Research Institute (DRI), Reno, NV. For quality-assurance purposes, additional samples collected on a 1-in-6 day schedule on 47 mm Teflon-membrane filters were submitted for gravimetric analysis to the South Coast Air Quality Management District (SCAQMD), Diamond Bar, CA. To detect possible sampler bias, the samplers were rotated throughout this study so that Teflon, quartz, and QA samples were collected from each of the samplers. Continuous hourly PM₁₀ measurements were made using a BAM, as described below. All sampler and monitor inlets were located on the roof of the CDF monitoring station and were at least 1 m but no more than 4 m from each other.

Filter-based PM₁₀ samples were collected in accordance with the requirements of US EPA Designation RFPS-1298-127 for PM₁₀ sample collection [14], following the instrument manual and the California Air Resources Board's Standard Operating Procedure, AQSB SOP 404 [15]. Briefly, preweighed Teflon-membrane and pretreated quartz-fiber filters in cartridges were obtained from the analytical lab and loaded into the sampling instruments in batches. The instruments were fitted with louvered PM₁₀ inlets, as specified in 40 CFR 50, Appendices J and L, and samples were collected at a calibrated flow rate of 16.7 L min^{-1} for 24 h. After removal from the sampler, exposed filters were stored and transported to the

analytical laboratory at 2 to 4 °C. For sample blanks, preweighed filters were obtained from the analytical lab and then stored along with exposed cassettes at 2 to 4 °C, then returned to the lab for analysis without being placed in a sampler.



Figure 2. The Partisol samplers and BAM 1020 monitors at the CDF sampling site. All sampler inlets (Partisols and BAMs) were approximately 4.0 m above ground level (Photo credit, David Cardiel).

Continuous hourly PM_{10} measurements were conducted using a MetOne Instruments BAM 1020 (Grants Pass, Oregon) (Figure 2), which is US EPA-designated FEM EQPM-0798-122 [14]. This instrument was operated in accordance with the US EPA requirements in 40 CFR 58 and its appendices, the SLOAPCD Standard Operating Procedure for the MetOne Instruments BAM 1020 [16], and the instrument manual. For comparison with the gravimetric data, 24 h BAM concentrations were calculated by averaging valid hourly data. For a 24 h mean BAM concentration to be valid, at least 75% of the constituent hourly values were required to be valid.

2.2. Laboratory Chemical Analysis

Detailed laboratory analyses were conducted for each of the PM_{10} filter samples, including particle mass, elements, ions, carbon fractions, and methanesulfonate, to identify potential source markers and to perform source apportionment [17,18].

The teflon-membrane filters, following exposure and shipping, were equilibrated in a clean room with controlled temperature (21.5 ± 1.5 °C) and relative humidity (RH; $35 \pm 5\%$) before gravimetric analysis to minimize particle volatilization and aerosol-liquid-water bias [19,20]. The filters were weighed before and after sampling using an XP6 microbalance (Mettler Toledo Inc., Columbus, OH, USA) at the DRI or a Sartorius MC5 microbalance (Data Weighing Systems, Inc., Wood Dale, IL, USA) at the SCAQMD, each with a sensitivity of ± 1 µg. A radioactive source (500 picocuries of Polonium210) and an electrostatic charge neutralizer were used to eliminate static charge on the filters. A total of 51 elements (from Na to U) were quantified on the Teflon-membrane filters using XRF (PANalytical Model Epsilon 5, Almelo, The Netherlands) [21].

Half of each quartz-fiber filter was extracted in distilled, deionized water (DDW) and analyzed for eight water-soluble ions, including chloride (Cl^-), nitrate (NO_3^-), sulfate (SO_4^{2-}), ammonium (NH_4^+), sodium (Na^+), magnesium (Mg^{2+}), potassium (K^+), and calcium (Ca^{2+}), via ion chromatography (Dionex ICS 5000+ IC systems, Thermo Scientific, Sunnyvale, CA, USA) [22]. A 0.5 cm² punch was taken from the other half of each quartz-fiber filter to quantify the OC, the EC, and eight thermal fractions (OC1-OC4, pyrolyzed carbon [OP], and EC1-EC3) following the IMPROVE_A thermal/optical protocol using the DRI Model 2015 Multiwavelength Carbon Analyzer (Magee Scientific, Berkeley, CA, USA) [23,24]. Methanesulfonate ($CH_3SO_3^-$), a marker species for oceanic biogenic materials, was measured using ion chromatography.

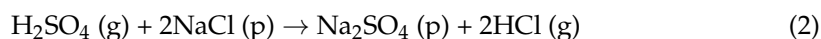
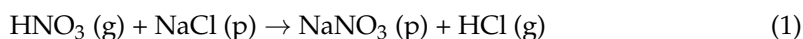
2.3. Data Analysis

The three independent 24 h PM₁₀ mass-concentration datasets (i.e., the SLOAPCD's BAM measurements; the gravimetric-mass concentration from the Teflon membranes, determined by the DRI; and the gravimetric-mass concentration from the Teflon membranes, determined by the SCAQMD) were compared via linear regression, both with and without an intercept term; Deming regression, both with and without an intercept term; and the 90th-percentile upper bound of the coefficient of variation (CVUB). While linear regression assumes that the values of the dependent variable are exactly known, Deming regression is an errors-in-variable model that relaxes this assumption. Deming regression is often used to determine the line of best fit when two variables are measured with errors [25]. Deming regression coefficients were calculated in the R software suite [26] using the "Deming" package [27] and assuming a constant coefficient of variation. The CVUB is the statistic used by the US EPA to evaluate the precision of collocated particulate matter samplers. The CVUB is based on the standard deviation of the percentage differences of mass concentrations from collocated samplers and was calculated according to the procedure in 40 CFR 58, Appendix A, Section 4.2. For low-volume PM₁₀ samplers, such as those used in this study, the EPA's data quality objective is a CVUB of less than 10%.

The identification of PM₁₀ sources and the estimation of source contributions used a weight-of-evidence approach [18,28]. First, the detailed chemical data were grouped into major constituent groups representing different sources (e.g., sea salt, mineral dust, traffic emissions, and regional/urban background), and their concentrations and contributions to the PM₁₀ were calculated. Next, the wind speed and direction on days exceeding the state 24 h mean PM₁₀ mass-concentration standard (50 µg m⁻³) were examined to infer the direction of PM₁₀ transport from the source to the receptor (CDF). The combination of windroses, PM₁₀ roses, and PM₁₀ compositions provided weighted evidence of PM₁₀ sources.

Fresh sea salt particles are generated through two main pathways: (1) bubble-bursting when air bubbles entrained by breaking waves rise to the surface and burst to create film and jet drops, and (2) spume drops when the wind shear is sufficiently high to tear water droplets off surface waves [29]. The composition of fresh sea salt is usually considered similar to that of bulk seawater, and the compositions with the highest mass percentages are Cl (55.04%), Na (30.61%), SO₄²⁻ (7.68%), Mg (3.69%), Ca (1.16%), and K (1.1%) [30]. Once in the air, the spray droplets are transported and dispersed by wind, and chemical reactions with other atmosphere constituents subsequently change their composition. Due to proximity to the ocean, sea salt particles may deposit on beach sands and may be resuspended as fresh or aged sea salt particles along with mineral dust.

One of the main chemical reactions during sea salt aging is chloride depletion, often observed in coastal regions, where particulate chloride is displaced as gas-phase hydrogen chloride (HCl) in atmospheric reactions with nitric and sulfuric acids [31];



The degree of chloride depletion can be estimated from the ratios of Cl⁻/Na⁺ and (Cl⁻ + NO₃⁻)/Na⁺.

As Na⁺ is conservative during sea salt aging, we separated the sea salt Na⁺ (ssNa⁺) into fresh sea salt Na⁺ (fsNa⁺) and aged sea salt Na⁺ (asNa⁺). The fresh sea salt (FS) was calculated as the sum of the measured Cl⁻ that had not been displaced, the corresponding fsNa⁺ had the same Na⁺/Cl⁻ ratio in the seawater, and the sea salt (ss) contributions of Mg²⁺, K⁺, Ca²⁺, and SO₄²⁻. As ssMg²⁺, ssK⁺, ssCa²⁺, and ssSO₄²⁻ do not change with aging, these ions were estimated using their ratios of total measured ssNa⁺ in typical fresh seawater [30,32,33]. The equation for estimating FS is

$$\text{FS} = \text{fsNa}^+ + \text{Cl}^- + \text{ssMg}^{2+} + \text{ssK}^+ + \text{ssCa}^{2+} + \text{ssSO}_4^{2-} \quad (3)$$

where $fsNa^+$ is estimated as $0.56 \times Cl^-$, $ssMg^{2+}$ as $0.12 \times ssNa^+$, ssK^+ as $0.036 \times ssNa^+$, $ssCa^{2+}$ as $0.038 \times ssNa^+$, and $ssSO_4^{2-}$ as $0.252 \times ssNa^+$.

The aged sea salt (AS) was estimated by balancing the excess Na^+ with NO_3^- and then with SO_4^{2-} [34]. The excess Na^+ was calculated as the molar equivalent difference between Na^+ and Cl^- [35]. The equation for estimating AS is

$$AS = asNa^+ + asNO_3^- + asSO_4^{2-} \quad (4)$$

where $asNa^+ = ssNa^+ - fsNa^+$, and $asNO_3^-$ and $asSO_4^{2-}$ are calculated by balancing $asNa^+$.

The measured PM_{10} species were grouped into seven major compositions, including fresh sea salt (FS); aged sea salt (AS); non-sea-salt sulfate ($nssSO_4^{2-}$), which was estimated as the total SO_4^{2-} minus the sea salt SO_4^{2-} ($ssSO_4^{2-}$); mineral dust (MD); elemental carbon (EC); organic matter ($OM = OC \times \text{multiplier}$); and other measured species. The sum of these seven composition groups was defined as the reconstructed mass, and the difference between the gravimetric and reconstructed masses was reported as the “unidentified” mass [36].

FS and AS were estimated using Equations (3) and (4), respectively. The MD was estimated as

$$MD = (3.48 \times Si) + (1.63 \times nssCa) + (2.42 \times Fe) + (1.94 \times Ti) \quad (5)$$

following the modified IMPROVE formula, where the non-sea-salt Ca ($nssCa$) is the total Ca minus the sea-salt Ca^{2+} ($ssCa^{2+}$) in Equation (3) [36,37].

A multiplier of 1.8 was used to convert OC to OM for nonurban aerosols [37,38]. The “Other” category is the sum of other measured ions (e.g., NH_4^+) and elements (e.g., Br and Ba) without double-counting. The reconstructed mass (RM) was calculated as

$$RM = OM + EC + nssSO_4^{2-} + FS + AS + MD + Others \quad (6)$$

3. Results

3.1. Data Quality Assurance

A total of 47 valid 24 h sample pairs were taken between April and October 2021 at the CDF monitoring site (Figures 1 and 2). Of these days (Figure 3), one equaled and eight exceeded the state 24 h mean PM_{10} mass concentration standard ($50 \mu g m^{-3}$) based on the gravimetric measurement of the particle mass and the measured flow volume from the Partisol sampler loaded with Teflon-membrane filters. One sample, from 7 October 2021, was identified as an outlier and removed from further analysis. On that day, the BAM recorded a 24 h average of $25 \mu g m^{-3}$ and the QA sample analyzed by the South Coast AQMD had a mass concentration of $25 \mu g m^{-3}$, while the mass concentration of the sample analyzed by the DRI was $90 \mu g m^{-3}$.

The relations between the 24 h PM_{10} mass concentrations determined by the various measurements (i.e., BAM and gravimetry performed by the DRI and the SCAQMD) were explored for quality-assurance purposes and for comparison with the results of Lewis et al. [13]. Since gravimetric-mass concentration is determined solely from Teflon-membrane filters, the gravimetric analysis for the sample pair may still have been valid even if a paired quartz-fiber filter were invalid or missing. Thus, there were 47 valid 24 h gravimetric-mass concentrations from the DRI analysis, with corresponding valid BAM concentrations, and 26 from the SCAQMD gravimetric analysis. As noted above, linear regression, Deming regression, and the CVUB were used to compare these datasets. For the regression analyses, the BAM concentrations were treated as the dependent variable and the gravimetric concentrations as the independent variable. The results are summarized in Tables 1 and 2.

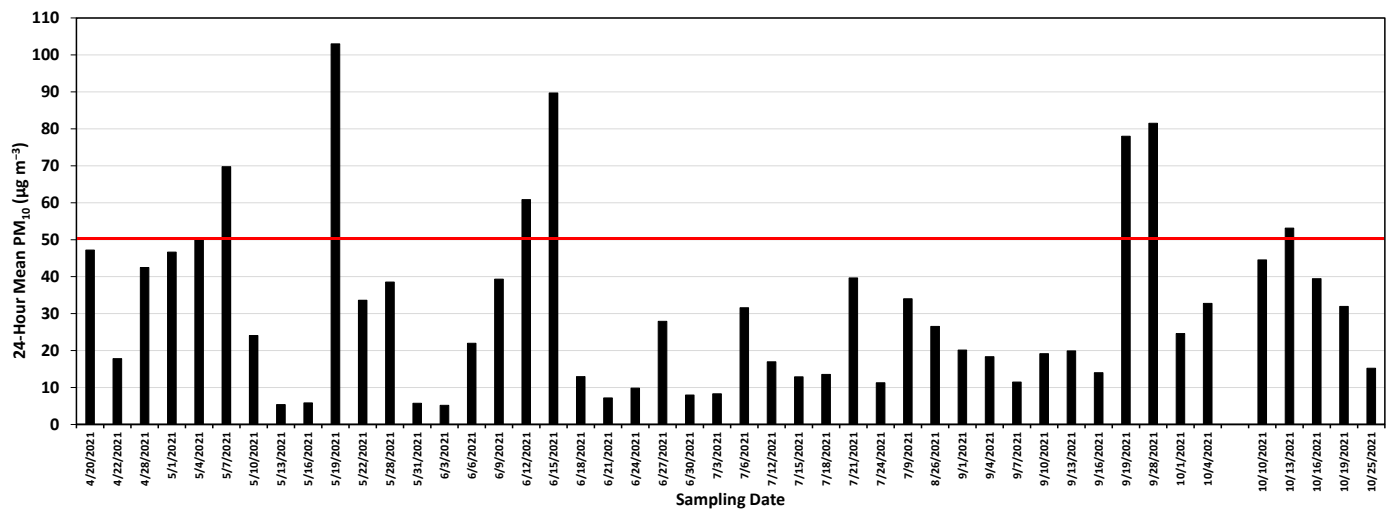


Figure 3. The validated mean 24 h PM_{10} ($\mu g m^{-3}$) concentration for the days sampled between April and October 2021. Concentration of PM_{10} was determined from gravimetric analysis of the Teflon-membrane filter. The horizontal line represents the state mean 24 h PM_{10} standard of $50 \mu g m^{-3}$.

Table 1. BAM vs. gravimetric PM_{10} concentration comparisons, linear regressions.

Comparison	Sample Size	Linear Regression		R^2	Linear Regression through the Origin	
		Slope (95% CI)	Intercept (95% CI)		Slope (95% CI)	R^2
SLOAPCD BAM vs. DRI Gravimetric	53	1.047 (1.023–1.071)	−0.421 (−1.323–0.481)	0.993	1.038 (1.024–1.053)	0.997
SLOAPCD BAM vs. SCAQMD Gravimetric	24	1.004 (0.956–1.051)	−0.128 (−1.675–1.419)	0.987	1 (0.973–1.027)	0.996

Table 2. BAM vs. gravimetric PM_{10} concentration comparisons—Deming regression and CVUB results.

Comparison	Sample Size	Deming Regression		Deming Regression through the Origin	CVUB
		Slope (95% CI)	Intercept (95% CI)	Slope (95% CI)	
SLOAPCD BAM vs. DRI Gravimetric	53	1.014 (0.981–1.046)	0.307 (−0.129–0.907)	1.032 (1.010–1.054)	6.44%
SLOAPCD BAM vs. SCAQMD Gravimetric	24	1.003 (0.947–1.060)	−0.236 (−1.076–0.605)	0.987 (0.947–1.027)	7.05%

The comparisons in Tables 1 and 2 show excellent agreement between the gravimetric and BAM measurements, with R^2 values greater than 0.98 and slopes near 1:1, giving confidence that the BAM data provided reasonable measurements of hourly and 24 h mean PM_{10} . In comparison of the DRI gravimetric and SLOAPCD BAM concentrations, the linear-regression models—both with and without an intercept—and the Deming model without an intercept all indicated a statistically significant but small bias of 4% to 5%. Nonetheless, with a CVUB of 6.44%, this pair of samplers was well within the EPA’s data quality objective for collocated monitors. In comparison of the SCAQMD gravimetric and SLOAPCD BAM concentrations, none of the regression models or the CVUB indicated a statistically significant difference between the measurements.

3.2. Fresh and Aged Sea Salt

Inorganic ions in this coastal environment without major local aerosol sources likely come from sea salt, mineral dust, and the regional/urban background. Figure 4 shows that measured cations are highly correlated with anions ($R^2 = 0.99$) with a regression slope of 1.04, indicating that most ions were measured with high quality and the particles were nearly neutral. The slightly higher-than-unity slope (1.04) is dominated by a few data points with high ion concentrations, which was probably caused by the carbonate (CO_3^{2-}) that is common in mineral dust but was not analyzed in this study.

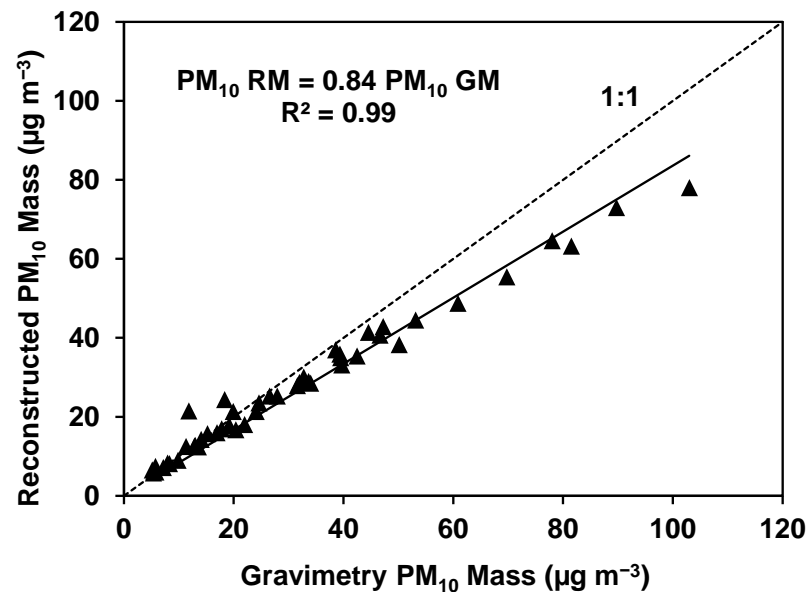


Figure 4. Correlation between water-soluble cations and anions.

Figure 5 shows that both Mg^{2+} and K^+ are highly correlated ($R^2 \geq 0.98$) with Na^+ , and the regression slopes are very close to the expected mass concentration ratios (0.12 for $\text{Mg}^{2+}:\text{Na}^+$ and 0.036 for $\text{K}^+:\text{Na}^+$) in seawater [30]. Therefore, Na^+ , Mg^{2+} , and K^+ mainly originate from fresh sea salt [35]. In contrast, Figure 6 shows that Ca^{2+} and SO_4^{2-} exceed the fresh seawater ratios for most samples and their correlations with Na^+ are lower than those in Figure 6. The excess Ca^{2+} and SO_4^{2-} indicate additional sources, likely minerals (e.g., CaCO_3) for the Ca^{2+} and the regional/urban background for the SO_4^{2-} . Water-soluble Ca^{2+} and SO_4^{2-} can also form from heterogeneous reactions between sulfuric acid (H_2SO_4) or sulfur dioxide (SO_2) and mineral dust [34,39,40].

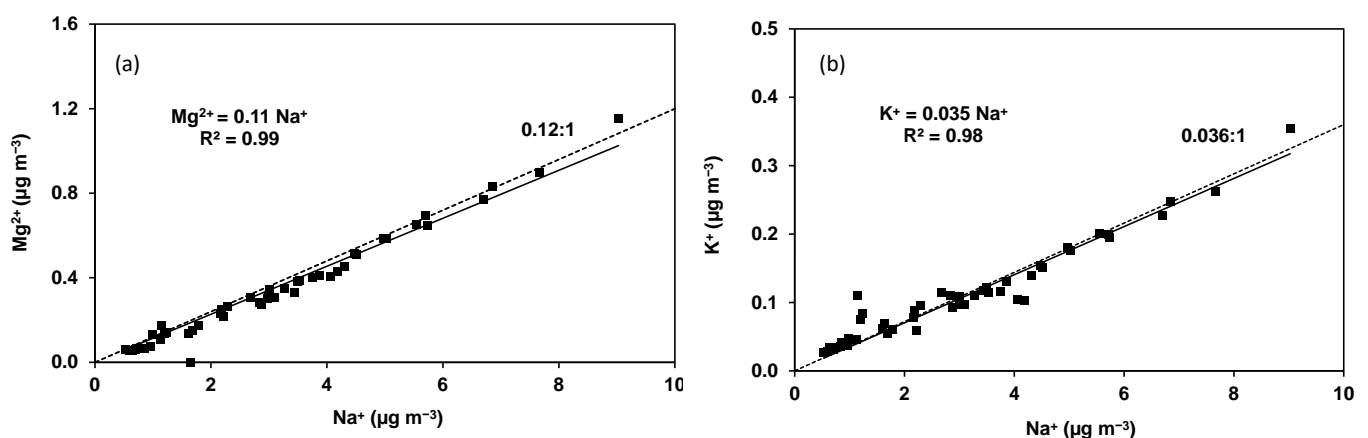


Figure 5. Correlations between: (a) Mg^{2+} and Na^+ , (b) K^+ and Na^+ . The dashed lines indicate ion ratios in fresh seawater.

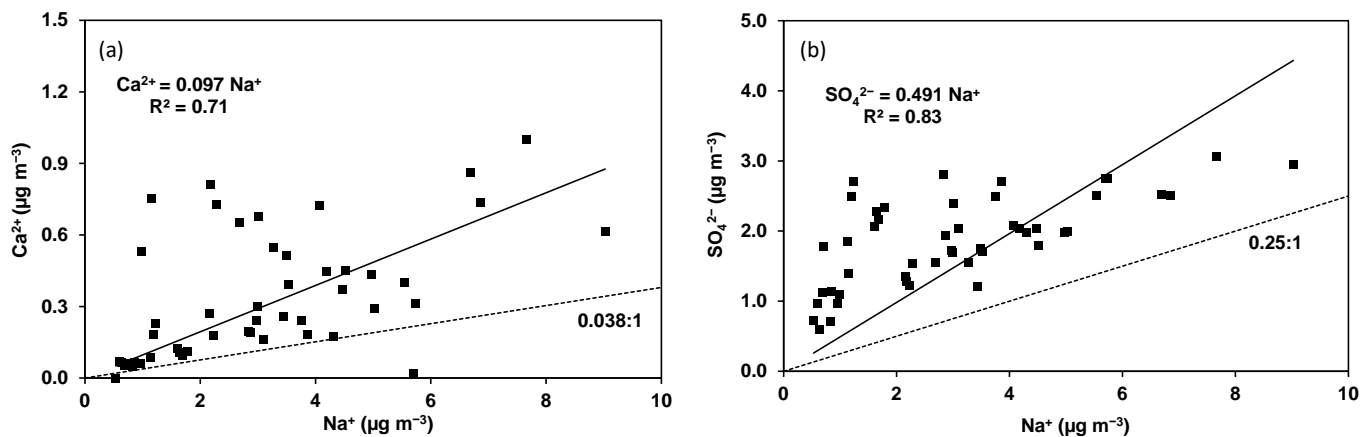


Figure 6. Correlations between: (a) Ca^{2+} and Na^+ , (b) SO_4^{2-} and Na^+ . The dashed lines indicate ion ratios in fresh seawater.

In the assumption that sea salt was the only source of Na^+ and Cl^- at the monitoring site, typical fresh sea salt particles have a Cl^-/Na^+ mass ratio of 1.8 [30]. Figure 7a shows that at the CDF, the average Cl^-/Na^+ ratio is 1.51: lower than 1.8 for all samples. Therefore, approximately 16% Cl^- was displaced by stronger acids (e.g., nitric and/or sulfuric acids). Figure 7b shows that most data points are below the 1:1 line, indicating that both NO_3^- and SO_4^{2-} were involved in the Cl^- displacement for most samples.

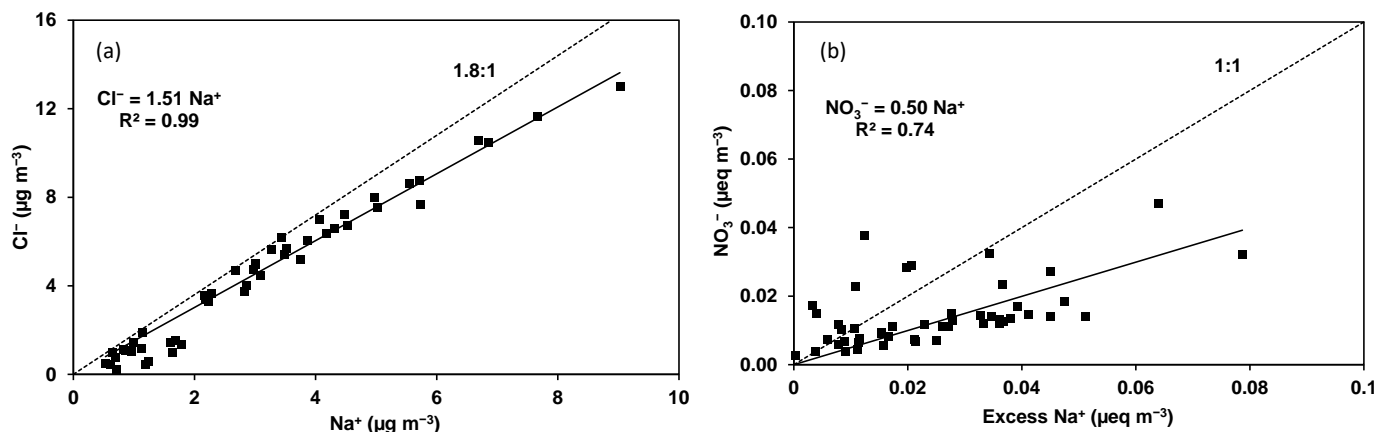


Figure 7. Correlations between: (a) Cl^- and Na^+ , (b) NO_3^- and excess Na^+ . Dashed line in (a) indicates the typical fresh sea-salt-particles' Cl^-/Na^+ mass ratio of 1.8. Dashed line in (b) is the 1:1 line.

Figure 8 shows that the AS/FS ratio decreases with the PM_{10} concentration when the PM_{10} concentrations are lower than approximately $40 \mu\text{g m}^{-3}$, and the ratio remains < 0.2 at higher PM_{10} concentrations, indicating that FS dominates SS during high- PM_{10} -concentration events.

3.3. PM_{10} Major Chemical Composition and Mass Reconstruction

The relation between the mass determined by gravimetric analysis and the reconstructed mass showed a strong correlation ($R^2 = 0.99$), indicating that the gravimetric and chemical measurements were of high accuracy (Figure 9). Since the slope (0.84) of the best-fit linear-regression line was less than unity, it indicated that there were constituents of the PM_{10} that were not accounted for by those measured in the laboratory analysis or in the mass reconstruction (Equation (6)). The unidentified mass is also shown as the difference between the gravimetric mass (represented by *) and the reconstructed mass (represented by the stacked bar height) in Figure 10. The attribution of the unidentified PM_{10} mass to a source is described later.

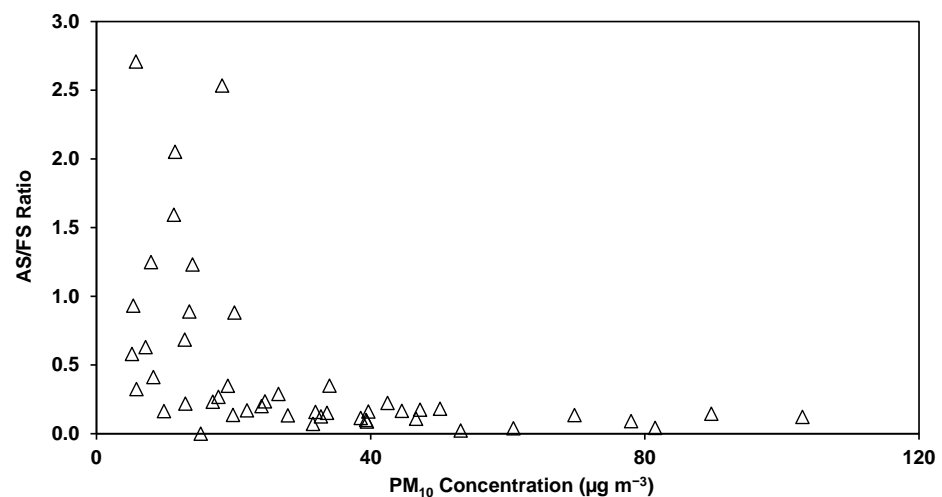


Figure 8. Ratio of aged over fresh sea salt (AS/FS) as a function of PM_{10} concentration.

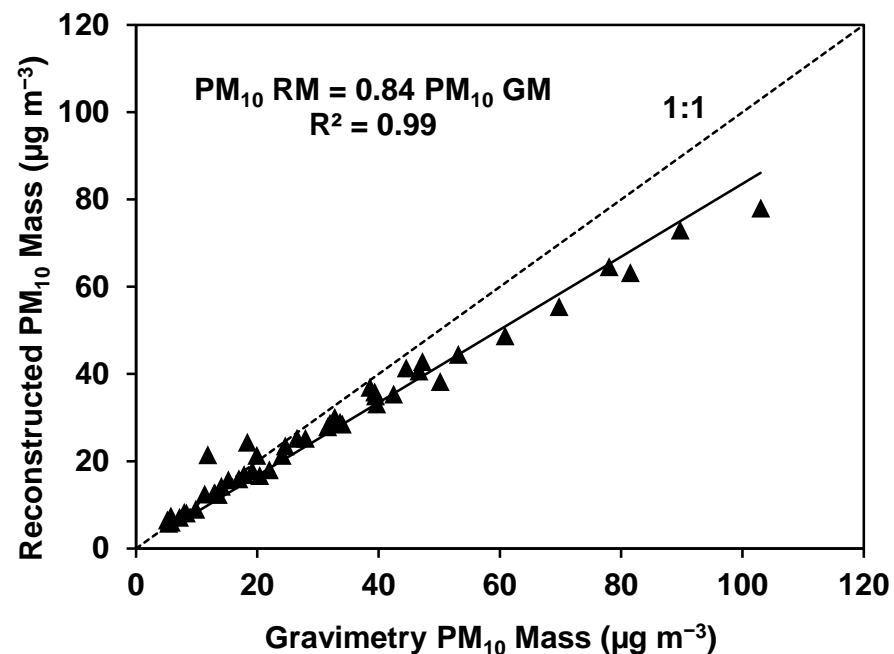


Figure 9. Correlation between reconstructed and gravimetric PM_{10} mass concentrations.

Figure 10 shows that mineral dust and sea salt had high concentrations during the high- PM_{10} days at the CDF monitoring station, representing influences from saltation-driven dust emissions and ocean sea spray, while OM was a minor contributor. Additionally, the concentrations of tracers for on-road traffic emissions (represented by EC) and regional pollution (represented by $nssSO_4^{2-}$, $nssNO_3^-$, and NH_4^+ (included in the others category)) were low. The concentration of methanesulfonate ($CH_3SO_3^-$) was $<1.2 \mu g m^{-3}$ for all sampling days. The PM_{10} mass percentages of the chemical constituents in Figure 11 show that while sea salt and mineral dust were the dominant PM_{10} constituents during high- PM_{10} -concentration days, organics and $nssSO_4^{2-}$ contributions were higher during lower- PM_{10} -concentration days.

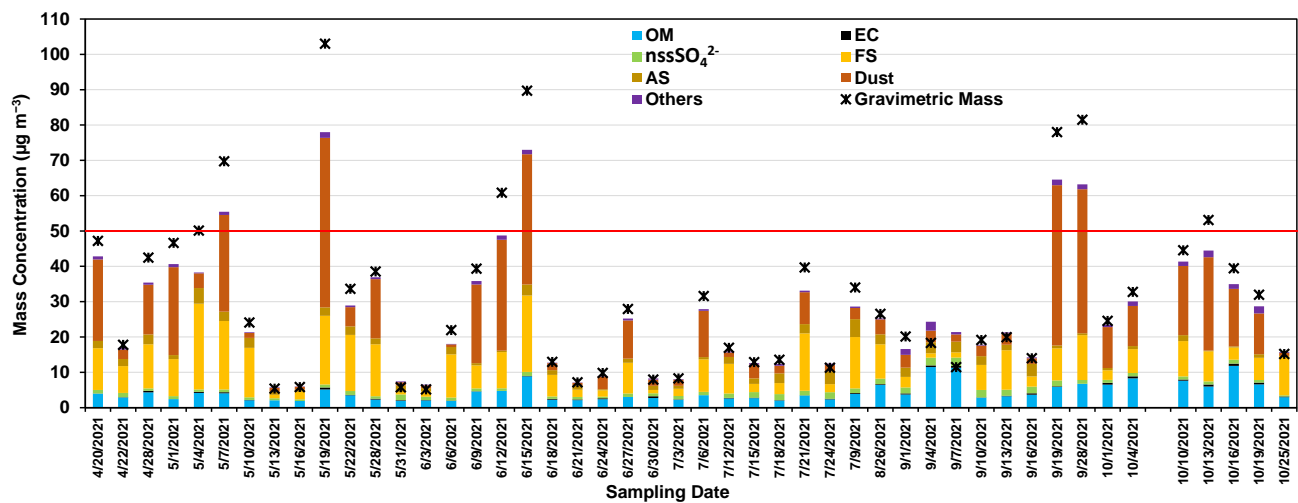


Figure 10. Concentration of PM₁₀ chemical constituents (stacked bars) and gravimetric mass (*) for the days sampled between April and October 2021. The horizontal line represents the state mean 24 h PM₁₀ standard of 50 µg m⁻³.

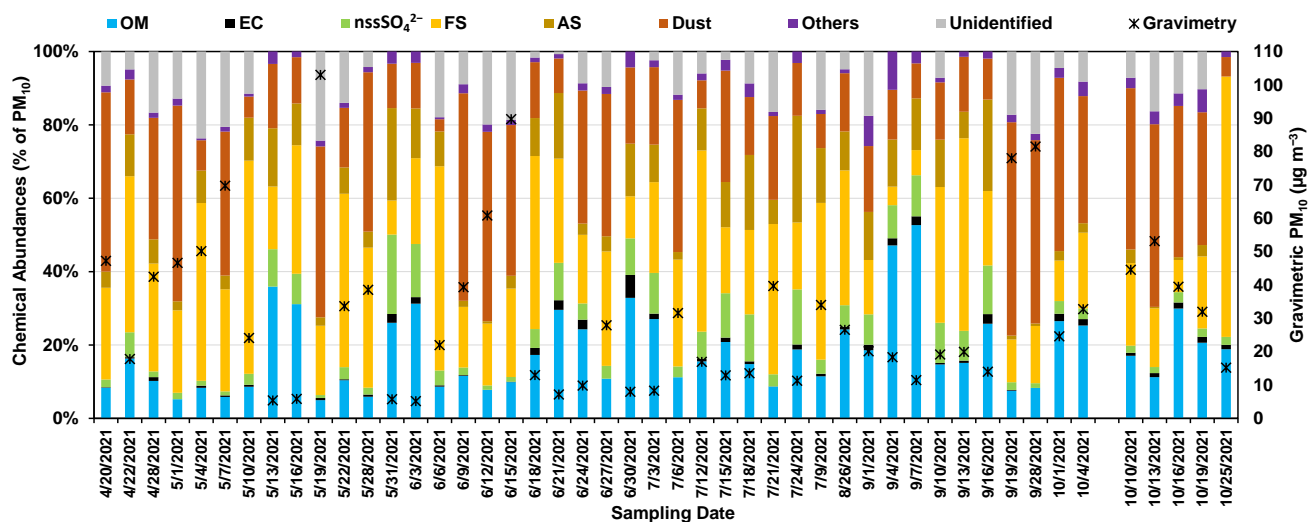


Figure 11. PM₁₀ mass percentages of chemical constituents (stacked bars) and gravimetric mass (*) for the days sampled between April and October 2021.

3.4. Source Attribution of PM₁₀ at the CDF

Of critical interest is the understanding of contributions from the direction of the ODSVRA to the PM₁₀ measured at the CDF on the days that exceeded the state 24 h PM₁₀ standard. During the monitoring period, eight exceedance days were identified to define the source attribution (Figure 3). The source attribution for these days was based on the chemical-speciation data and using Equation (3) (FS), Equation (4) (AS), Equation (5) (MD), the OM, the EC, and the non-SS sulfate to estimate the relative contributions to the total reconstructed mass (Equation (6)). Also included in the source attribution was the category “Others” that represented the sum of other measured ions and elements not accounted for in the above categories. For each of the identified exceedance days, the 24 h mean PM₁₀ concentration, the wind rose, the PM₁₀ rose, the source attribution, and the attribution of the PM₁₀ mass based on the hours of transport from the direction of the ODSVRA to the CDF are shown in Table 3. The PM₁₀ roses and attribution of hours when PM₁₀ was being transported to the CDF from the direction of the ODSVRA are based on hourly measurements of wind speed and direction and hourly BAM-measured PM₁₀.

Table 3. Days that exceeded the state 24 h mean PM₁₀, wind and PM₁₀ directional relations, and the attribution of PM₁₀ mass based on the hours of transport from the direction of the ODSVRA to the CDF.

Date	24 h PM ₁₀ (µg m ⁻³)	Wind Rose	PM ₁₀ Rose	Source Attribution	% Mass from Direction of ODSVRA
4 May 2021	50				58
7 May 2021	70				84
19 May 2021	103				89

Table 3. Cont.


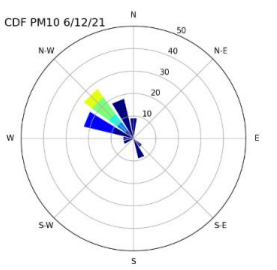
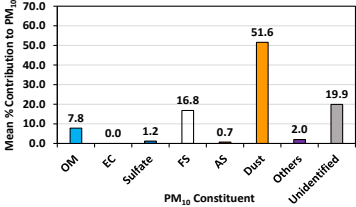


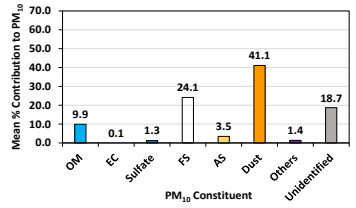
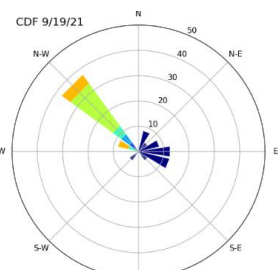
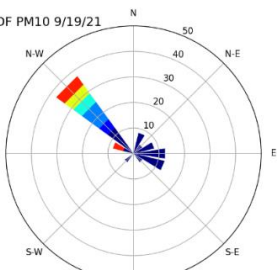
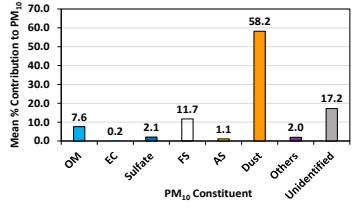
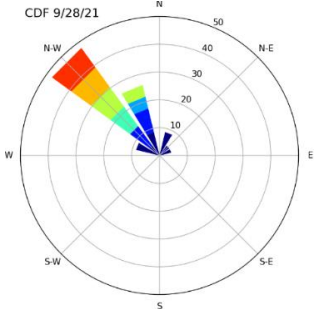
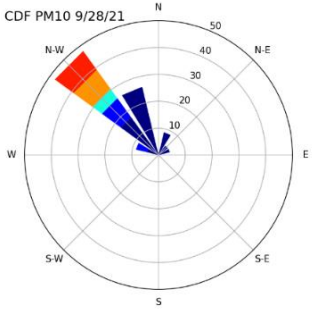
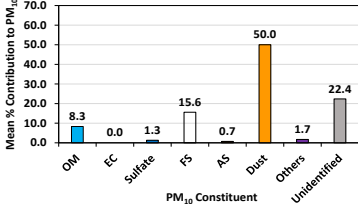

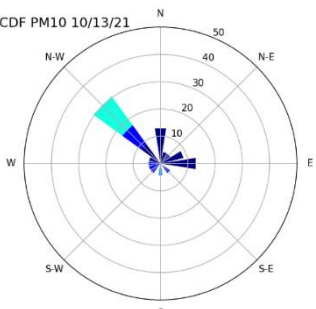
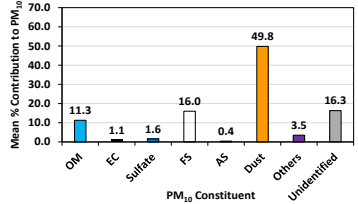
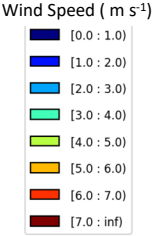
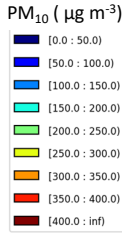
Date	24 h PM ₁₀ (µg m ^{−3})	Wind Rose	PM ₁₀ Rose	Source Attribution	% Mass from Direction of ODSVRA
12 June 2021	61				71
15 June 2021	90				93
19 September 2021	78				85

Table 3. Cont.

Date	24 h PM ₁₀ (µg m ^{−3})	Wind Rose	PM ₁₀ Rose	Source Attribution	% Mass from Direction of ODSVRA
28 September 2021	82				92
13 October 2021	53				63 (one hour of missing BAM data)
					

3.4.1. Compiled Source Attribution for Exceedance Days in 2021

For the exceedance days identified for the period of April–October 2021, for the sources defined for each individual day (excluding 7 October 2021), the composition percentages from each of the bar charts, shown in Table 3, were used to calculate a mean source attribution for the exceedance day. This attribution is presented in Figure 12. The dominant source of the PM₁₀ is MD (43.1% \pm 15.3%), followed by SS (22.4% \pm 11.7% for FS and 2.6% \pm 2.8% for AS) and the unidentified category (20.4% \pm 2.9%).

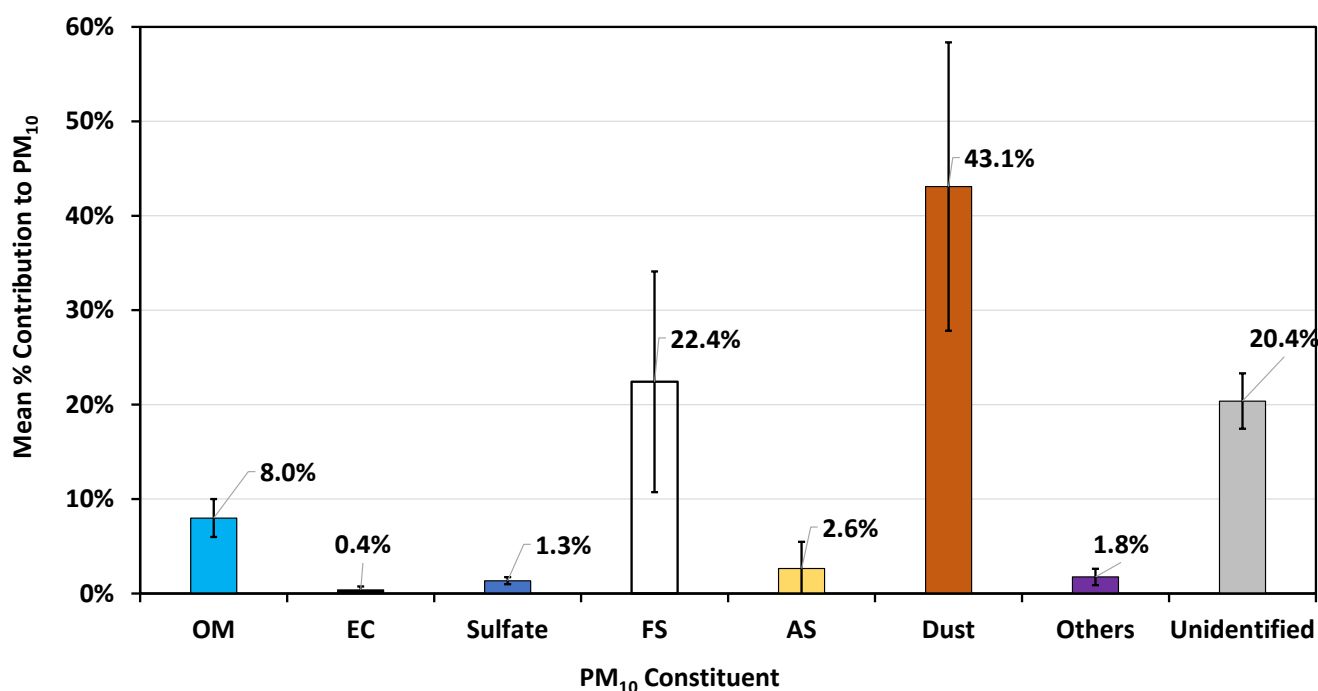


Figure 12. The mean source attribution of PM₁₀, representing the eight exceedance days between April and October 2021. Note: OM, organic matter; EC, elemental carbon; FS, fresh sea salt; and AS, aged sea salt. Error bars represent the standard deviation of the mean based on the eight sample days.

3.4.2. Compiled Source Attribution for Non-Exceedance Days in 2021

For the non-exceedance days identified for the period of April–October 2021, for the sources defined for each individual day, the composition percentage from each day was used to calculate a mean source attribution for a non-exceedance day. This attribution is presented in Figure 13.

The dominant source of the PM₁₀, as shown in Figure 13, was sea salt (fresh plus aged, 40.5% \pm 24.0%), followed by mineral dust (24.2% \pm 14.6%), OM (22.4% \pm 16.6%), sulfate (7.5% \pm 6.0%), others (2.8% \pm 2.5%), and unidentified (6.6% \pm 6.0%). The contributions from AS on non-exceedance days (10.8% \pm 8.3%) were much higher than those on exceedance days (2.6% \pm 2.8%), indicating that larger fractions of AS were collected at the CDF on days with a wider range of wind directions and lower wind speeds. The contributions from EC and non-SS nitrate (included in others) remained low, similarly to on the mean exceedance day (Figure 13). Sulfate increased, as more sources were likely in inland areas than areas to the west of the CDF. The source attribution for the mean non-exceedance days represented a day with a lower probability of winds that would entrain sand and emit dust within the ODSVRA, as well as a much greater degree of mixing with a wider range of wind direction.

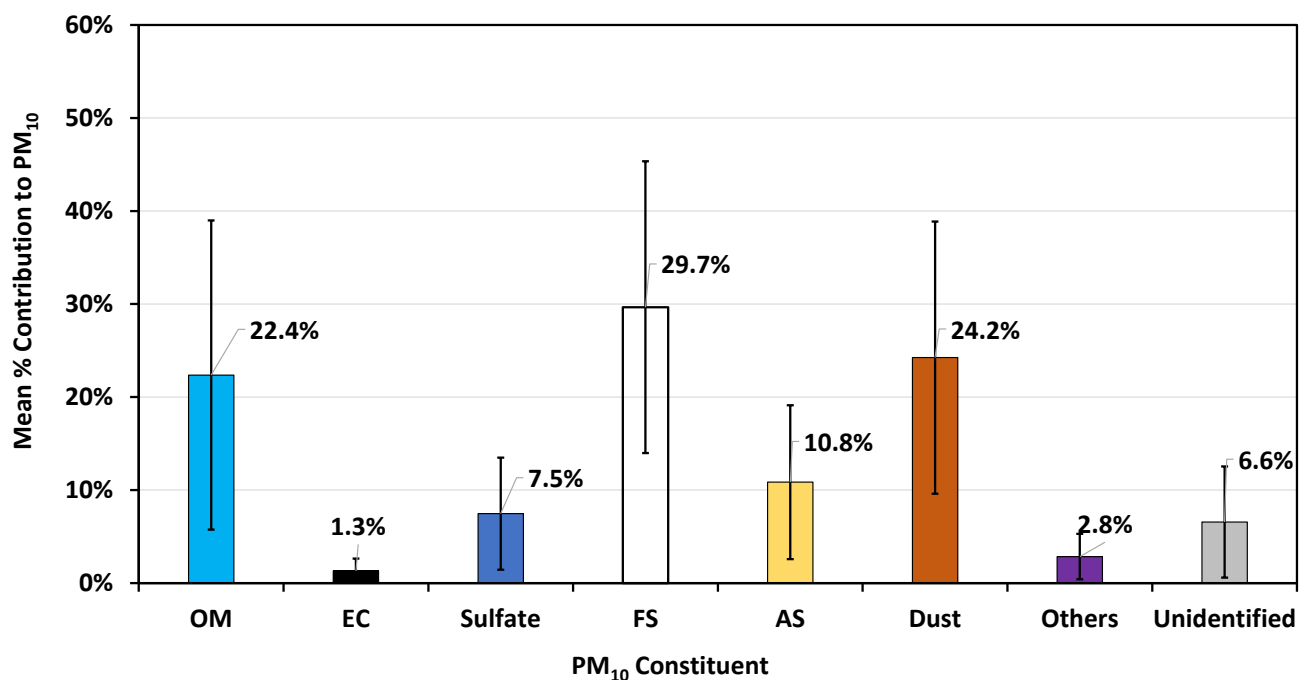


Figure 13. The mean source attribution of PM₁₀, representing the non-exceedance days between April and October 2021. Error bars represent the standard deviations of the means based on 39 sample days.

3.5. Exceedance Days Related to Wind Speed Magnitude, Duration, and Wind Direction Persistence at the CDF and the S1 Tower, 2019–2022

We examined the relation between days that met or exceeded the state 24 h mean PM₁₀ standard (based on averaging hourly PM₁₀ BAM data) and meteorological conditions, principally wind speed, wind direction, and precipitation conditions at the CDF and S1 tower monitoring locations for the period of 2019–2022, to evaluate the conditions that can lead to an exceedance of the state PM₁₀ standard. Based on Gillies et al. [2], we assumed the threshold for saltation within the ODSVRA was associated with a wind speed of 8 m s^{−1} measured at 10 m AGL at the S1 tower (Figure 1). To account for the wind speed gradient from S1 to the CDF, we examined the correspondence of 10 m AGL wind-speed values at the S1 tower between 7.75 m s^{−1} and 8.25 m s^{−1} with the 10 m AGL wind-speed values at the CDF. This distribution had a skewness of −0.099 and an excess kurtosis of −0.57. Based on these moderate values for the third and fourth moments, we chose the mean value of 3.6 m s^{−1} at the CDF to indicate that it was highly probable that the saltation threshold within the ODSVRA had been achieved.

To isolate the effect of wind, bearing PM₁₀, that had passed over the ODSVRA, we segregated the data based on wind direction ranges of 236–326° to represent the ODSVRA-influenced direction and 327–235° to represent the non-ODSVRA-influenced transport direction. The fractions of the 24 h periods for the wind direction ranges of 236–326° and 327–235° for the 20 days with the highest 24 h mean PM₁₀ values (ordered by total PM₁₀, descending from left to right) in 2019–2022 are shown in Figure 14. Of the total number of exceedances (201) in this period, 153 had >50% of the total daily PM₁₀ associated with the wind direction range of 236–326°. Two of the days in Figure 14, with <50% of their daily PM₁₀ values within the wind direction range of 236–326°, can be linked to regional events: 28 October 2019 was due to particulate matter being transported from the San Joaquin Valley [11] to San Luis Obispo Co., and 14 September 2020 due to wildfire smoke [41].

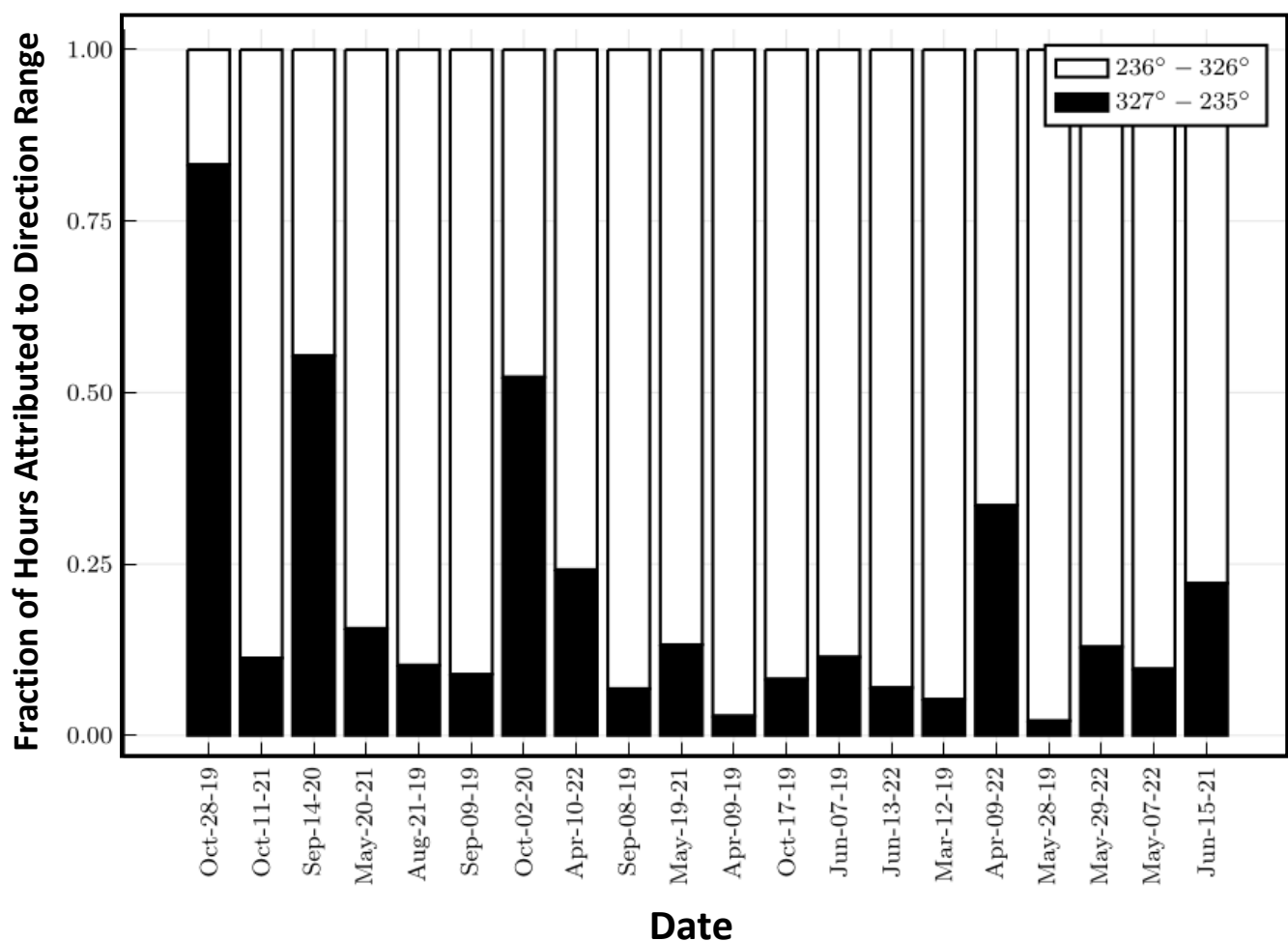


Figure 14. The fractions of the 24 h periods for the wind direction ranges of 236–326° (white portion of bar) and 327–235° (black portion of bar) for the 20 days with the highest 24 h mean PM₁₀ values above 50 µg m^{−3}, 2019–2022.

4. Discussion

4.1. Exceedance Days Related to Wind Speed Magnitude and Duration and Wind Direction Persistence

The wind and PM₁₀ roses shown in Table 3 indicate that for the identified exceedance days from April to October 2021, wind direction and associated elevated PM₁₀ were westerly to northwesterly with respect to the CDF. These days also had periods of time when wind speeds from this directional range exceeded 3.6 m s^{−1}, as measured at the CDF. For the longer period, 2019–2022, it is clear from the wind and PM₁₀ data records that exceedance of the state 24 h PM₁₀ standard had the greatest likelihood of occurring when the wind direction at the CDF was between 236 and 326°, bringing PM₁₀ to the CDF from the direction of the ODSVRA, and that as wind speed increased above 3.6 m s^{−1}, the probability of exceedance increased further.

4.2. Source Attribution on Exceedance Days

The source attributions for the identified exceedance days (Table 3) and the mean attribution from the eight identified days (Figure 12) suggest that the MD component (43.1% ± 15.3%) of the PM₁₀ was the principal source, followed by sea salt (25.0% ± 14.5%), on these days. The vertical flux of mineral dust particles from a source area, based on the physics of the dust emission process [42–44], scales nonlinearly with wind shear stress and horizontal saltation flux. Therefore, as wind speed, shear stress, and saltation flux

increased, the dust-sized particles, including those in the PM₁₀ size fraction, increased in number and mass concentration rapidly.

The other constituent of PM₁₀ that could increase as wind speed increases is sea salt. The production of sea spray on the open ocean is a function of wave height, wind history, wind shear, and water viscosity [45]. Production of sea spray by breaking waves is due to wind shear (primarily at the wave crest), splashing, and popping of breaker-entrained air bubbles rising to the free surface [46]. In combination, these processes will input more sea spray into the air as the wind speed increases. Upon evaporation of the liquid sea spray droplets, sea salt particles are created and their number and mass concentration in the atmosphere contribute a greater fraction to the overall PM₁₀. The chemical speciation of the sea salt fractions, fresh and aged, does not unambiguously resolve what fraction is directly attributable to sea spray, as sea salt particles could also originate from saltating sand as a result of sea salt particles or sea spray droplets being deposited previously to the sand surfaces. This separation of sea salt contribution in airborne PM₁₀ remains unresolved. If it is predominantly from evaporating sea spray droplets, then the contribution of this source will remain uncontrolled. If, however, a significant fraction of sea-salt PM₁₀ is derived from saltation and resuspension of deposited particles, then dust-control methods that reduce saltation will also reduce the input of sea-salt-particle contributions to downwind PM₁₀ when regional winds in the area are generally west to northwest.

The unidentified constituent of 20.4% ($\pm 2.9\%$) cannot be unambiguously resolved due to three analytical challenges. The first challenge is to account for the mass of PM₁₀ that is related to the presence of the oxide and carbonate components of the minerals that were not resolved by XRF or the other analytical methods. The second challenge is finding the accurate multiplier to convert OC to OM. A multiplier of 1.8, representative of nonurban aerosols, is used in Equation (6) [37,38]. Multiplier values ranging from 1.2 for fresh engine exhaust to 2.2 for aged aerosols sampled in remote areas have been reported [36]. Using a multiplier of 2.2 instead of 1.8 would reduce the unidentified fraction to 18.6% ($\pm 3.2\%$). Due to the small difference, a less-extreme multiplier of 1.8 was used. The third challenge is to measure particle-bound water content. The filters were weighed at 21.5 (± 1.5) °C and 35% ($\pm 5\%$) RH. This RH is lower than the efflorescence RHs of the main salt forms NaCl (43%), NaNO₃ (40%), and Na₂SO₄ (55%) [47]; therefore, the salt particles were likely in a dry state. However, McInnes et al. [48] observed that water made up 9% of submicron marine aerosol mass when weighted at 35% RH. Additionally, minerals often exist in hydrated phases, including water in crystal structures [49]. Currently, there are no standard ways to accurately determine mineral compositions or particle-bound water content in aerosol samples.

We note that the unidentified fraction (20.4% \pm 2.9% of PM₁₀) from this study is much lower than that reported by Lewis et al. [13], i.e., 69% ($\pm 18\%$) for all samples and 82% ($\pm 14\%$) for designated high-PM₁₀ days. Lewis et al. [13] speculated that ammonium nitrate, semivolatile organic compounds, and aerosol water were major contributors to their unidentified mass because these were not measured. Figure 7b shows that for these samples, most NO₃[−] is associated with Na⁺, not NH₄⁺. The sums of the NH₄⁺ and the NO₃[−] were 1.4% ($\pm 1.2\%$) and 5.2% ($\pm 3.4\%$) of PM₁₀ on exceedance and non-exceedance days, respectively, showing that NH₄NO₃ is a much smaller contributor to PM₁₀ than speculated by Lewis et al. [13]. Unfortunately, Lewis et al. [13] did not measure carbon or ions, and their data cannot be subjected to a quality check between the reconstructed and gravimetric masses, as shown in Figure 9. Their differences between the gravimetric and BAM data were much larger than those shown in Tables 1 and 2, indicating potential errors in their filter collection.

Lewis et al. [13] found only a moderate correlation ($R^2 = 0.71$) between their gravimetric PM₁₀-mass concentrations and the BAM PM₁₀ measurements made simultaneously, a few meters away. They also reported a significant bias between the datasets, with a slope and an intercept of 0.54 and 5.3 $\mu\text{g m}^{-3}$, respectively, for the linear regression of their gravimetric-mass concentrations in the BAM measurements. This indicates that at higher PM₁₀ levels,

their gravimetric measurements tended to be much less than the BAM measurements. In contrast, we found high correlations and low biases between our collocated gravimetric and BAM measurements (Tables 1 and 2) of PM_{10} . Lewis et al. [13] attributed the bias they observed to unmeasured semivolatile species—including ammonium nitrate, organic material, and water—that they assumed were lost from their gravimetric samples prior to analysis. This explanation is unlikely, as we did not observe this bias in our measurements, and furthermore, measured ammonium nitrate was found to be only a minor contributor to PM_{10} in our samples, along with relatively low contributions from carbonaceous particulate-matter constituents.

It is more likely that most of the unidentified mass represents the oxide components of the quartz and feldspar minerals common to the sands and of the carbonate minerals and/or the hydrated water in the clay minerals of the Oceano Dunes, as well as less-common minerals and their associated oxides. Equation (5) is a simplification for resolving very generalized mineral dust that was developed for rural sites in the IMPROVE network and cannot be made specific to a geographic area [50]. We arrived at the conclusion that the unidentified mass was largely oxide-associated and potentially some carbonate, as the wind and PM_{10} roses (Table 3) indicated that transport to the CDF for the identified exceedance days was dominated by periods when the wind direction was from the ODSVRA and the ocean. Our conclusion is further supported by the relation shown in Figure 15, which shows that the MD and unidentified PM_{10} concentrations increase as a function of the total 24 h PM_{10} measured with the BAM at the CDF when the wind direction range at the CDF is between 236° and 326° . That they increase as a function of increasing total PM_{10} for the same directional range supports that they are linked with the same source, i.e., saltation-driven dust emissions.

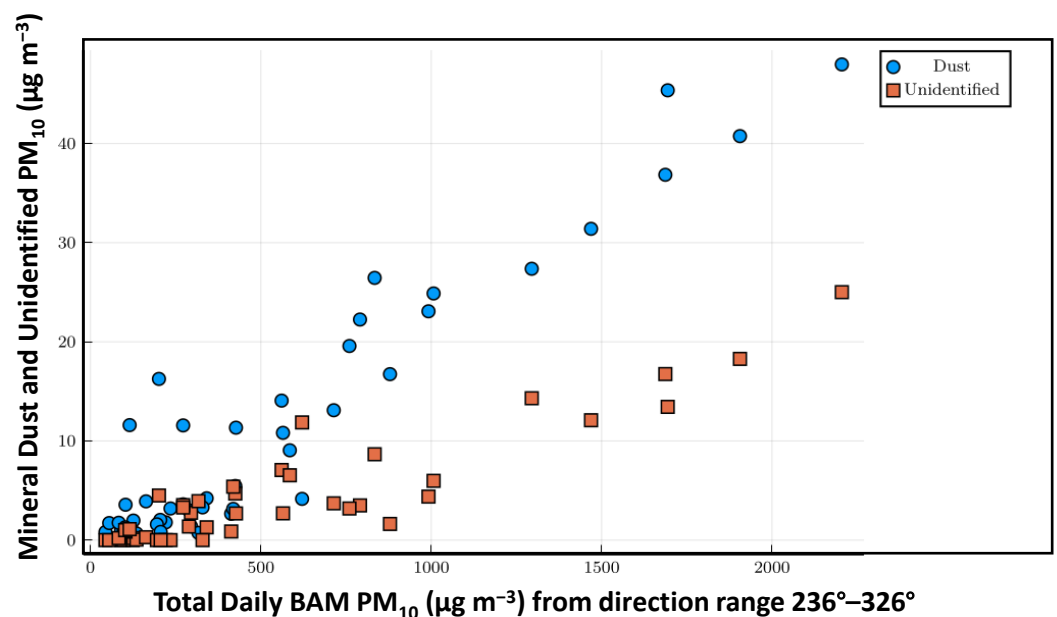


Figure 15. The relation between the MD and unidentified components of the PM_{10} and the total daily PM_{10} calculated from the BAM for all the valid sampling days from April to October 2021.

Assuming, as we suggest, that the unidentified component represents uncharacterized components of mineral-dust PM_{10} particles (i.e., the oxide components of the mineral particles), the range of attribution of MD to PM_{10} mass concentration on a generalized exceedance day (Figure 12) in April–October 2021 would be 45.3–81.7%, with sea salt accounting for a range between 10.5% and 39.5%.

As the OM and EC components were quite low on the exceedance days, there was no indication of combustion processes as a significant contributor. Other significant PM_{10} sources between the CDF and the ODSVRA, for the semivolatile particles speculated by

Lewis et al. [13], are implausible under the associated wind conditions, as upwind of the CDF is mainly open vegetation-covered areas until the eastern edge of the Oceano Dunes is reached. The presence of a significant source of semivolatile particles would have been accounted for in the quantification of the OM component, but an 8.0% attribution of OM in the PM_{10} , as found in this analysis, suggests that significant contributions from semivolatile particles is unlikely. To further support this argument, Figure 16 shows the relation between the OM (which includes semivolatile species), the EC and the total 24 h PM_{10} as measured with the BAM at the CDF when the wind direction range was $327\text{--}235^\circ$ (i.e., not from the direction of the ODSVRA) for all the valid sample days.

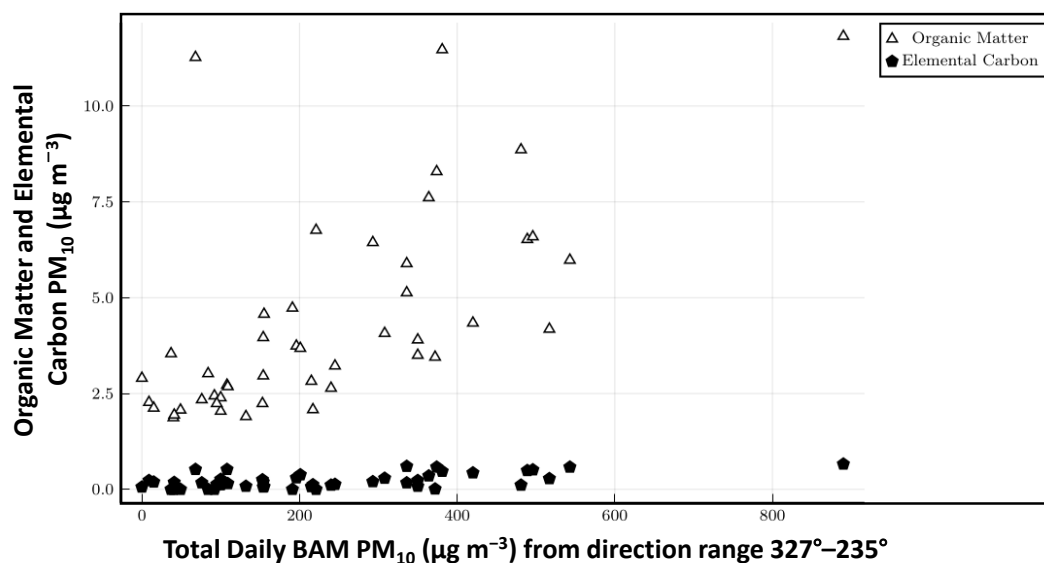


Figure 16. The relation between the OM and EC components of the PM_{10} and the total daily PM_{10} calculated from the BAM for all the valid sampling days from April to October 2021.

Under these conditions, the EC was relatively invariant while the OM generally increased with increasing total PM_{10} , suggesting that the OM composition of the PM_{10} increased when transport to the CDF was not from the direction of the ODSVRA and there were greater contributions from combustion sources of particulate matter.

The other constituents of the PM_{10} (Figure 11), i.e., EC, OM, nitrate, and sulfate, were generated by sources that do not increase their emission strength as a function of increasing wind speed, as was the case for mineral dust emissions and sea salt. Under higher wind speeds, the PM_{10} from these sources would be more efficiently dispersed, which would lower their concentration and contribution to the total PM_{10} during a 24 h period if the winds were westerly.

4.3. Source Attribution for Non-Exceedance Days in 2021

The non-exceedance-day source attribution does not provide much useful information in terms of air-quality management with respect to the PM_{10} originating from the ODSVRA and reflects more the regional attribution of sources when MD is not actively being emitted in the ODSVRA under conditions of elevated wind speeds for westerly winds. The unidentified fraction ($6.6\% \pm 6.0\%$) on the mean non-exceedance day was much lower than on the mean exceedance day ($20.4\% \pm 2.9\%$), supporting our inference that a large portion of the unidentified fractions is likely related to mineral dust (i.e., oxides and/or carbonate and hydrated water in minerals), which had much higher concentrations on exceedance than non-exceedance days.

5. Conclusions

On days when the 24 h PM_{10} concentration equaled or exceeded the State of California Standard of $50 \mu\text{g m}^{-3}$ at the CDF monitoring station, mineral dust was a consequential

contributor. For eight exceedance days between May and October 2021, mineral dust contribution ranged between 8.3% and 58.2%, with a mean-exceedance-day attribution of 43.1% ($\pm 15.3\%$). Assuming most of the unidentified mass represents the oxide components of the various minerals in the Oceano Dune sands, the mean-exceedance-day contribution of mineral dust increased to 63.5% ($\pm 18.2\%$). The source of this component of the PM_{10} is attributable to the wind-driven saltation and dust-emission processes within the ODSVRA. Exceedance days, as measured at the CDF, are most likely to occur when dust-laden air is transported from the direction of the ODSVRA to the CDF monitoring station. Over a three-year period, 2019–2022, >50% of exceedance days occurred when winds were from the direction range of $236\text{--}326^\circ$, with wind speed $\geq 3.6\text{ m s}^{-1}$ measured at the CDF, which likely corresponds with above threshold wind speed conditions for saltation and dust emissions as measured within the ODSVRA at the S1 tower.

Based on the results presented, the mitigative actions taken by California State Parks to reduce dust emissions are wholly justifiable as a management strategy to achieve the requirement of the Stipulated Order of Abatement of lowering PM_{10} to achieve the stated air-quality objective. Mineral dust was the largest contributor to the PM_{10} on days that exceeded the state standard for PM_{10} during the observation period, and controlling dust emission is the only viable strategy, as the other sources, particularly if the significant contribution of sea salt ($25.1\% \pm 14.5\%$) is predominantly generated by wind and wave actions, cannot be controlled through an intervention strategy. If NaCl is also being derived from saltation and dust emissions, suppression of saltation via the methods being used within the ODSVRA is also the appropriate means to lower this PM_{10} constituent originating from the park.

Author Contributions: Conceptualization, K.A.T. and J.A.G.; methodology, K.A.T., D.A.C., X.W., S.K. and J.A.G.; validation, K.A.T., X.W. and S.K.; formal analysis, K.A.T., X.W., E.F.-C. and J.A.G.; writing—original draft preparation, X.W. and J.A.G.; writing—review and editing, K.A.T., X.W., J.A.G. and E.F.-C. All authors have read and agreed to the published version of the manuscript.

Funding: This research was funded by the California Department of Parks and Recreation, Contract C1953001 to DRI.

Institutional Review Board Statement: Not applicable.

Informed Consent Statement: Not applicable.

Data Availability Statement: Data are available from the DRI following a request to California State Parks, Off-Highway Motor Vehicle Recreation Division, 715 P Street, Sacramento, CA 95814.

Acknowledgments: We would like to acknowledge the support of C. Gibbons (SLOAPCD), who supported the field measurement campaign, and the intellectual contributions from E. Withycombe (California Air Resources Board, retired). T. Carmona of Parks provided the map. We also gratefully acknowledge the support provided by California State Park Project Managers R. Glick and J. O'Brien to carry out this work. The material is courtesy of California State Parks, 2022.

Conflicts of Interest: The authors declare no conflict of interest. The funders had no role in the design of this study; in the collection, analyses, or interpretation of data; in the writing of this manuscript; or in the decision to publish the results.

References

1. Gillies, J.A.; Etyemezian, V.; Nikolich, G.; Glick, R.; Rowland, P.; Pesce, T.; Skinner, M. Effectiveness of an array of porous fences to reduce sand flux: Oceano Dunes, Oceano CA. *J. Wind. Eng. Ind. Aerodyn.* **2017**, *168*, 247–259. [\[CrossRef\]](#)
2. Gillies, J.A.; Furtak-Cole, E.; Nikolich, G.; Etyemezian, V. The role of off-highway vehicle activity in augmenting dust emissions at the Oceano Dunes State Vehicular Recreation Area, Oceano, CA. *Atmos. Environ.* **2022**, *13*, 100146. [\[CrossRef\]](#)
3. Huang, Y.; Kok, J.F.; Martin, R.L.; Swet, N.; Katra, I.; Gill, T.E.; Reynolds, R.L.; Freire, L.S. Fine dust emissions from active sands at coastal Oceano Dunes, California. *Atmos. Chem. Phys.* **2019**, *19*, 2947–2964. [\[CrossRef\]](#)
4. Mejia, J.F.; Gillies, J.A.; Etyemezian, V.; Glick, R. A very-high resolution (20 m) measurement-based dust emissions and dispersion modeling approach for the Oceano Dunes, California. *Atmos. Environ.* **2019**, *218*, 116977. [\[CrossRef\]](#)

5. Swet, N.; Hilgendorf, Z.; Walker, I. UCSB Historical Vegetation Cover Change Analysis (1930–2020) within the Oceano Dunes SVRA 2022. Available online: [https://ohv.parks.ca.gov/pages/1140/files/Memo%20Scientific%20Basis%20for%20Possible%20Revision%20of%20the%20Stipulated%20Order%20of%20Abatement%20\(SOA\).pdf](https://ohv.parks.ca.gov/pages/1140/files/Memo%20Scientific%20Basis%20for%20Possible%20Revision%20of%20the%20Stipulated%20Order%20of%20Abatement%20(SOA).pdf) (accessed on 3 January 2023).
6. Walker, I.J.; Hilgendorf, Z.; Gillies, J.A.; Turner, C.M.; Furtak-Cole, E.; Nikolich, G. Assessing performance of a “nature-based” foredune restoration project, Oceano Dunes, California, USA. *Earth Surf. Process. Landf.* **2022**, *48*, 143–162. [\[CrossRef\]](#)
7. Furtak-Cole, E.; Gillies, J.A.; Hilgendorf, Z.; Walker, I.J.; Nikolich, G. Simulation of flow and shear stress distribution on the Oceano Dunes, implications for saltation and dust emissions. *Environ. Fluid Mech.* **2022**, *22*, 1399–1420. [\[CrossRef\]](#)
8. Wolfe, S.A.; Nickling, W.G. The protective role of sparse vegetation in wind erosion. *Prog. Phys. Geogr.* **1993**, *17*, 50–68. [\[CrossRef\]](#)
9. San Luis Obispo County; Air Pollution Control District. Nipomo Mesa Particulate Study, San Luis Obispo Air Pollution Control District. 2007. Available online: <https://storage.googleapis.com/slocleanair-org/images/cms/upload/files/Phase1PMStudyReport2.pdf> (accessed on 4 January 2023).
10. Craig, J.; Cahill, T.A.; Ono, D. South County Phase 2 Particulate Study. San Luis Obispo County Air Pollution Control District. 2010. Available online: https://storage.googleapis.com/slocleanair-org/images/cms/upload/files/PM2-final_report_with_appendices.pdf (accessed on 5 January 2023).
11. San Luis Obispo County; Air Pollution Control District. 2018 Annual Air Quality Report, San Luis Obispo Air Pollution Control District. 2019. Available online: <https://storage.googleapis.com/slocleanair-org/images/cms/upload/files/2018aqrt-FINAL.pdf> (accessed on 5 January 2023).
12. Swet, N.; Elperin, T.; Kok, J.F.; Martin, R.L.; Yizhaq, H.; Katra, I. Can active sands generate dust particles by wind-induced processes? *Earth Planet. Sci. Lett.* **2019**, *506*, 371–380. [\[CrossRef\]](#)
13. Lewis, S.L.; Russell, L.M.; McKinsey, J.A.; Harris, W.J. Small contributions of dust to PM_{2.5} and PM₁₀ concentrations measured downwind of Oceano Dunes. *Atmos. Environ.* **2022**, *294*, 119515. [\[CrossRef\]](#)
14. US Environmental Protection Agency. List of Designated Reference and Equivalent Methods, United States Environmental Protection Agency. 15 December 2022. Available online: <https://www.epa.gov/system/files/documents/2022-12/ListofFRMandFEM.pdf> (accessed on 5 January 2023).
15. California Air Resources Board. AQSB SOP 404: Standard Operating Procedures for Thermo Scientific Partisol Model 2025i Sequential Air Sampler, California Air Resources Board, Monitoring and Laboratory Division, 2020; California Air Resources Board: Sacramento, CA, USA, 2020.
16. San Luis Obispo County; Air Pollution Control District. Standard Operating Procedures for MetOne Instruments BAM 1020 Beta Attenuation Particulate Matter Monitor, San Luis Obispo Air Pollution Control District, 2014; San Luis Obispo County Air Pollution Control District: San Luis Obispo, CA, USA, 2014.
17. Chow, J.C.; Watson, J.G. Chemical Analyses of Particle Filter Deposits. In *Aerosols Handbook: Measurement, Dosimetry, and Health Effects*, 2nd ed.; Ruzer, L., Harley, N.H., Eds.; CRC Press/Taylor & Francis: New York, NY, USA, 2013; pp. 179–204.
18. Watson, J.G.; Chow, J.C.; Engling, G.; Chen, L.-W.A.; Wang, X.L. Source Apportionment: PRINCIPLES and Methods. In *Airborne Particulate Matter: Sources, Atmospheric Processes and Health*; Harrison, R.M., Ed.; Royal Society of Chemistry: London, UK, 2016; pp. 72–125.
19. Watson, J.G.; Tropp, R.J.; Kohl, S.D.; Wang, X.L.; Chow, J.C. Filter processing and gravimetric analysis for suspended particulate matter samples. *Aerosol Sci. Eng.* **2017**, *1*, 93–105. [\[CrossRef\]](#)
20. South Coast Air Quality Management District. SOP 00104: Standard Operating Procedure for Weigh Room Operations and Weighing of PM_{2.5} Samples; South Coast Air Quality Management District: Diamond Bar, CA, USA, 2018.
21. Watson, J.G.; Chow, J.C.; Frazier, C.A. X-ray fluorescence analysis of ambient air samples. In *Elemental Analysis of Airborne Particles*; Landsberger, S., Creatchman, M., Eds.; Gordon and Breach Science: Amsterdam, The Netherlands, 1999; Volume 1, pp. 67–96.
22. Chow, J.C.; Watson, J.G. Enhanced ion chromatographic speciation of water-soluble PM_{2.5} to improve aerosol source apportionment. *Aerosol Sci. Eng.* **2017**, *1*, 7–24. [\[CrossRef\]](#)
23. Chen, L.-W.A.; Chow, J.C.; Wang, X.L.; Robles, J.A.; Sumlin, B.; Lowenthal, D.H.; Zimmermann, R.; Watson, J.G. Multi-wavelength optical measurement to enhance thermal/optical analysis for carbonaceous aerosol. *Atmos. Meas. Tech.* **2015**, *8*, 451–461. [\[CrossRef\]](#)
24. Chow, J.C.; Watson, J.G.; Chen, L.-W.A.; Chang, M.C.O.; Robinson, N.F.; Trimble, D.; Kohl, S. The IMPROVE_A temperature protocol for thermal/optical carbon analysis: Maintaining consistency with a long-term database. *J. Air Waste Manag. Assoc.* **2007**, *57*, 1014–1023. [\[CrossRef\]](#)
25. Martin, R.F. General Deming regression for estimating systematic bias and its confidence interval in method-comparison studies. *Clin. Chem.* **2002**, *46*, 100–104. [\[CrossRef\]](#)
26. R Core Team. R: A Language and Environment for Statistical Computing; R Foundation for Statistical Computing: Vienna, Austria, 2021; Available online: <https://www.R-project.org/> (accessed on 15 December 2022).
27. Therneau, T.; Deming, T.-S. Passing-Bablok and Total Least Squares Regression, R package version 1.4. 2018. Available online: <https://CRAN.R-project.org/package=deming> (accessed on 15 December 2022).
28. Wang, X.L.; Chen, L.-W.A.; Lu, M.; Ho, K.-F.; Lee, S.-C.; Ho, S.S.H.; Chow, J.C.; Watson, J.G. Apportionment of vehicle fleet emissions by linear regression, positive matrix factorization, and emission modeling. *Atmosphere* **2022**, *13*, 1066. [\[CrossRef\]](#)
29. Veron, F. Ocean spray. *Annu. Rev. Fluid Mech.* **2015**, *47*, 507–538. [\[CrossRef\]](#)

30. Seinfeld, J.H.; Pandis, S.N. *Atmospheric Chemistry and Physics: From Air Pollution to Climate Change*, 2nd ed.; John Wiley & Sons: New York, NY, USA, 2012.
31. McInnes, L.M.; Covert, D.S.; Quinn, P.K.; Germani, M.S. Measurements of chloride depletion and sulfur enrichment in individual sea-salt particles collected from the remote marine boundary layer. *J. Geophys. Res. Atmos.* **1994**, *99*, 8257–8268. [\[CrossRef\]](#)
32. Cheung, K.; Daher, N.; Shafer, M.M.; Ning, Z.; Schauer, J.J.; Sioutas, C. Diurnal trends in coarse particulate matter composition in the Los Angeles Basin. *J. Environ. Monit.* **2011**, *13*, 3277–3287. [\[CrossRef\]](#)
33. Lowenthal, D.; Kumar, N. Light Scattering from Sea-Salt Aerosols at Interagency Monitoring of Protected Visual Environments (IMPROVE) Sites. *J. Air Waste Manag. Assoc.* **2006**, *56*, 636–642. [\[CrossRef\]](#) [\[PubMed\]](#)
34. Zhuang, H.; Chan, C.K.; Fang, M.; Wexler, A.S. Formation of nitrate and non-sea-salt sulfate on coarse particles. *Atmos. Environ.* **1999**, *33*, 4223. [\[CrossRef\]](#)
35. Bardouki, H.; Liakakou, H.; Economou, C.; Sciare, J.; Smolík, J.; Ždímal, V.; Eleftheriadis, K.; Lazaridis, M.; Dye, C.; Mihalopoulos, N. Chemical composition of size-resolved atmospheric aerosols in the eastern Mediterranean during summer and winter. *Atmos. Environ.* **2003**, *37*, 195–208. [\[CrossRef\]](#)
36. Chow, J.C.; Lowenthal, D.H.; Chen, L.-W.A.; Wang, X.L.; Watson, J.G. Mass reconstruction methods for PM_{2.5}: A review. *Air Qual. Atmos. Health* **2015**, *8*, 243–263. [\[CrossRef\]](#) [\[PubMed\]](#)
37. Simon, H.; Bhawe, P.V.; Swall, J.L.; Frank, N.H.; Malm, W.C. Determining the spatial and seasonal variability in OM/OC ratios across the US using multiple regression. *Atmos. Chem. Phys.* **2011**, *11*, c2933–c2949. [\[CrossRef\]](#)
38. Hand, J.L.; Copeland, S.A.; McDade, C.E.; Day, D.E.; Moore, J.C.T.; Dillner, A.M.; Pitchford, M.L.; Indresand, H.; Schichtel, B.A.; Malm, W.C.; et al. Spatial and Seasonal Patterns and Temporal Variability of Haze and Its Constituents in the United States, IMPROVE Report, V. Cooperative Institute for Research in the Atmosphere, Fort Collins, CO. 2011. Available online: <https://vista.cira.colostate.edu/Improve/spatial-and-seasonal-patterns-and-temporal-variability-of-haze-and-its-constituents-in-the-united-states-report-v-june-2011/> (accessed on 7 January 2023).
39. Pakkanen, T.A. Study of formation of coarse particle nitrate aerosol. *Atmos. Environ.* **1996**, *30*, 2475–2482. [\[CrossRef\]](#)
40. Usher, C.R.; Michel, A.E.; Grassian, V.H. Reactions on mineral dust. *Chem. Rev.* **2003**, *103*, 4883–4940. [\[CrossRef\]](#)
41. San Luis Obispo County; Air Pollution Control District. 2021 Ambient Air Monitoring Network Plan, San Luis Obispo Air Pollution Control District. 2021. Available online: <https://storage.googleapis.com/slocleanair-org/images/cms/upload/files/2021-network-plan-for-publication.pdf> (accessed on 5 January 2023).
42. Lu, H.; Shao, Y. A new model for dust emission by saltation bombardment. *J. Geophys. Res. Atmos.* **1999**, *104*, 16827–16842. [\[CrossRef\]](#)
43. Shao, Y. *Physics and Modelling of Wind Erosion*; Kluwer Academic Publishers: Dordrecht, The Netherlands, 2000.
44. Shao, Y. A model for mineral dust emission. *J. Geophys. Res.* **2001**, *106*, 20239–20254. [\[CrossRef\]](#)
45. Ovadnevaite, J.; Manders, A.; de Leeuw, G.; Ceburnis, D.; Manahan, C.; Partanen, A.-I.; Korhonen, H.; O'Dowd, C.D. A sea spray aerosol flux parameterization encapsulating wave state. *Atmos. Chem. Phys.* **2014**, *14*, 1837–1852. [\[CrossRef\]](#)
46. Erinin, M.A.; Wang, S.D.; Liu, R.; Towle, D.; Liu, X.; Duncan, J.H. Spray generation by a plunging breaker. *Geophys. Res. Lett.* **2019**, *46*, 8244–8251. [\[CrossRef\]](#)
47. Martin, S.T. Phase transitions of aqueous atmospheric particles. *Chem. Rev.* **2000**, *100*, 3403–3454. [\[CrossRef\]](#)
48. McInnes, L.M.; Quinn, P.K.; Covert, D.S.; Anderson, T.L. Gravimetric analysis, ionic composition, and associated water mass of the marine aerosol. *Atmos. Environ.* **1996**, *30*, 869–884. [\[CrossRef\]](#)
49. King, J.; Etyemezian, V.; Sweeney, M.; Buck, B.J.; Nikolich, G. Dust emission variability at the Salton Sea, California, USA. *Aeolian Res.* **2011**, *3*, 67–79. [\[CrossRef\]](#)
50. Malm, W.; Sisler, J.; Huffman, D.; Eldred, R.; Cahill, T. Spatial and seasonal trends in particle concentration and optical extinction in the United States. *J. Geophys. Res.* **1994**, *99*, 1347–1370. [\[CrossRef\]](#)

Disclaimer/Publisher's Note: The statements, opinions and data contained in all publications are solely those of the individual author(s) and contributor(s) and not of MDPI and/or the editor(s). MDPI and/or the editor(s) disclaim responsibility for any injury to people or property resulting from any ideas, methods, instructions or products referred to in the content.

Oceano Dunes State Vehicular Recreation Area Dust Control Program

DRAFT 2023 Annual Report and Work Plan

ATTACHMENT 11-03

**DRAFT DRI Report PI-SWERL September 2022 Results and Implications for
Emission/Dispersion Modeling (Fall 2022)**

**SAG Comments on PI-SWERL September 2022 Results and Implications for
Emission/Dispersion Modeling (February 10, 2023)**

THIS PAGE WAS INTENTIONALLY LEFT BLANK.

Oceano Dunes State Vehicular Recreation Area Dust Control Program

DRAFT 2023 Annual Report and Work Plan

ATTACHMENT 11-03

**DRAFT DRI Report PI-SWERL September 2022 Results and Implications for
Emission/Dispersion Modeling (Fall 2022)**

THIS PAGE WAS INTENTIONALLY LEFT BLANK.

PI-SWERL September 2022 Results and Implications for Emission/Dispersion Modeling

In September 2022 DRI undertook a PI-SWERL measurement campaign to quantify emissivity of key areas that, subsequently, had either not been measured following a major change to the area (e.g., foredune restoration areas) or had not been measured for a number of years. The campaign was timed to occur prior to the opening of the beach area in front of the foredune restoration area and the corridor between the restoration area and the plover enclosure to OHV activity that was scheduled for October 1, 2022. The timing of the campaign coincided with the relaxation of restrictions to access the areas related to protecting sensitive species.

The areas of the ODSVRA that were measured in September 2022 were the six foredune restoration areas, the corridor between foredune restoration area #6 and the plover enclosure, the plover enclosure, and the beach to the west of the plover enclosure above the high tide line. Measurements were also made in the corridors between restoration areas, #3 and #4, and #5 and #6. At the time the campaign was planned to occur it was expected that the western half of the corridors would have been impact-free since the area was OHV-restricted beginning in March 2022, however, there was evidence that these corridors had been disturbed by sand-moving operations shortly before the measurements were taken. The eastern half of the corridors were continually impacted by OHV activity as they provide access to public toilets.

PI-SWERL measurements of emissivity have been typically carried out in the month of May, however, during May 2022 the areas chosen for testing in September 2022, are usually off-limits due to access restrictions during the nesting/fledgling period of the western snowy plover and California least tern. Although not ideal for developing the long-term emissivity record for similar weather conditions, it was deemed necessary to acquire these emissivity measurements as they currently are represented in the DRI emission model by unsubstantiated emissivity relationships. The developed emissivity relations are needed as input to the DRI emission/dispersion model to provide the most up-to-date estimates of total mass emissions based on the meteorology of the 10 baseline days from May 2013, as the selected areas have undergone substantial modification or multiple year periods of restricted OHV activity in recent years.

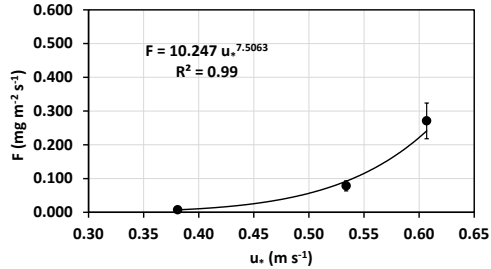
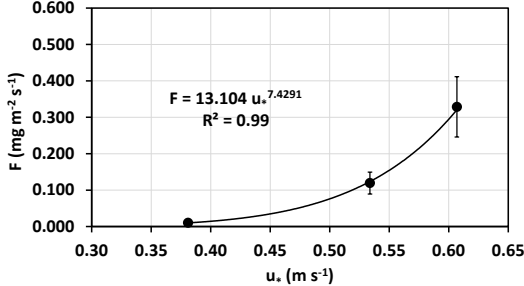
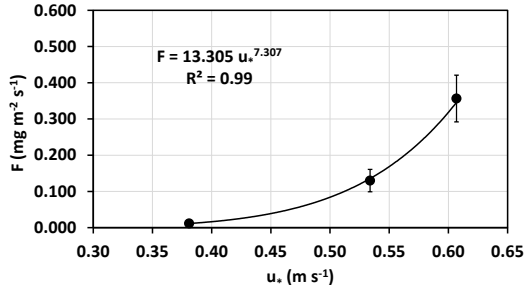
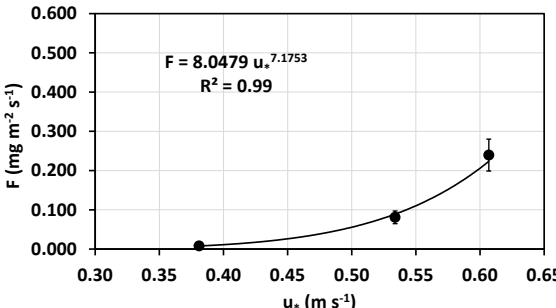
In the last iteration for modeling, as provided in the 2022 ARWP, the mass emissions and PM_{10} at the CDF and Mesa2 receptor sites the DRI model used the following relations:

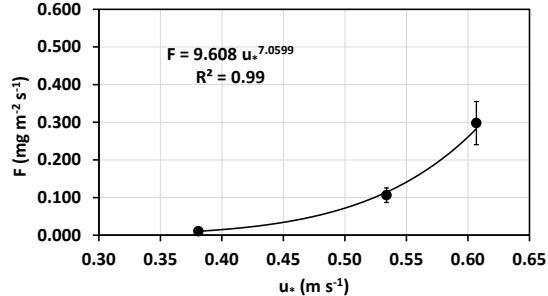
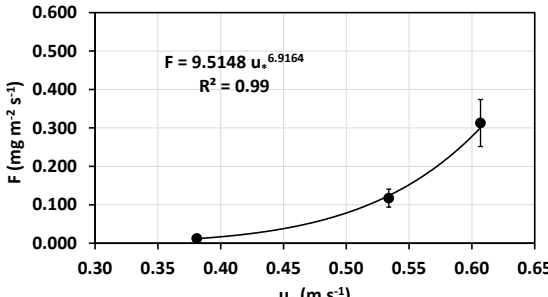
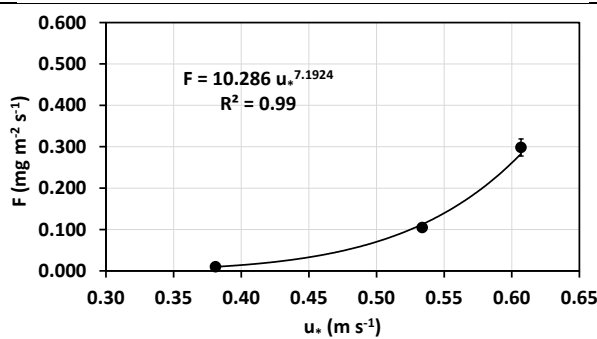
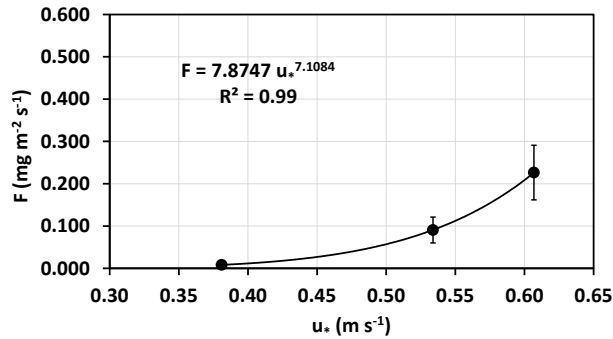
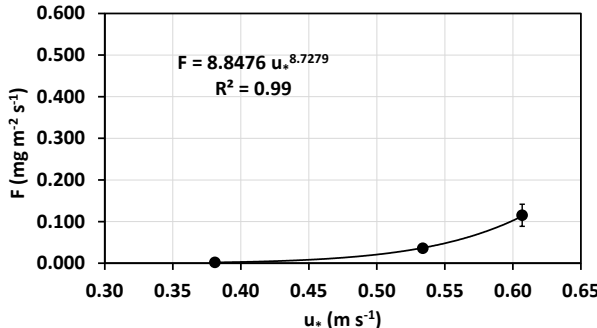
1. Foredune restoration areas: PM_{10} emissivity is equal to the mean emissivity for all non-riding areas (using the 2019 PI-SWERL grid) and this applies equally to the entire 48 acres.
2. Plover nesting enclosure: PM_{10} emissivity is equal to 50% of the actual mean emissivity for the nesting enclosure, based on the 2019 PI-SWERL emissions grid.
3. Beach (west of foredune restoration areas) and corridors between foredune restoration areas: PM_{10} emissivity in these areas is equal to the mean emissivity for all non-riding areas (using the 2019 PI-SWERL grid). No zonal or gradation in emissivity as a function of longitude is applied.

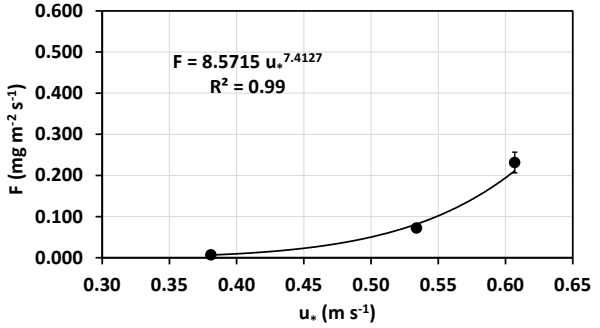
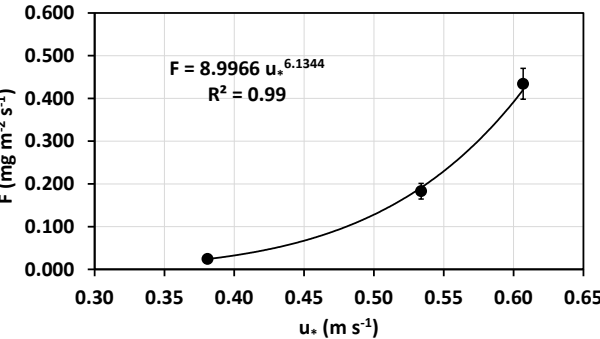
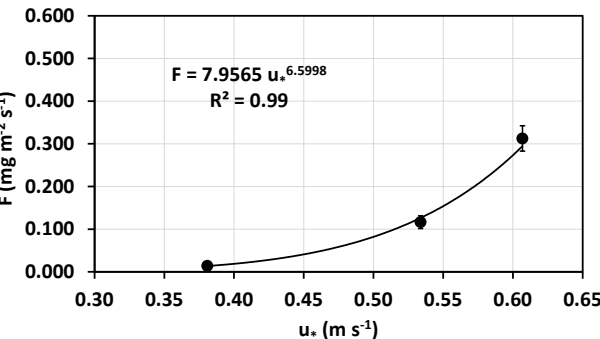
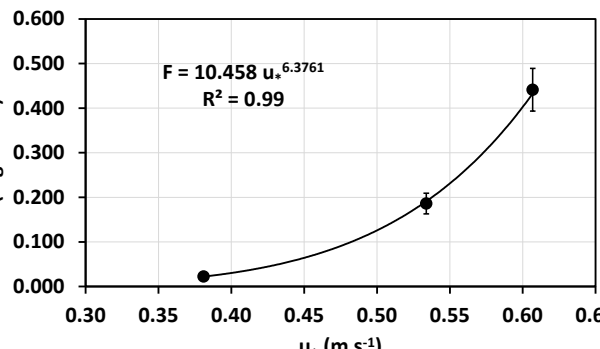
PI-SWERL measurements September 2022

The PI-SWERL testing, i.e., areas tested, number of tests conducted at each location, and the mean emissivity relation for the identified area are shown in Table 1.

Table 1. Areas tested, number of tests conducted at each location, and the mean PM₁₀ emissivity relations.

Test Area	Number of Tests	Mean Emissivity Relation for PM ₁₀ $F \text{ (mg m}^{-2} \text{ s}^{-1}) = a u_*^b \text{ (m s}^{-1})$
Restoration Area #1	16	 <p>$F = 10.247 u_*^{7.5063}$ $R^2 = 0.99$</p>
Restoration Area #2	15	 <p>$F = 13.104 u_*^{7.4291}$ $R^2 = 0.99$</p>
Restoration Area #3	16	 <p>$F = 13.305 u_*^{7.307}$ $R^2 = 0.99$</p>
Restoration Area #4	22	 <p>$F = 8.0479 u_*^{7.1753}$ $R^2 = 0.99$</p>

Restoration Area #5	17	 <p> $F = 9.608 u_*^{7.0599}$ $R^2 = 0.99$ </p>
Restoration Area #6	24	 <p> $F = 9.5148 u_*^{6.9164}$ $R^2 = 0.99$ </p>
Restoration Areas Combined	110	 <p> $F = 10.286 u_*^{7.1924}$ $R^2 = 0.99$ </p>
Plover Exclosure	23	 <p> $F = 7.8747 u_*^{7.1084}$ $R^2 = 0.99$ </p>
Beach (west of plover ex.)	16	 <p> $F = 8.8476 u_*^{8.7279}$ $R^2 = 0.99$ </p>

Corridor between RA#6 and plover ex. (no OHV)	12	 <p> $F = 8.5715 u_*^{7.4127}$ $R^2 = 0.99$ </p>
Corridor between RA#6 and plover ex. (OHV)	9	 <p> $F = 8.9966 u_*^{6.1344}$ $R^2 = 0.99$ </p>
Corridor between RA#6 and plover ex. (combined)	21	 <p> $F = 7.9565 u_*^{6.5998}$ $R^2 = 0.99$ </p>
All Corridors Combined (OHV and non-OHV)	52	 <p> $F = 10.458 u_*^{6.3761}$ $R^2 = 0.99$ </p>
		Error bars represent the Standard Error ($SE = (\text{Std. Dev. of the Mean} / (\# \text{tests} - 1)^{0.5})$)

September 2022 PI-SWERL Relations Compared with Previous Year Relations

The mean emissivity relation of the six restoration areas combined is compared with the mean non-riding area emissivity relation for the period 2013-2019 and for just the 2019 data in Fig. 1. The mean emissivity of the restoration area is lower, on average, by a factor of 0.38 than the mean non-riding area emissivity for the period 2013-2019 and a factor of 0.50 lower than the mean non-riding area emissivity for 2019.

The mean emissivity relation of the plover enclosure is compared with the mean non-riding area emissivity relation for the period 2013-2019 and for just the 2019 data in Fig. 2. The mean emissivity of the plover enclosure area is lower by a factor of 0.31 than the mean non-riding area emissivity for the period 2013-2019 and a factor of 0.41 lower than the mean non-riding area emissivity for 2019.

The mean emissivity relation of the beach area west of the plover enclosure is compared with the mean non-riding area emissivity relation for the period 2013-2019 and for just the 2019 data in Fig. 3. The mean emissivity of the beach area is lower by a factor of 0.12 than the mean non-riding area emissivity for the period 2013-2019 and a factor of 0.16 lower than the mean non-riding area emissivity for 2019.

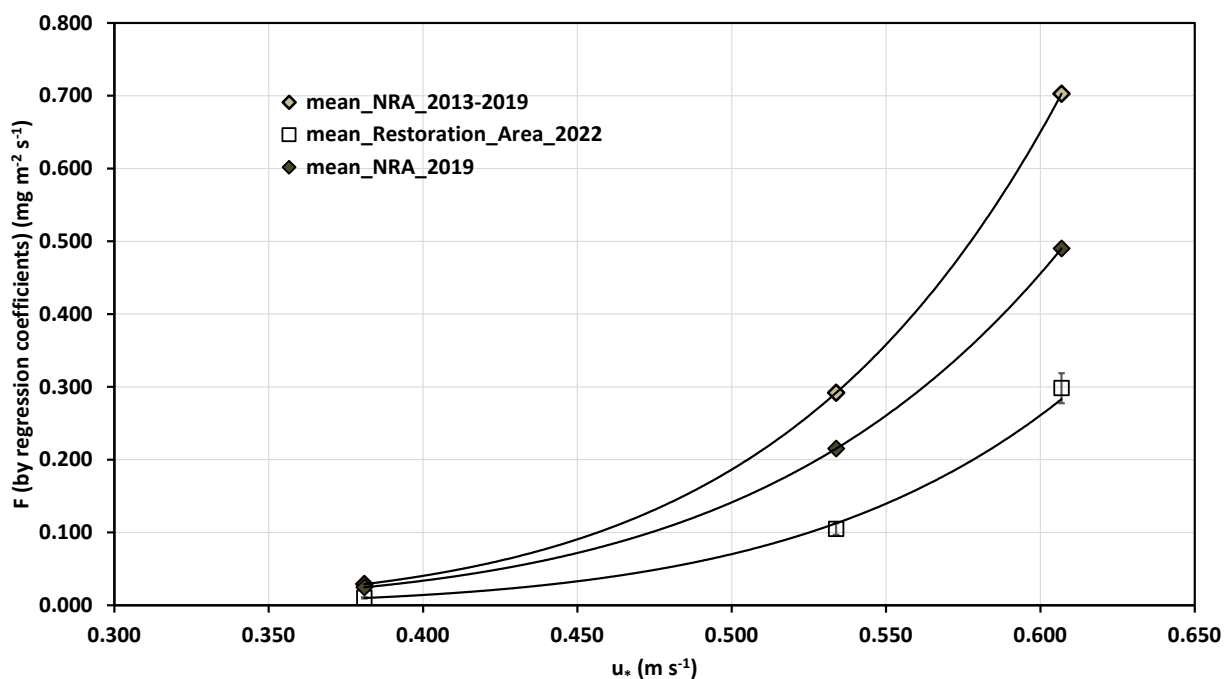


Figure 1. The mean emissivity relations for the non-riding area (NRA) for all data 2013-2019, for data from 2019, and the restoration areas combined (September 2022). The 2013-2019 and 2019 data are represented by the regression-derived emissivity coefficients for the relation $F=au_*^b$. The 2022 data are the mean F values for the three PI-SWERL u_* set points with the error bars representing the Standard Error ($SE=(\text{Std. Dev. of the Mean}/(\#tests-1)^{0.5})$).

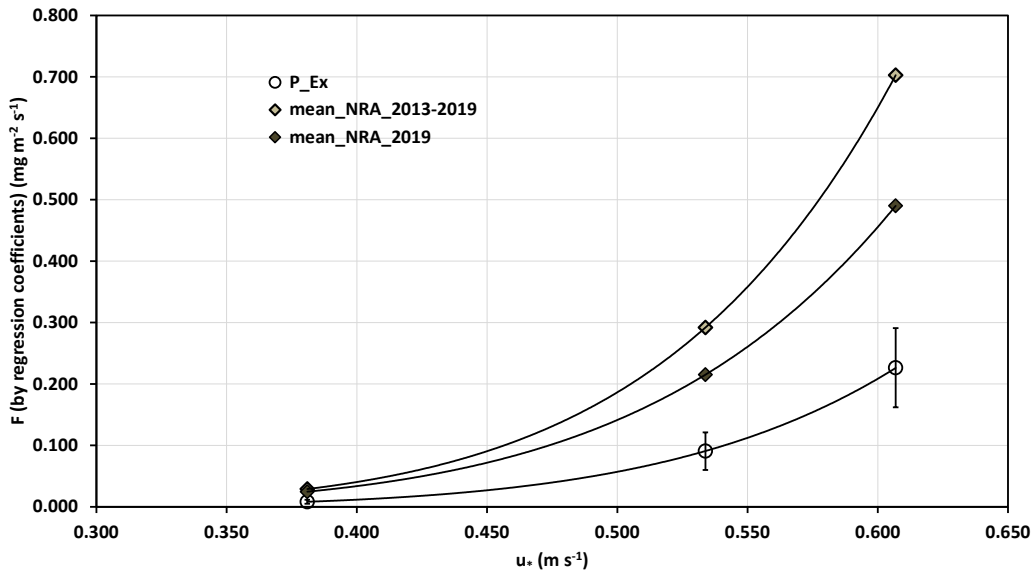


Figure 2. The mean emissivity relations for the non-riding area (NRA) for all data 2013-2019, for data from 2019, and the Plover Exclosure area (September 2022). The 2013-2019 and 2019 data are represented by the regression-derived emissivity coefficients for the relation $F=au^*{}^b$. The 2022 data are the mean F values for the three PI-SWRL u^* set points with the error bars representing the Standard Error ($SE=(\text{Std. Dev. of the Mean}/(\# \text{tests}-1)^{0.5})$).

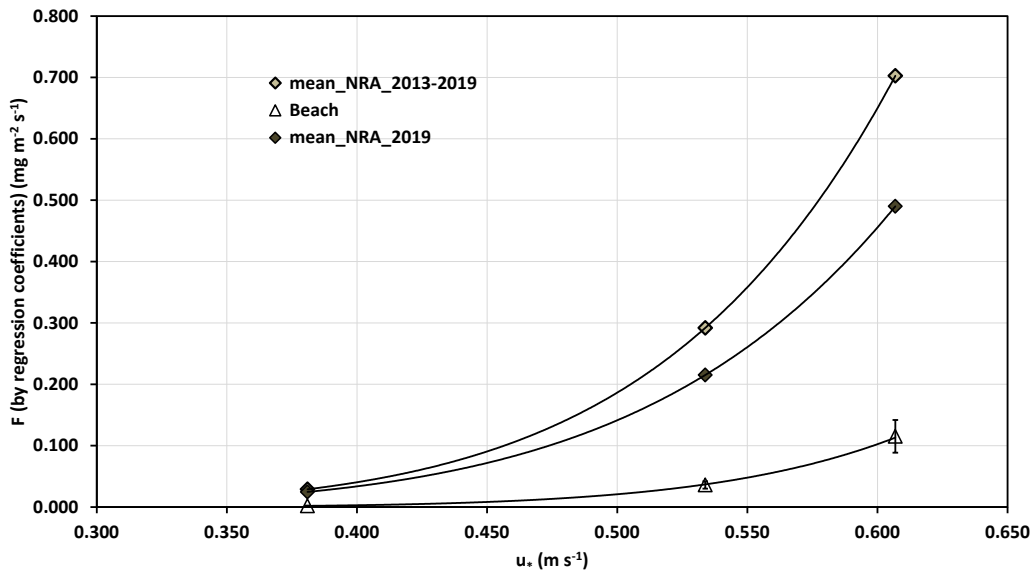


Figure 3. The mean emissivity relations for the non-riding area (NRA) for all data 2013-2019, for data from 2019, and the beach area west of the Plover exclosure (September 2022). The 2013-2019 and 2019 data are represented by the regression-derived emissivity coefficients for the relation $F=au^*{}^b$. The 2022 data are the mean F values for the three PI-SWRL u^* set points with the error bars representing the Standard Error ($SE=(\text{Std. Dev. of the Mean}/(\# \text{tests}-1)^{0.5})$).

The corridors between the foredune restoration areas and between restoration area #6 and the plover enclosure have a more complex impact history from OHV and Parks activity than the areas that are completely secure from activities other than access by people on foot. They also represent quite a small proportion of the total area that is accounted for in the emission/dispersion model. The mean emissivity relation for all the tests carried out in the corridors, both OHV and non-OHV impact portions (but potential disturbance by Parks activities) is shown in Fig 4. This relation is also shown with the non-riding area relations for 2013-2019 and just 2019. The mean emissivity of the corridors is similar to the 2019 mean non-riding area relation.

The PI-SWRL measurements made in September 2022 indicate that the areas tested have emissivity relations that result in lower emissions of PM_{10} for equivalent shear velocities than the longer term, i.e., 2013-2019 mean non-riding emissivity relation, and the 2019 mean non-riding area emissivity relation. The data from 2019 represent the highest number of tests and greatest spatial coverage for the non-riding areas since the initial PI-SWRL survey of 2013. The emissivity relations established for the areas tested in 2022 (Table 1) are all lower than the mean emissivity relation established for the non-riding area in May 2022.

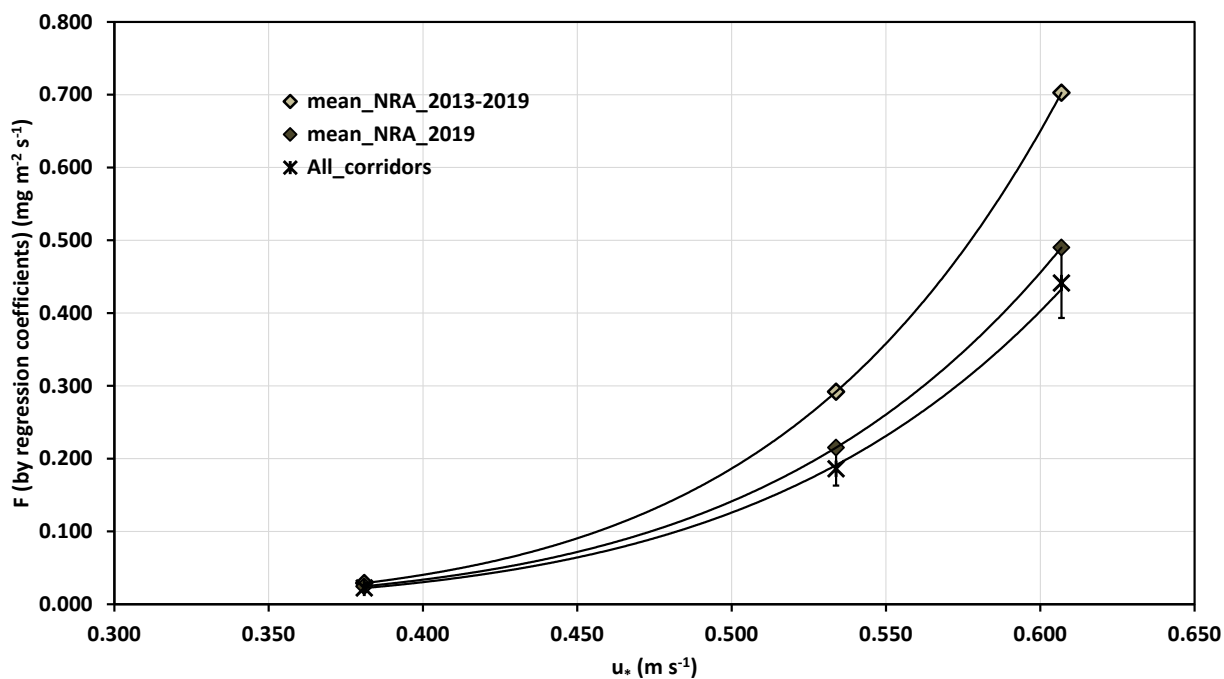


Figure 4. The mean emissivity relations for the non-riding area (NRA) for all data 2013-2019, for data from 2019, and all the corridor measurement data combined (September 2022). The 2013-2019 and 2019 data are represented by the regression-derived emissivity coefficients for the relation $F=au_*^b$. The 2022 data are the mean F values for the three PI-SWRL u_* set points with the error bars representing the Standard Error ($SE=(\text{Std. Dev. of the Mean}/(\# \text{tests}-1)^{0.5})$).

The areas of highest potential emissions are the corridors between the restoration area treatments and the plover exclosure. These areas were subject to some OHV and Parks maintenance activities prior to testing, which are expected to increase emissivity. We recommend that the mean corridor emissivity relation (Table 1, Fig. 4) be used for the next model iteration.

The foredune restoration treatment areas have quite similar emissivity relations, but treatment areas 1, 2 and 3 are more emissive than 4, 5, and 6. An Analysis of Variance (ANOVA) between these two groups, however, indicates that the mean emissivity values for each PI-SWRL u+ step are not significantly different. This suggests that for the next model iteration that using the mean emissivity relation (Table 1, and Fig. 1) for the 48 acres restoration area should be acceptable.

At the time of the September 2022 PI-SWRL measurement campaign the plover exclosure had been restricted from OHV activity since March 2021. Prior to that it experienced OHV and camping activities except during the period April-October when these activities were prohibited. The September 2022 PI-SWRL measurements indicate that at that time the emissivity of the plover exclosure was lower than the mean non-riding area emissivity for 2013-2019 and for the mean non-riding area emissivity as measured in 2019. The 2022 ARWP had proposed that the plover exclosure emissivity be set equal to 50% of the actual mean emissivity for the nesting exclosure, based on the 2019 PI-SWRL emissions grid. Upon review of the PI-SWRL test locations in 2019, the overlap in positions with the test locations in 2022 is limited, so no comparison is drawn between the 50% actual mean emissivity for the nesting exclosure in 2019 and the measured relation in 2022. We recommend that the 2022 relation be used to represent the plover exclosure in the next model iteration.

The beach area west of the foredune restoration area has the lowest emissivity of all the areas tested in September 2022. This area has had OHV activity restricted from March to September 2022. The low emissivity is likely a result of the lack of OHV activity, as well as the continual transfer of sand from the surf zone to the beach by wave action and subsequent transport by the wind. The sand exiting the surf zone should be essentially clean of PM₁₀ particles and clay coatings that are removed by continual movement of the sand particles in the swash zone. This area along with the restoration area have undergone significant reduction in emissivity compared to the conditions in 2019 for areas that were defined as being in the beach and camping area at that time and part of the ODSVRA known as the LaGrande tract (Fig. 5). The emissivity relations for the beach and camping in 2019 and the mean restoration and beach area measured in September 2022 are shown in Fig. 6.

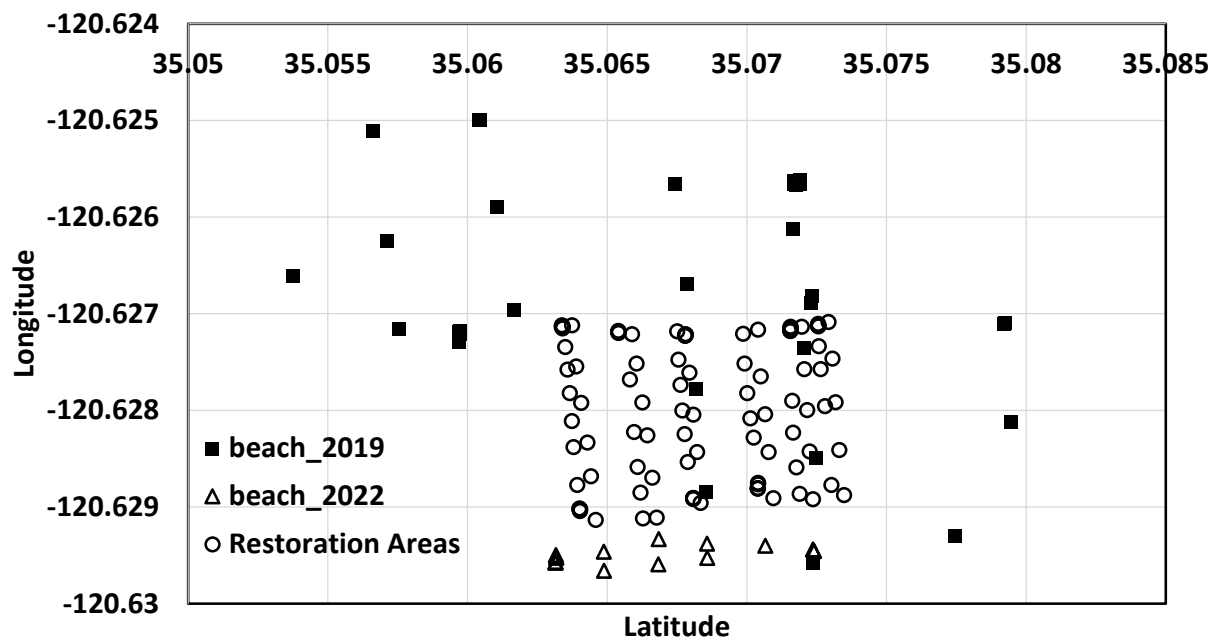


Figure 5. The PI-SWERL test positions in the beach and camping areas (part of the Lagrande tract) 2019, and the beach and restoration area PI-SWERL test locations in September 2022.

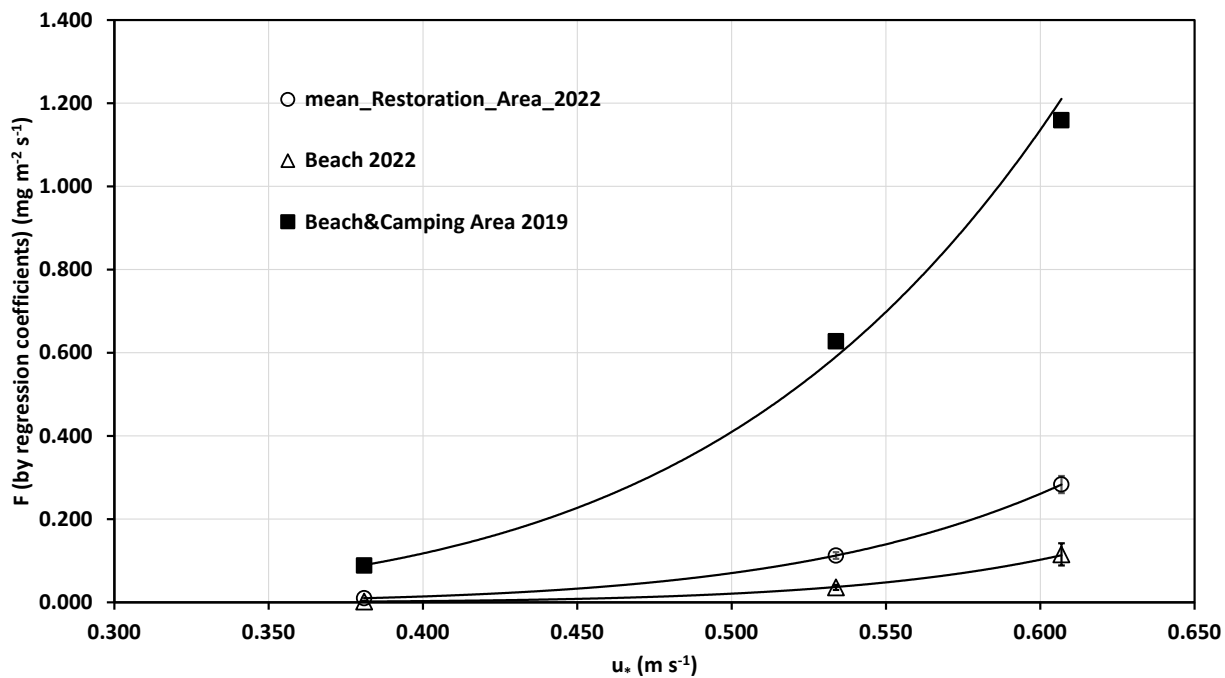


Figure 6. The mean emissivity relations for the beach and camping area 2019, and the beach and restoration areas, September 2022.

Conclusions

For the next model iteration to estimate the total PM₁₀ emission as a function of the 10 baseline wind days of May 2013 and model-estimated values for the 24-hour PM₁₀ concentration at CDF and Mesa2, DRI recommends the adoption of the following relations for emissivity based on the September 2022 PI-SWRL measurement campaign:

48 acre foredune restoration area: $F \text{ (mg m}^{-2} \text{ s}^{-1}) = 10.286 u_*^{7.1924}$

Plover exclosure: $F \text{ (mg m}^{-2} \text{ s}^{-1}) = 7.8747 u_*^{7.1084}$

Beach Area west of Restoration area (during seasonal OHV exclusion period):

$F \text{ (mg m}^{-2} \text{ s}^{-1}) = 8.8476 u_*^{8.7279}$

All access corridors in the vicinity of the foredune restoration areas and plover exclosure:

$F \text{ (mg m}^{-2} \text{ s}^{-1}) = 10.458 u_*^{6.3761}$

Oceano Dunes State Vehicular Recreation Area Dust Control Program

DRAFT 2023 Annual Report and Work Plan

ATTACHMENT 11-03

**SAG Comments on PI-SWERL September 2022 Results and Implications for
Emission/Dispersion Modeling (February 10, 2023)**

THIS PAGE WAS INTENTIONALLY LEFT BLANK.

February 10, 2023

Memo: SAG review of Desert Research Institute (DRI) report, “PI-SWERL September 2022 Results and Implications for Emission/Dispersion Modeling”

From: Scientific Advisory Group (SAG)

To: Jon O’Brien, California Department of Parks and Recreation (CDPR)

Cc: Sarah Miggins, California Department of Parks and Recreation (CDPR)
Liz McGuirk, California Department of Parks and Recreation (CDPR)

Executive Summary

The SAG recognizes the importance of PI-SWERL (Portable In-Situ Wind EROsion Laboratory) measurements to inform modeling of PM₁₀ emissions reduction benefit resulting from dust control management actions at the Oceano Dunes State Vehicular Recreation Area (ODSVRA). The DRI report entitled “PI-SWERL September 2022 Results and Implications for Emission/Dispersion Modeling” describes the results of a recent September 2022 PI-SWERL campaign that sought to quantify PM₁₀ emissivity in three different zones of management: (1) permanent plover enclosure, (2) seasonal enclosures, and (3) foredune restoration area. In the 2022 Annual Report and Work Plan (ARWP), all of these areas were identified as requiring further study to refine PM₁₀ emissions estimates via the DRI Emission/Dispersion Model, with the goal of reporting updated modeling of PM₁₀ emissions for the 2023 ARWP.

Although the SAG recognizes the importance of these recent PI-SWERL measurements to inform potential refinements to DRI Emission/Dispersion Modeling of PM₁₀ emissions, we request that this DRI report be substantially revised to address several important issues:

- I. **Context setting.** The DRI report dives directly into describing the new PI-SWERL measurements without providing adequate background on why they were collected or how they could be used to inform refinements to the DRI Emission/Dispersion Model.
- II. **Sampling approach.** The DRI report provides limited information on the strategy for choosing where to collect PI-SWERL measurements. Because there is a large degree of heterogeneity in vegetation and sediment characteristics within ODSVRA management zones, the sampling strategy could strongly influence the resulting PM₁₀ emissivity curves. Further contextual information on sampling locations amidst the complex topography and relative to past campaigns is also needed.
- III. **Proposed modeling updates.** On the basis of new PI-SWERL measurements, the DRI report proposes changes to the DRI Emission/Dispersion Model to better characterize the PM₁₀ emissivity associated with specific dust control management actions (i.e., permanent plover enclosure, seasonal enclosures, and foredune restoration area). However, some potentially complicating factors need to be considered and addressed. These include the ramifications of the PI-SWERL sampling strategy (as discussed above in terms of representativeness and overall uncertainty), the influence of seasonal

variations in PM₁₀ emissivity due to moisture conditions, and the implications of assuming averaged values rather than spatially distributed/weighted emissions rates.

- IV. **Adaptive management considerations.** In addition to informing the DRI Emission/Dispersion model, PI-SWERL measurements may also help to inform future adaptive management decisions, such as regarding dust control effectiveness of the different foredune treatments. Interpretation of existing PI-SWERL data and planning for future PI-SWERL campaigns should consider a long-term strategy for adaptive management.
- V. **Specific comments.** The SAG also notes numerous specific points within the text, table, and figures that require further clarification.

Because of these issues, the SAG is not yet ready to endorse DRI's proposed approach to modeling PM₁₀ emissivity for the permanent plover enclosure, seasonal enclosures, and foredune restoration area. Once the above issues are adequately addressed, the SAG would be happy to review a revised version of this DRI report. A full set of SAG comments follows in the subsequent pages of this review.

Respectfully,

The Scientific Advisory Group¹

Raleigh L. Martin (Chair of SAG), Bernard Bauer, Mike Bush, Leah Mathews, William Nickling, Carla Scheidlinger, Ian Walker

¹ As an author of the DRI report, SAG member John A. Gillies did not contribute to this review.

I. Context setting

The SAG infers that this DRI report was prepared to address the need to further refine approaches to modeling the effectiveness of dust control measures at the ODSVRA toward reducing PM₁₀ emissions. Once these modeling approaches are agreed upon, DRI would then presumably implement refinements to the DRI Emission/Dispersion Model, which would then serve as the basis for PM₁₀ emissions estimates presented in the 2023 ARWP.

However, this context is not immediately clear upon reading the present report. As a result, there is a risk that the results could be misinterpreted. Therefore, the SAG recommends that the DRI report be revised to provide such context, so that the purpose and intended use of the PI-SWERL measurements is clear to the reader. What is the motivation for the PI-SWERL campaign? How will PI-SWERL measurements be used to improve the existing DRI Emissions/Dispersion existing? In the subsequent paragraphs, the SAG attempts to provide such context.

In its February 2022 memo describing possible revisions to the Stipulated Order of Abatement (SOA), the SAG recommended several refinements to how the DRI Emission/Dispersion Model is used to simulate the effect of dust mitigation measures on PM₁₀ emissions reductions (SAG, 2022a). In response to these SAG recommendations, the 2nd Draft 2022 ARWP, prepared by the California Department of Parks and Recreation (CDRP) in consultation with the SAG, presented PM₁₀ emissions values calculated based on DRI model runs that implemented several of these model refinements (CDPR, 2022). In its review of the 2nd Draft 2022 ARWP (SAG, 2022b), the SAG approved of the implementation of some of these model refinements (e.g., the use of increased PM₁₀ emissions within temporary fence arrays), but the SAG sought further justification for the specific implementation of several other DRI model refinements:

- (1) **Permanent plover enclosure.** Emissivity values for the permanent enclosure (a.k.a. the plover nesting area enclosure) need to be further justified. The current assumption that this area has experienced a 50% reduction in PM₁₀ emissivity relative to conditions prior to establishment of the enclosure (as estimated by 2019 PI-SWERL measured enclosure area emissivity) may underestimate the actual PM₁₀ emissions of this area. The current assumption would imply that the emissivity is less than half of the mean emissivity of all non-riding areas. (See comment “E.2” in SAG review of 2022 ARWP.)
- (2) **Seasonal enclosures.** Emissivity values for the seasonal enclosures (i.e., seasonal foredune, beach, and open corridors) need to be further justified. The current assumption that such areas experience PM₁₀ emissions equivalent to mean non-riding areas may underestimate the actual emissions of these areas, given that seasonal enclosures experience vehicular disturbance during almost half of the year. (See comment “E.3” in SAG review of 2022 ARWP.)
- (3) **Underlying emissivity grid.** The use of an amalgamated 2013-2019 PI-SWERL emissivity grid for the pre-disturbance scenario, versus use of the 2019 PI-SWERL emissivity grid for mitigation scenarios, is potentially an “apples-to-oranges” comparison that needs to be further justified. The issue is that the 2013 PI-SWERL grid, used as the “baseline year” under the previous terms of the SOA, appears to display anomalously high PM₁₀ emissivity as compared to any other year or long-term trend. By including 2013 emissivity data for the baseline and pre-disturbance scenario, CDPR may therefore

be claiming credit for a greater percentage emissions reduction than is actually merited. (See comment “C” in SAG review of 2022 ARWP.)

On October 21, 2022, the San Luis Obispo County Air Pollution Control District (SLOAPCD) conditionally approved the 2nd Draft 2022 Annual Report and Work Plan (SLOAPCD, 2022). However, the SLOAPCD shared many of the SAG’s concerns about modeling assumptions, which may be crediting CDPR dust mitigation measures with achieving a greater level of PM₁₀ emissions reductions than may actually be merited. Therefore, as the condition for its approval of the 2022 ARWP, SLOAPCD mandated that these model issues be addressed in the 2023 ARWP. SLOAPCD’s conditional approval letter stated, “Emission calculations in the 2023 ARWP shall be based on assumptions recommended by the SAG and preapproved, in writing, by the APCO.”

In addition to these major concerns about modeling assumptions, the SAG’s review of the 2022 ARWP (SAG, 2022b) also noted several lower priority issues to be addressed in future modeling of dust mitigation scenarios. Though not of primary importance to SLOAPCD’s conditional approval of the 2022 ARWP, the SAG notes these model needs again here for context:

- (a) **Foredune restoration area.** Assumed PM₁₀ emissivity values for the foredune restoration area need to be further justified. Though use of mean non-riding area emissivity (as estimated by mean 2019 PI-SWERL measured non-riding area emissivity) is reasonable, the overall approach to modeling PM₁₀ emissions from the foredune should be revisited at some point. As noted in Walker et al. (2023), dust control potential is one of six criteria against which the foredune restoration project is being assessed. Further study is needed to understand the effect of the foredune on PM₁₀ emissions mitigation, including changes over time. (See comment “5” in SAG review of 2022 ARWP.)
- (b) **Use of zonal averages.** For those mitigation measures for which PM₁₀ emissivity is assumed to equal mean non-riding area emissivity, a mean value encompassing all 2019 measured non-riding area PI-SWERL measurements is assumed. However, it has been noted that there is a north-south gradient in PM₁₀ emissivity (Gillies et al., 2022), which justified use of zonal average non-riding area PM₁₀ emissivity values when modeling the pre-disturbance scenario (SAG, 2022a). The use of total mean (rather than zonal mean) non-riding area emissivity should be further justified. (See comment “5” in SAG review of 2022 ARWP.)

The above provides a summary of the recent history possibly motivating the current DRI report, including concerns previously expressed by the SAG about assumptions underlying the DRI Emission/Dispersion Model. The SAG encourages DRI to describe this context when updating their present report. (When doing so, it is okay to quote verbatim from the above passages as appropriate.) In addition, the SAG encourages DRI to provide some more general background and synthesis on all PI-SWERL measurements taken since 2013, including discussion of objectives for each measurement campaign, preliminary analysis and interpretation of year-to-year changes (especially 2013 as an outlier year), and the effects of seasonality (e.g., moisture, temperature, etc.).

II. Sampling approach

Aside from an overall description of the number of PI-SWERL tests performed by test area (Table 1) and a crude graphical representation for some of the sample points (Fig. 5), the current DRI report says very little about the approach to selecting locations for PI-SWERL tests. Such information is critically important, as it could strongly influence the resulting PM₁₀ emissivity curves used for the DRI Emission/Dispersion Model. The SAG encourages DRI to further describe several aspects of the sampling approach:

- Provide a map that shows locations of all PI-SWERL measurements.
- Provide a discussion of sampling strategy, if any (e.g., stratified-random approach or operator judgement). What was the goal for characterizing each area/zone?
- Provide a summary of descriptive statistics associated with measurements (e.g., mean, median, and measures of dispersion) to assess scatter.

Explanation and mapping of how the 2022 measurements correspond to prior PI-SWERL campaigns and measurement locations is also important. Such information can be used to help explain the rationale and context more clearly. It would also be useful to see a few photos of sampling locations within each of the foredune restoration treatments to help explain, with additional text, how locations were chosen within the complex terrain, vegetation cover, and lag surfaces within the treatment plots. From this, some further explanation is needed on how representative the samples in each treatment plot are and how they support the plot-wide averaging approach that was implemented.

As will be described in further detail in the next section, some additional sampling issues that need to be explained further include the following:

- There is a wide variation in the areal density of PI-SWERL tests within each management area. For example, more tests were performed within Foredune Restoration Area 6 than in the entire Plover Exclosure, despite the latter covering a much larger spatial area. Please explain the rationale for the number of tests performed in each area, and how this affects the uncertainty of results.
- What is the effect of performing tests in September? How might the results be different if collected at another time of year? This is particularly important for the Seasonal Exclosures, which were sampled toward the end of the exclosure period.

III. Proposed modeling updates

As noted above, the present DRI study is designed to improve characterization of PM₁₀ emissivity associated with specific dust control management actions at the ODSVRA. In particular, the PI-SWERL tests undertaken by DRI in September 2022 directly address the higher priority modeling needs described in items (1) and (2) above, as well as the lower-priority modeling need described in item (a) above. As for higher priority need (3) and lower priority need (b), these are potentially mooted by the existence of actual emissivity data, though specific issues may remain. Each of these items are described in further detail below:

Permanent plover exclosure (i.e., item (1) above)

PI-SWERL tests were undertaken across the plover exclosure, and an overall emissivity relationship was established based on the average of these measurements (Table 1). As shown in Fig. 2, the mean emissivity curve for the plover exclosure area is substantially lower than would be expected if assuming a mean non-riding area relationship (either from 2013-2019 data, or from just 2019 data). Also, it appears that mean emissivity values are less than half of either of these non-riding area relationships. *(NOTE: The language used in the DRI report, “lower by a factor of 0.31” for 2013-2019 and “[lower by] a factor of 0.41” for 2019 is potentially misleading and should be restated as “69% lower” [than 2013-2019] and “59% lower” [than 2019 only].)*

The use of actual PI-SWERL data is an improvement over the status quo (i.e., using the mean emissivity relationship for non-riding areas), but some potentially complicating factors need to be considered:

- The plover exclosure is larger and potentially more varied than the seasonal exclosures and foredune restoration area, yet only 23 PI-SWERL measurements were used to define the emissivity relationship for this area (as compared to 110 for the combined foredune restoration areas and 52 for the combined seasonal exclosures). What was the sampling strategy deployed, and how is confidence established that this is representative of the full plover exclosure area?
- How would the results be different if collected at another time of year? Measurements were collected in September, one of the driest times of year. Possibly, emissivity values would be lower if collected earlier in the year. It is not possible to collect measurements during spring/summer plover nesting, but measurements collected immediately prior to such nesting (e.g., in February) could add to the confidence of these relationships.

Seasonal exclosures (i.e., item (2) above)

PI-SWERL tests were undertaken in several types of seasonal exclosures, including the beach west of the foredune restoration areas and the corridors between foredune restoration areas and adjacent to the plover exclosure. *(NOTE: The DRI report refers to these beach and corridor areas as all being adjacent to the plover exclosure, which appears to be a typo and should be corrected.)* Emissivity relationships were established for each of these areas (Table 1). As shown in Fig. 3, the mean emissivity curve for the beach west of the foredune restoration area is substantially lower than would be expected if assuming a mean non-riding area relationship (either from all data in 2013-2019, or from data just in 2019). As shown in Fig. 4, the mean emissivity curve for the corridors between the foredune restoration areas and adjacent to the plover exclosure are roughly equal to the mean non-riding area relationship for 2019 data.

Overall, these findings make sense, but some potentially complicating factors need to be considered:

- The PI-SWERL tests were made near the end of the 5-month exclosure period, which may represent the lowest emissivity time of year due to the absence of recent disturbance (though some complicating factors include recent disturbance by sand moving operations, along with seasonally higher emissivity during the fall dry period). How would the measurements be different if measured at another time of year, such as just before the exclosure period (i.e., February), when these areas have experienced several months of continuous vehicular impact?
- As noted above, the DRI report may incorrectly state the locations of PI-SWERL tests. It should be confirmed whether these locations in fact align with the locations identified as providing “additional dust control benefit” in Fig. 2-2 or the 2022 ARWP (CDPR, 2022).

Foredune restoration area (i.e., item (a) above)

PI-SWERL tests were undertaken in each of the 6 foredune restoration areas, and emissivity relationships were established for each of these areas (Table 1). As shown in Fig. 1, the mean emissivity curve across the 6 foredune restoration areas is substantially lower than would be expected if assuming a mean non-riding area relationship (either from all data in 2013-2019, or from data just in 2019). There is some variability across the 6 specific foredune restoration areas (Table 1), with the treatment areas in the north (i.e., 1-3) experiencing higher PM₁₀ emissivity than treatment areas in the south (i.e., 4-6). However, an ANOVA test indicates a lack of significant difference among these areas, suggesting the use of a single mean PM₁₀ emissivity curve to represent all foredune areas.

The use of actual PI-SWERL data is an improvement over the status quo (i.e., using the mean emissivity relationship for non-riding areas), but some potentially complicating factors need to be considered:

- What was the sampling strategy within each of the foredune restoration zones? This strategy could strongly influence the emissivity relationship obtained, given the heterogeneity in sediment characteristics and surface exposure. Parts of each restoration zone are covered by vegetation, and thus would be presumed to not produce appreciable PM₁₀ emissions.
- How would the results be different if collected at another time of year? Measurements were collected in September, one of the driest times of year. Possibly, emissivity values would be lower if collected earlier in the year. It is not possible to collect measurements during spring/summer plover nesting, but measurements collected immediately prior to such nesting (i.e., in February) could add to the confidence of these relationships.
- Is the overall emissivity relationship for the foredune restoration areas (i.e., Fig. 1) affected by the approach to averaging? Was the average across the foredune restoration zone weighted by the relative area of each zone?
- Given the potential for the foredune areas to evolve in future years, it may be necessary to complete further PI-SWERL tests on a periodic basis.

Implications for future modeling (including items (3) and (b) above)

Based on the above data collection, the DRI report recommends a set of approaches to modeling PM₁₀ emissivity for each management area studied (see Table 1 below). Overall, these proposed new modeling approaches offer a potentially significant improvement over previous modeling approaches. However, some of the specific issues identified above need to be addressed. Potentially this would require further PI-SWERL data collection over time and at different times of year. In addition, the permanent plover enclosure would potentially benefit from a larger number of PI-SWERL sample points (whereas the other areas could potentially suffice with fewer sample points). In all cases, further information on sampling strategies needs to be provided to establish confidence in these modeling approaches.

As for the issue regarding the use of zonal means (i.e., item (b) above), this issue is mooted by the fact that mean 2019 PI-SWERL non-riding PM₁₀ emissivity curves are no longer being used to estimate dust control effectiveness for these restoration and enclosure areas.

Table 1. DRI proposed approaches to modeling PM₁₀ emissivity for specific dust control management areas.

Dust control management area	Previous modeling approach (i.e., 2022 ARWP)	Proposed new modeling approach
Permanent plover enclosure	Use 50% of mean 2019 PI-SWERL plover enclosure PM ₁₀ emissivity curve	Use mean 2022 PI-SWERL plover enclosure PM ₁₀ emissivity curve
Seasonal beach enclosures	Use mean 2019 PI-SWERL non-riding PM ₁₀ emissivity curve	Use mean 2022 PI-SWERL seasonal beach enclosure PM ₁₀ emissivity curve
Seasonal corridor enclosures	Use mean 2019 PI-SWERL non-riding PM ₁₀ emissivity curve	Use mean 2022 PI-SWERL seasonal corridor PM ₁₀ emissivity curve
Foredune restoration area	Use mean 2019 PI-SWERL non-riding PM ₁₀ emissivity curve	Use mean 2022 PI-SWERL foredune restoration area PM ₁₀ emissivity curve

Summary

In general, DRI's proposed new approaches to modeling PM₁₀ emissivity for the permanent plover enclosure, seasonal beach enclosures, seasonal corridors, and foredune restoration area could be adopted for modeling PM₁₀ mitigation effectiveness in the 2023 ARWP. However, before moving forward with such modeling, it would help if the DRI report could be updated to clarify approaches to the following specific issues:

- **Permanent plover enclosure:** Explain the PI-SWERL sampling strategy and possible implications of collecting data at the end of the dry season (i.e., September). In addition, verify the percentage emissions reductions (i.e., addressing possible typos in the current report).
- **Seasonal beach/corridor enclosures:** Verify the actual locations of PI-SWERL tests (i.e., addressing possible typos in the current report) and possible implications of

collecting data after several months without off highway vehicle (OHV) impacts (i.e., at the end of the exclosure period).

- **Foredune restoration area:** Explain the PI-SWERL sampling strategy and possible implications of collecting data at the end of the dry season (i.e., September). In addition, consider introducing weighted averaging to represent the relative contribution of each treatment area to the overall mean foredune emissivity curve.

As noted above, it would help in all cases to provide further context on the 2022 PI-SWERL campaign, including a map of the specific locations of PI-SWERL tests and an explanation for the sampling strategy. In addition, to account for dynamic changes in PM₁₀ emissivity conditions, future assessments of dust control effectiveness should be based on repeat PI-SWERL campaigns conducted periodically (e.g., every couple of years).

IV. Adaptive management considerations

The report suggests that foredune restoration emissivity be averaged across all treatment plots for the purposes of the refined model. However, there may be some utility in keeping the treatment plots discrete for the purposes of understanding their respective emissivity contributions and for informing adaptive management decisions. It is unclear, however, whether or not distinguishing emissivity at this level of resolution will make much of a difference in the overall modeling of PM₁₀ dispersion to receptor sites. That said, if there is utility in plot-scale emissivity measurements for identifying which treatments are having greater impacts on reducing PM₁₀ delivered to the receptor sites, then this could help to inform future adaptive management decisions. In addition, it should be noted that foredune treatment area 1 is a control surface with no actual treatment, and some rationale should be provided for including it in the overall average.

Consider including a more extensive discussion about a long-term strategy for future PI-SWERL measurement campaigns and how best to integrate information from past campaigns, especially the seemingly anomalous 2013 measurements. In particular, it may be useful to identify a number of control sites that are measured consistently so as to parameterize the importance of seasonality and time of day on the overall results. This information can feed into an adaptive management process regarding the general performance of both the foredune restoration site and the plover exclosure over time.

V. Specific Comments

1) Page 1

- a) In the second paragraph (and elsewhere), please be consistent with using the terminology “foredune restoration area” rather than just “restoration area.”
- b) In the second paragraph, please provide further information about the sand moving operations and who engaged in this work.
- c) In the third paragraph, please provide a definition for “emissivity relations” [relationships?].

- d) In item 2 in the list, please clarify what is meant here. Is it assumed that the *present* emissivity is 50% of what had been *measured* in 2019?
- e) In item 3 in the list, please clarify if such a longitudinal function is assumed within the foredune restoration area.

2) Table 1

- a) Please define F , u^* , a , and b . It can be inferred from the graphs that F is probably the emissivity, u^* is the shear velocity, and a and b are fitting parameters. But these should be explicitly defined within the report.
- b) Restoration Areas Combined: How were measurements combined? Simple average or areal weighting? Note that there are different numbers of measurements in each restoration area. Was each restoration area averaged first, before taking a combined mean of the 6 individual restoration area average? Why include Restoration Area 1, which is a control zone with no treatment?
- c) Why were the Corridors between Restoration Area 6 and the Plover Exclosure combined (i.e., second to last panel from bottom)?
- d) What is the intention of combining the OHV and non-OHV corridor results (i.e., last panel on bottom)? Would it not make more sense to look at these separately and then compare them to similar 2019 data (i.e., riding and non-riding areas, respectively)?
- e) Why use standard error (SE) rather than standard deviation? If SE is to be used as an indicator of uncertainty around the mean, then why not conduct some sort of uncertainty analysis in the modeling effort (for future consideration)?

3) Figures 1-4

- a) These figures all include curves for “mean NRA 2019” and “mean NRA 2013-2019,” and the narrative for each basically says that the new 2022 measurements display much lower PM₁₀ emissivity than those prior means. Why not collapse all these curves into a single figure so that the reader is able to compare the new results for the restoration areas vs. plover exclosure vs. beach vs. corridors? (With the caveat that OHV and non-OHV should be separated, as described above.)

4) Page 7

- a) The last sentence in the paragraph preceding Figure 4 states, “...for the non-riding area in May 2022.” Is this a typo? Were there PI-SWERL measurements taken in May 2022? If so, where were they? Alternatively, is this referring to an analysis that was published in May 2022? If so, please provide a citation and context for the referenced values.

5) Page 8

- a) The first paragraph on this page recommends the use of the mean corridor emissivity relation (Table 1, Figure 4) in the next model iteration. Please provide justification as to why the mean for multiple different surfaces is actually meaningful to use. What is the logic/rationale?
- b) For the foredune restoration areas, it is recommended to use the mean emissivity of all the PI-SWERL measurements in all the treatment areas. Following on the comment above regarding Table 1, why does this recommendation make sense when area 1 is a control with no treatment at present? Also, does the model take into account percent cover by vegetation in each of these areas or does it apply the mean emissivity to the entire surface area?
- c) In the third paragraph, the meanings of “actual” and “measured” should be clarified.

- d) In the fourth paragraph, “know” should be replaced with “known.”
- 6) Figure 5
 - a) As presently displayed, this is not very useful. The figure is a distorted representation of actual spatial dimensions. Why not put a map/image underneath so that we can see where these measurements were taken? In addition, please show the positions of *all* September 2022 PI-SWERL tests, including those within the Plover Exclosure (potentially via a separate figure panel).

References

- CDPR, 14 September 2022, 2nd DRAFT 2022 Annual Report and Work Plan, https://storage.googleapis.com/slocleanair-org/images/cms/upload/files/2ndDraft2022ARWP_2022914.pdf
- Gillies, J.A., Furtak-Cole, E., Nikolich, G., and Etyemezian, V., 2022. The role of off-highway vehicle activity in augmenting dust emissions at the Oceano Dunes State Vehicular Recreation Area, Oceano, CA. *Atmospheric Environment: X*, 13, 100146, <https://doi.org/10.1016/j.aeaoa.2021.100146>
- SAG, 07 February 2022, Memo: Scientific Basis for Possible Revision of the Stipulated Order of Abatement (SOA), [https://ohv.parks.ca.gov/pages/1140/files/Memo%20Scientific%20Basis%20for%20Possible%20Revision%20of%20the%20Stipulated%20Order%20of%20Abatement%20\(SOA\).pdf](https://ohv.parks.ca.gov/pages/1140/files/Memo%20Scientific%20Basis%20for%20Possible%20Revision%20of%20the%20Stipulated%20Order%20of%20Abatement%20(SOA).pdf)
- SAG, 27 September 2022, Memo: SAG Review of CDPR “2nd DRAFT 2022 Annual Report and Work Plan” (dated September 14, 2022), <https://storage.googleapis.com/slocleanair-org/images/cms/upload/files/SAG%20comments%202022%20ARWP%20-%2020220914%20version%20-%20final.pdf>
- SLOAPCD, 21 October 2022, Conditional Approval of California Department of Parks and Recreation’s 2022 Annual Report and Work Plan in Response to Stipulated Order of Abatement Number 17-01, <https://storage.googleapis.com/slocleanair-org/images/cms/upload/files/Final%20Conditional%20Approval%20-%20Revised.pdf>
- Walker, I.J., Hilgendorf, Z., Gillies, J.A., Turner, C.M., Furtak-Cole, E., Nikolich, G., 2023, Assessing performance of a “nature-based” foredune restoration project, Oceano Dunes, California, USA. *Earth Surface Processes and Landforms*, 48, 1-20, <https://doi.org/10.1002/esp.5478>

Oceano Dunes State Vehicular Recreation Area Dust Control Program

DRAFT 2023 Annual Report and Work Plan

ATTACHMENT 11-04

**SAG DRAFT SAG Framework for Assessing Excess Emissions of PM₁₀ from the ODSVRA
(January 30, 2023)**

**DRI DRAFT SAG Framework for Assessing Excess Emissions of PM₁₀ from the ODSVRA
(April 2023)**

**SAG Review of DRI Draft SAG Framework for Assessing Excess Emissions of PM₁₀ from the
ODSVRA (April 19, 2023)**

**FINAL SAG Framework for Assessing Excess Emissions of PM₁₀ from the ODSVRA
(June 21, 2023)**

THIS PAGE WAS INTENTIONALLY LEFT BLANK.

Oceano Dunes State Vehicular Recreation Area Dust Control Program

DRAFT 2023 Annual Report and Work Plan

ATTACHMENT 11-04

**SAG DRAFT SAG Framework for Assessing Excess Emissions of PM₁₀ from the ODSVRA
(January 30, 2023)**

THIS PAGE WAS INTENTIONALLY LEFT BLANK.

January 30, 2023

Memo: Framework for Assessing “Excess Emissions” of PM₁₀ from the Oceano Dunes

From: Scientific Advisory Group (SAG)

To: Jon O’Brien, California Department of Parks and Recreation (CDPR)
Karl Tupper, San Luis Obispo County Air Pollution Control District (SLOAPCD)

Cc: Sarah Miggins, California Department of Parks and Recreation (CDPR)
Liz McGuirk, California Department of Parks and Recreation (CDPR)
Gary Willey, San Luis Obispo County Air Pollution Control District (SLOAPCD)

Introduction

The Stipulated Order of Abatement (SOA), as amended by the SLOAPCD Hearing Board in October 2022, requires that dust mitigation plans at the Oceano Dunes State Vehicular Recreation Area (ODSVRA) “be designed to eliminate emissions in excess of naturally occurring emissions from the ODSVRA that contribute to downwind violations of the state and federal PM₁₀ air quality standards.” The amended SOA requires that such an “excess emissions goal” be approved by the SLOAPCD Hearing Board by October 16, 2024 (SLOAPCD Hearing Board, 2022). For the purposes of assessing progress toward eliminating such excess PM₁₀ emissions, it is therefore necessary to identify a simple but objective framework for establishing a “naturally occurring” PM₁₀ baseline against which “excess emissions” can be evaluated.

To establish such a framework for assessing “excess emissions” of PM₁₀ from the ODSVRA, the SAG proposes that CDPR leverage and extend the approach developed by Gillies et al. (2022) for comparing total PM₁₀ (TPM₁₀) to total wind power density (TWPd). By this approach, variations in observed ambient PM₁₀ concentration are represented by TPM₁₀, while variations in the dust-mobilizing wind strength are represented by TWPd. For any particular PM₁₀ monitoring site, the relationship between TPM₁₀ and TWPd is expected to remain constant, unless upwind management changes (or other factors) enhance PM₁₀ dust emissions (causing an increase in the TPM₁₀:TWPd ratio) or reduce PM₁₀ dust emissions (causing a decrease in the TPM₁₀:TWPd ratio).

The purpose of this memo is to propose an approach for determining the relationship between TPM₁₀ and TWPd that is representative of “naturally occurring” emissions as measured at any given monitoring site downwind of the ODSVRA (e.g., CDF or Mesa2). Specifically, naturally occurring TPM₁₀ versus TWPd would be estimated by modeling PM₁₀ concentrations and wind speeds for the “pre-disturbance” emissions scenarios established by the SAG in its February 2022 memo (SAG, 2022). Such modeling could utilize the Desert Research Institute (DRI) emissions-dispersion model (Mejia et al., 2019). Going forward, actual observed TPM₁₀ and TWPd at any given monitoring site (e.g., CDF or Mesa2) could then be compared to the expected TPM₁₀:TWPd ratio for naturally occurring emissions. If observed values of this ratio

were to significantly exceed expected “naturally occurring” values, this could be attributed as “excess emissions” as specified by the amended SOA (see Fig. 1 below).

Although the feasibility of this TPM₁₀:TWPD approach to assessing excess emissions has not yet been tested, the data and the modeling strategies already exist to begin evaluating this concept. The SAG recommends that this proposed TPM₁₀:TWPD approach be developed in an iterative fashion, first performing some initial DRI model runs to establish a proof of concept. Then, if the proposed framework appears viable, it could be further refined toward establishing a benchmark for naturally occurring TPM₁₀:TWPD against which future observed variations in TPM₁₀:TWPD could be compared. In the end, a successful framework for assessing excess emissions should accommodate wide year-to-year variability in wind and PM₁₀ conditions, and it should also account for ongoing questions about the attributability of PM₁₀ from the ODSVRA versus exogenous sources.

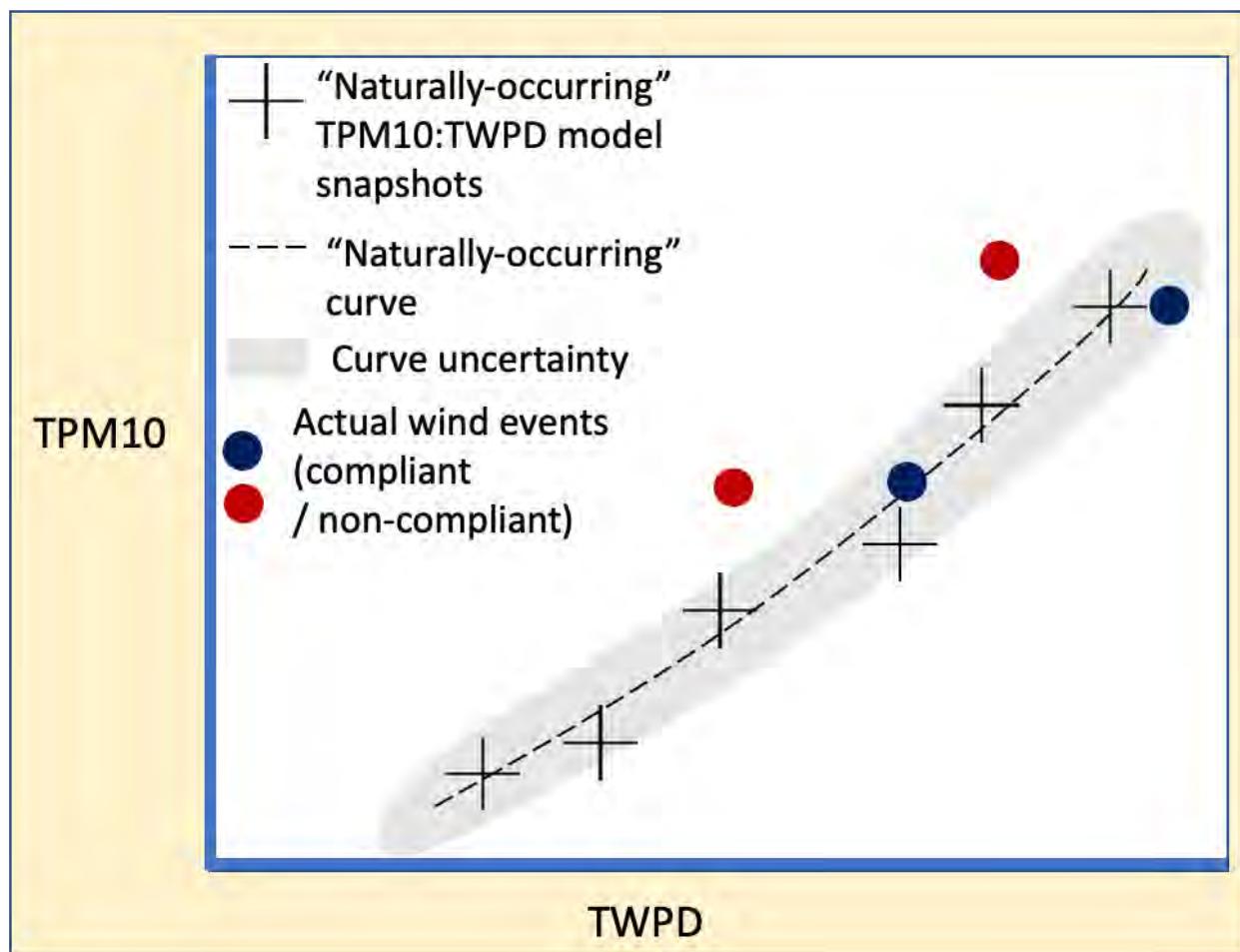


Figure 1. Concept for setting a “naturally occurring” emissions baseline for TPM₁₀ relative to TWPD. Diagram is conceptual and does not reflect actual data or modeling.

Scientific Basis

Recent scientific developments provide a basis for the proposed framework for assessing excess PM₁₀ emissions:

1. **Pre-disturbance emissions scenarios.** In February 2022, the SAG established a process for modeling PM₁₀ associated with “pre-disturbance emissions scenarios” based on known historic vegetation cover and assumed PM₁₀ emissivity prior to significant vehicular disturbance (SAG, 2022). Existing data on historic vegetation cover (Swet et al., 2022) and PM₁₀ emissivity relationships for undisturbed locations at the ODSVRA (Gillies et al., 2022) inform such pre-disturbance modeling. **The pre-disturbance scenario approach, which is codified in the amended SOA, could serve as the basis for identifying a “naturally occurring” baseline against which future changes in airborne PM₁₀ are considered.**
2. **TPM₁₀:TWPDP framework.** Published reports (e.g., Gillies et al., 2022) establish the ratio of total PM₁₀ emissions (TPM₁₀) to total wind power density (TWPDP) as a useful way to account for year-to-year variations in wind events when examining long-term increments of progress resulting from ODSVRA dust mitigation measures. TPM₁₀:TWPDP provides an average, over a defined period of time, for the PM₁₀ measured at a receptor site (e.g., CDF) relative to the effective dust-mobilizing strength of wind at a meteorological monitoring site (e.g., S1). **This allows for calculation of emissions under any given meteorological condition, and the TWPDP can be applied to both disturbed (current/future) and undisturbed (pre-disturbance, or “natural” surface conditions).**

Together, these two bodies of knowledge allow, conceptually, for the calculation of how much TPM₁₀ *would have been* generated from a surface undisturbed by vehicular activity under specific wind conditions (TWPDP) of the present day. Comparing that TPM₁₀ number to what was *actually observed* at the ODSVRA at any given time period in the future will allow for determining if the TPM₁₀ observed was in excess of what would have been generated for the observed TWPDP during that time period, but on an undisturbed ODSVRA surface.

Proposed Implementation

The SAG proposes an iterative implementation, which would first determine the efficacy of the TPM₁₀:TWPDP framework before fully establishing its use for regulatory assessment of “excess” emissions based on PM₁₀ observations at monitoring sites. In particular, the SAG recommends pursuing the following steps toward implementing this framework:

1. **Modeling.** Thus far, the TPM₁₀:TWPDP framework has been applied only to observations. Establishing a “naturally-occurring” curve (i.e., as in Fig. 1 above) would require obtaining model snapshot values for TPM₁₀ and TWPDP from DRI model simulations of pre-disturbance scenarios. TPM₁₀ could be derived by adding up hourly modeled PM₁₀ concentrations at CDF, and TWPDP could be calculated by compiling hourly modeled

wind speed data at the latitude and longitude of the S1 Tower at the reference height of 10 meters above ground level. As a first step to determine feasibility of this modeling approach, a subset of days from existing model runs could be queried to obtain the values for each modeled day. As established in the SOA, these initial model runs could be based on known meteorological conditions for a subset of high wind days in 2013. The following values would be obtained and then preliminary comparisons among these values could be performed as a proof of concept for the proposed modeling approach:

- (a) **Modeled TPM_{10} values for known 2013 emissions conditions**, i.e., model runs from the SOA Particulate Matter Reduction Plan (CDPR, 2019).
 - (b) **Modeled TPM_{10} values for estimated pre-disturbance emissions conditions**, i.e., model runs underlying the February 2022 SAG memo (SAG, 2022).
 - (c) **Modeled TWPDP values at S1 tower for 2013 meteorology scenarios**. These should be equivalent for (a) and (b) above, as the same set of meteorology scenarios (i.e., high wind days in 2013) would be utilized for modeling both the 2013 and pre-disturbance emissions conditions.
 - (d) **Observed TWPDP values at S1 tower for 2013 meteorology scenarios**, i.e., calculated based on actual measured wind speeds at the S1 tower. Assuming the model is accurate, such observed TWPDP values should be similar to those obtained via modeling for the same set of days in (c) above.
2. **Naturally occurring TPM_{10} :TWPDP curve**. Assuming it is possible to obtain modeled TPM_{10} and TWPDP for a collection of representative days for the pre-disturbance scenario in step 1 above, the next step would be to determine whether it is possible to establish a meaningful “naturally occurring” TPM_{10} :TWPDP curve. The idealized conceptual diagram in Fig. 1 shows a smooth increase in TPM_{10} versus TWPDP, but the actual model runs may display a much larger amount of scatter. This scatter could be reduced by increasing the timescale of model snapshots (i.e., each point in the TPM_{10} :TWPDP curve would represent a series of days rather than a single day) but with the tradeoff that temporal precision is reduced. An acceptable balance for this tradeoff would need to be determined. In addition, an approach to accounting for exogenous sources of PM_{10} (i.e., PM_{10} observed at monitoring sites that originate outside the ODSVRA) may need to be developed.
3. **Observed TPM_{10} and TWPDP**. Assuming it is possible to establish a meaningful TPM_{10} :TWPDP curve in step 2 above, the next step would be to compare such a curve to actual observations of TPM_{10} and TWPDP. The proposed approach assumes a straightforward comparison between measured TPM_{10} :TWPDP data points and the modeled “naturally-occurring” curve. Even if it is possible to establish this modeled curve with a high degree of certainty, it remains possible that the variability of observed TPM_{10} :TWPDP values would be so large that comparisons between these observations and the modeled “naturally-occurring” curve would be statistically insignificant. Do such comparisons make sense for TPM_{10} :TWPDP values computed over 24-hour periods? If not, would it help to calculate TPM_{10} :TWPDP values over longer time scales (i.e., over a month or season), such that this variability would be reduced while still providing a meaningful result? Preliminary comparisons between observations and the naturally occurring TPM_{10} :TWPDP benchmark relationship would need to be performed to establish the viability of such comparisons and to inform any fine tuning that may need to be performed.

The SAG recommends that CDPR commission modeling and data retrieval actions as per the three initial steps proposed above, with the goal of evaluating viability and identifying further implementation steps in the context of “Monitoring and Adaptive Management” for the upcoming 2023 Annual Report and Work Plan (ARWP). Because testing and implementation of the proposed framework is necessarily iterative, CDPR may wish to commission the work one step at a time, and then to share the results of each step with the SAG for review and consultation on next steps. If all three proposed initial steps are completed to the satisfaction of the SAG, CDPR, and SLOAPCD, these parties could then work toward codifying a process, subject to the approval of the SLOAPCD Hearing Board, to allow for regular assessments of excess PM₁₀ emissions relative to the naturally occurring baseline. For example, a chart such as that in Fig. 1 could be established for each PM₁₀ monitoring site such that emissions that exceed the “naturally occurring” envelope would be treated as non-compliant under the terms of the SOA. Procedures for responding to the occurrence of such non-compliant events would need to be established, such as via adaptive management actions toward additional dust mitigation to bring ODSVRA PM₁₀ dust emissions back in compliance with the SOA.

Respectfully,
The Scientific Advisory Group

Raleigh Martin (Chair of SAG); Bernard Bauer; Mike Bush; John A. Gillies; Leah Mathews; William Nickling; Carla Scheidlinger; Ian Walker

References

- CDPR, 10 June 2019, Oceano Dunes State Vehicular Recreation Area Draft Particulate Matter Reduction Plan, https://storage.googleapis.com/slocleanair-org/images/cms/upload/files/Draft_PMRP_20190606.pdf
- Gillies, J.A., Furtak-Cole, E., Nikolich, G. & Etyemezian, V., 2022, The role of off-highway vehicle activity in augmenting dust emissions at the Oceano dunes state vehicular recreation area, Oceano, CA. Atmospheric Environment: X, 13, 100146.
<https://doi.org/10.1016/j.aeaoa.2021.100146>
- Mejia, J.F., Gillies, J.A., Etyemezian, V., Glick, R. (2019). A very-high resolution (20 m) measurement-based dust emissions and dispersion modeling approach for the Oceano Dunes, California. Atmospheric Environment, 218, 116977,
<https://doi.org/10.1016/j.atmosenv.2019.116977>
- SAG, 07 February 2022, Memo: Scientific Basis for Possible Revision of the Stipulated Order of Abatement (SOA),
[https://ohv.parks.ca.gov/pages/1140/files/Memo%20Scientific%20Basis%20for%20Possible%20Revision%20of%20the%20Stipulated%20Order%20of%20Abatement%20\(SOA\).pdf](https://ohv.parks.ca.gov/pages/1140/files/Memo%20Scientific%20Basis%20for%20Possible%20Revision%20of%20the%20Stipulated%20Order%20of%20Abatement%20(SOA).pdf)
- SLOAPCD Hearing Board, 14 October 2022, Case No. 17-01, Order to Modify Existing Stipulated Order of Abatement, <https://storage.googleapis.com/slocleanair-org/images/cms/upload/files/SOA%2017-01%20Second%20Amendment%20Final%20Adopted%2010-14-2022%20%26%20Filed.pdf>
- Swet, N., Hilgendorf, Z., Walker, I., February 2022, UCSB Historical Vegetation Cover Change Analysis (1930-2020) within the Oceano Dunes SVRA,
[https://ohv.parks.ca.gov/pages/1140/files/Memo%20Scientific%20Basis%20for%20Possible%20Revision%20of%20the%20Stipulated%20Order%20of%20Abatement%20\(SOA\).pdf](https://ohv.parks.ca.gov/pages/1140/files/Memo%20Scientific%20Basis%20for%20Possible%20Revision%20of%20the%20Stipulated%20Order%20of%20Abatement%20(SOA).pdf),
Attachment 2

Oceano Dunes State Vehicular Recreation Area Dust Control Program

DRAFT 2023 Annual Report and Work Plan

ATTACHMENT 11-04

DRI DRAFT SAG Framework for Assessing Excess Emissions of PM₁₀ from the ODSVRA

(April 2023)

THIS PAGE WAS INTENTIONALLY LEFT BLANK.

Framework for Assessing “Excess Emissions” of PM₁₀ from the Oceano Dunes

Phase 1: Modeled TPM₁₀ for CDF, Mesa2, and S1 tower, and TWPDP for S1 tower for 1939 (as previously modeled) and 2013 (as previously modeled)

To test the proof of concept that a relation between Total PM₁₀ (TPM₁₀ $\mu\text{g m}^{-3}$) and Total Wind Power Density (TWPDP W m^{-2}) could be established using modeled hourly PM₁₀ concentrations at CDF and Mesa2, and 10 m above ground level wind speed (AGL) at the S1 tower, DRI extracted these data from previous emission and dispersion model runs representing the 1939 “pre-disturbance condition” (vegetation mask and model emissivity parameters set by the SAG, 2022) and the 2013 baseline condition (no dust controls in place, 2013 PI-SWERL emissivity grid). The meteorology (i.e., wind field conditions) were identical in both model runs based on wind fields generated for days between May 15 and July 13 in 2013.

From the existing model runs, individual days were queried to obtain the hourly predicted values of PM₁₀ at CDF, Mesa2, and S1 tower, and wind speed at 10 m AGL at the S1 tower for each modeled day. A total of 60 days (1440 hours) were extracted from the model runs between May 15 and July 13, 2013. Initially, for each day the 24 hourly values were summed to calculate daily TPM₁₀ ($\mu\text{g m}^{-3}$) and TWPDP (W m^{-2}) values, for the 1939 and 2013 emissivity grids with the 2013 wind fields applied for both cases. In previous estimates of the relation between TPM₁₀ and TWPDP, the summation was calculated for only above threshold wind speed, which at S1 tower for years since 2013 has been set at 8.5 m s^{-1} (Gillies et al., 2022).

For the first case, all hourly (model-estimated) data used for calculating TPM₁₀ ($\mu\text{g m}^{-3}$) and TWPDP (W m^{-2}), the relation between these two variables is shown in Fig. 1 for CDF, Mesa2, and at the S1 tower. As Fig. 1 shows, in all three cases the 2013, TPM₁₀ and TWPDP relations show an “excess of emissions” compared with the 1939 case. The data in each case show clustering of lower TPM₁₀ and TWPDP values below approximately TWPDP=2000 W m^{-2} , which likely represent a non-emitting condition within the ODSVRA, i.e., wind is likely below the 8.5 m s^{-1} threshold speed for saltation and dust emissions. Filtering the hourly data to remove hours with 10 m AGL wind speed $< 8.5 \text{ m s}^{-1}$, the relations for CDF, Mesa2, and at the S1 tower are shown in Fig. 2. Filtering for above threshold wind speed, the number of days is reduced to 23 and the range of hours over threshold is 1 to 8 for given day. With hours below the threshold wind speed of 8.5 m s^{-1} for each day removed, the goodness of fit and the slope decrease for the TPM₁₀ and TWPDP relations. The 2013 data still exhibit an “excess of emissions” compared with the 1939 case.

As a “proof of concept” for using model-generated hourly data to quantify whether a particular year’s windy season emissions are “in excess” of the 1939 pre-impact emissivity and vegetation conditions, the relations shown in Figs. 1 and 2 suggest that it is feasible. Outstanding issues to be settled are the 1939 emissivity grid, what filtering of the wind speed data should be considered, and what criteria can be used to judge that the condition of “excess emissions” has been exceeded for a specified period of time for a given year.

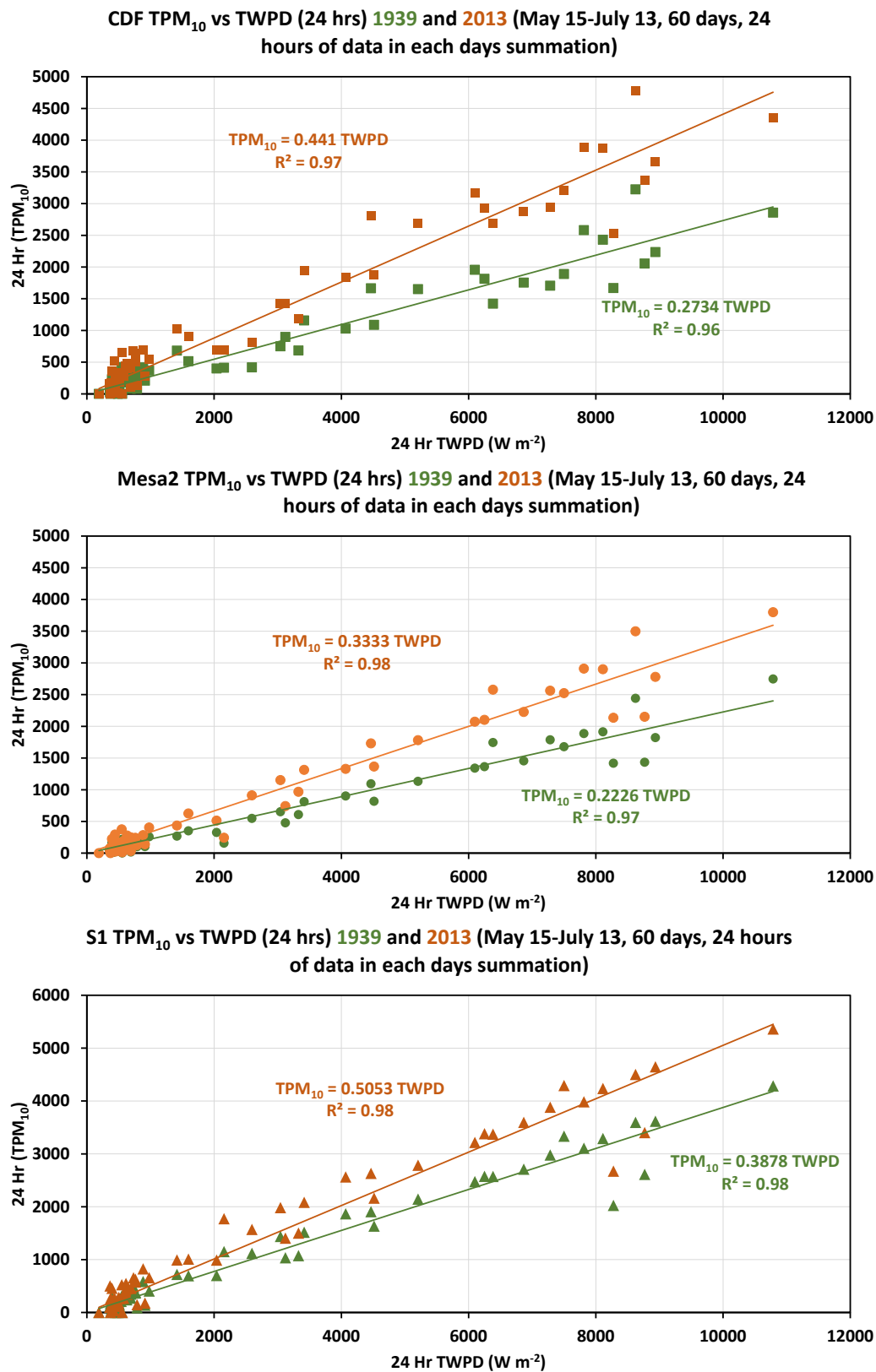


Figure 1. TPM₁₀ and TWPD relations for CDF, Mesa2, and S1 tower for all hours for each of the 60 days.

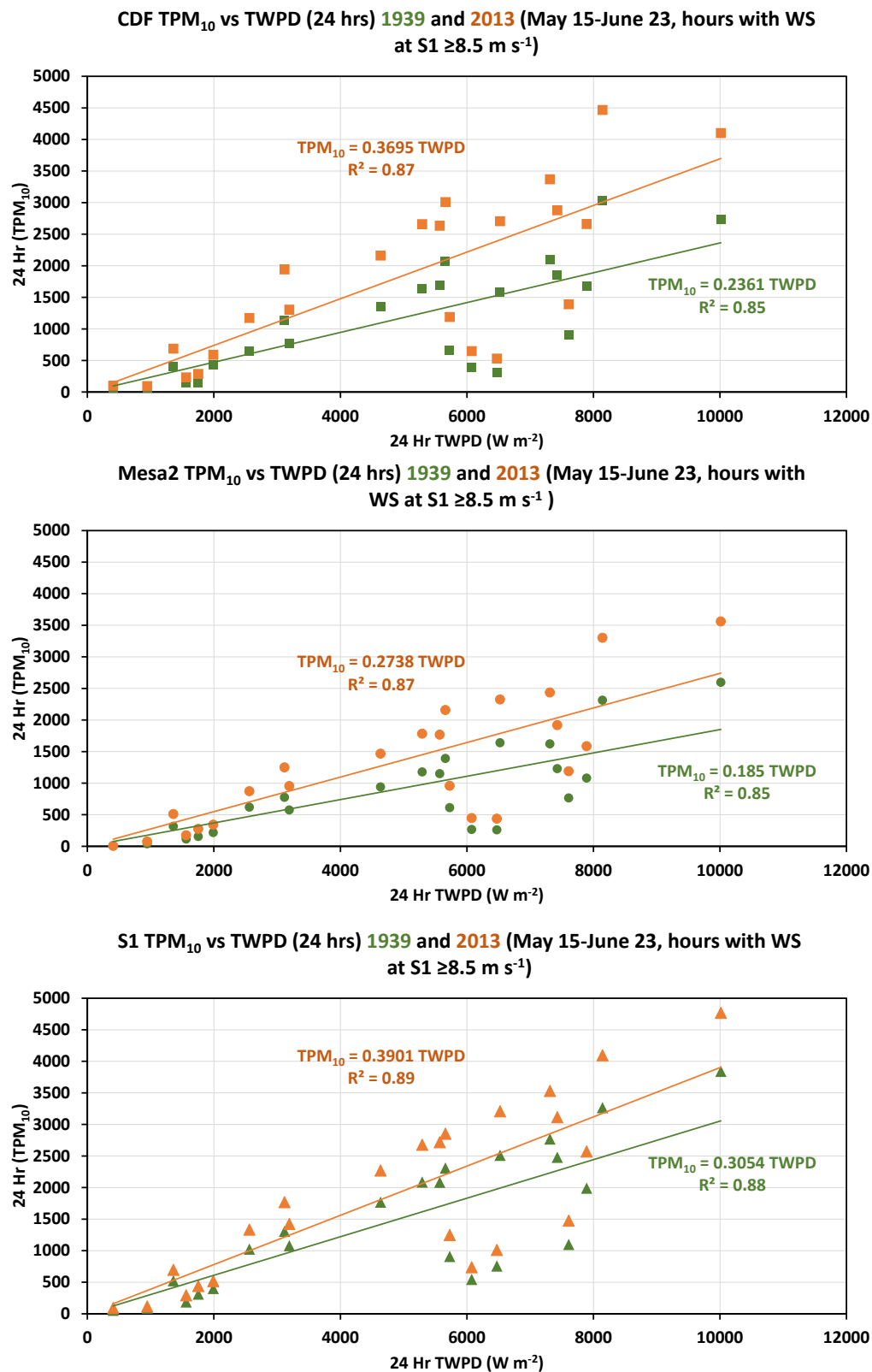


Figure 2. TPM₁₀ and TWPD relations for CDF, Mesa2, and S1 tower. Summations based on using only hours when wind speed at S1 tower are ≥ 8.5 m s⁻¹ for a modeled day.

Observed and Modeled TWPD values at S1 tower for 2013 meteorology

As part of the proposed implementation for evaluating “excess emissions”, SAG requested that observed TWPD (i.e., calculated based on measured wind speed 10 m AGL at S1 tower) be compared with modeled TWPD. For the same days as represented in Figs. 1 and 2, the relation between hourly modeled wind speed and measured wind speed for the S1 tower is shown in Fig. 3. The modeled 10 m AGL wind speed is highly correlated with the measured wind speed, but it is biased lower by approximately 10% across the range of the observations (Fig. 3).

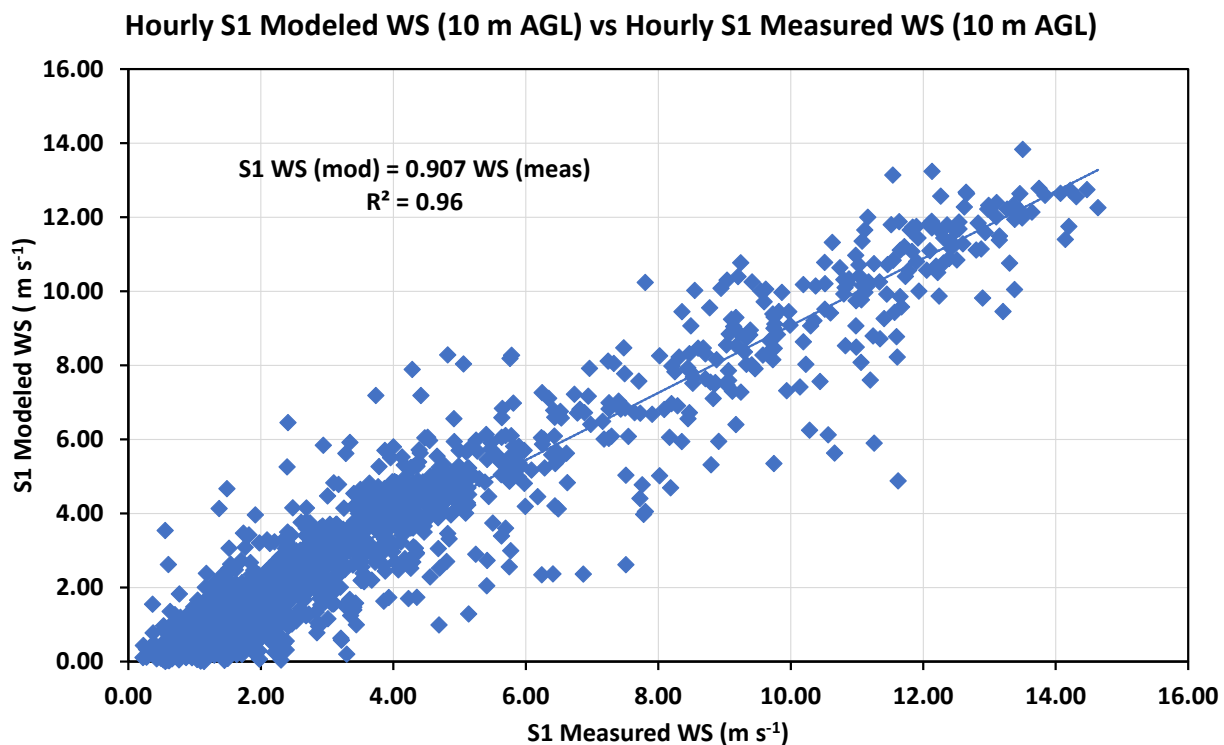


Figure 3. The relation between modeled 1 hour wind speed and measured 1 hour mean wind speed at S1 Tower for 60 days between May 15 and July 13, 2013.

The TWPD for measured and modeled values was calculated by summing the 24 hourly values in each of the 60 days. The relation between modeled and measured TWPD for the available days is highly correlated as shown in Fig. 4. The low bias in the modeled hourly wind speed values, however, is amplified upon the conversion to WPD due to the cubing of the wind speed. This results in the modeled TWPD values being approximately 23% lower than the calculated WPD (based on measured wind speed) across the range of observations.

Using 24-hour TWPD calculated from measured hourly S1 tower data and modeled 24-hour TPM₁₀ to define the relation between them results in correlations that are as high as between modeled TWPD and modeled TPM₁₀, however, the slope of the relationship for each of the sites, Mesa2, CDF, and S1 are lower due to the higher TWPD values calculated from the measured wind speeds for S1 tower. The

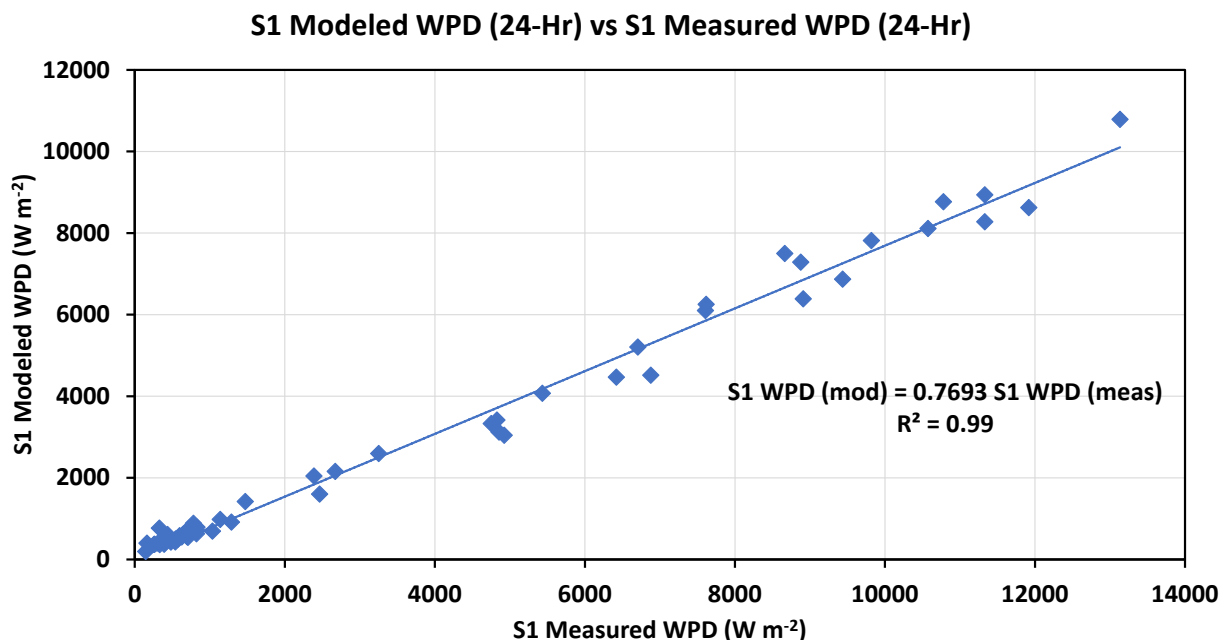


Figure 4. The relation between modeled 24-hour TWPd and 24-hour measured WPD at the S1 Tower for 60 days between May 15 and July 13, 2013.

differences between the relation for modeled and measured TWPd for each of the sites, CDF, Mesa2, and S1 tower is shown in Fig. 5.

As there will only be modeled values of hourly wind speed and PM_{10} for the 1939 emissivity grid, a question arises as to how to best determine whether a current year condition, for example a day when the 24-hr mean PM_{10} at CDF is much higher than the State standard of $50\ \mu g\ m^{-3}$, is in a condition of “excess emissions”. Measured PM_{10} and measured wind speed can be acquired most rapidly, but the known biases in the model present an issue of a direct comparison with the 1939 modeled TPM_{10} and TWPd relationship.

The biases in the modeled hourly wind speed and PM_{10} data were presented and described in detail in Mejia et al. (2019). As observed for wind speed (Fig. 3), the model also underestimates PM_{10} (see Mejia et al., 2019, Figs. 12 and 13), less so when 24-hour PM_{10} is $>50\ \mu g\ m^{-3}$ (Mejia et al., 2019). Modeled wind speed and PM_{10} cannot be readily generated for an identified period (e.g., daily, or monthly) in a current year to ascertain whether a condition of “excess emission” exists. This would require generating the wind field (using newly-acquired meteorological data and the CalMet part of the emission/dispersion model) for the time interval in question. This wind field would then be used to generate the PM_{10} concentrations using the Lagrangian Particle Dispersion component of the model for the current year emission grid. This raises the question, should, in the case of the 1939 emission scenario, the modeled data be adjusted by the identified biases between measured and modeled to generate the 1939 TPM_{10} , TWPd relation? This would expedite the comparison of current year observations of TPM_{10} and TWPd with the 1939 TPM_{10} and TWPd relation to evaluate (e.g., the day after the event) whether a period of high PM_{10} concentrations represented a condition of “excess emissions”.

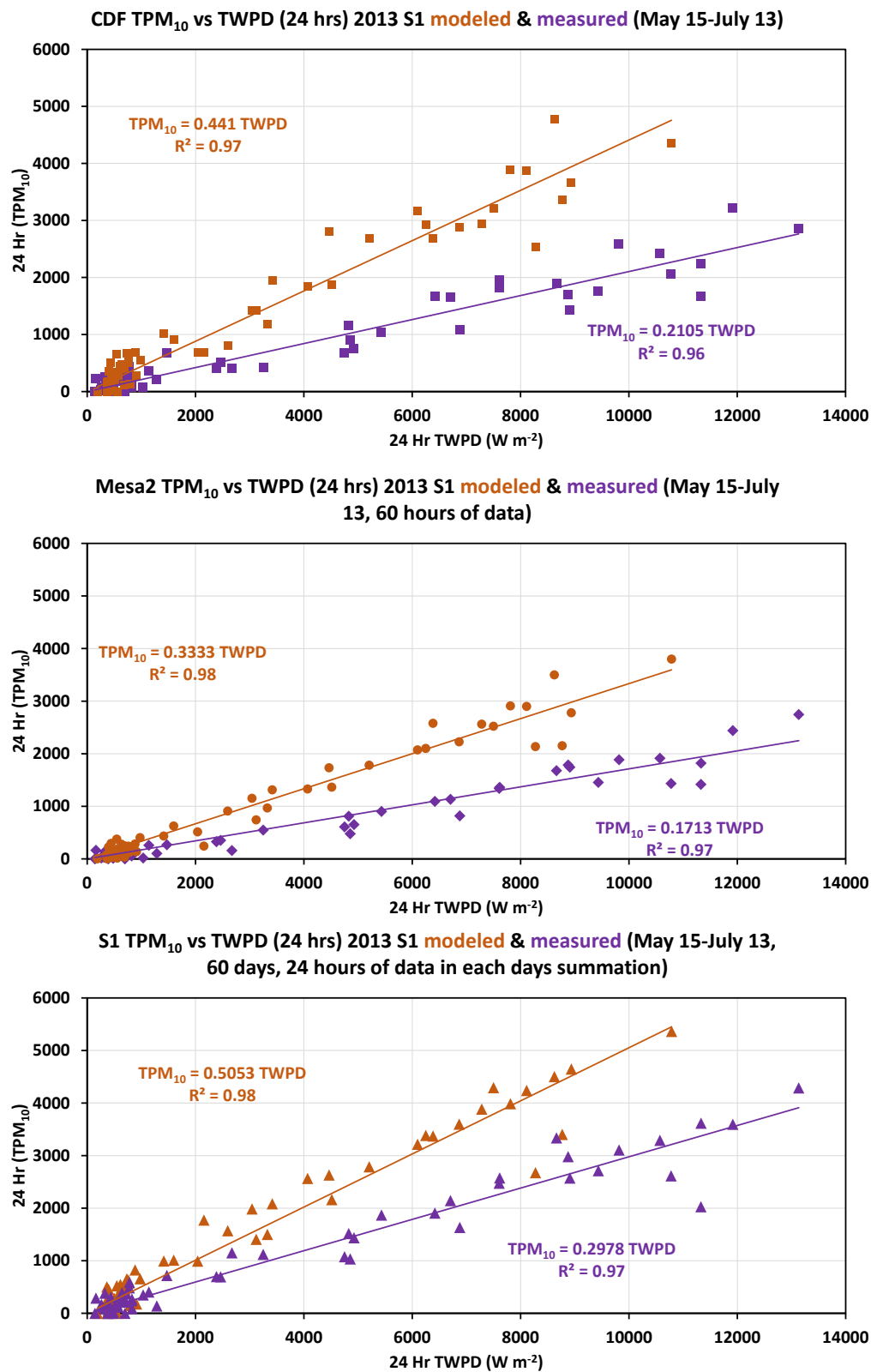


Figure 4. The relation between modeled 24-hour TPM₁₀ and 24-hour modeled and measured WPD at CDF, Mesa2 and S1 Tower for 60 days between May 15 and June 23, 2013.

The confirmation, i.e., acceptance or rejection of the identified condition could be completed later using modeled data. For example, after the end of the end of the wind season (approximately October). The determination of the time frame for evaluating the condition of “excess emissions” seems to require clarification within the SOA to guide an agreed upon framework for its implementation.

THIS PAGE WAS INTENTIONALLY LEFT BLANK.

Oceano Dunes State Vehicular Recreation Area Dust Control Program

DRAFT 2023 Annual Report and Work Plan

ATTACHMENT 11-04

**SAG Review of DRI Draft SAG Framework for Assessing Excess Emissions of PM₁₀ from the
ODSVRA (April 19, 2023)**

THIS PAGE WAS INTENTIONALLY LEFT BLANK.

April 19, 2023

Memo: SAG review of Desert Research Institute (DRI) report, “Framework for Assessing ‘Excess Emissions’ of PM₁₀ from the Oceano Dunes Phase 1”

From: Scientific Advisory Group (SAG)

To: Dr. Jack Gillies¹, Desert Research Institute

Cc: Jon O’Brien, California Department of Parks and Recreation (CDPR)

Following recommendations arising from the SAG in-person meeting held February 23-24, 2023, the Desert Research Institute (DRI) undertook a preliminary assessment of the viability of an excess emissions framework based on an expected relationship between Total PM₁₀ (TPM₁₀; $\mu\text{g m}^{-3}$) and Total Wind Power Density (TWPD; W m^{-2}). The framework was initially proposed in a SAG Memo (“SOA Excess Emissions Framework”, January 30, 2023) that lays out a multi-step implementation process, the first stage consisting of the extraction of information from existing DRI model runs to determine whether it is feasible to create a ‘naturally-occurring’ curve that characterizes the pre-disturbance conditions at the Ocean Dunes State Vehicular Recreation Area (ODSVRA). It was anticipated that there would be a positive (increasing) relationship between dust emissions and wind power that could be characterized by a curve that might take the form of Figure 1.

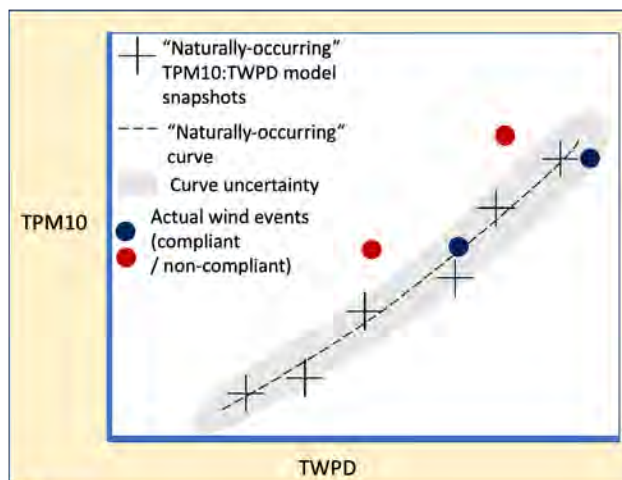


Figure 1. Concept diagram for setting a “naturally occurring” emissions baseline for TPM₁₀ relative to TWPD. Diagram does not reflect actual data or modeling.

Real measurements of dust concentrations and wind speeds in today's environment can be plotted on the diagram and compared to the pre-disturbance curve (derived from modeling) to determine whether PM₁₀ concentrations were in compliance with excess emissions regulations. Assessment of compliance would be made depending on whether the measurements fall above (non-compliant) or below (compliant) the curve, recognizing that there is uncertainty associated with

defining the 'naturally occurring' conditions. This uncertainty is graphically represented by the grey area surrounding the dashed curve in Figure 1.

The DRI proof-of-concept document suggests that such a curve could be created (see Figure 2) and that it is linear, as was anticipated based on a well-known cubic relationship between wind speed and particle emission from the surface. For the purposes of the proof-of-concept report, DRI used modeled hourly S1 tower wind speed (10 m above ground level) versus modeled hourly PM₁₀ concentrations at CDF (or Mesa2 or S1). DRI extracted these data from previous emission and dispersion model runs representing the 1939 “pre-disturbance condition” (vegetation mask and model emissivity parameters set by the SAG, 2022) and the 2013 baseline condition (no dust controls in place, 2013 PI-SWERL emissivity grid) using the wind conditions for days in 2013, as defined in the SOA.

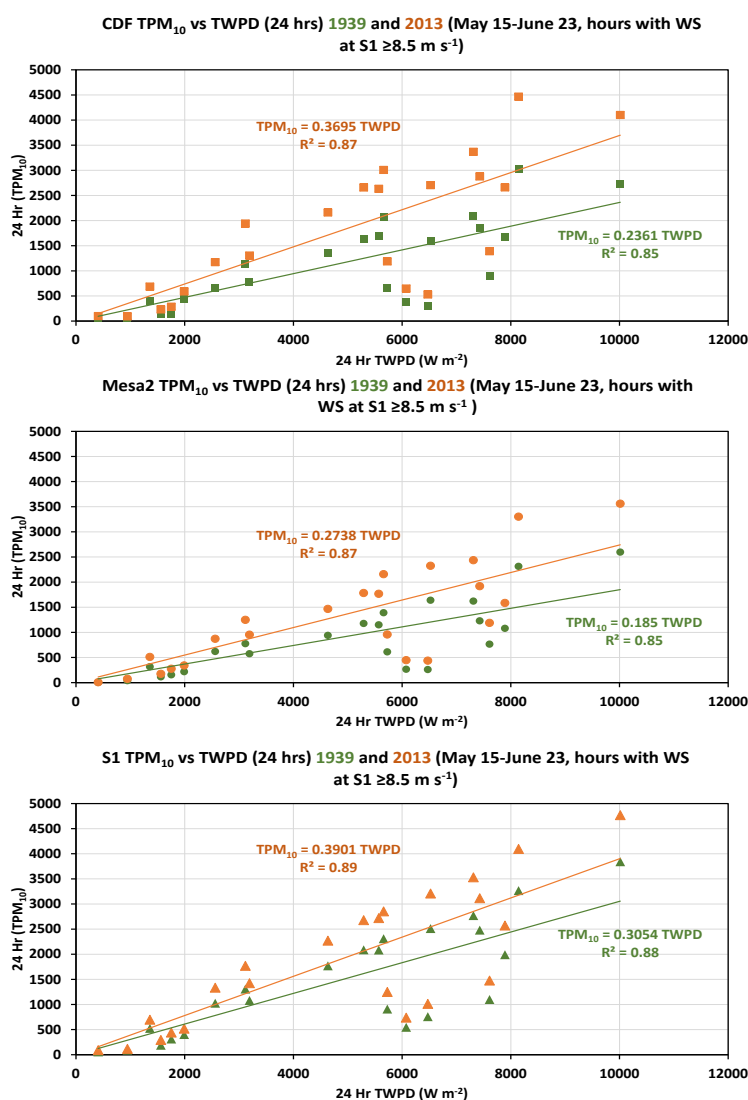


Figure 2. TPM₁₀ and TWPDP relations for CDF, Mesa2, and S1 tower. Summations based on using only hours when wind speed at S1 tower are $\geq 8.5 \text{ m s}^{-1}$ for a modeled day. See DRI report for additional details.

DRI concludes that these figures suggest that “it is feasible” to use “model-generated hourly data to quantify whether a particular year’s windy season emissions are ‘in excess’ of the 1939 pre-impact emissivity and vegetation conditions.” The SAG concurs. However, the DRI report also notes that when comparing observed (measured) data with modeled data, a source of bias is introduced because the wind model consistently underpredicts the actual wind speeds measured at the S1 tower (10 m above ground level) by approximately 10%. As a consequence, PM₁₀ emissions are also underpredicted (as described in Mejia et al., 2019).

There are significant ramifications for the excess emissions framework embodied in Figure 1. Even relatively small underpredictions of wind speed become important when estimating TWPD because of the cubic relation between wind speed and TWPD. DRI estimates that modeled TWPD values will be approximately 23% smaller than TWPD values based on wind speed measurements. Ultimately, this will produce a 'naturally occurring' curve (based on model results) in Figure 1 that is positioned above a similar curve that might have been based on measurements (had they been available). In short, the inherent bias would lead to measured data being preferentially (and artificially) positioned in the 'compliant' region of Figure 1 unless the bias is accounted for in the modeling leading to the 'naturally occurring' curve.

The SAG thanks DRI for undertaking this proof-of-concept investigation into the proposed excess emissions framework. The results are generally quite encouraging. It is particularly gratifying that the relationship between Total PM₁₀ (TPM₁₀) and Total Wind Power Density (TWPD) is linear and that the statistical correlation is quite good ($R^2 \geq 0.85$). This suggests that the proposed methodology for evaluating excess emissions is on a firm foundation. Nevertheless, the model bias is problematic for operationalizing the methodology, and it will need to be addressed.

The SAG makes the following observations (in no implied order of importance) regarding next steps in the iterative plan toward implementation:

1. The key concept in the proposed excess emissions framework is determining whether a close statistical relationship can be established between TPM₁₀ and TWPD for the pre-disturbance scenario. The DRI document indicates that this is feasible, and SAG is in general agreement. Moving forward, care needs to be taken that the regression statistics (R^2 , confidence intervals, statistical significance) are not influenced by clustering of points at small values of TPM₁₀ and TWPD (as seems to be the case in Figure 1 of the DRI report), and that when calculating the final version of the 'naturally occurring' curve the points are evenly distributed across the range of TWPD (the independent variable). In this regard, two issues require further discussion: (a) eliminating points below some threshold TWPD level, partly because they dominate the data set, but mainly because such low-emission days do not contribute to the management challenge; and (b) sub-sampling or selecting data values to create even increments along the TWPD axis, which may also involve some sort of averaging process to capture the most likely TPM₁₀ for any given TWPD value (or value bin).
2. The second set of figures in the DRI document (Figure 2 above) shows the relationship between TPM₁₀ and TWPD for days above threshold conditions for dust emission. There are five points that fall well below the line, in the zone of $5000 < \text{TWPD} < 8000$, and these

points strongly influence the slope of the regression. Most of the other points fit the linear trend well, but at a steeper slope. It would be useful to know whether those five points are somehow different in terms of meteorological conditions or some other factor.

3. Following this second point, it is essential that confidence bands be placed around the regression lines (as a surrogate for the grey zone in Figure 1 above) to parameterize the uncertainty in the pre-disturbance conditions. As a starting point, it would be instructive to include 90% confidence intervals around the regression curve. Ultimately, it will be essential for SAG to discuss, with CDPR and APCD, how to establish such confidence (uncertainty) bands for purposes of determining excess emissions because a non-compliant day would ostensibly fall above the upper confidence bands (rather than just the curve itself). The wider the confidence bands, the more likely it will be for measurements to fall within the compliant zone. This is a statistical matter, but it requires CDPR and APCD personnel to agree on an acceptable level of uncertainty.
4. The form of the regression equations included in the DRI report suggest that the regression fits have been constrained to pass through the origin (0,0) given that there are no offsets in the equations (only slopes). Although it seems reasonable to predict that there would be zero emissions at zero wind, it is similarly reasonable to assume that there would be zero (or at least minimal) emissions up to a certain wind threshold. In the latter case, there should be an offset to TWPD that aligns with the threshold. This should be explored as there are implications for the slopes of the regression curves, and hence a potential shift in the evaluation metrics leading to non-compliance.
5. The issue of model bias will require extensive discussion to address. There would seem to be three obvious approaches: (a) devise a simple bias correction algorithm such as a fractional multiplier to adjust the modeled pre-disturbance TPM_{10} values to bring them in-line with measured TPM_{10} values (using a training data set of present-day measured and modeled values that is yet to be determined); (b) devise a simple bias correction algorithm such as a fractional multiplier to adjust the modeled wind speeds to bring them in-line with measured wind speeds, and then to use these adjusted wind speeds to model the pre-disturbance scenario PM_{10} values used to generate the 'naturally occurring' curve (in Figure 1); and (c) undertake a model recalibration exercise to correct for the bias within the model itself.

SAG encourages ongoing discussions with DRI, CDPR, and APCD personnel as we work collectively on the next implementation steps leading toward a robust excess emissions framework.

Respectfully,

The Scientific Advisory Group¹

Bernard Bauer (Chair), Carla Scheidlinger (Vice-Chair), Mike Bush, Leah Mathews, Ian Walker.

Acknowledgement: Raleigh Martin (former Chair of SAG) provided feedback on the DRI document a few days after leaving his post as an official member of SAG.

¹ As an author of the DRI report, SAG member John A. Gillies did not contribute to this review.

Oceano Dunes State Vehicular Recreation Area Dust Control Program

DRAFT 2023 Annual Report and Work Plan

ATTACHMENT 11-03

FINAL SAG Framework for Assessing Excess Emissions of PM₁₀ from the ODSVRA

(June 21, 2023)

THIS PAGE WAS INTENTIONALLY LEFT BLANK.

For FINAL SAG/DRI Report see Attachment 6

THIS PAGE WAS INTENTIONALLY LEFT BLANK.

Oceano Dunes State Vehicular Recreation Area Dust Control Program

DRAFT 2023 Annual Report and Work Plan

ATTACHMENT 12

**ODSVRA Public Relations Campaign
(State Parks ARWP Work Product)**

THIS PAGE WAS INTENTIONALLY LEFT BLANK.

Placeholder. ODSVRA Public Relations Campaign is being finalized.

THIS PAGE WAS INTENTIONALLY LEFT BLANK.

Oceano Dunes State Vehicular Recreation Area Dust Control Program

DRAFT 2023 Annual Report and Work Plan

ATTACHMENT 13

**2022/2023 ODSVRA Dust Control Program Vegetation Restoration Projects
(State Parks ARWP Work Product)**

THIS PAGE WAS INTENTIONALLY LEFT BLANK.

2023-2024 Project List (subject to change)						
Project Name	Project Acreage	Total Plants	Plants Per Acre	Native Seed (lbs)	Native Seed (lbs per Acre)	Large Straw Bales (3X4X8 ft)
New Planting Areas						
North Boy Scout Camp 2021-WF-01	21.7	62,228	2,868	274	12.6	260
Eucalyptus Tree (east) 2021-WF-02	10.8	32,197	2,981	152	14.1	130
Eucalyptus Tree (west) 2022-ST-02	5.0	13,525	2,705	64	12.8	12
Subtotal	37.5	107,950	2,879	490	13.1	402
Supplemental Areas						
Eucalyptus Tree (south) 2022-VG-10	2.4	7,015	2,923	35.0	14.6	29
Subtotal	2.4	7,015	2,923	35	14.6	29
Total	39.9	114,965	2,881	525	13.2	431

THIS PAGE WAS INTENTIONALLY LEFT BLANK.